In-Situ Vadose-Zone Monitoring and Hydrologic Evaluation of Sulfide-Mine Mill-Tailings Wastes at Waite Amulet, Quebec.

by

Mark R. Woyshner

Department of Civil Engineering
McGill University, Montreal (Quebec)
Research Thesis Adviser: Dr. R. Yong, Ph.D.

May, 1992

A Thesis submitted to
the Faculty of Graduate Studies and Research
in partial fulfillment of the requirements
of the degree of
Masters of Science

Abstract

A thorough review of soil-water energy theories and soil-moisture measurement techniques are presented. Monitoring of piezometric head and soil-moisture potential and content at 3 vertical profiles was conducted along a cross section through Waite Amulet tailings, Quebec. Results characterized the subsurface hydrology during the fall of 1990, a recharge period, which shed light on the hydrologic controls of tailings oxidation.

Infiltration rates, wetting front velocities, hydraulic conductivities, and field capacity were determined. The presence of a tree cover increases infiltration by a factor of three. Recharge peaks reflected the conversion of tension-saturated to pressure-saturated porewaters. And, a water balance showed soil-moisture storage was 53% of precipitation, saturated-zone recharge 31%, evapotranspiration 12%, and runoff 4%.

The reliability of time-domain reflectometry to predict gravimetric water content of oxidized tailings was 88%. Heat dissipation sensors detected small dial fluctuations in response to evapotranspiration. Gypsum blocks proved valuable in detecting wetting fronts.

Résumé

Une revue des théories portant sur l'énergie des sols et de l'eau ainsi que sur les techniques permettant de mesurer le contenu en eau des sols est présentée. Des mesures de niveau piézométrique, de potentiel hydraulique et de teneur en eau du sol ont été mesurés sur trois profils verticaux le long d'une section à travers le parc à résidus miniers Waite Amulet, situé dans le nord du Québec. Les résultats ont servi à caractériser l'hydrologie souterraine durant l'automne 1990, soit une période de recharge, afin d'identifier les contrôles hydrologiques de l'oxydation des déchets solides miniers.

Les taux d'infiltration, la vitesse du front d'infiltration, la conductivité hydraulique et la capacité de retention d'eau ont été determinés. La présence d'arbres a augmenté l'infiltration par un facteur de trois. Les pics de recharge ont reflété la transition de conditions de saturation par tension à des conditions de saturation par pression. De plus, le bilan hydrique a montré une proportion d'emmagasinement d'humidité équivalente à 53% des précipitations, une recharge de la zone saturée à 31%, une évapotranspiration de 12% et un écoulement de surface de 4%.

La fidélité de la réflectométrie en domaine du temps pour prédire le contenu gravimétrique en eau des résidus oxydés a été de 88%. Les détecteurs de dissipation de chaleur ont identifié de légères fluctuations diurnes en réponse à l'évapotranspiration. Des blocs de gypse ont été utiles pour détecter le front d'infiltration d'eau.

Acknowledgements

The author is grateful for the opportunity to collaborate with the hydrogeotechnical group at the "Centre de technologie Noranda". In particular, the author wishes to sincerely thank Dr. Ernest Yanful, Ph.D., and Luc St-Arnaud, M.Eng., for their invaluable guidance and assistance throughout the breadth of this work. Working with them has been professionally rewarding as well as thoroughly enjoyable. In addition, interactions with S. Aiken, S. Payant, and K. Shikatani during field activities were particularly helpful and enjoyable. It is recognized that the "Centre de technologie Noranda" provided partial funding for this study.

The author is greatly appreciative for having the fortune to study with Professor Raymond Yong, Ph.D. Having him as a mentor has been invaluable to the author; through Dr Yong's challenges and enlightened guidance, the author has grown intellectually and matured academically. Their relationship has been most rewarding for the author.

This study could not have materialized without the love and support of the author's spouse, Dr. Louise Gaston, Ph.D. She provided financial stability during the course of the graduate studies of the author, and her insight into life has broadened the author's perspective while providing a ground for reality. Indeed, she is full of love.

Furthermore, the author would not have completely understood how to translate the acquired academic knowledge to current environmental problems without his spiritual growth developed in parallel during graduate studies. With this balance he can make better choices.

The author has fully appreciated the experience of graduate studies at McGill University, and he is thankful for the opportunity given to him by Dr. Yong and the Department of Civil Engineering and Applied Mechanics.

Table of Contents

List of Figures

List of Tables

1.0 WASTES OF SULPHIDE ORE, MINING AND MILLING

The Canadian mining industry produces in excess of 500 million tonnes of solid waste each year (IGWGMI, 1988). The mining and milling waste water is typically treated during the operation and discharged to receiving waters. The remaining waste, which is primarily the waste rock and mill tailings, generally remains on site as surface deposits of the mining operation. These rock dumps and tailing ponds are the most visible environmental impact of mining and milling waste, some of which can be physically managed though the recontouring and revegetation of mine sites during continuing operations and upon abandonment.

Sulphide ore contains marketable metalliferous minerals in association with sulphur. The mining of sulphide ore is a principal generator of waste in the Canadian mineral industry. Much of this waste is acid discharge generating and poses a significant environmental problem.

1.1 MINING AND MILLING PROCESSES

Mining operations generally consist of underground and surface methods which produce solid and liquid waste. Underground mines involve relatively little surface disturbance. The waste rock produced from the extension of the access tunnels and the low grade ores are stockpiled, with some reuse as mine backfill. The waste, as a percentage of the total underground mined material, ranges from near zero in the case of iron ore to 10 to 20 percent for the non-ferrous metals. Comparatively, these values for open-pit mines are about 40% for iron ore and 65% for non-ferrous metals. Surface methods (e.g., open pit and strip mining) usually require the removal of large quantities of material in addition to the ore body, and result in the disturbance of a considerable area of land. Surface mining generates large quantities of solid waste material, which for open pit mining is approximately 50 times that produced by

underground mining. Although about 6 times as much water flows though open pit mines, the water flow per tonne of ore removed is about twice that for underground types. Figure 1.1 compares the product and byproduct quantities of open-cast and underground extraction.

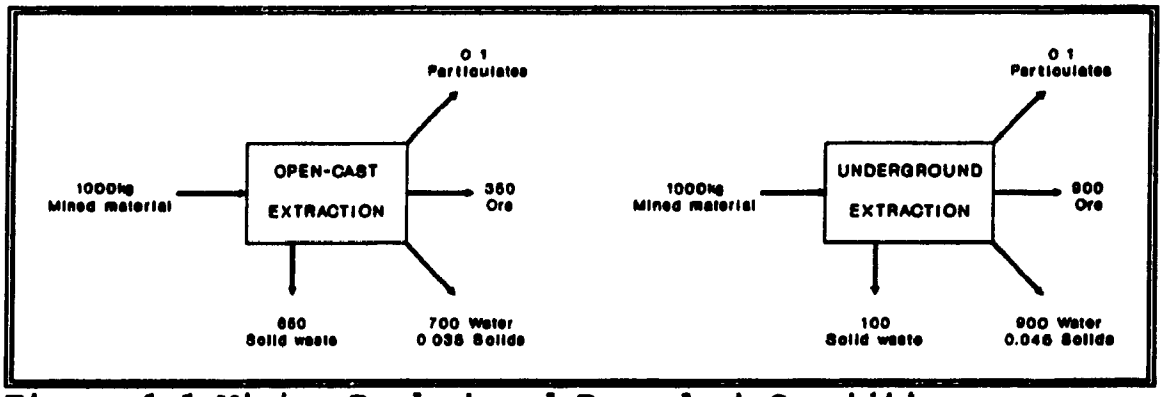

Figure 1.1 Mining Product and Byproduct Quantities (after Ripley *et al., 1987*).

In the milling process beneficiation is the concentration and preparation of the ore for subsequent stages of processing such as smelting, leaching, or refining (Fig. 1.2). Ore milling generally removes unwanted ore constituents, alters the physical properties of the ore (e.g., particle size and moisture content), and increases the desired mineral concentration (i.e., ore upgrade). Milling generally consists of three steps: (1) preparation, whereby the ore is comminuted by crushing and/or grinding; (2) concentration, whereby the desired ore is separated from the other ore material; and (3) dewatering. In some cases, other treatment may follow the concentration step and be included in the milling process. Waste from the milling process consist of finely ground material generated from the concentration stage which typically accumulates as a sludge in tailings ponds near the mine site.

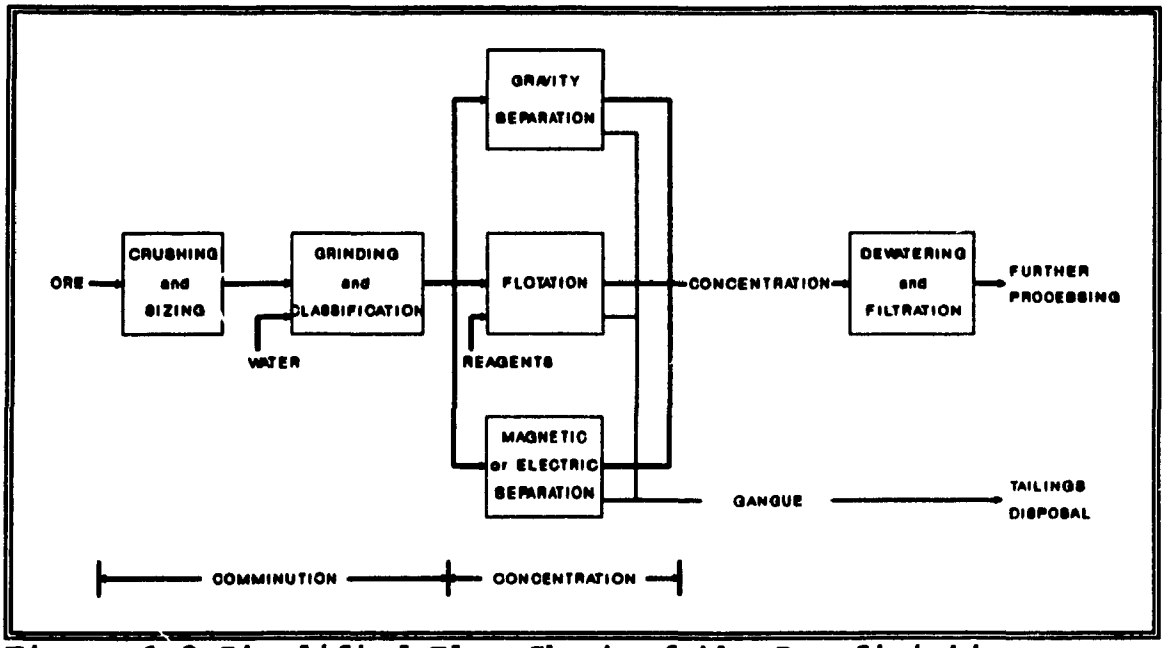

Figure 1.2 Simplified Flow Chart of the Beneficiation Phase (after Ripley *et al.*, 1978).

1.2 MINING WASTE

The principal solid waste disposal problem in the mining industry is the handling and relocation of the overburden and the waste rock. The overburden is the soft material (i.e., the soil and unconsolidated material) which needs no blasting for its removal. The overburden is typically set aside and reused in the closure and reclamation activities. The waste rock (gangue) is consolidated material which contains no ore or ore which is not economically feasible to remove. Waste rock can be reused as mine backfill, road construction, or sold.

The geometry and depth of the ore body and the characteristics of the geologic formation generally dictate the mine design and the quantity of waste produced. The rate of production of overburden and waste rock generally increase with depth of ore bodies mined and with decreasing ore grade. Greater overburden problems are associated with open pit and strip mining methods, however the production of

waste rock by underground methods also contributes to the production of solid waste.

The liquid waste of a mining operation is the hydrologic drainage from the mining site, which includes where mine openings intersect the water table, percolation from waste rock and mill tailings piles, and surface runoff. The drainage is a contamination problem because the mine site comprises reduced oxidation states of the elemental metal and sulphur in the ore formation (e.g., pyrite). When exposed to the atmosphere, it is oxidized and the pH of the drainage is lowered, whereby increasing the solubility and mobility of the heavy metals. This "acid mine drainage" has a significant environmental impact lasting for hundreds of years following mine closure.

1.3 MILLING WASTE

Solid wastes in the milling process consist of the host rock for the minerals which have been removed by various concentration processes. The host rock has essentially no value and, as wastes, they are known as tailings which are deposited in settling basins (tailing ponds), or mud lakes in the form of slurry. The solids are allowed to settle in the settling basin, and the effluent is decanted from the cleanest portion. It is treated, recycled into the mill, or discharged into receiving waters. The solid residue piles, if not properly managed, constitute sources of dust and sediment to be potentially eroded by runoff to streams. Vegetation stabilization is the most common method of minimizing the generation of dust and sediment from tailing piles. Tailings, however, are a principal source of acid mine drainage.

The principal source of liquid waste in the milling process consists of the wastewater decanted from the tailing ponds. The decanted water typically contains some suspended solids and sometimes low concentrations of cyanide and other

dissolved ions. Cyanide is contributed to the mill waste waters by reagents used in the flocculation depression of the various minerals. In addition, several other ions present in some mill tailings pond effluent are derived from the same source.

1.4 ENVIRONMENTAL IMPACT OF ACID MINE DRAINAGE

Most Canadian base metal, precious metal, and uranium mines contain mineralization, either in the ore or the surrounding waste rock, which is a combination of elemental metal and sulphur. These sulphide minerals (e.g., lead, copper, nickel, zinc, iron, and silver) are unstable and oxidize when exposed to oxygen and water at the surface. Their weathering follows well established mineral oxidation sequences. The following overall stoichiometric reactions characterize the oxidation of pyrite (Stumm and Morgan, 1981):

$$FeS_2(s) + 3.5O_2 + H_2O \rightleftharpoons Fe^{2+} + 2SO_4^{2-} + 2H^+ \quad (a)$$

$$Fe^{2+} + S_2^{2-} + 3.5O_2 + H_2O \rightleftharpoons Fe^{2+} + 2SO_4^{2-} + 2H^+ \quad (a')$$

$$4Fe^{2+} + O_2 + 4H^+ \rightleftharpoons 4Fe^{3+} + 2H_2O \quad (b)$$

$$FeS_2(s) + 14Fe^{3+} + 8H_2O \rightleftharpoons 15Fe^{2+} + 2SO_4^{2-} + 16H^+ \quad (c)$$

$$Fe^{3+} + 3H_2O \rightleftharpoons Fe(OH)_3(s) \quad (d)$$

In reaction sequential order, pyrite is oxidized by oxygen (a) or is dissolved (pK_s = 18.4) and then oxidized (a'). The ferrous iron formed is oxidized extremely slowly (b; the rate limiting reaction half-time is on the order of 1000 days) and the resultant Fe(III) is rapidly reduced by pyrite (c), releasing additional acidity and new Fe(II) iron to enter the cycle (via reaction b). Ferric hydroxide may also precipitate and serve as a reservoir for soluble Fe(III) (d).

Following sulfide oxidation (a or a'), oxygen is involved only indirectly in the oxidation of Fe(II)(b), the oxygenation of FeS_2 (a) being no longer significant. At pH levels less than 3.5, the oxidation of Fe(II)(b) is catalyzed by obligate anaerobic bacteria (*T. ferrooxidans*). Carbon dioxide (CO_2) is the principal carbon source and growth control for *T. ferrooxidans* and its availability regulates the kinetics of Fe(II) oxidation (b). If Fe(II) is removed by percolation (to deeper soil regions of negligible O_2 and bacteria), then the availability of O_2 by diffusion is rate limiting for the oxygenation of FeS_2.

These reactions yield sulfuric acid which increases the solubility of heavy metals and promotes their mobility. Initially the reaction rates are relatively moderate; as the reactions proceed, however, temperature and acidity increase, resulting in an increased reaction rate. At the lower pH levels (pH 2 to 4) bacteria catalyze the reactions and reaction rates can increase two to three orders of magnitude.

Acid mine drainage principally develops from mill tailings and waste rock piles, the walls of the underground mines, and open pits. Acid mine drainage may also develop in areas where mine openings intersect the water table. Untreated acid mine drainage can contaminate surface and ground waters, contaminate drinking water supplies, and degrade fish and wildlife habitat and plant communities.

2.0 STATEMENT OF THE PROBLEM AND THESIS OBJECTIVES

The unsaturated zone of mill tailings is the region where sulfide mineral weathering is at a maximum. The oxidation of these minerals releases metals, sulfate, and acidity to the tailings pore-water which subsequently participate in other reactions. An understanding of unsaturated zone flow of water provides and insight into the hydrologic controls on tailings mineral oxidation and pore-water evolution.

This thesis is an *in-situ* study of the flow of water in the vadose-zone of a (typical) mill tailings. The results provide: (1) guidelines to the installation an *in-situ* geohydrologic monitoring system in actively oxidizing mill tailings; and, (2) preliminary information on the hydrologic controls as they presently exist at an *in-situ* study site. In addition to exploring the site hydrologic dynamics, the study provides insight to the tailings hydrologic cycle: infiltration, evaporation, evapotranspiration, soil moisture storage, percolation, watertable fluctuation, recharge, runoff and streamflow generation. The results provide a site water balance, establish the hydrologic controls in the vadose zone, and ultimately contribute to the overall understanding of the oxidation process and pore-water evolution.

An *in-situ* geohydrologic approach to mine and mill solid waste oxidation is a dynamic systems approach typically based on measurements of soil-moisture content and hydraulic potential (i.e., the energy state of water in soil), in addition to the inflows and outflows of the hydrologic system. Continuous *in-situ* monitoring of these parameters along a vertical profile provides a one-dimensional view of the system's dynamics. Several vertical profiles, strategically placed with regard to hydrologic interpretation of the site, can contribute to the hydrologic characterization of the site. Actively oxidizing tailings

and rock piles, however, support highly corrosive pore-water environments posing particular difficulties to field study. The development and testing of a continuous monitoring system suitable for actively oxidizing pore-water environments is, therefore, a principal objective of this thesis (Table 2.1).

The development of the monitoring system centers on a theoretical review of soil-water physics (Chapter 3) and literature review of soil-water measurement techniques (Chapter 4). Laboratory testing of the system was limited to that needed for equipment familiarity and calibration. Laboratory tests of the system to evaluate accuracy, reliability and limitations were not conducted as they are beyond the scope of this Masters level thesis; much of which, though, has been evaluated and appear in the reviewed literature.

Table 2.1. Statement of the Problem and Thesis Outline.

PROBLEM:	(1) *In situ* monitoring of the flow regime at mine and mill solid waste sites (i.e., AMD sites). (2) Hydrologic controls of an AMD tailings site.
APPROACH:	(1) Theoretical review of soil-water physics (Ch.3). (2) Literature review of soil-water measurement techniques (Ch.4). (3) *In situ* hydrologic monitoring of the tailings vadose-zone: (a) Study site background (Ch.5), (b) Site investigative methodology (Ch.6).
RESULTS:	(1) *In situ* monitoring of at the study site and performance of the monitoring system: (a) Presentation of data (Ch.7), (b) Discussion (Ch.8). (2) Hydrologic analysis (Ch.9).

The field site at which the monitoring system was installed is a de-watered tailings pond which poses several unanswered hydrologic questions. The site background is presented in Chapter 5 which reviews previous geotechnical, hydrogeologic, and geochemical investigations, in addition

to the site climatological and geographic setting. The thesis investigative methodology of the tailings site (Chapter 6) describes the continuous geohydrologic monitoring (*in situ*) and periodic soil-moisture measurement of the tailings during a test period. The monitoring results from the test period (Chapter 7) provide preliminary *in-situ* data to explore the unanswered hydrologic questions and evaluate the monitoring system's performance. The fundamental questions posed include:

(a) What is the infiltration capacity of the tailings surface, and what storm events exceed the infiltration capacity, resulting in Hortonian overland flow?

(b) Are there partial-area or variable-source-area contributions to overland flow and how does the watertable fluctuation contribute to these areas?

(c) With little infiltrating water, are there significant increases in the hydraulic gradient of the saturated zone due to the conversion from tension-saturated water of the capillary fringe to pressure-saturated porewaters?

(d) What are the typical exfiltration hydraulic gradients and evapotranspiration estimates?

(e) What is the soil moisture storage capacity of the tailings? How does infiltration contribute to soil moisture storage and recharge to the saturated zone of the tailings, and what storm events contribute to recharge?

(f) What are the hydrogeologic properties with regard to Darcian flow?

(g) What are the dynamics of the tailings hydrologic system.

(h) What are the quantitative changes of the hydrologic system (i.e., water balance) during the monitoring period.

A discussion of the results (Chapter 8) provides interpretation of the data regarding the hydrologic system dynamics and controls (questions posed), and monitoring system performance. Employing the monitoring results, a hydrologic analysis (Chapter 9) provides a water balance of the vadose zone for the period of study (i.e., in the Autumn of 1990). The summary and conclusions are presented in Chapter 10 along with further recommendations.

3.0 THEORY OF SOIL-WATER ENERGY

Energy, being the capacity to do work, is associated with flow (or transformations). A change in energy is work. Water, like other substances, moves in the direction of an energy gradient, from high to low, liberating energy as it moves. As long as energy can be lost as the result of water movement, movement will continue. Equilibrium[1] can only be reached when further movement does not result in any further energy loss (i.e., water moves toward the region of lowest energy).

Fluid flow, as a mechanical process (i.e., hydraulic flow), represents work, and hydraulic flow is the sum of its static pressure, kinetic, and gravitational potential energies (i.e., Bernoulli's equation). Hydraulic flow velocities are extremely low in soil and the kinetic energy component is generally neglected. Soil water will also move by thermal energy gradients and by physico-chemical energy gradients (i.e., by molecular diffusion), which are generally associated with the interaction of clay and water. In addition to fluid flow, the movement of moisture in soils can also occur in the vapor phase by a thermal gradient and a vapor pressure gradient.

Table 3.1 summarizes the theories of soil-water energy. Soil structure fundamentally controls soil-water interactions. Soil-water energy is presented with an explanation of the soil-water retention mechanisms and a summary of the analytical approaches to the soil-water system. The soil-water energy characterization is reviewed as an integral relationship in soil moisture research.

---

[1]With regard to equilibrium and in situ soil water, it rarely, if ever, exists. However, for all practical purposes, water retained in soil beyond the direct influence of surface evaporation and evapotranspiration and groundwater discharge can be loosely considered in a state of equilibrium (e.g., drainage to field capacity following saturation).

Table 3.1. Summary of the Theories of Soil-Water Energy.

I. Soil Structure	
II. Water Retention Mechanisms:	(1) Surface Tension (2) Osmotic Imbibition (3) Adsorption
III. Analytical Approaches:	(1) Static Approach (a) Pore Geometry Concept (b) Potential Concept (2) Dynamic Approach (3) Balance Approach (4) Systems Approach
IV. Soil-Water Energy Characterization	

3.1 SOIL STRUCTURE AND SOIL WATER

The components and structure of soil fundamentally control soil-water interactions, the mechanisms of water retention, and the movement of soil water. An ideal granular, transported soil which has not been compressed is typically composed of weathered silts and sands with a porosity of 25 to 50 percent. Because of the relatively small surface area to volume ratio of silt and sand, the soil-particle surface forces of these soils do not significantly contribute to the characterization the soil structure. Instead, the soil structure (i.e., packing) is strongly influenced by particle shape and size distribution, typified by soil grains and soil voids. Though the larger soil voids often contain smaller grains, the soil voids of a granular soil are generally considered large with respect to a clay soil.

Clay is characterized by fine particles (<0.002 mm), composed mainly of hydrous silicates of alumina with, in some cases, iron or magnesium. The developed double-diffuse ion layer (Gouy-Chapman) at surfaces of clay minerals varies with the clay mineral type and the pore water chemistry. When coupled with the large surface area to volume ratio, the surface forces of the clay particles tend to dominate

with regard to soil behavior. As a result, the clay fabrics that develop are comprised of clay particles arranged in random, flocculated, or oriented distributions. Comprehensive texts such as Yong and Warkentin (1975) or Mitchell (1976) can be referred to for further discussions on soil behavior and soil structure.

The interparticle attraction and repulsion forces, principally governing the development of the clay fabric, are controlled by the extent of the diffuse ion layer. Clearly defined aggregates of clay particles, termed cluster units or fabric units, additionally develop in clay soils. Cluster units also contain domain units which are small groups of clay particles acting as a single clay particle. A typical clay soil might be composed of cluster units with slightly oriented clay minerals and a porosity of 40 to 70 percent. A soil composed of clay, silt, and sand (loam) would develop a structure of soil grains, voids, and clay arrangements.

Soil structures generally include a variety of pore sizes. The larger pores are between sand grains and/or cluster units, and the smaller pores are between clay aggregates and minerals. In general, water flows through the larger voids (macro-pores) by advection and diffuses into the clay cluster units and domains (through micro-pores).

3.2 WATER RETENTION MECHANISMS

Soil water can generally be divided into three groups based on the amount of energy required to remove the water from the soil. The water which occupies the larger soil voids (macro-pores) typically drains to a field capacity[1]. The water remaining in the macro-pores ordinarily requires very little energy for its removal, only a minor elevation above room temperature is adequate. The water which occupies the interparticle voids of a clay aggregate (micro-pores) and, in some cases, the interlayers of clay minerals can be driven off at relatively low temperatures (100 to 150 °C). While at still higher temperatures (>300 °C) adsorbed water and the water bonded in the crystal lattice (lattice OH water) is lost. While not directly related, the amount of energy required to remove water from soil can generally be considered an indicator of the water retention mechanism. These mechanisms include: surface tension, osmotic imbibition, and adsorption.

---

[1]Field Capacity (FC). The condition reached when a soil holds the maximum possible amount of water in its voids and pores after excess moisture has drained away; a measure of the volume of water a soil can hold under these conditions. The percentage of water remaining in the soil (either by weight or volume) after the soil has been saturated and free drainage has practically ceased (typically 2 to 3 days). The term is obsolete in technical work but useful as an in situ descriptive term. For many soils FC is in the range of 1/10 to 1/3 bar suction, commonly taken as 1/3 bar. In groundwater hydrology FC is thought of as a minimum value of water content in an unconfined aquifer following the lowering of the water table and the drainage of the larger voids (i.e., the porosity less the specific yield).

3.2.1 Surface Tension

Surface tension, by definition, is a property possessed by liquid surfaces whereby they appear to be covered by a thin elastic membrane in the state of tension. The phenomenon is due to the unbalanced molecular cohesive forces near the surface. Surface tension and the angle of contact of the air-liquid surface to a solid are fundamental to capillarity. This property holds water in soil as films around individual particles and in pore spaces. It accounts for the rise of soil water above the height at which it could be held by hydrostatic pressure.[1] Generally speaking, water retained by surface tension (i.e., in the macro-pores and on the surfaces, adjoining the individual particles of sand, silt, and clay aggregates) requires the least energy for its removal. For a more rigorous description of surface tension and capillarity, see Appendix A.

3.2.2 Osmotic Imbibition

Osmosis is the diffusion of a solvent into a more concentrated solution in order to equalize the concentration. Strictly, diffusive flux is proportional to the gradient of chemical potential, but for most practical applications, it is taken as proportional to the gradient of concentration of the substance (see Denbigh, 1981, pp. 86-87). Imbibition (from chemistry) is the absorption or adsorption of a liquid by a solid or a gel, accompanied by swelling of the gel.

Water held by osmotic imbibition is adsorbed water caused by the chemical concentration gradient at the diffuse ion layer. In the soil-water system, the pore water is attracted to a clay particle where ion concentrations are

---

[1]In groundwater hydrology, the hydraulic rise is represented as the capillary fringe above the water table, often referred to as the tension-saturated zone.

higher, as described by the diffuse ion layer concept. The water retained by osmotic imbibition is typically the water which diffuses into the micro-pores of the clay aggregates. Water molecules, in continuous attempt to dilute the concentration of exchangeable cations adsorbed at the clay surface, move toward the clay mineral. Because they do not have sufficient energy to displace the adsorbed ions the concentration gradient remains unchanged. Other water molecules, also influenced by osmosis, subsequently replace this water. Therefore, water retained by osmotic imbibition can be envisioned as water without structure held in motion between clay minerals and, in some cases, between the mineral layers. Water in soil micro-pores, influenced by both osmotic imbibition and surface tension, generally requires more energy for its removal than water retained in the macro-pores.

Water held by osmotic imbibition is similar in energy to that held by the hygroscopic mechanism of soil science, which suggests a similar physical mechanism. Hygroscopic water (from soil science) is the water adsorbed by a dry soil from an atmosphere of high relative humidity (typically, 98% relative humidity at 25°C) and water lost from an air dry soil when it is heated to 105°C. This definition implies adsorption by a vapor pressure gradient with the atmosphere, and not that of a concentration gradient. Regardless, the vapor pressure of soil-water is decreased with an increase in solute concentration because the solute decreases the partial molar free energy of the water, and at thermodynamic equilibrium, the free energy of the soil water is stabilized by the gradients of chemical potential and vapor pressure at a constant temperature.

Hygroscopic water and water held by osmotic imbibition differ in the degree of saturation. Water held by osmotic imbibition occurs at higher degrees of soil saturation (even at 100% saturation, in ground water), whereas hygroscopic

water is in equilibrium with atmospheric water (i.e., a very low degree of saturation), and therefore, solely soil water. In addition, osmotic imbibition is dependent on the surface charge density of the soil particles (chiefly clay particles) -- a soil with a low surface charge density and a high solute concentration may exhibit a low osmotic imbibition and an elevated hygroscopic water content.

3.2.3 Adsorption

Adsorption, in the context of the soil-water system (hydration), is the bonding of water molecules to mineral surfaces (chiefly clay) by physicochemical forces and having physical properties substantially different from soil pore-water. Adsorbed water forms a thin film which is somewhat rigidly held by the clay particle. The water is held by hydrogen bonds and van der Waals bonds to both the clay surface and to the adsorbed cations (cation solvation). Because of this molecular bonding (which is "secondary" bonding), adsorbed water requires the most energy for its removal. The water in the clay mineral layers (lattice OH water) is held in the crystalline structure by "primary" molecular bonds (ionic and covalent) and is generally not considered as adsorbed (or retained) water. Adsorbed water and lattice OH water requires extreme amounts of energy for its removal (300 - 1000 °C).

The mechanism of water retention by adsorption can be envisioned to grade into the mechanism of water retention by osmotic imbibition. The first layer of water molecules is held to the clay surface (and adsorbed cations) by hydrogen bonding. The second layer is held to the first, again by hydrogen bonding, but the force beccmes weaker with distance as the orienting influence of the clay surface on the water molecules decreases. Each successive layer is held less strongly, and the bonding quickly decreases to that of free water. In addition, water forms hydroxocomplexes (adsorbed)

with aqueous metal ions, of which there is a higher concentration at the charged surface (in the diffuse ion layer). At distances from the clay mineral surface, osmotic imbibition develops as the dominant water retention mechanism. The energy required to remove adsorbed water decreases with distance from the clay surface.

3.3 ANALYTICAL APPROACHES TO THE SOIL-WATER SYSTEM

Analytic scientific approaches have been developed and defined by various researchers. Approaches applicable to soil systems have been summarized by Richter (1987). An expansion of his summary, incorporating concepts advanced by other researchers, has been applied here to define the approaches that appropriately characterize the soil-water system.

3.3.1 Static Approach

Statics is used to describe equilibrium conditions. In nature, however, the soil-water system is rarely, if ever, at complete equilibrium. Precipitation and evaporation, heating and cooling, and gravitation all induce fluxes of water in soils. These fluxes, in turn, alter the state of chemical equilibrium. In addition, soil-chemical changes (e.g., salinization, redox reactions) may osmotically induce soil-water movement. Nevertheless, concepts of water in soil have been advanced to characterize the state of soil-water at a given time and these concepts are essential to the understanding of soil-water retention.

Soil-water retention can be described by the concept of the soil-water system geometry. This approach attempts to describe the soil structure, the shapes and sizes of the pores and particles, the shapes of the water films, and the amount of water in the voids; giving rise to the "capillary tube" theory to account for the capillary fringe, and the

"ink-bottle" theory to account for hysteresis[1] loops associated with relationship plots. Soil-water retention can also be described with a concept of potential (i.e., the energy state of water in soil) which does not consider the pore space geometry but specifies only the energy with which water is held in a soil. It should be thought of as a "black box" approach, providing incomplete knowledge of how water is retained in soil. The coupling of the geometric and potential concepts provides an unabbreviated characterization of soil-water retention.

3.3.1.1 Pore geometry concept

There exists a variety of pore geometries in soils which is defined by the soil structure. Early geometric concepts (late 1800's) considered soil voids as bundles capillary tubes which, by surface tension, related capillary rise to the capillary radius (Appendix A); although, this overestimates height calculations of the capillary fringe. Further developments of geometric concepts approximated soil particles with uniform spheres and packing configurations, advancing a mathematical description of the pressure difference across a spherical curved air-water surface within a soil-pore (Appendix A). Though not an accurate representation of most soil structures, experiments designed to test the theory demonstrated that water retention in sands can be explained by surface-tension forces and that a hysteresis loop exists in the relation of soil-water content

---

[1]Hysteresis is a term borrowed from the study of magnetism and used to describe a bivariate plot, which evidences a loop form and therefore a different value of the dependent variable, according to whether the independent variable is increasing or decreasing. Hydrologic examples include relations between: (1) matric potential and soil-water content; (2) river discharge and water stage; and (3) suspended sediment and solute concentrations and river discharge.

to tension suction (matric potential). A more complete representation of soil structures includes variously sized macro-pores and micro-pores inter-connected though openings of various sizes ("breathing" channels). A description of this system requires a statistical approach. For a more complete discussion on geometric concepts, refer to Yong and Warkentin (1975).

Hysteresis in the relationship between soil suction by tension and soil-water content is commonly observed and is a

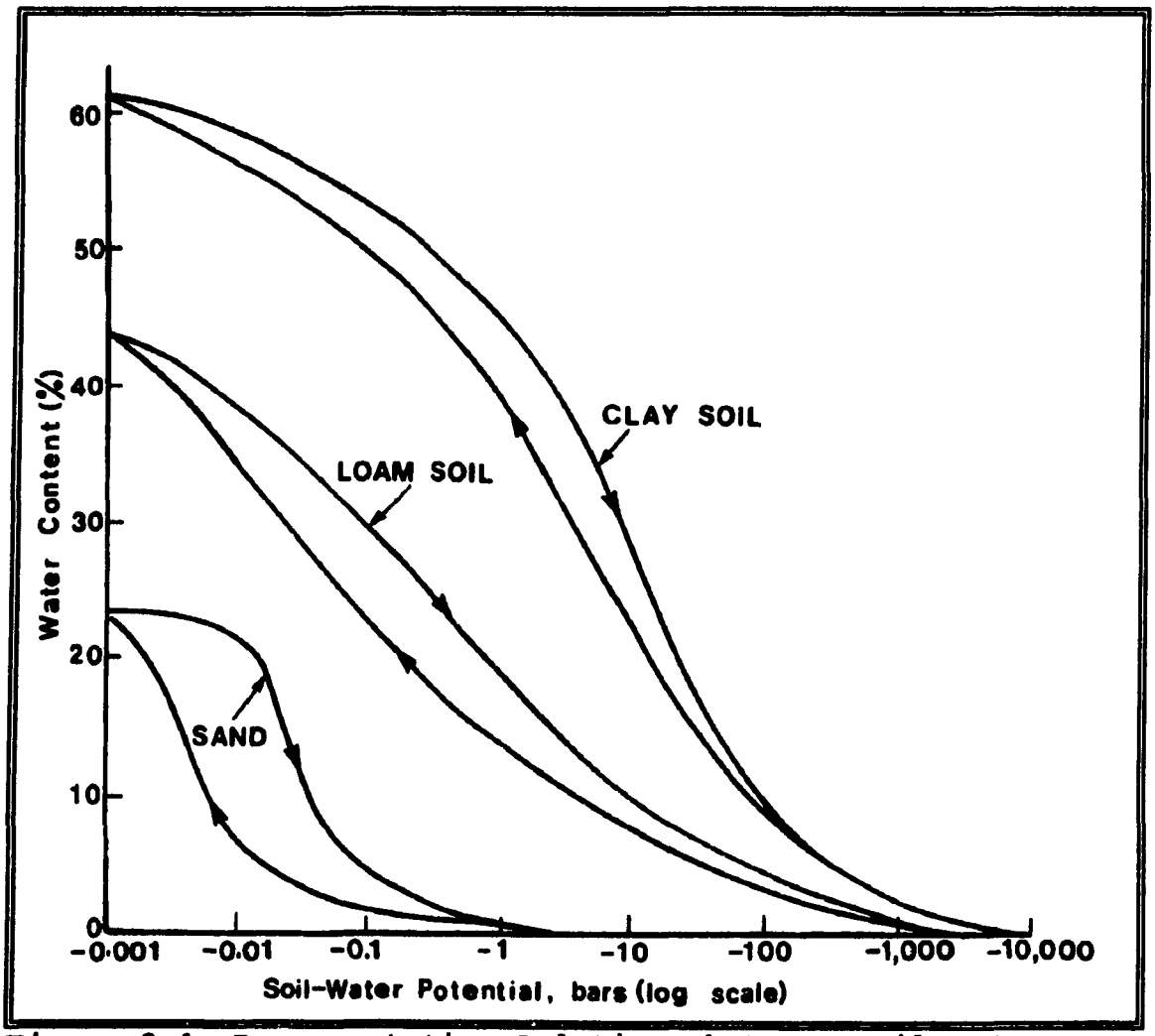

Figure 3.1. Representative Relations between Soil-Water Potential and Soil-Water Content for Different Soils (after Yong and Warkentin, 1975).

source of error when using soil suction measurements to estimate water content (Fig. 3.1). With silty and sandy soils, hysteresis is chiefly caused by different pore and pore inter-connection diameters. The drying or emptying of a series of interconnected pores does not occur until the negative pressure (suction) is high enough to exceed the surface tension forces in the pore with the smallest diameter. Complete wetting does not occur until the negative pressure is low enough to allow the largest pore to fill. Therefore, at the same pressure, a sample has a higher water content on drying than on wetting. This phenomenon is known as the "ink bottle" effect (Fig. 3.2); the neck diameter, which controls the emptying, is smaller than the main pore space, and wetting advances through the larger diameter, main pore space. Refer to Hillel (1972) or Iwata and Tabuchi (1988) for extended references on hysteresis.

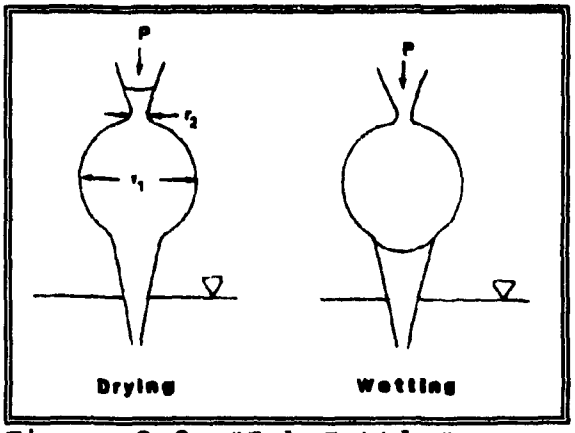

Figure 3.2. "Ink Bottle" Representation of Hysteresis in Soils due to Drying and Wetting (after Yong and Warkentin, 1975).

Hysteresis in clay soils results from three additional effects: (1) contact-angle effect, by which the contact angle, and hence the radius of curvature, is greater in an advancing meniscus than a receding meniscus; (2) particle rearrangement by swelling, shrinking, or aging resulting in changes is soil structure; and, (3) air entrapment. Refer to Hillel (1972) for further discussion.

3.3.1.2 Potential Concept

Visualizing the soil-water phenomena as an energy state yields the application of classical physics and, as a result, more advances in describing soil-water have emerged with the potential concept. Work must be done to extract water from soil and the amount of work required per unit mass of water extracted increases as the amount of water remaining in the soil decreases. The soil-water potential is defined as the work done on a unit mass of water required to move it from a free water surface to a point in the soil. It is a negative value in the unsaturated zone and a positive value in the saturated zone; free water is defined as having zero potential (for a more rigorous definition see Appendix A). The soil suction (the negative of soil-water potential, a positive value) is generally restricted to the work required to remove soil water against the surface tension forces of the soil (matric suction) and the osmotic forces of the soil solution (osmotic suction).

The total soil-water potential may be divided into many component potentials such as gravitational, osmotic, capillary, pneumatic, piezometric, and others. Simplifying this, the total potential can be described with three potentials: pressure potential, osmotic potential, and gravitational potential. Capillary, pneumatic, and piezometric are usually considered together as pressure potential; a saturated medium has a positive pressure potential and a unsaturated medium (vadose zone) has a negative pressure potential (matric potential). The pressure potential plus the gravitational potential is the hydraulic potential[1].

---

[1]Hydraulic potential is typically expressed in terms of head, i.e., energy per unit weight (see Appendix A5 or Freeze and Cherry, 1979, pp.18-22).

3.3.2 Dynamic Approach

The spacial and temporal changes in pore geometry and soil-water potential describe the movements of soil-water, and movements are described by kinetics (Greek *kinein* = to move). The kinetic approach focuses on the process, the flow or change, without asking why something happens. The dynamic perspective (e.g., Greek *dynamike* theory of forces and movements) is characterized by the principal of "causality", i.e., the combination of the cause (force) and the movement or change as the effect. An example is the hydraulic flow equation, Darcy's law in which water flow (effect) is proportional to the gradient of hydraulic potential (cause). Other similar examples are Fick's law of diffusion, Fourier's law of heat conduction, and Ohm's law of electrical conduction. These are linear phenomenological laws in the field of non-equilibrium thermodynamics of irreversible processes. The dynamic approach is typically applied, but not restricted, to the rapid changes in soils, the components of heat, gas, water and ions. Established texts in groundwater hydrology or hydrogeology can be referred to for discussions of fluid flow and solute transport in porous medias.

3.3.3 Balance Approach

For a complete quantitative description of the changes of water in the soil profile, the dynamic approach is not sufficient. Dynamics only quantitatively describes the velocity (or volume) of flow, and not the interrelations of a hydrologic system. Dynamics only describes the flow density of rapid components and not the changes in concentration. The effect of flows into and out of soil compartments must be considered, i.e., the balance approach (e.g., Greek *oikos* = household; balance regime of the world, of nature). The principal of balance is the methodological

basis of every material or energy regime and is commonly applied in hydrology as the "water balance".

The principal of balance coupled with the Darcian flow equation in which the hydraulic potential gradient is the driving force provides a reasonable quantitative approach of subsurface flow for most hydrologic systems (e.g., equation of continuity for fluid flow, or Richards' equation for unsaturated flow). Similarly, the transport of solutes is typically characterized by the principal of balance by mass conservation coupled with gradients of concentration and hydraulic potential (i.e., fluxes). These types of coupling begins to describe soil-water as a system. Although for many circumstances, it is possible to formulate simple models based solely on the principal of balance, if simple assumptions or probabilistic modes can be used instead of dynamic equations.

3.3.4 Systems Approach

A system is an amount of objects (elements) and the relation between the objects and their properties (Hall and Fagen, 1956). Investigations of the interactive flows between a complex, limited part of reality (a system) and its surroundings reveals and expresses how the system behaves. Using this approach, the conclusions for macroscopic systems will differ from those for microscopic systems. Each system is simultaneously a subsystem (element) of a larger system, but itself consists of different elementary systems which have properties different from its elements. For this reason, a system is defined as an integrated entirety whose properties are different from the properties of its elements.

The systems approach is particularly highlighted in thermodynamics and ecology. The relations and interactions between systems and subsystems are mediated by material and energy flows, which can be vectoral flows (transport) or

scalar flows (transformations). Thermodynamics is the science of heat, more generally of the energetic transformation that accompany material transports and transformations. The "open" system of thermodynamics has a methodological significance in ecology.

Equilibrium thermodynamics of "closed" systems (i.e., thermostatics) is mainly used for estimating the efficiency of systems that use chemical energy; a distinct part of the energy is always lost as heat. A description of the system is attained by state equations (e.g., PV = nRT) which combine material state variables, and are therefore formulated for equilibria in closed systems. A closed system only exchanges heat with the surroundings. State changes in thermostatics can only be described by the idealized term: "reversible" process (no heat and entropy is produced). Reversible processes do not exist in nature, however, there are processes where entropy production is very small (e.g., dissolution and ion exchange).

Non-equilibrium thermodynamics of irreversible processes assumes the transition to an "open" system (i.e, a system than exchanges matter and energy with the surroundings). This branch of thermodynamics deals with entropy production of steady-state transport processes. Natural transport processes, like irreversible processes, derive their spontaneity from a degradation of energy from a high ordered form to a low degree of ordering, which implies a production of entropy. Generally, each gradient of the system is related by a phenomenological coefficient to each flux such that the fluxes and forces are coupled. Entropy production associated with transport processes may be expressed as a sum of the products of independent fluxes with their conjugated driving forces. More state variables are generally required to characterize processes, than in the case of equilibrium (thermostatics). In general, a rapid process has higher entropy production and is more

irreversible than a slow process. Non-equilibrium thermodynamics has a more general significance if the dynamics of the process in a system is described correctly. Equilibrium is then included as a special case.

The first and second laws of thermodynamics state that the total energy content of the universe is constant and the total entropy is continually increasing. Closed systems reach equilibrium at minimum energy and maximum entropy. Open systems (e.g., living systems) minimize their entropy by importing energy (e.g., negative entropy) and exporting entropy (e.g., matter) to the surroundings, thereby increasing total entropy (of the surroundings). An important consequence of open systems in a stationary state, is that they organize themselves with a constant material composition and according to the principal of minimizing entropy production, which results in maximizing the utilization of energy and minimizing energy dissipation (entropy). Living systems can never obtain an equilibrium state, but rather they obtain a stationary state. Equilibrium is death.

Researchers have adopted systemic approaches to hydrologic systems. The system processes are governed by the principles of conservation of mass, energy, and charge. In applications to the transport of soil water, the thermodynamic gradients that are commonly considered include temperature, chemical constituent concentration, and hydraulic potential. The development and applications of the thermodynamic approach to soil-water can be found in Hillel (1972) and in Iwata and Tabuchi (1988). The "Thermodynamics of Soil Solutions" is covered by Sposito (1981). And, for a recent review of subsurface hydrochemical models utilizing thermodynamic approaches refer to Mangold and Tsang (1991). In soil and ecosystem energy models which utilize a systemic approach (Ulrich, 1987; Runge, 1973; and Jenny, 1961), soil-

water components are flux variables in the transport process.

3.4 Soil-Water Energy Characterization

The functional relation of soil-water content to soil-water potential (Fig. 3.3), termed the "soil-water energy characteristic", describes the intrinsic energy state of soil-water with regard to the moisture history of the soil. The bivariate plot illustrates the hysteresis loop encountered in soil moisture research as a soil sample passes from a saturated state to a desaturated state until an oven dry condition is reached (desorption), and the return to a saturated state (absorption). The plot is

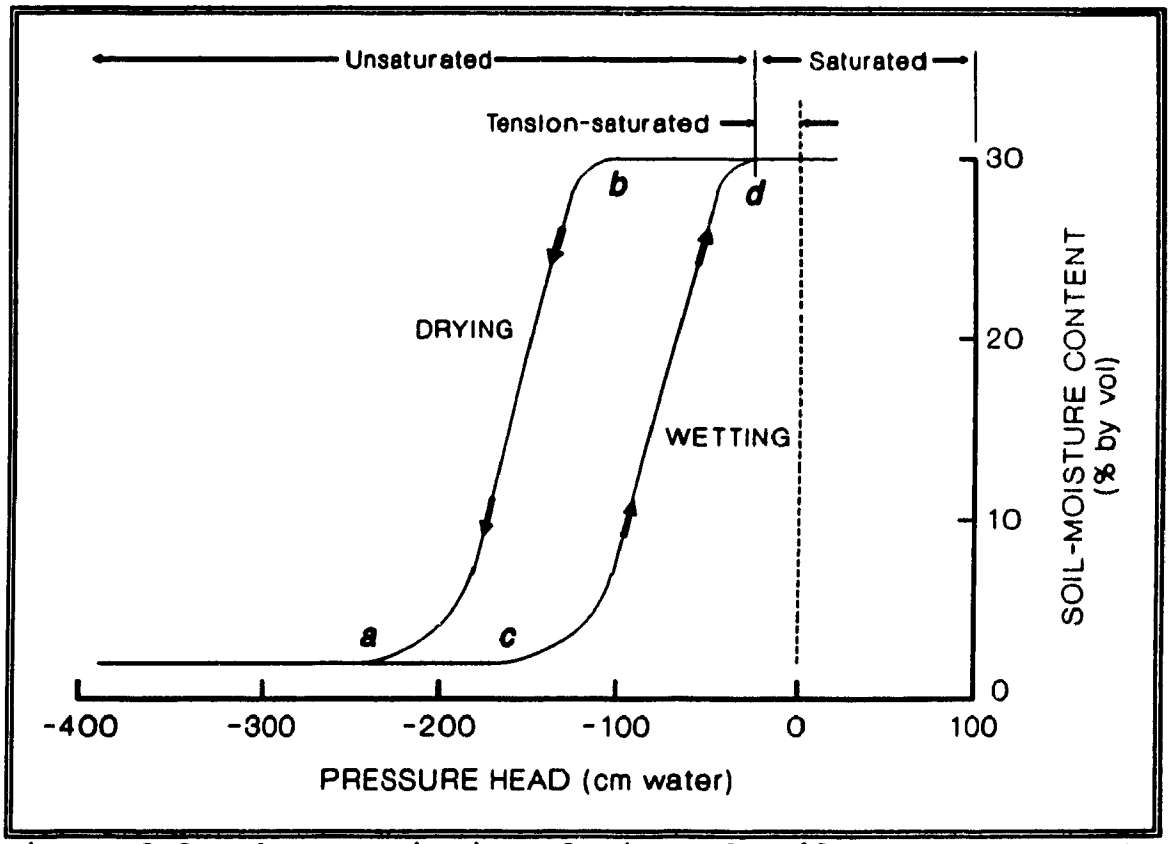

Figure 3.3. Characteristic Relation of Soil-Water Content to Pressure Head for a Naturally Occurring Sand Soil (adapted from Freeze and Cherry, 1979, and Lambe and Whittman, 1969).

characteristic to the soil composition and structure and is, therefore, unique to a particular soil.

Several soil properties can be evaluated from the soil-water energy characteristic curve. The air-entry value (Ψ_A, *d* on Fig 3.3) is the soil-water potential value at which the wetting curve reaches saturation (porosity); this value represents the soil-water potential at the minimum height of the capillary fringe. Lambe and Whittman (1969) refers to this point as the *minimum capillary head* (h_{cn}). A minimum capillary head is typical of rising watertable conditions. The highest elevation above a free water surface at which complete saturation exists is referred by Lambe and Whittman (1969) as the *saturation capillary head* (h_{cs}); it is the lowest potential at saturation, located on the drying curve (*b* on Fig 3.3). A saturation capillary head is typical of falling watertable conditions. The highest elevation to which any continuous channel of water exists above a free water surface, the *maximum capillary head* (h_{cx}), is located on the drying curve at a water content approximately equal to field capacity (*a* on Fig 3.3). The distance from a free water surface to the highest elevation that capillary water would rise in dry soil is called the *capillary rise* (h_{cr}) which is located on the wetting curve (*c* on Fig 3.3).

The slope of the energy characterization curve represents the unsaturated storage property of soil, termed specific moisture capacity (C). The maximum rate of change of the slope (the maximum specific moisture capacity) indicates the dominant void size involved in water retention, which represents the "ink bottle" effect.

The "ink bottle" effect increases as the soil-grain size, and hence the pore void size, increases. The "ink-bottle effect also increases as size-class and roundness sorting increases, and as packing decreases. The residual soil-water content of granular soil (i.e., the soil-water content following the emptying of the dominant void size)

generally reflects soil-water held by retention mechanisms other than that manifested solely by surface tension (e.g., a high residual water content in a granular soil generally indicates some water held by osmotic imbibition).

A further analysis of the soil-water energy characteristic for the identification of the "ink bottle" effect can be developed by plotting the differential in

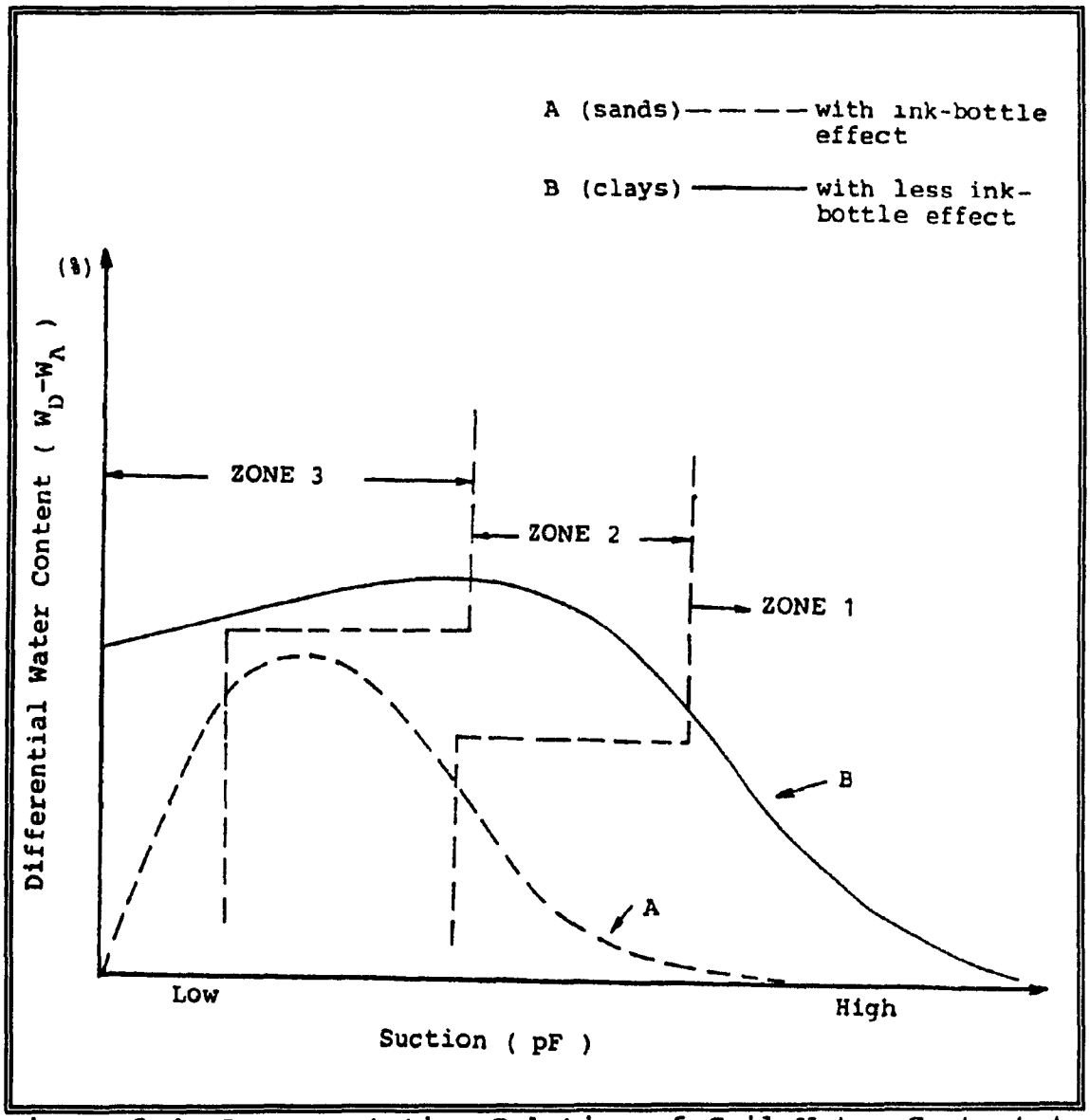

Figure 3.4. Representative Relation of Soil-Water Content to Differential Soil Suction (after Wang, 1986).

water content (the drying value less the wetting value) against the soil-water potential (Fig. 3.4) (Yong *et al.*, 1982).

The descriptive characteristics distinguishing the "ink bottle" effect, as summarized by Wang (1986), are: (1) the differential water content at the starting point (Ψ=0) is nearly zero, indicating no change or nearly reversible change in volume; (2) the curve peaks quickly at low suction values (high soil-water potential), indicating the dominant void size; and, (3) the differential water content varies widely with the high suction range (low soil-water potential) after passing its peak, indicating the extent to which the breathing channels participate in the retention of water.

Clay soils typically exhibit volume changes which are measurable in terms of the resultant effect on dry density. By including dry density as a third variable in the soil-water energy characterization, the relational surface plot (Fig. 3.5) more completely describes the energy state of clay soil (Yong, 1980). The measurement of soil volume while evaluating the soil-water energy characteristic permits the following properties and behavior of soils to be evaluated (Wang, 1986): (1) soil-water potential characteristics; (2) air-entry properties; (3) volume change behavior; and, (4) interfabric unit stability characteristics.

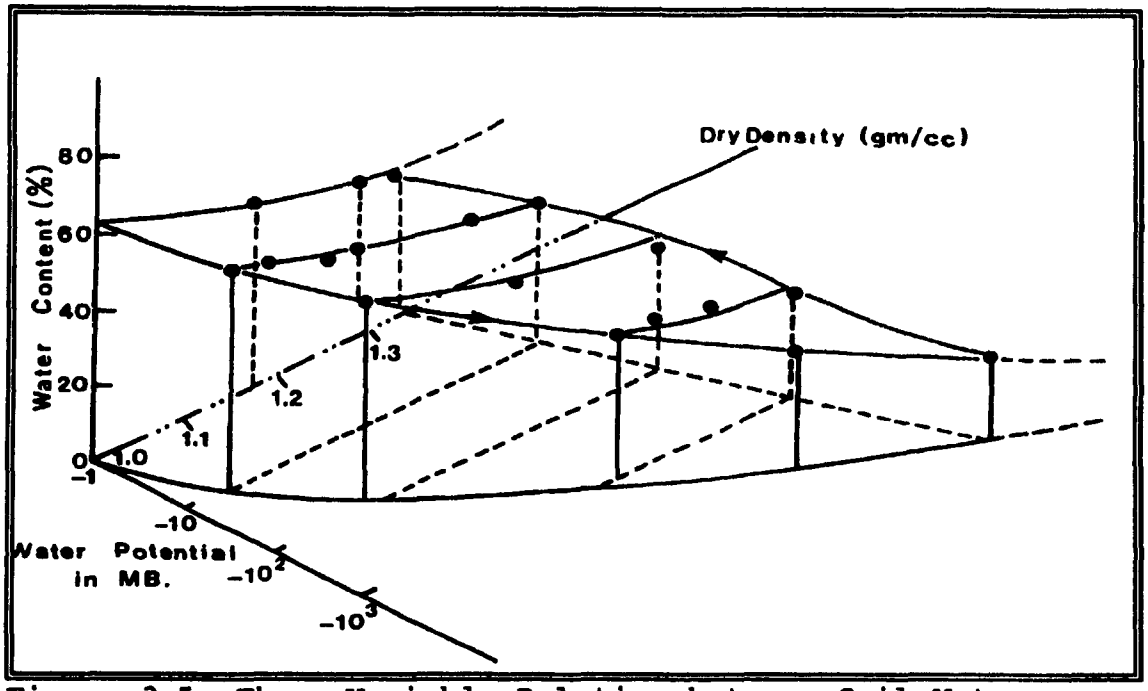

Figure 3.5. Three Variable Relation between Soil-Water Potential, Soil-Water Content, and Dry Density (after Yong and Warkentin, 1975).

3.5 The Relevance of Soil-Water Energy to this Thesis.

This field study examines the hydrologic controls of mill tailings. In this circumstance, the soil advective flux of water in the vadose zone is of primary concern. At this scale, the dominant water retention mechanism is surface tension.

Surface tension is described with the potential concept which is used to determine the direction and (dynamic) flux of soil moisture. The flux of soil moisture is used with soil-moisture content measurements to develop a soil-water budget.

The characteristic relation of soil-water potential and moisture content is useful to validate soil-moisture measurements with regard to antecedent moisture conditions and spacial relations. The estimation of the extent of the capillary fringe and dominant void size evacuation can also be evaluated.

4.0 *In-situ* Measurement Techniques of Soil-moisture

Related through the soil-water energy characteristic, the measured values of soil-water content (θ) and potential (ψ) are fundamental to soil moisture research. A review of the methods of soil-moisture determination (Schmugge, 1980; Gardner, 1986) describes current measurement techniques of soil-water content and potential. Directed by their reviews, a summary of current measurement techniques is presented (Table 4.1).

Table 4.1. Review of Soil-Moisture Measurement Techniques.

Soil-Water Content:	(1) Gravimetric Method (2) Nuclear Methods (a) neutron thermalization (b) gamma ray or neutron attenuation (3) Absorbent Blocks and Porous Ceramics (4) Time-Domain Reflectometry (electromagnetic method)
Soil-Moisture Potential:	(1) Tensiometer (2) Peltier Thermocouple Psychrometer (3) Electrical Resistivity Porous Block (4) Thermal Conductivity Porous Block

4.1 *In-Situ* Measurement of Soil-water Content

Several methods exist to measure the quantity of water in soils, of these, most can be found in Gardner (1986). The methods can be summarized by four groups: (1) gravimetry method; (2) nuclear methods (e.g., neutron thermalization and gamma ray or neutron attenuation); (3) methods employing absorbent blocks and porous ceramics; and, (4) Time-domain reflectometry.

4.1.1 Gravimetric Method

Soil-water content by gravimetry is simply determined by weighing the sample before and after drying it at 103°C. This method is the most accurate and reliable, as it is a direct measurement method, but suffers from being time

consuming and results in the destruction of the sample, and therefore cannot be automated. For these reasons, the gravimetric method is often used in field investigations to validate measurements by indirect methods.

4.1.2 Nuclear methods

Neutron thermalization[1] method measures the density of thermal neutron cloud surrounding a fast neutron source placed in soil. The density of this cloud, as determined by the concentration and capture cross section, represents an equilibrium between the rate of emission of fast neutrons, their thermalization by nuclei (typically those of hydrogen), and their capture by absorbing nuclei. If the capture cross section remains constant with regard to everything except water (e.g., chemical composition and bulk density), then the volumetric soil-water content may be calibrated to the thermal neutron density.

Gamma ray[2] attenuation measures the degree to which a beam of monoenergetic gamma rays is attenuated or reduced in intensity in passing through a soil column. The measurement is dependent on the overall density of the column and if the density of the soil less its water content is constant, then changes in the attenuation represents changes in water content. The gamma ray attenuation method, therefore, can

---

[1]Due to similar mass, hydrogen nuclei have a marked property for scattering and slowing neutrons which is exploited in the neutron method for measuring soil-water content. High-energy neutrons (0.1 to 10 Mev.) emitted from a radioactive substance such as radium-beryllium or americium-beryllium neutron source are slowed and changed in direction by elastic collisions with atomic nuclei. This process is called *thermalization*, the neutrons being reduced in energy to about the thermal energy of atoms in a substance at room temperature (Gardner, 1986).

[2]Gamma rays are short, highly penetrating X-rays emitted by radioactive substances during their spontaneous disintegration.

also measure bulk density. Measurement techniques using neutron attenuation are similar to those using gamma rays, but more specific to water.

The methods of neutron thermalization and gamma ray and neutron attenuation, although well accepted, are less desired where soils vary in chemical concentration and density. The presence of hydrogen other than as water (e.g., in clay structure or organic matter) also introduces error in the measurement. In addition, the instrument does not automate measurements well and poses health or regulatory problems when used incorrectly or left on site.

4.1.3 Porous-absorbent Blocks and Ceramics

The electrical and thermal conductivity and electrical capacitance of porous materials are sensitive to water content. As a result, soil-moisture probes utilizing these concepts perform well. Equilibrium of the porous-absorbent block with soil-water, however, is an energy state equilibrium which is related to the soil-water content through antecedent soil-moisture conditions (i.e., moisture wetting or drying history). In other words, the water content of a porous block is most reasonably calibrated to soil suction (Section 4.2); calibration to soil-water content involves the hysteresis often encountered in the soil-water energy characterization (Section 3.4).

4.1.4 Time-Domain reflectometry (TDR)

The measurement of soil-water content by TDR method has an advantage over other methods because it is a non-destructive technique that is nearly independent of soil density, texture, solute concentration, and temperature. Measurements can be quickly replicated at a given site or profile, with prospect for automation. These attributes appear attractive and therefore TDR was investigated and

used in this thesis to measure *in-situ* soil-water content, although not without calibration by gravimetry.

Soil-moisture content has been recognized for some time to influence the dielectric properties of soil (Smith-Rose, 1933; Nikodem, 1966; Hoekstra and Delancy, 1974; Hallikainen *et al.*, 1985). The dielectric constant of water at 20°C is 80.36, where that of air is 1 and of soil particles is 3 to 7. The measurement of dielectrics in the time domain was demonstrated to be simpler and less expensive than other electromagnetic techniques (Fellner-Feldegg, 1969; Chudobiak *et al.*, 1979). As a result, the use of time-domain reflectometry has been developed as a method of soil-water content determination (Davis, 1975; Davis and Chudobiak, 1975; Davis and Annan, 1977; Topp *et al.*, 1980).

The measurement of soil-moisture content by TDR method is chiefly a radar technique where a fast rise-time voltage pulse is propagated down a cable, through the soil and reflected back. The measurement of travel time through the soil-transmission line yields a measurement of "apparent" dielectric constant (K_a) of the soil, with which soil-moisture content (θ) may be calculated from relations provided by Topp *et al.* (1980), or other soil-specific relations.

The TDR instrument consists of four principal components (Fig. 4.1): (1) a pulse generator which produces a high-frequency, wide-band, fast rise-time step (typically on the order of 10^{-10} sec.); (2) a timing control which synchronizes all the timing for the pulser; (3) a sampling receiver which transforms a high frequency signal into a lower frequency output; and (4) a display (typically an oscilloscope). The step voltage pulse (or signal), leaving the TDR instrument, travels along a coaxial line, to the soil-transmission line (rods) which serve as conductors through the soil (Fig 4.1). At the end of the soil rods, the signal reflects and returns back to the TDR receiver.

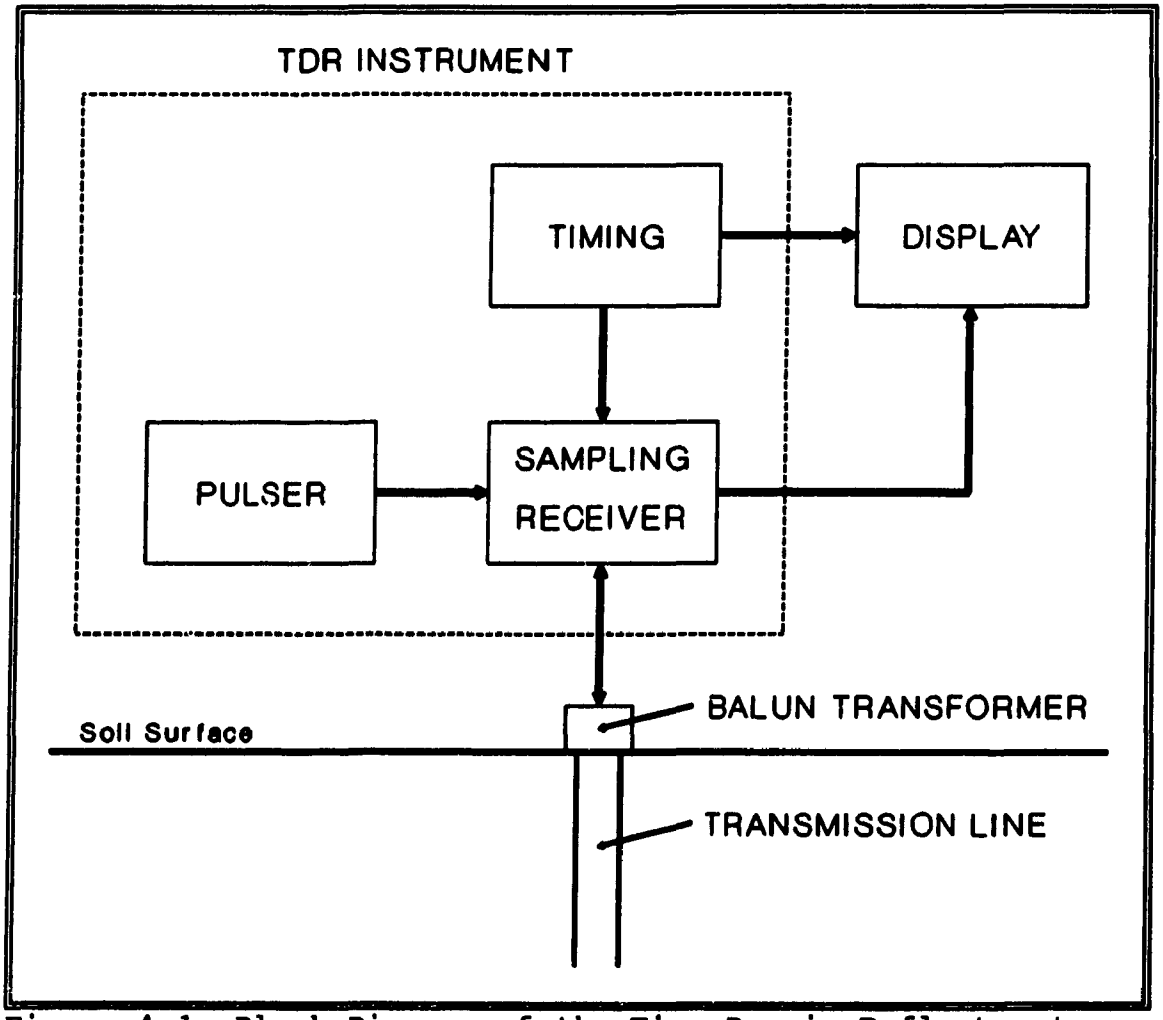

Figure 4.1. Block Diagram of the Time-Domain Reflectometry Instrument (after Topp and Davis, 1985).

The receiver monitors the voltage pulse and detects reflections from the transmission line by employing a sampling technique to measure the high-frequency signals. The sampling principle is analogous to the principle of optical stroboscopes. The receiver also produces a low-frequency (audio frequency) facsimile output which is displayed on an oscilloscope.

To determine soil-water content, the output trace (Fig. 4.2) is visually analyzed on the oscilloscope (or plotted hard-copy). Data can also be collected via an (optional) RS232 port and plotted and analyzed on computer. Software

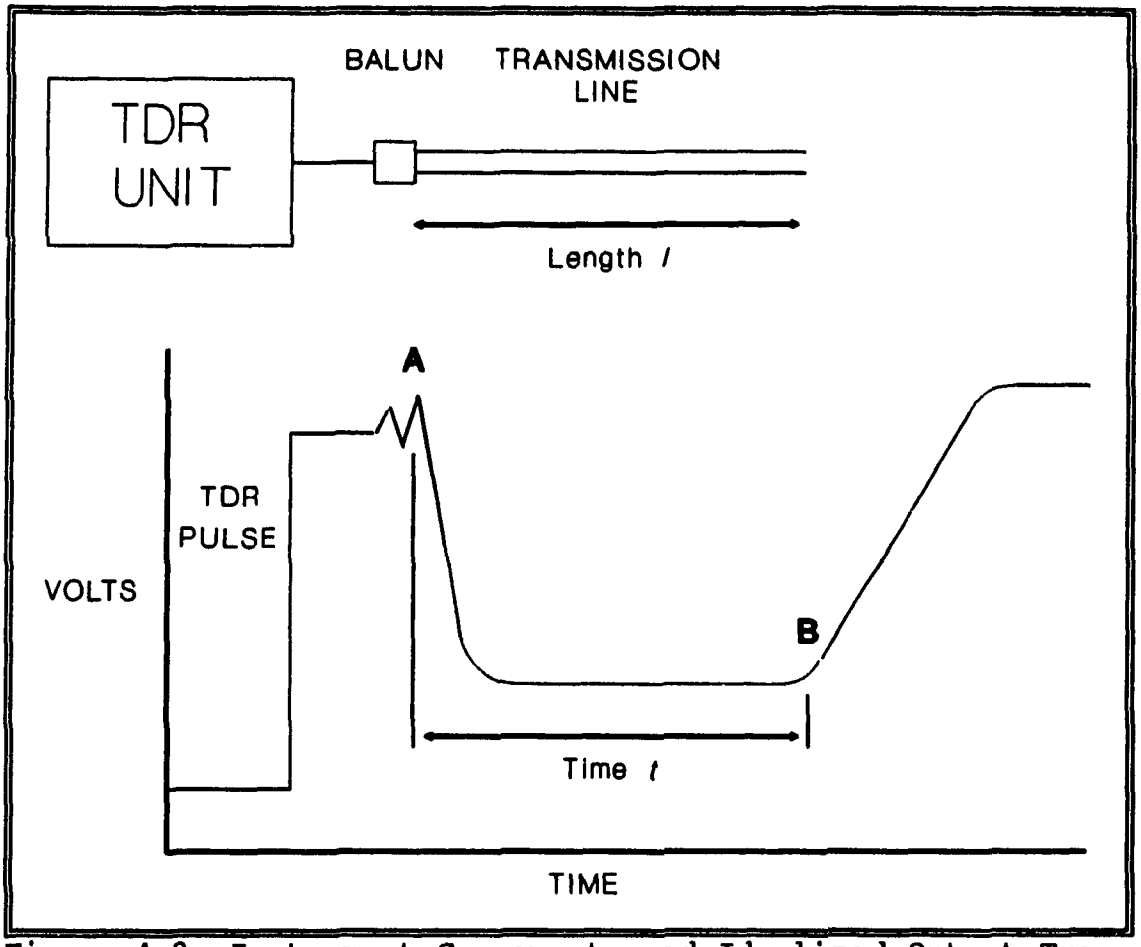

Figure 4.2. Instrument Components and Idealized Output Trace of the TDR Soil-Moisture Content Measurement Method (after Topp and Davis, 1985).

routines have been developed to perform this task (Baker and Allmaras, 1990; Heimovaara and Bouten, 1990). Some systems have also included an algorithm to calculate the soil-moisture content (Campbell Scientific, Inc., 1991; Soilmoisture Equipment, Corp., 1990).

A transmission line consists of a conducting medium (2 conductors) and a dielectric[1] medium which occupies the space between and around the conductors. A coaxial line has

---

[1]A dielectric is a non-conductor and is capable of supporting an electric stress. Refer to Appendix B for notes on charge and dielectrics.

a shield conductor surrounding a dielectric material which surrounds a center conductor. In the soil-transmission line the rods serve as the conducting medium and the soil is the dielectric medium. The high-frequency TDR pulse propagates through the dielectric medium guided by the conductors. This is analogous to radio or television signals propagating through space, although, broadcast signals are higher in power and need no conductors to guide the wave. TDR wave propagation is different from low-frequency or direct current systems in which the current travels in or along the surface of the conductors.

When there is a discontinuity (or impedance difference) in the transmission line, a fraction of the wave is reflected back towards the source. The transmission line coming from the TDR instrument is a coaxial wire and unbalanced[1] which transmits well the TDR frequency signal. At the connection of the coaxial wire to the soil rods, a discontinuity, the reflected signal indicates the beginning of the soil-transmission line. The difference between this and the reflection at the end of the soil rods provide the time measurement, central in the calculations of soil-water content (Fig. 4.2).

The connection of the coaxial wire to the soil rods represents a potential for a large impedance mismatch resulting in signal loss; it is usually beneficial to minimize the signal loss and maximize the signal energy entering the soil. In particular, the paired transmission line (2 rods) suffers unwanted signal loss and noise due to impedance mismatch between the probe and the coaxial cable,

---

[1]A transmission line is balanced when the voltages of the two conductors at any transverse plane are equal in magnitude and opposite in polarity with respect to ground; otherwise it is unbalanced (Markus, 1966). A parallel transmission line is typically balanced and a coaxial transmission line is unbalanced.

even with an impedance-matching transformer, a balun[1]. Other soil-transmission line configurations, incorporating three and four parallel rods and resembling a coaxial configuration, have been reported to improved wave propagation through the soil and the resulting TDR trace output (Zegelin and White, 1989).

Attenuation (or losses) in the coaxial cable may be minimized with either short-length leads or a large-diameter cable. A maximum length of 5 m is suggested for an RG58, 50 ohm coaxial cable to maintain the signal rise time (Zegelin *et al.*, 1992), however Herkelrath *et al.* (1991) found that cable length had little effect on calibration up to a length of 27 m. Lower loss coaxial cable (e.g., RG213) may be used for longer runs, however the size and relative inflexibility of the cable is inconvenient. If 2-conductor line must be used between the balun and the soil rods, a shielded 300 ohm TV line (Belden no. 8290) is recommended (Topp and Davis, 1985).

It is often desirable to maximize the volume of soil sampled in order to reduce the effects of soil variability. This is done with TDR by extending length and diameter of the soil rods, and the rod-to-rod spacing. Determining the water content from the signal propagation velocity is independent of the geometry of the soil-transmission line (Topp *et al.*, 1982b). The maximum limits, though, depend on the electrical properties of the soil; wave attenuation increases with an increase in soil electrical properties (e.g., electrical conductivity; clay mineral & organic mater content; soil-water content). Therefore, the design of the

---

[1]In order to match the impedance of the soil-transmission line with a 50 ohm coaxial cable, a broad-frequency bandwidth, impedance-matching transformer is utilized. The Anzac model TP103 balun has been successfully used for this purpose (Topp and Davis, 1985).

soil-transmission line is often site specific, depending on soil type.

Regarding transmission-line design, several items are noteworthy. There is a strong measurement weighting close to the 2 conductors of the 2-rod probe, and to the center conductor of the 3-rod probe (Knight, 1991), and sensitivity falls off rapidly with distance from the conductors (Baker and Lascano, 1989; Knight, 1991). Zegelin *et al.* (1992) has documented no difference in performance of 3-rod probes with rod-to-rod spacing varying from 1.5 cm to 10 cm. Zegelin *et al.* (1992) further suggest other important points. Small diameter rods have around them small measurement regions, and to ensure a representative water-content measurement the rod diameter should be at least ten times the average soil particle diameter (D_{50}). For probes less than 5 cm in length, large errors in θ are due to the resolution limits of the TDR instrument.

Paired transmission rods having a center-to-center spacing of 5 cm is a practical compromise. With this spacing and a worst case scenario (i.e., a heavy clay soil at high water content), the resolution limit is 7.5 cm (Topp and Davis, 1985). Generally, in clays and soils containing free salts, the signal penetration is less than 1 m. At maximum, the penetration range is up to tens of meters in sand and gravels (Davis *et al.*, 1983).

A potential source of error in TDR measurements arises from air gaps around the rods of the soil-transmission line (Annan, 1977). Gaps occur during rod installation or in swelling soils. Refer to Topp and Davis (1985) and Topp *et al.*, (1982b) for installation methods. Rod coatings and covers also cause error in the measurement and should not be used. Deviations from the rods being parallel generally do not significantly affect the soil-water content measurement (Davis, 1975; Stein and Kane, 1983), although the changing impedance induced along the probe may affect the precision

with which the travel time is determined, which therefore is conveyed to the measurement of K_a and θ.

The TDR signal propagation velocity (in addition to the amplitude and polarity of the reflected signal) is dependent on the electrical properties of the materials composing the transmission line. Although the properties of dielectrics, which is represented by the dielectric constant, is fundamentally a complex electrical concept, simplifying assumptions and conditions facilitate the utilization of these principles for soils. The dielectric constant (K) is related to the signal propagation velocity (v) by:

$$v = \frac{c}{K^{1/2}} = \frac{c}{(K'[1+(\tan^2\delta)^{1/2}]/2)^{1/2}} \qquad (4.1)$$

where, c = propagation velocity of and electromagnetic wave in free space (vacuum) (3 x 10^8 m/sec);
K′ = real dielectric constant;
tan δ = the loss tangent;

$$\tan\delta = \frac{K'' + (\frac{\sigma_{dc}}{\omega \varepsilon_o})}{K'} \qquad (4.2)$$

where, K" = dielectric loss;
ε_o = permittivity of free space ($10^{-9}/36\pi$ F/m);
σ_{dc} = zero frequency DC conductivity (S/m); and
ω = angular frequency ($2\pi f$ radian/sec);

The loss tangent is a ratio of the imaginary component to the real component of the complex dielectric. The real part is a measure of the energy stored by the dipoles aligned in an applied electromagnetic field. The imaginary part is a measure of the energy dissipation rate in the medium; K" represents losses by molecular vibration and rotation and the term $\sigma_{dc}/\omega\varepsilon_0$ represents losses by conductivity (see Appendix B and Schmugge *et al.*, 1980).

In soils over a frequency range of 10 MHz to 1 GHz, the loss tangent is typically much less than 1 (i.e., the imaginary losses negligible) and therefore, K'≈K (Davis and Annan, 1977); thus,

$$v = \frac{c}{K_a^{1/2}} \qquad (4.3)$$

Because the effect of electric loss, though not measurable, exists in this estimation of the dielectric constant (K), it is the termed an "apparent" dielectric constant (K_a).

In practice, the velocity (v) is obtained from the given length of the transmission line in the soil (the travel time being 2L) and by the measurement of the signal 2-way travel time (t) in the soil using TDR (Fig. 4.2).

$$K_a = \left(\frac{c}{v}\right)^2 = \left(\frac{ct}{2L}\right)^2 = \left(\frac{15\ t[ns]}{L[cm]}\right)^2 \qquad (4.4)$$

where, t = 2-way travel time; and,
L = the known length of the soil-transmission rods.

Because the dielectric constant of water substantially differs from that of the solid and gas phases of soil (Appendix B), the dielectric constant of soil is strongly dependent on its water content (Topp *et al.*, 1980).

$$\theta_v = (4.3x10^{-6})K_a^3 - (5.5x10^{-4})K_a^2 + (2.92x10^{-2})K_a - (5.3x10^{-2}) \qquad (4.5)$$

They concluded that the high-frequency dielectric constant is only weakly dependent on soil type, density, temperature, and pore-water conductivity. If, although, the electrical nature of the soil is high (e.g., by ions or surface charge), the estimate of the dielectric constant (and θ) is lower than expected, presumably caused by structured "ice-like" water which has a lower dielectric constant than liquid water. Under such conditions, the imaginary losses

are not negligible. At sites where temperature extremes are encountered the dielectric constant of water must be adjusted (e.g., Handbook of Chemistry and Physics, 1974; Hasted, 1973); at 50°C, the temperature correction to 25°C is almost 11%.

The potential of TDR for the measurement of soil-water content and other applications has been investigated with regard to: (1) TDR probe design (Topp *et al.*, 1982b; Topp *et al.*, 1984; Topp and Davis, 1985; Zegelin and White, 1989); (2) comparison with nuclear methods (Keng and Topp, 1983; Drungil *et al.*, 1989); (3) soil moisture in gravelly soils (Drungil *et al.*, 1989); (4) infiltration and advancing wetting fronts (Topp and Davis, 1981; Topp *et al.*, 1982a; Topp *et al.*, 1983; Ledieu *et al.*, 1986); (5) water balance (Zegelin *et al.*, 1992); (6) irrigation scheduling (Topp and Davis, 1985); (7) unfrozen water content of frozen soils (Patterson and Smith, 1981; Hayhoe *et al.*, 1983; Stein and Kane, 1983, with comment by Patterson and Smith, 1985, and Topp and Davis, 1985; Patterson and Smith, 1984); (8) measurement of soil electrical conductivity and salinity (Dalton *et al.* 1984; Dasberg and Dalton, 1985; Dalton and Van Genuchten, 1986; Topp *et al.*, 1988; Yanuka *et al.*, 1988); and, (9) contaminant detection (Yong and Hoppe, 1989). Roth *et al.* (1990) attempted to predict the relation between θ and K_a on the individual dielectric constants of the three soil components (soil particles, air, and water).

The measurement of soil-moisture content by the measurement of a TDR propagation velocity through soil has generally been favorable when compared to other techniques, although not without prudent methodology. Under ideal conditions, TDR has a maximum resolution in θ of 0.002 in sandy soils with little solute content (Zegelin *et al.*, 1982). As clay content and electrical conductivity increases, the resolution decreases.

4.2 *In-Situ* Measurement of Soil-water Potential

Soil-water potential is measured *in situ* by four methods: (1) Tensiometer; (2) Peltier Thermocouple Psychrometer; (3) Electrical Resistivity Porous Block; and (4) Thermal Conductivity Porous Block. Of these, only the thermocouple psychrometer measures total potential, while the others measure pressure potential. The tensiometer is a direct measurement of matric potential while the porous blocks are indirect measurements of matric potential. Piezometers measure hydraulic head in saturated soil.

4.2.1 Tensiometer

The soil-water pressure potential by tension can be directly measured with a tensiometer (Gardner et al., 1922; Richards and Gardner, 1936; Richards, 1949; Richards, 1986). They are the most widely used means of evaluating *in-situ* soil potential, but suffer from having a limited suction range (typically 0 to 0.85 bars), being maintenance intensive, being inoperable at freezing air temperatures, and are difficult to install in stony soils. When equipped with pressure transducers, they are capable of continuous monitoring (Marthaler et al., 1983; Lowery, 1986; and references within). A recent review of tensiometers can be found in Stannard (1990).

A tensiometer is an instrument consisting of a tube closed at the bottom with a ceramic cup and at the top with a pressure measurement device (e.g., manometer, Bourdon gage or pressure transducer) (Fig. 4.3). In the absences of a pressure gauge, direct reading may be obtained by the height of the air pocket within the tensiometer (Villa Nova et al., 1989). Water in the tensiometer is in contact with the soil water though the ceramic tip. As the soil dries, the tension is exerted on the water in the tensiometer and the suction (negative pressure) is measured within the tensiometer. Water in the tensiometer is lost as vapor through the

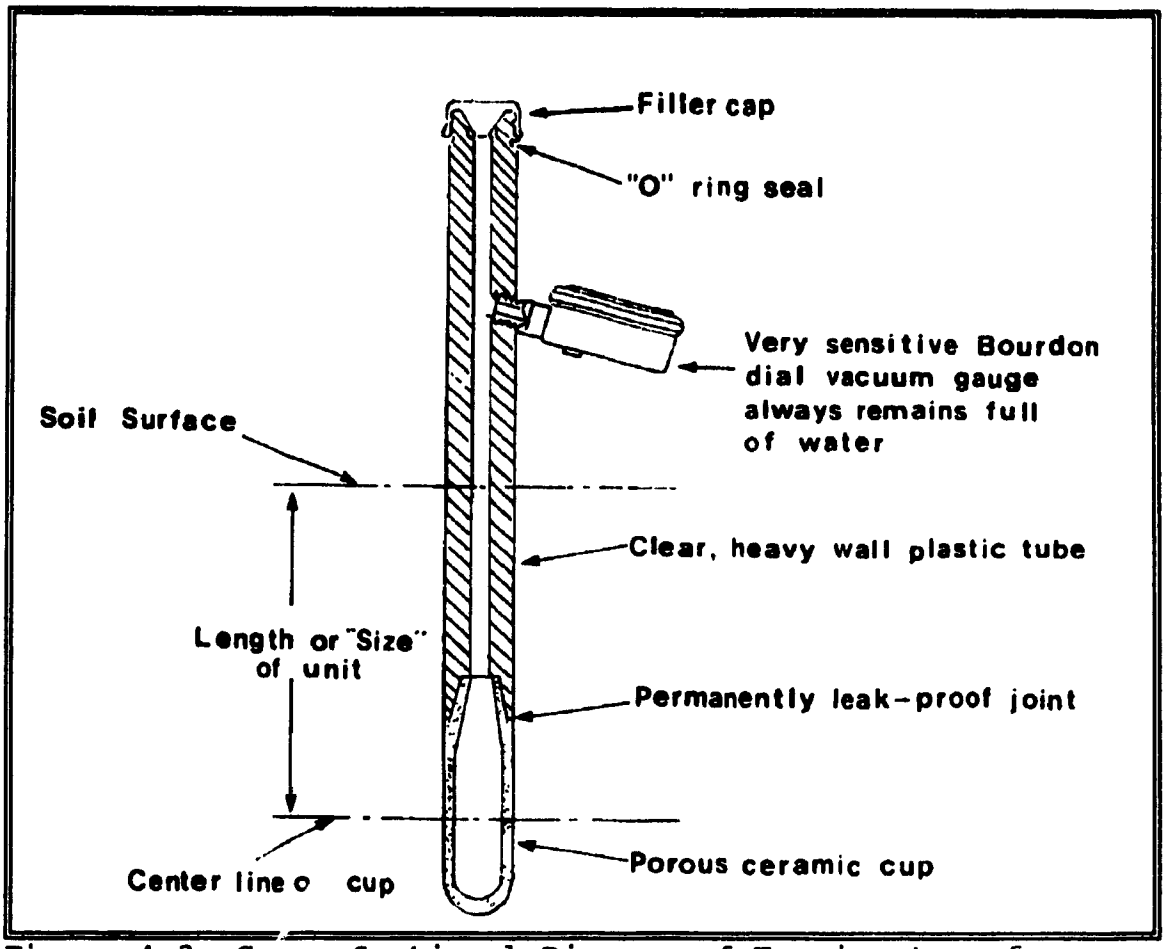

Figure 4.3. Cross-Sectional Diagram of Tensiometers for Field Use in Soil-Water Potential Measurement (after Yong and Warkentin, 1975).

ceramic cup and replacement is required (about every weak depending on the pressure and size of the tensiometer).

The instrument typically measures matric (capillary) potential but if the wall material (porous ceramic) of a tensiometric cup completely restricts the passage of solute ions, the pressure measured by the tensiometer is equal to the value of the total potential (osmotic potential and matric potential). Standard tensiometers, however, allow movement of salt through the porous membrane and hence they do not measure osmotic potential. The tensiometer could also measure positive pressures.

The pore size of the ceramic cap directly affects the minimum suction value (air entry value) and the hydraulic conductivity of the tensiometer. The air entry value (bubbling pressure) is the pressure required to force air through a saturated ceramic pore; that is, the pressure greater than that of the water pressure which is under the meniscus of the air-water interface. Because the air entry value is governed by the size of the largest diameter pores, the effective pore size of a ceramic cap is based on the air entry value. Ceramic caps with high air entry values have small pores and as a consequence a slower exchange of water (a smaller hydraulic conductivity), which results in a lag in the readings. Therefore, the standard tensiometer maximizes both the bubbling pressure and response time, resulting in a bubbling pressure of 0.85 bars. The physical properties of porous ceramics appear in Table 4.1 (Soilmoisture Equipment, Inc., 1987).

Table 4.2. Physical Properties of Porous Ceramics.

Air Entry Value (bar)	Bubbling Pressure (psi)	Approximate Porosity (% vol)	Saturated Hydraulic Conductivity (cm/s)	Pore Size (μm)	Flow[1/] Rate (mL/hr/ cm^2/14.7 psi)
0.5	7 to 9	50	3.11×10^{-5}	6.0	180
1.0[2/]	19 to 28	45	8.60×10^{-6}	2.5	50
1.0	20 to 30	34	3.46×10^{-7}	2.1	2
2.0	35 to 45	38	1.73×10^{-7}	1.2	1
3.0	46 to 70	34	1.70×10^{-7}	0.8	1
5.0	80	31	1.21×10^{-7}	0.5	0.7
15	220	32	3.59×10^{-9}	0.16	0.015

1/ through a standard 1/4 inch plate.
2/ high flow.

Porous ceramics generally contain various proportions of kaolin, alumina, ball clay, and other feldspathic materials. There are certain cation exchange effects exhibited by the porcelain material. They, however, generally tend to reach an equilibrium.

4.2.2 Peltier Thermocouple Psychrometer

Like the tensiometer, the thermocouple psychrometer is an instrument utilizing a porous ceramic cap in contact with soil. However, instead of measuring pressure changes caused by the movement of water through the porous cup, it measures vapor pressure. In this way, the ceramic cap acts like a soil pore void in which the measurement of vapor pressure is made. The determination of soil-water potential by the measurement of vapor pressure has theoretical advantages; the vapor pressure is a well defined thermodynamic quantity which depends upon both the matric and osmotic components of total potential. Therefore, it is capable of measuring the total potential.

The theory of how the Peltier[1] Thermocouple Psychrometer operates has been described in detail (Spanner, 1951; Rawlins, 1966; Rawlins and Dalton, 1967; Dalton and Rawlins, 1968; Peck 1968, 1969; Rawlins, 1971; Scotter, 1972). A thermocouple junction is fixed inside a small ceramic bulb (Fig. 4.4). A cooling current is applied which condenses water on the junction. The cooling current is released and the water is allowed to evaporate. As this water evaporates, it cools the junction. The rate of evaporation is inversely related to the vapor pressure in the bulb. The cooling is measured as the voltage output of

---

[1]Peltier Effect (*Elec. Eng.*). The phenomenon whereby heat is liberated or absorbed at a junction where an electric current passes from one metal to another. The heating or cooling of the junction depends on the direction of the electrical current.

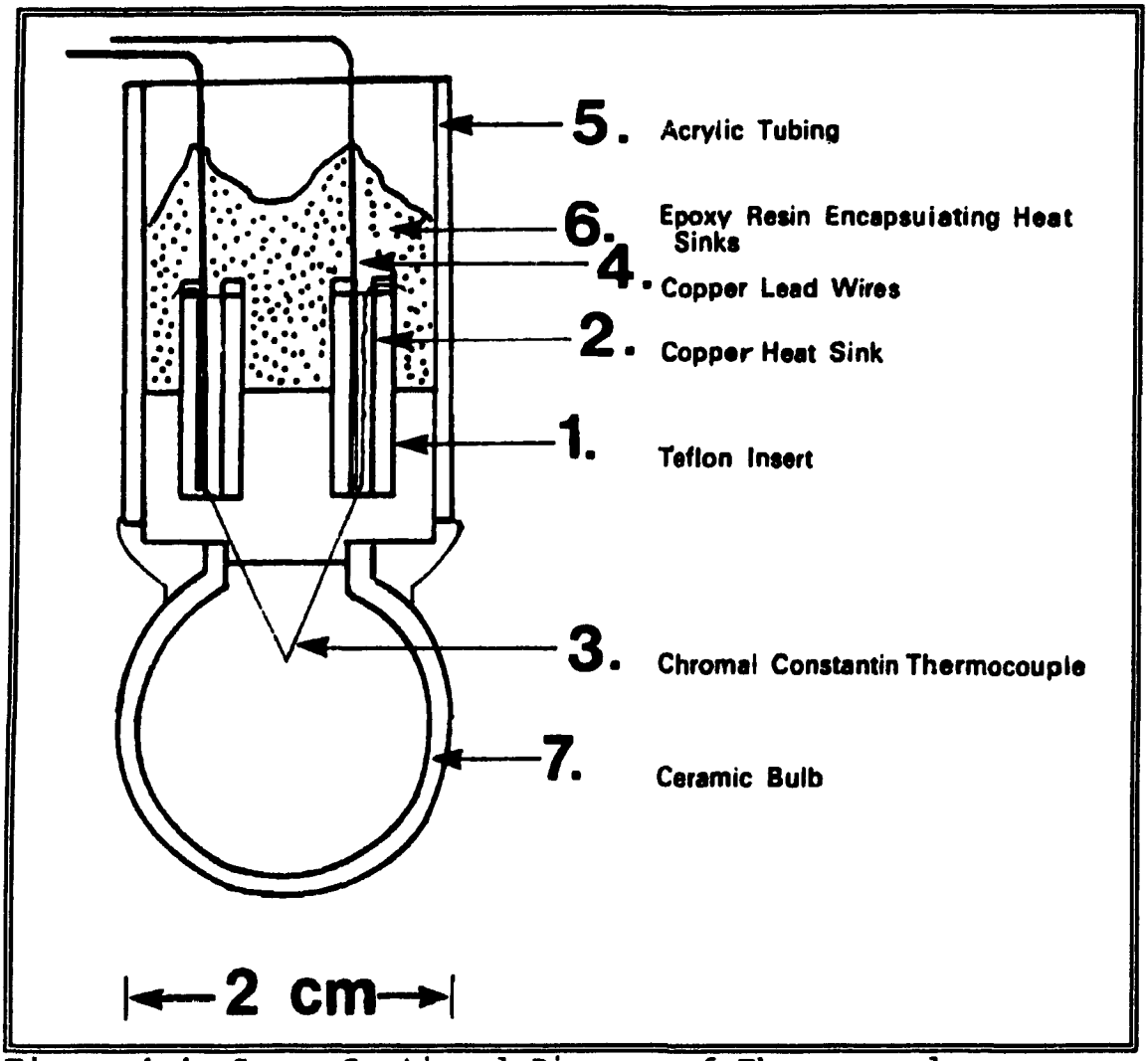

Figure 4.4. Cross-Sectional Diagram of Thermocouple Psychrometer for Soil-Water Potential Measurement (after Yong and Warkentin, 1975).

the thermocouple. Since the vapor pressure is temperature dependent, a second thermocouple is added to measure the temperature. The vapor in the ceramic bulb is in equilibrium though the ceramic pores with the vapor pressure in the soil and the measurement of vapor pressure can be converted to soil-water potential.

The precision of the psychrometer used in the laboratory is typically 0.1 bar, but the precision of *in-situ* measurements is more on the order of 0.5 bar. At potentials around -15 bar, vapor equilibrium is established

quickly and the readings take only a few minutes. At higher potentials (-1 bar), however, the readings may take hours. Calibration procedures can be found in Brown and Bartos (1982).

4.2.3 Electrical Resistance of Absorbent Blocks

It is possible to measure the water content of soil by measuring the resistance between two electrodes, mounted in a porous block and implanted in the soil. The units are commonly called "Gypsum Blocks", or Bouyoucous moisture blocks after the person who developed the idea (Bouyoucous and Mick, 1940). As the soil dries, the pores of the block, which are in contact with the soil, lose water and electrical capacitance increases. The electrical resistance is then correlated to soil-water potential which is measured by other methods.

The electrical resistivity of porous blocks varies with its water content, which because it is in equilibrium with the soil, responds to fluxes driven by changes in soil-water potential. However, the measurements also depend upon the electric solutes present in the fluid. Blocks made of inert materials such as nylon (Bouyoucous, 1949), plaster of Paris (Bouyoucous, 1953), or fiberglass (Colman and Hendrix, 1949) are highly sensitive to small variations in salinity of the soil solution; while, gypsum blocks maintain a nearly constant electrolyte concentration corresponding primarily to that of its saturated solution of calcium sulfate. This tends to buffer the effect of small to moderate variations in the soil solution. However, since gypsum is soluble, these blocks eventually deteriorate in the soil.

Porous blocks embedded in the soil tend to equilibrate with the soil moisture (matric) suction. Prior to installation, it is often beneficial to calibrate the probes to soil suction in a pressure plate apparatus (Fredlund and Wong, 1989) or by other methods (Reynolds et al., 1987).

Often gypsum blocks can be grouped by saturated resistance while calibrating only a few per group. The calibrated measurements, although, may be complicated by changes in soil water chemistry (i.e., electrical conductance).

Because of changes in soil-water chemistry, measurements of soil-moisture potential by electrical resistance blocks is likely to be of less accuracy and less reliable than those by other methods. On this basis and considering the solubility of gypsum, they have been more dependable in drier ranges (xeric soils) than in wetter ranges (mesic soils). In addition they are able to operate over the full range of tension and can be automated (Strangeways, 1983).

Regarding changes in soil chemistry, gypsum blocks will clearly measure a lower resistance with pore waters of higher electrical conductance. As a soil dries its pore water increases solute concentration, and the electrical conductance of the pore water also increases. The electrical conductance of the soil, though, decreases due to the absence of water, the electrical conducting medium. A gypsum block in equilibrium with the soil will therefore measure a higher resistance during drying periods.

4.2.4 Thermal Conductivity of Porous Blocks

Similar to the concept supporting the gypsum block, the thermal conductivity (heat dissipation) of a porous block (of low heat diffusivity) is sensitive to water content and can be used as an index to soil-water potential (Shaw and Bauer, 1939a,b; Johnson, 1942; Bloodworth and Page, 1957; Dejager and Charles-Edwards, 1969; Phene et al., 1971a,b). In general, air is a better thermal insulator than water and as air is replaced by water the thermal conductivity of the porous medium increases.

The heat dissipation[1] sensor consists of a miniature heater and a temperature sensing element encased in a porous ceramic (Fig. 4.5). The temperature sensing element is typically a thermocouple. When placed in soil, equilibrium is conserved as water flows between the porous block and the soil; as water content within the block increased, so does the thermal conductivity. The temperature of the block is measured before and after a known quantity of heat is delivered to the block, and the change in temperature (ΔT) represents heat dissipation; more heat will dissipate through the block with higher water contents, resulting in a smaller ΔT. Consequently, ΔT is inversely proportional to the water content of the porous block. And because the water content in the block is directly proportional soil-water matric potential, the temperature rise within the porous block (ΔT) is inversely proportional to soil-water matric potential.

Heat dissipation sensors are independent of soil texture, temperature, and salinity. Phene (1986) analyzed the practical strengths and weaknesses of the heat dissipation method which also appears in Phene et al. (1987). In summary, they have a response time of less than one hour (between 0.1 and 1 bar suction) and can be calibrated over a wide range of suction (0.1 to 15 bars).

---

[1]Like hydraulic conductivity, *Thermal conductivity (k)* is a linear coefficient that measures the ability to conduct heat. Similarly, *Thermal diffusivity (K)* is the ability to diffuse thermal influences, which accounts for the heat capacity of a substance; *heat capacity (C)* is the ability of a substance to store heat ($J\ m^{-3}\ K^{-1}$). Thermal diffusion controls temperature wave velocity and thermal influence depth ($K=k/C$). *Thermal admittance (μ)*, on the other hand, is a measure of the ability of a surface to accept or release heat. Refer to Oke (1987), pp.43-45. To avoid confusion between these inter-linked thermal properties, the term heat dissipation is used for this sensor.

They found that the accuracy depends upon the accuracy of the temperature measurement and the calibration which is linear between 0.1 and 3 bars. However, an inflection in the calibration curve has been noted at 1.75 bars (Sattler and Fredlund, 1989). Calibration procedures can be found in Fredlund and Wong (1989).

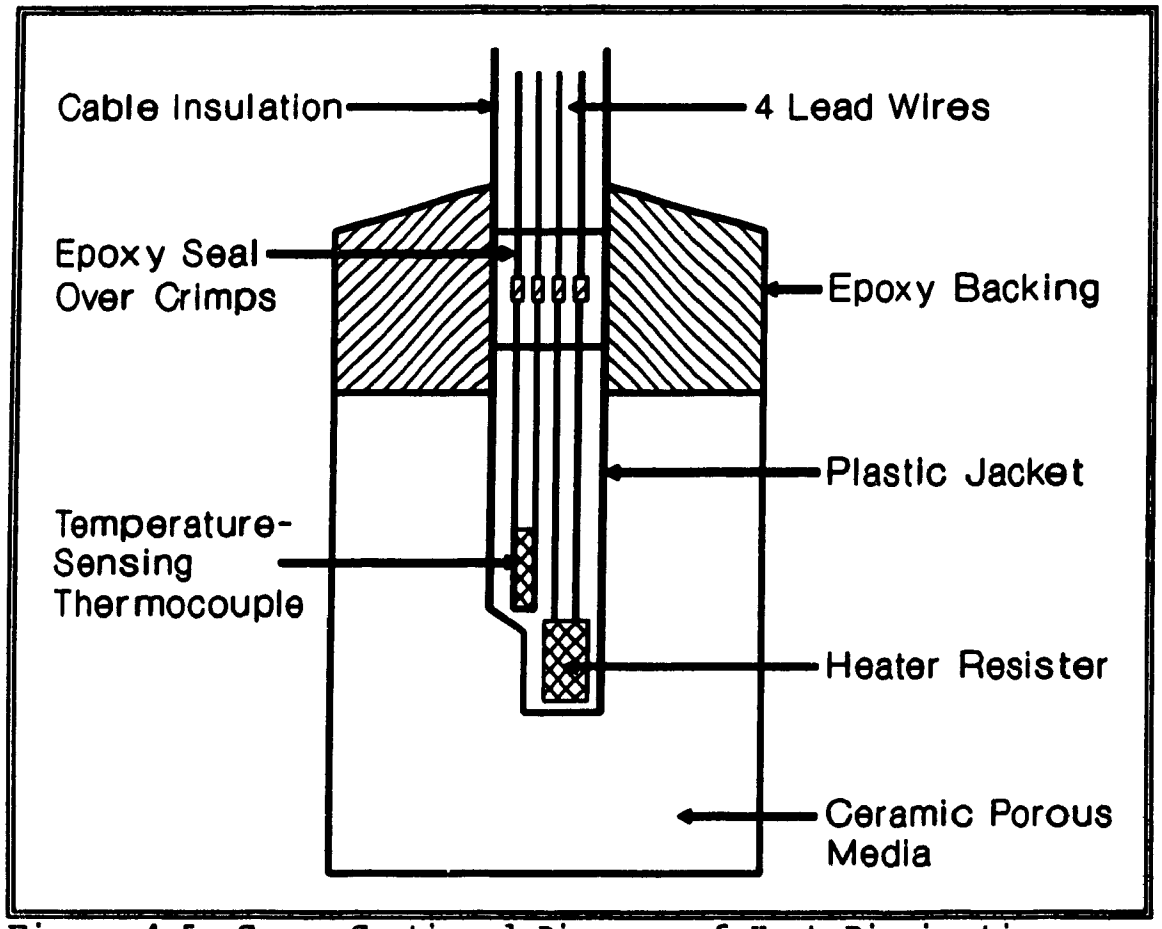

Figure 4.5. Cross-Sectional Diagram of Heat Dissipation Sensor for Soil-Water Potential Measurement (after Slattler and Fredlund, 1989).

4.3 Piezometers, a Measurement of Hydraulic Head

In the saturated medium, measurements of hydraulic potential is governed by the hydraulic head, which is composed of the elevation head and the pressure head (velocity head is negligible in most groundwater bodies). The basic device for the measurement of hydraulic head is a tube or pipe in which the elevation of a water level can be determined. In the laboratory, the tube is called a manometer, and in the field the pipe is called a piezometer. Automated measurements are typically conducted with submersible pressure transducers located in the piezometer. In this case, the method is termed pressure-transducer piezometry.

A piezometer tube, to the soil, is sealed along its length or a partial length (a plug) with typically a bentonite slurry. It is open to water flow at the bottom and open to the atmosphere at the top. The intake, which is located at the base of the piezometer, is usually a section of slotted or screened pipe or manufactured porous tip. The intake is designed to allow the inflow of water but not of soil particles. Water enters the piezometer at a fixed elevation and rises in the piezometer until the head of the water in the tube balances the water pressure at the entry point. The depth of the water in the piezometer is known as the pressure or piezometric head.

5.0 STUDY SITE BACKGROUND

Located in western Quebec, near the town of Rouyn-Noranda (Fig. 5.1), the Waite Amulet mill processed approximately 8.74 million tonnes of sulfide ore and produced concentrates of Cu and Zn between 1929 and 1962. In addition, the mill generated approximately 5.9 million tonnes of mill tailings, contained in an elevated 41 ha tailings dam.

The tailings are located at 48° 19′ latitude north and 79° 05′ longitude west of Greenwich at an nominal elevation of 315 meters above mean sea level (N. Amer. Datum 1927). It is situated at the western edge of Plateau D'Abitibi in the Outaouais Supérieur climatic region. The area of coverage can be located on the 32D/6 Rivière Kanasuta SE quadrant 1:50,000 map or the 32D Noranda-Rouyn 1:250,000 map.

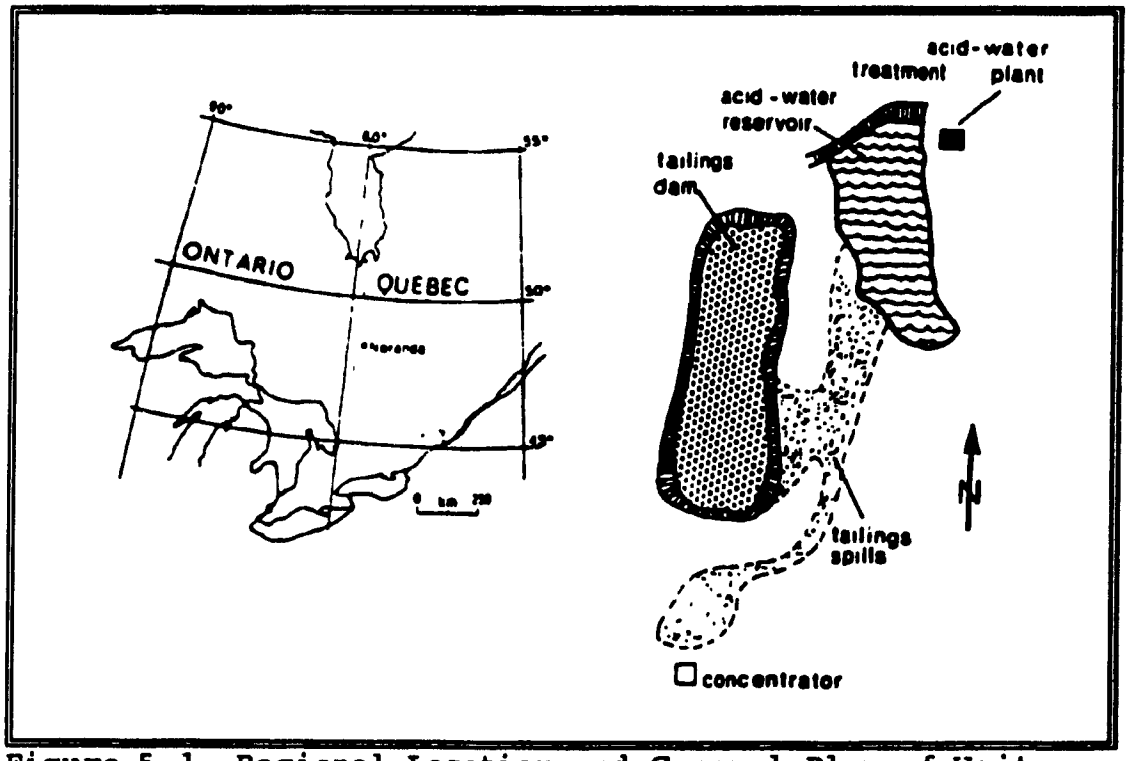

Figure 5.1. Regional Location and General Plan of Waite Amulet Tailings (after Blowes and Jambor, 1988).

The boreal climate of the region is classified as a subpolar, subhumid, continental climate -- $1_1 3_2 C_2+$ by Litynski (1987, 1983), where 1_1 is -1.5 to 1.9 mean annual temperature, 3_2 is 800 to 950 mm annual precipitation, C_2 is 50 to 62 percent continental, and + is an index of concordance. A climatic summary can be found in Table 5.1.

There are several climatic stations within proximity of Waite Amulet (Table 5.2). At permanent stations, net observations are conducted twice each day, and at synoptic stations, net observations are conducted every six hours. Data from synoptic stations are typically reduced and made available to the public prior to data from permanent stations.

Table 5.1. Regional Climatological Summary.

Month	Mean Daily Temp. (C)	Daily Max. Temp. (C)	Daily Min. Temp. (C)	Total PPT (mm)	Fraction as Snowfall (%)	Calculated Lake Evaporation (mm) a/
January	-17.5	-10.5	-22.5	53.0	94	-
February	-15.0	-8.0	-22.5	50.0	93	-
March	-8.0	-1.5	-15.0	50.0	73	-
April	1.5	6.5	-5.0	50.0	-	-
May	8.5	15.5	2.0	62.5	-	107.5
June	14.5	21.5	8.0	100.0	-	119.3
July	17.5	21.5	11.0	100.0	-	128.2
August	15.0	23.5	9.5	100.0	-	102.3
September	10.5	21.5	5.0	112.5	-	58.3
October	5.0	16.0	0.0	76.0	-	-
November	-3.0	9.5	-7.0	75.0	-	-
December	-13.0	-8.0	-18.0	62.5	88	-
Annual	1.5	7.0	-5.0	900	27	515.6

Source: Isopleth maps constructed by Ministère de L'environnment du Québec; period of record = 1951-80 (Canadian Climate Normals data).

a/ Source: Environment Canada, Canadian Climatic Normals, vol.9, 1951-80; Amos Station.

Table 5.2. Meteorological Stations near Waite Amulet, Quebec.

STATION NAME	STATION NUMBER	CLASS	LATITUDE deg	LATITUDE min	LONGITUDE deg	LONGITUDE min	ALTITUDE meters	STATION BEGAN	PPT	PPT RATE	AIR TEMP	VEG TEMP	SOIL TEMP	AIR HUMID	INSOL	SOLAR RAD	EVAP	WIND	SOIL HUMID	SNOW	PPT QUAL
Waite Amulet	-	-	48	19	79	5	315	-	*	*	*		*				*				
Amos	7090120	P	48	34	78	8	310	1913	*	*	*	*	d	*	*	d	*	*		*	
Clericy	7081716	A	48	22	78	51	274	1986		*											
Duparquet	709BBDH	P	48	31	79	16	290	1914	*		*			d							d
Evain	708B309	P	48	15	79	6	302	1986		*	*	*	*	*		*		*	*	*	
Lac Berry	709CEE9	P	48	48	78	18	305	1973	*		*			d							
La Sarre	7094120	P	48	48	79	12	274	1951	*		*										
Manneville	7084560	P	48	33	78	29	311	1949	*		*				*						d
Montbeillard	7085102	P	48	5	79	16	274	1972	*		*			d							d
Mont Brun	7085106	P	48	25	78	44	305	1980	*		*			*							*
Palmarolle	7095785	P	48	40	79	10	276	1986	*		*	*	*	*			*		*		
Poularies	7096215	P	48	41	78	59	290	1969	*		*			*	*						d
Riviere Heva	7096621	P	48	14	78	12	305	1984	*	*	*										
Riviere Kinojevis	7086630	P	48	13	78	52	290	1974	*		*			*							*
Rouyn Airport	7086720	C	48	13	78	50	301	1949						*				*			
Taschereau	7098360	P	48	40	78	42	310	1953	*		*										
Val-D'Or Airport	7098600	C	48	4	77	47	337	1949	*	*	*		*	*	*			*		*	

P: permanent station A: automatic station C: synoptic station *: currently measured d: measurement discontinued.

The Waite Amulet tailings are rich in sulfide minerals, principally pyrite and pyrrhotite, and oxidize readily when exposed to water and atmospheric oxygen. The oxidation of the sulfide minerals has generated low pH waters with high concentrations of SO_4^{2-}, Fe^{2+}, and other metals. The movement of the tailings-derived waters away from the impoundment and to the adjoining surface and ground water systems constitutes an important environmental problem. The site remediation to date has included the construction and operation of an acid water treatment plant to treat the tailings runoff (1984 to present) and the revegetation of the tailings surface (1978-79).

Revegetation consisted of neutralizing the tailings surface with 44 tonnes per hectare of agricultural limestone and applying 2.2 tonnes per acre of fertilizer because the tailings were devoid of any nutrients. Birds foot trefoil[1] (*Lòtus*) and a companion crop of creeping red fescue[2] (*Festuca rùbra*) were planted. Aspen-birch groves subsequently established in isolated woodlands.

Several studies have been conducted at the Waite Amulet tailings site. A hydrogeochemical investigation, conducted by the Centre de Technologie Noranda, began in 1985 and encompassed three phases. The site reconnaissance (phase I; Siwik, 1986) included a geophysical investigation, a drilling program, and a saturated zone pore water sampling program (Blackport, 1986), in addition to a bacteria count (Ferroni and Leduc, 1985). The hydrogeological exploration, which involved further drilling and sampling (Blackport, 1987), was completed during phase II of the investigation

---

[1]Trefoil is any of several trifoliolate leguminous herbs, having compound leaves with three leaflets. Birds foot trefoil is a large genus, *Lòtus*, of the *Papilionoideae* bean subfamily of the *Leguminosae* pea family.

[2]Fescue is the genus *Festuca* of tufted perennial grasses with panicled spikelets.

(Siwik *et al.*, 1987). Mineralogical analysis were also conducted (Petruk and Pinard, 1986; Jambor, 1986, 1987a, and 1987b) and a hydrogeochemical study of the unsaturated zone was completed (Blowes and Cherry, 1987). Phase III of the investigation (Siwik *et al.*, 1988) included the monitoring and sampling of the tailings runoff and baseflow (seeps), the measurement of pore oxygen gas concentration, moisture content, and grain size distribution of the tailings to one meter depth, and further measurement of hydraulic conductivities of the saturated zone (Noranda). A supplementary report was also produced on the porewater geochemistry and mineralogy (Blowes and Jambor, 1988). An extensive review and analysis of the generation and evolution of acidic pore waters at the Waite Amulet tailings was conducted by Yanful *et al.* (1990) which included a hydrogeologic evaluation and modelling (flownet) and preliminary hydrologic analysis. This document concluded the investigative effort conducted by the Centre de technologie Noranda.

5.1 REVIEW OF STUDY SITE FINDINGS

Beneath the tailings, a variable bedrock topography composed of fractured granodiorite underlies a southwesterly dipping clay mantle which ranges in thickness from 2 to 20 m on a north-south transect. The tailings also vary in thickness, ranging from 2 m in the north to 15 m in the south. Because the mill discharge to the tailings was at the southern end, the tailings are much more fine-grained in the northern region (d_{50} = 0.007 mm) than in the south (d_{50} = 0.14 to 0.17 mm). The tailings are well sorted (d_{10} = 0.001 mm, north; d_{10} = 0.02 mm, south); the fine-grained tailings in the north contain 17 to 22% clay and 10% silt size fractions and the coarse-grained tailings in the south contain 5% clay and 1 to 3% silt size materials. The

reported porosity of the tailings averages 0.27 and that of the underlying clay, 0.43.

The tailings surface slopes gently to the north. Runoff from the south appears to pond in the central portion of the tailings. Runoff from the north also ponds in places but also enters a channel and flows off the tailings, to the north (Fig. 5.2). The water table (Fig. 5.3) is highest in elevation in the north-central portion of the tailings where it is just below the tailings surface, and drops towards the south (5.5 m below surface) and towards the west (4 m below surface). Seeps rim the base of the tailings dam faces, indicating the watertable location. Tailings runoff and baseflow seepage discharge to a treatment plant collection pond which is underlain by clay (Fig. 5.2).

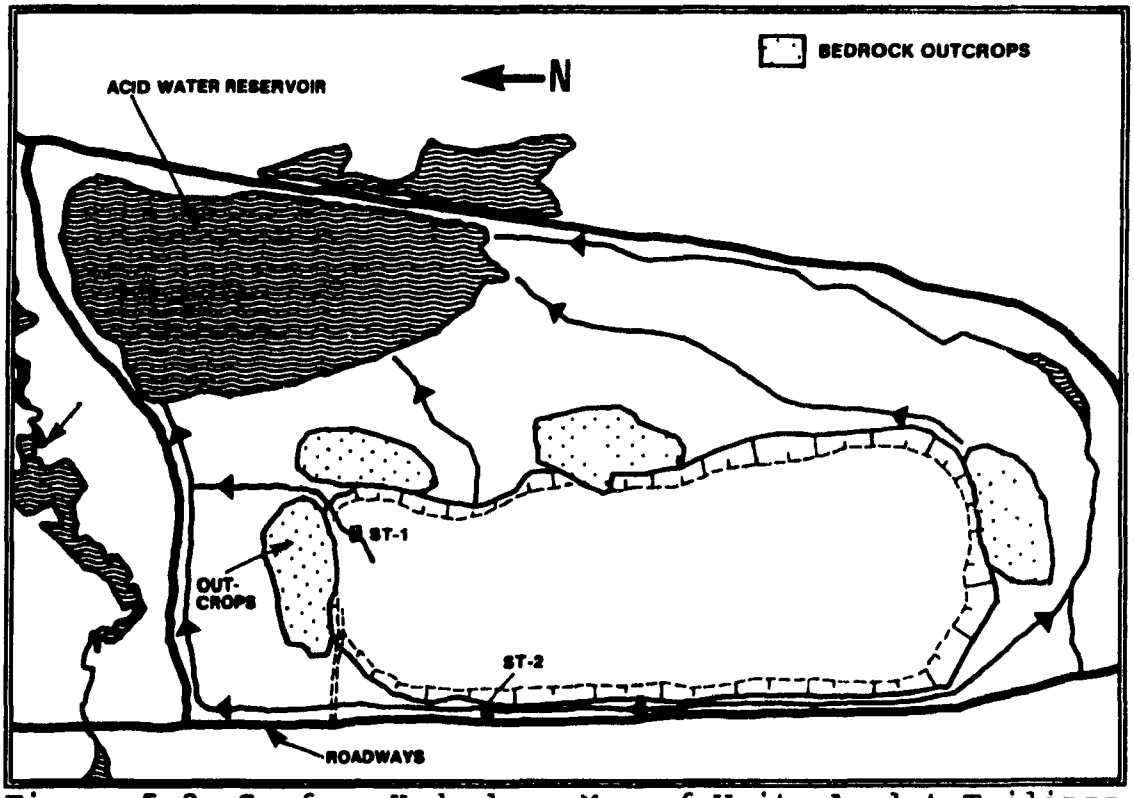

Figure 5.2. Surface Hydrology Map of Waite Amulet Tailings (after Yanful *et al.*, 1990).

Saturated hydraulic conductivity measurements (K_s) of the tailings range from 10^{-5} to 10^{-4} cm/s in the vadose zone (measured with a constant head test using a Guelph permeameter) and from 5 x 10^{-6} to 2 x 10^{-4} cm/s in the saturated zone (measured with a falling head test in piezometers). Hydraulic conductivity measurements of the clay underlying the tailings range from 10^{-7} to 10^{-4} cm/s (currently under revision by Noranda). Preliminary estimates indicate that a portion of the infiltrating water may be flowing into the underlying clay layer (currently under investigation by Noranda).

Weathering of the tailings follows well established mineral oxidation sequences (Stumm and Morgan, 1981) (Section 1). The oxidation of Fe^{2+} is the rate controlling

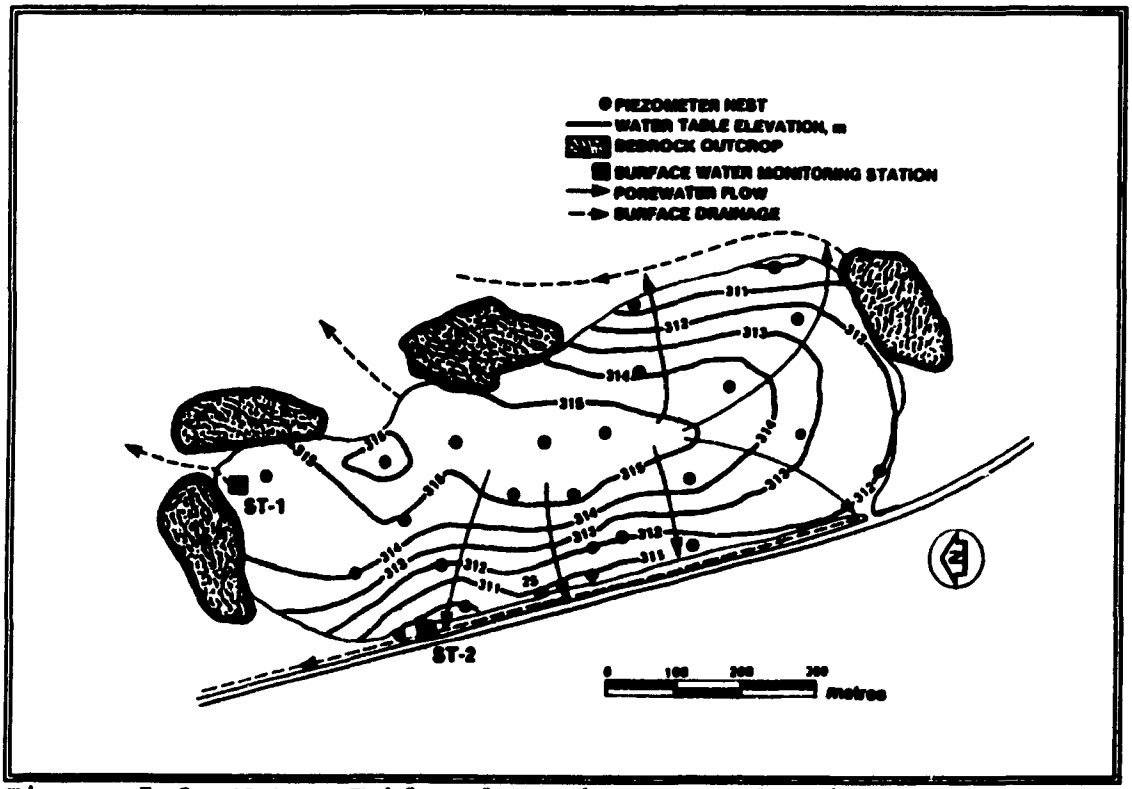

Figure 5.3. Water Table Elevation Map of Waite Amulet Tailings, October 1986 (after Yanful *et al.*, 1990).

reaction which is regulated by the activity of acidphillic bacteria (*T. ferrooxidans*). If the diffusion rate is low, iron oxidation can be controlled by O_2 availability, and *T. ferrooxidans* activity by CO_2 availability. In these circumstances, the diffusion rate of O_2 and CO_2 into the tailings controls the rate of sulfide oxidation, and hence the rate of acid generation. Gaseous oxygen profiles indicate a decrease with depth to 0.5 to 0.7 m with estimated diffusion coefficients in the range of 3.0 to 4.2 x 10^{-7} cm^2/s. Bacteria counts of *T. ferrooxidans*, an obligate anaerobe, correlate with the termination of the O_2 profile. The highest populations in the south-end tailings lie at 0.5 m depth, although they decrease sharply to almost zero at 1.1 m depth. *T. ferrooxidans* is absent below the water table.

The availability of CO_2, the principal carbon source and growth control for *T. ferrooxidans*, regulates the kinetics of Fe(II) oxidation. The observed levels of CO_2 in the tailings vadose zone generally increase with depth from 0.2 to 6.5%, with maximum levels occurring where the O_2 profiles terminate, and the bacterial count is a maximum. The increase is presumed to be due to a buffering reaction ($CaCO_3 + 2H^+ = Ca^{2+} + H_2CO_3^*$), driven by the percolation of acidic porewaters. CO_2 availability does not appear to limit bacterial growth. Soil temperature measurements suggest that bacteria activity in the shallow soil zone may increase during hot summer days.

Pyrite alteration intensity decreases with depth. The near surface zone is strongly oxidized, indicated by the destruction of most pyrite and pyrrhotite with immature gossan[1] development. Principal alteration products are

---

[1]Gossan *(Mining)*. The oxidized upper portion of a vein of lode of sulphide minerals. Sometimes devoid of a $ value owing to the action of circulating water.

oxyhydroxides and sulfates. Underlying the heavily oxidized zone is an intermediate zone of weak alteration which is succeeded by a zone of negligible sulfide alteration. The bulk of the tailings sulfides have been unaffected by alteration. A hardpan formation is present in some areas, principally at the tailings dam but also elsewhere (phase III, p. 13).

By sulfide oxidation, Fe(II) and SO_4^{2-} concentrations are high (a maximum of 10 g/L) in the unsaturated zone -- highest in the intermediate alteration zone. Concentrations of other metals are also elevated in the unsaturated zone and follow a mobility order. The maximum concentrations of other metals are (in mg/L): Mn = 50, Zn = 250, Ni = 15, Co = 8.9, Pb = 5.1, Cu = 90, Cr = 4. Porewater electrical conductance (E_c) is very high in the unsaturated zone (37,000 μS/cm, Table D3.3). Low pH porewaters (< 4.0) are restricted to the upper zone of the tailings. As waters percolate, the pH is raised by H^+ consuming mineral-dissolution reactions (principally carbonate dissolution).

The pH at the water table is about 5 and at greater depths in the tailings the pH increases to 6 to 7. E_c is high at the water table (measured up to 25,000 μS/cm) and decreases to 2000 to 1000 μS/cm in the deeper tailings. Dissolved Fe(II) (and other metals) are generally high in the shallow saturated zone (Fe = 6 g/L max.) and decrease with depth (Fe = 50 to 100 mg/L). Sulfate concentrations also follow a similar trend. Iron precipitates from solution largely as ferric hydroxide ($Fe(OH)_3$; pK_s = 37.2) but also as siderite ($FeCO_3$; pK_s = 10.7). Geochemical calculations indicate favorable conditions for siderite formation deep in the tailings and siderite has been found in the tailings cores.

Acidity is produced at the seepage face where Fe(II) oxidizes to Fe(III) as oxygen becomes readily available and iron hydroxide precipitates, coating the bottom of the ditch

with a red sludge (pH < 4.0). Maximum concentrations are typically 2.5 g/L Fe_T (1.3 g/L Fe^{2+}), 2.5 mg/L Cu, 0.6 mg/L Pb, 8.0 mg/L Zn, 500 mg/L Ca, 800 mg/L Mg, and 7.5 g/L SO_4. Runoff from the tailings surface (north-end channel) has typical baseflow concentrations less than 10 mg/L Fe_T, 3.5 mg/L Fe^{2+}, 1 mg/L Cu, 0.2 mg/L Pb, 5 mg/L Zn, 400 mg/L Ca, 150 mg/L Mg, and 2000 mg/L SO_4. Within the acid treatment pond the pH is less than 3.5 and maximum concentrations are 1000 mg/L Fe and 50 mg/L Zn.

6.0 Investigative Methodology at Waite Amulet Tailings

The investigative methodology fundamentally centers on two items (Table 6.1): (1) continuous *in-situ* monitoring of soil-moisture potential and groundwater hydraulic head; and, (2) periodic manual measurements of soil-moisture content. Precipitation and evaporation data were also collected to characterize the soil/atmosphere hydrologic fluxes. These data were used to characterize the two surfaces with regard to the transient flow in the soil-water system (i.e., dynamics and quantitative changes).

Table 6.1. Methods of Measuring Hydrologic Parameters.

Soil Moisture Potential:	(1) Heat dissipation sensors, (2) Tensiometer, (3) Gypsum blocks.
Soil-moisture Content:	(1) Time-domain reflectometry, (2) Gravimetric.
Groundwater Hydraulic Head:	Pressure-transducer piezometry.
Precipitation:	Tipping-bucket rain gauge.
Evaporation:	U.S."Class A" evaporation pan.
Temperature:	(1) Soil temperature with thermocouples, (2) Air temperature with a thermistor.

Soil temperature measurements are measured in the heat dissipation method of soil-moisture potential measurement; although these temperature data ostensibly may be used in an energy balance (e.g., to measure soil evaporation), they were not directly used in this thesis study. This methodology would require the collection of other data (e.g., net solar radiation and sensible and latent heat fluxes) which is beyond the scope of this study. The temperature results, however, are explored in the discussion section.

6.1 Location of monitoring sites.

A network of piezometer nests remaining from previous hydrogeologic investigations scatter the tailings surface. Two cross sections are also located through the western half of the tailings from the groundwater divide to the western seepage collection ditch (Fig. 6.1). The cross sections were initially placed to calibrate the flownet modelling (Yanful *et al.*, 1989). The topography along the sections steps from the tailings top surface to benches lower in elevation.

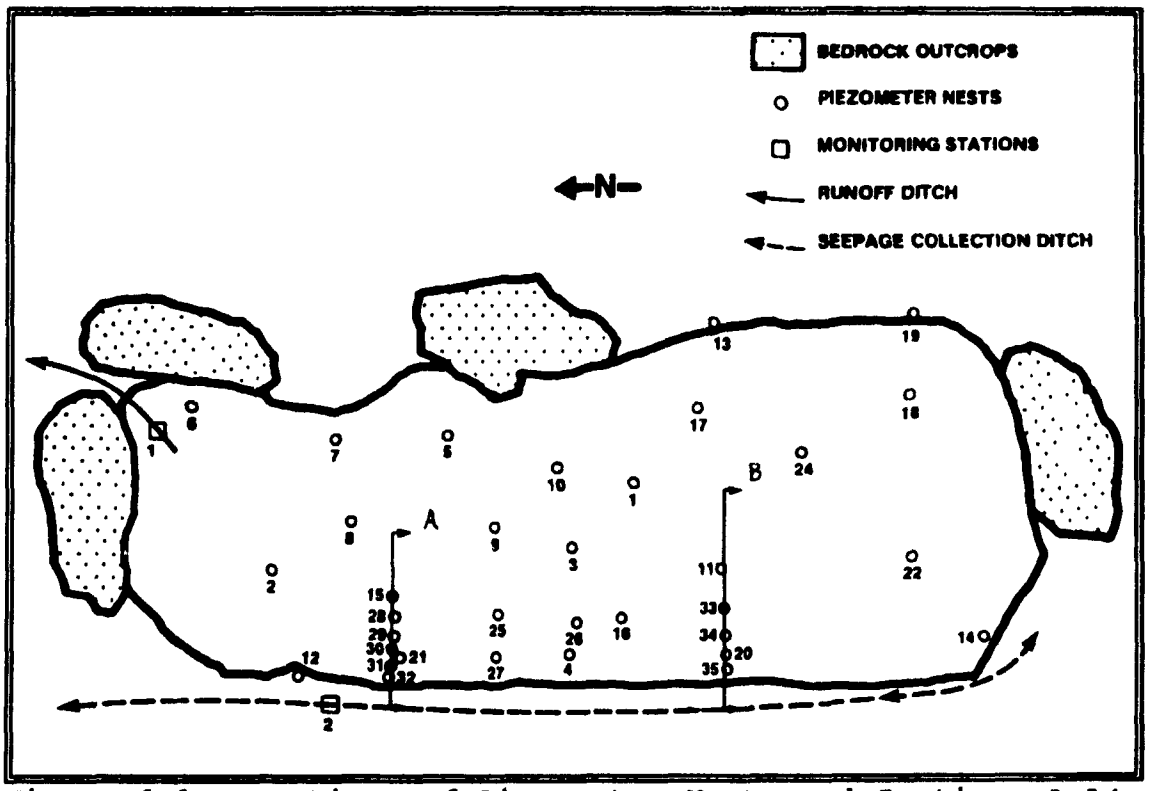

Figure 6.1. Locations of Piezometer Nests and Sections A-A′ and B-B′ at Waite Amulet (after Yanful *et al.*, 1990).

Section A-A′ (Fig. 6.2) was selected for this thesis study on the basis of its central proximity to a weir at surface water station #2 (ST2); although ST2 was not used in this study, it measured surface and seepage flow from the tailings during previous studies and may be subsequently employed. The selection of section A-A′ is also based on the defined westward tailings-water flow parallel to the section A-A′.

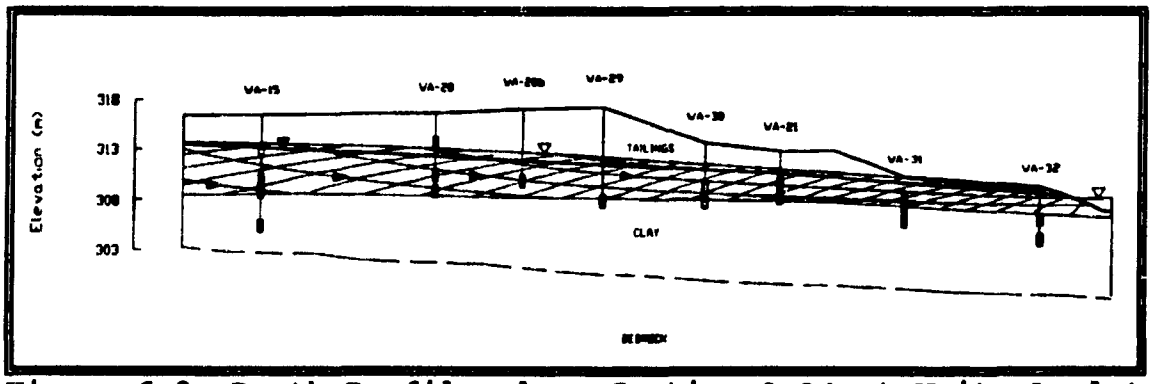

Figure 6.2. Depth Profile along Section A-A′ at Waite Amulet (after Yanful *et al.*, 1990).

At section A-A′, three vertical profile vadose-zone monitoring nests were located (Fig. 6.3): two on the tailings top surface (WA15) and one on the tailings bench (WA30). At WA15 the nest was located next to the piezometer nest in an open grass-legume field. The other nest was located in close proximity to the piezometer nest (approx. 15 m) in an aspen-birch grove established approximately 10 to 15 years ago. At WA30, the vadose-zone monitoring nest was located in a grass-legume field next to the piezometer nest.

Each vadose-zone monitoring nest was coupled with an existing piezometer nest in which groundwater hydraulic head was measured. A level survey was conducted to establish the elevations of the ground surface and of each uncapped piezometer top, from which periodic depth-to-water measurements were conducted. At each monitoring site,

groundwater hydraulic head and soil-water matric potential were measured once ever hour (employing a data logger) and soil-water content was manually measured at periodic intervals. Precipitation and evaporation measurements were conducted at ST1 (Fig. 5.2).

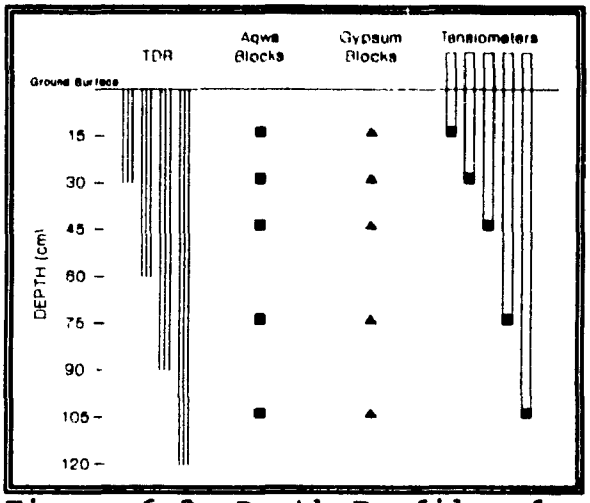

Figure 6.3. Depth Profile of Vadose-Zone Monitoring Nests, Waite Amulet.

6.2 Measurement of Soil-water Potential

Soil-water potential was measured by three methods which utilized: (1) heat dissipation sensors (i.e., agwa blocks), (2) tensiometers, and (3) gypsum blocks. Peltier thermocouple psychrometers were not used for several reasons: (1) their measurement time increases with increased soil-water potentials (higher sensor humidity), and may be up to several hours at -1 bar. They are therefore more appropriately used in warm dry climates; (2) the thermocouples within the sensor are exposed, offering a short sensor life in corrosive soil environments; and (3) they require an accurate measurement device and are therefore better coupled with data acquisition systems, than with inexpensive data-logging systems.

All of three sensors were installed with a inch diameter auger[1] at depths 15, 30, 45, 75, and 105 cm below the tailings surface. The bore hole was back-filled and packed with tailings and sealed at the surface with native clay.

---

[1]Insertion tool, 240 series, Soilmoisture Equipment Corp., Santa Barbara, CA, USA.

6.2.1 Heat Dissipation Sensors

Heat dissipation sensors measure matric potential over a wide range of values. They are independent of soil texture, temperature, and chemistry, capable of continuous monitoring by inexpensive data logging systems, and maintenance free. For these reasons, heat dissipation sensors were selected as the principal device for soil-water potential measurement.

The employed heat dissipation[1] sensor consisted of a 1 kohm miniature heater and a type T thermocouple encased in a inch by inch diameter porous ceramic. The measurement entailed (in sequence) a temperature measurement, the delivery of 10 volts for 60 seconds, and a second temperature measurement. The temperature rise is inversely proportional to soil-water potential.

Each heat dissipation sensor was individually calibrated by the manufacturer to 1 bar suction in a pressure plate apparatus (procedures similar to Fredlund and Wong, 1989); calibrations to higher suction values significantly increased the cost of each sensor. A 1 bar calibration, seemed adequate for a silty soil in a subpolar, subhumid, continental climate based on the soil-water characteristic for Waite Amulet tailings (Fig. 6.4a,b) and the climatic records (Table 5.1). Measurements greater than the reported inflection point of the calibration (i.e., 1.75 bars; Sattler and Fredlund, 1989), were expected to be few and only during summer dry spell. They were estimated with the use of the gypsum block measurements or by the general form of the published heat dissipation sensor calibration curves (Sattler and Fredlund, 1989); these values are considered less accurate.

---

[1]Agwa-II sensor, Agwatronics Inc., Merced, CA, USA.

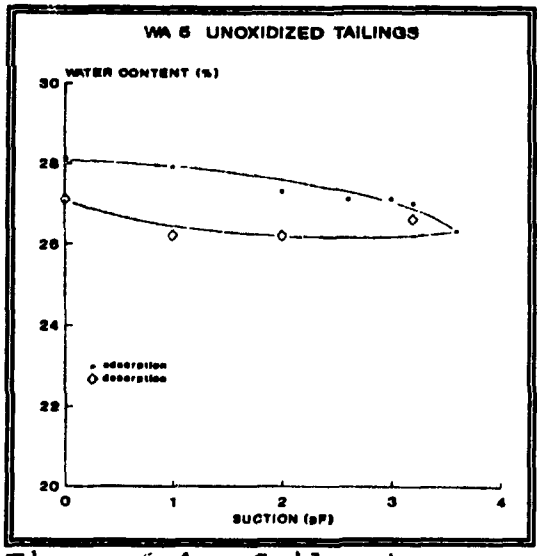

Figure 6.4a. Soil-water Energy Characteristic Curve near Piezometer Nest WA5 (after GRC, 1990).

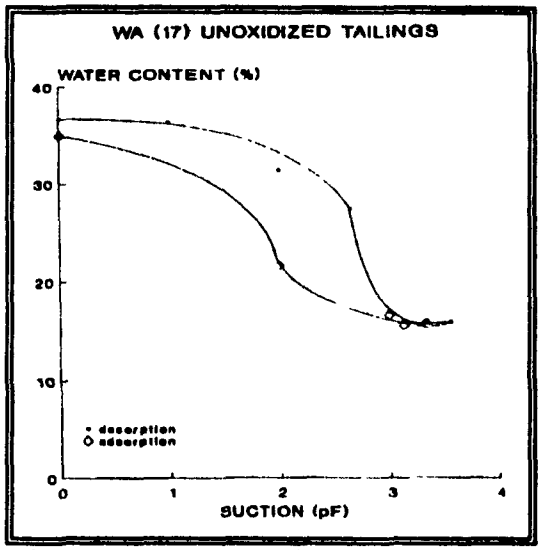

Figure 6.4b. Soil-water Energy Characteristic Curve near Piezometer Nest WA17 (after GRC, 1990).

6.2.2 Tensiometers

Tensiometers measure matric potential directly and were therefore used to validate measurements by the thermal conductivity blocks. The narrow suction range of the tensiometer (0 to 0.85 bars) is not expected to greatly limit its use at Waite Amulet. Each tensiometer[1] was each equipped with a pressure transducer[2] to facilitate automated measurement. The pressure transducer was attached with a reducing bushing (#B-4-RB-2). However, because tensiometers suffer from freezing air temperatures and are maintenance intensive, their reliability confines their use and an incomplete record of measurement was anticipated. The pressure transducers that were attached to the tensiometers were calibrated prior to installation.

---

[1]Model #2725 Series, Soilmoisture Equipment Corp., Santa Barbara, CA, USA.

[2]Model #PX180-015GV, -15 to 15 psig, Omega Engineering, Inc., Stamford, CT, USA.

6.2.3 Gypsum Blocks

Gypsum blocks are inexpensive probes which operate over a wide range of suction and are capable of automated measurement. They measure the electrical resistance within a block of gypsum which varies chiefly with the soil-water matric potential, but also with wide variations in soil chemistry. The electrical conductance (E_c) of tailings pore waters is reported to be high in the unsaturated zone, the actively oxidizing region (maximum 37,000 μS/cm, Appendix C8.3), and decreases in the deeper tailings chiefly by $Fe(OH)_3$ and $CaSO_4$ precipitation (1000 to 2000 μS/cm, Yanful *et al.*, 1989). The gypsum block measurements are, therefore, expected to vary with both soil-water potential and E_c. As a result, their purpose in the system design is to monitor a related trend, rather than absolute values of soil-water potential and E_c. Because of this coupling of ψ with E_c, the gypsum blocks were not calibrated to matric potential prior to installation, although a generalized calibration which is provided by the manufacturer was used to estimate the soil-water potential (Fig. 7.16b).

6.2 Measurement of Soil-water Content

Time-domain reflectometry (TDR), being independent of temperature and nearly independent of soil density, texture, and chemistry, was used to make repeated manual measurements of soil-water content. Occasional measurements of soil-water content by gravimetric method (Gardner, 1986) were also conducted to validate the TDR measurements.

At each monitoring nest, four vertical TDR soil transmission lines were installed: 30, 60, 90, and 120 cm in length. A horizontal placement of the transmission lines was not used because the installation requires trenching which disturbs the soil structural integrity. Each soil transmission line was a 3-rod design (Zegelin, 1989), but modified to accommodate budgetary constraints (Fig 6.5).

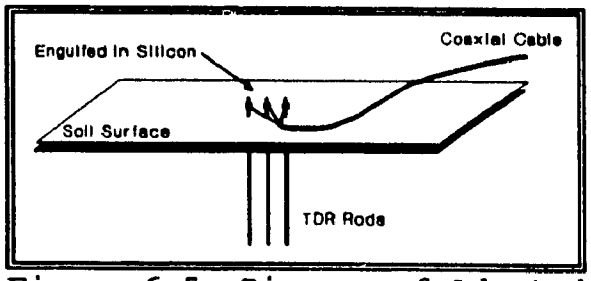

Figure 6.5. Diagram of Adapted 3-rod TDR Soil Transmission Line.

Stainless steel rods with rod-length dependent diameters (generally, 1/8 inch diameter by 30 cm length, 3/16 inch diameter by 60 cm length, and 1/4 inch diameter by 90 cm and greater length) were driven directly in the tailings with a guide to maintain an equal spacing of 3 cm. Approximately 1½ cm of each rod extended out from the tailings surface to which the coaxial cable was connected. The center conductor of the coaxial cable was connected to the center rod of the soil transmission line and the shield conductor of the coaxial cable was divided and connected to the two outside rods of the soil transmission line. Each conductor was connected to the rod with and aluminum fuse clip and secured with galvanized steel wire ties (Fig 6.5). The three contacts were emersed from the soil surface to the wire in one continuous body of silicon gel. At the other end of a 2 m 50 ohm coaxial cable (RG58/U; Beldon #8240) a BNC plug connected the cable to the TDR instrument. No balun is used with the 3-rod design.

6.3 Measurement of Groundwater Hydraulic Head

At each monitoring site a previously existing piezometer nest was utilized to measure hydraulic heads. At WA15 there are four piezometers: WA15-2 at 3.46 m depth, WA15-1 at 6.51 m depth, WA15-4 at 7.71 m depth, and WA15-3 at 10.22 m depth. The deepest piezometer (WA15-3) has a 1.2 m screened segment and is located at the base of the clay (½ m above bedrock), the other three piezometers have a 15 cm screened segment and are located in unoxidized tailings. At WA30 there are two piezometers, WA30-2 at 4.56 m depth and WA 30-1 at 6.06 m depth, with the deeper piezometer located

at the clay-tailings contact. Each piezometer was equipped with a submersible pressure transducer[1] and each pressure transducer was calibrated prior to installation. The pressure transducers were measured by a data logger once every hour and converted to pressure head meters of water units. Previously measured hydraulic conductivities for some of the piezometers are: $10^{-4.33}$ cm/s for WA15-1, $10^{-5.65}$ cm/s for WA15-4, and $10^{-4.07}$ cm/s for WA15-3.

Depth-to-water from the top of piezometer were periodically measured with a manually operated electronic water level meter to validate the pressure transducer measurements. The water level record for each piezometer was converted to hydraulic head (the base of the "V" of the weir at ST1 is elevation equal to zero).

6.4 Measurement of Temperature

Air temperature is typically measured in a standard National Weather Service type instrument shelter (i.e., cotton region type), with the bottom of the 0.3 m^3 ventilated white wooden shelter standing 1.22 m (4 ft) above the ground. Because of budgetary constraints, this type of shelter was not available. Air temperature was alternatively measured four feet above the ground in the aspen-birch grove at monitoring station WA15t; solar radiation exposure errors in the measurement were, therefore, limited. The measurement was made with a Fenwal Electronics UUT51J1 thermistor[2].

Tailings temperature was measured with type T thermocouples which were located in the thermal conductivity sensors. The thermocouple reference temperature at the data

---

[1]PDCR 830 Series, Druck Inc., New Fairfield, CT, USA.

[2]Model 107 temperature probe, Campbell Scientific Canada Corp., Edmonton, Alberta; corporate office, Logan, UT, USA.

logger wiring panel was measured with a Fenwal Electronics UUT51J1 thermistor.

6.5 Measurement of Precipitation and Evaporation

Precipitation and Evaporation were measured at ST1 (Fig. 5.2). Precipitation was measured with a tipping bucket rain gauge located in the center of a circular wind shield. Evaporation was measured in a US Weather Bureau Class A stainless steel evaporation pan placed on timber supports. Hourly measurements were recorded in data logger[1] memory.

6.6 Data Logger Configuration

Data logging monitoring systems[2] were installed at WA15 and WA30. Monitoring station WA15 measured two vadose zone nests (Fig. 6.3), one in the grass and the other in the trees (WA15g and WA15t), and the groundwater piezometer nest (WA15). Monitoring station WA30 measured a vadose zone nest and a groundwater piezometer nest. At each monitoring nest site the thermal conductivity sensors, gypsum blocks, pressure-transducer tensiometers, and pressure-transducer piezometers were measured once every hour. At WA15t air temperature was also measured every hour. The hourly measurements and daily averages of all data were recorded in data logger memory and on a back-up cassette tape.

---

[1]Lakewood Dataloggers, Edmonton, Alberta, Canada.

[2]Campbell Scientific Canada Corp., Edmonton, Alberta.

7.0 Presentation of the Results

The results of the soil-water monitoring are presented for the period September 13 through November 23, 1990, which characterizes the autumn season. Because of equipment delivery delays and laboratory testing and calibration, field activities did not begin until August 15, 1990. Four site visits were conducted: August 15-24, September 7-14, October 1-7, and November 19-23.

Table 7.1. Monitoring Period for each Parameter.

Aug 1 - Nov 23	Precipitation; Evaporation (no data).
Aug 17 - Nov 23	Pressure-transducer Tensiometers (no data).
Sep 13 - Nov 23	Air Temperature; Gypsum Blocks; Soil-water Content by TDR; Pressure-transducer Piezometers.
Oct 7 - Nov 23	Soil Temperature and Soil-water Potential by Heat Dissipation Sensors.
Oct 7 and Nov 23	Gravimetric Soil-water Content.

Monitoring started on September 13 with measurements of pressure-transducer piezometers, gypsum blocks, soil-water content by TDR, and air temperature. On October 7 measurements of soil temperature and soil-water potential from the heat dissipation sensors began. Pressure-transducer tensiometers were installed on August 17 but freezing air temperatures by early September dictated their removal; no useable data was obtained. Gravimetric soil-water content measurements were conducted on October 7 and November 23.

The climatic station at ST1 was installed in late July. The precipitation data is presented from August 1 through November 20. The evaporation-pan water-level sensor failed and no usable data was obtained.

7.1 Precipitation

Hourly totals (mm/hr) of precipitation at Waite Amulet were measured with a tipping bucket rain gauge, located at ST1 (Fig. 5.2), as per Section 6.5. From this station record, the daily precipitation totals during the period of study period (Table 7.2) are illustrated with the records of Val D'Or Airport (Fig. 7.1).

Table 7.2 Precipitation at Waite Amulet, 1990.

	AUG (mm)	SEP (mm)	OCT (mm)	NOV (mm)
1	0.0	2.6	0.6	0.0
2	0.0	0.0	0.6	0.0
3	0.0	0.0	8.4	1.8
4	15.0	2.6	1.2	0.0
5	4.2	0.0	0.0	0.0
6	1.0	2.6	0.0	0.0
7	15.2	0.0	0.0	0.0
8	0.0	0.0	0.0	0.0
9	0.0	9.4	0.0	0.0
10	1.2	0.0	23.4	0.0
11	0.0	12.0	0.0	0.0
12	0.0	0.2	0.0	0.0
13	0.0	2.4	0.0	0.2
14	2.2	8.4	5.0	10.0
15	0.0	0.0	5.0	8.0
16	9.6	0.0	9.4	2.0
17	1.0	0.0	1.0	0.0
18	0.0	0.8	17.4	0.0
19	0.0	4.2	0.0	0.4
20	0.0	0.2	7.4	0.0
21	0.0	28.4	7.6	-
22	0.0	3.0	0.0	-
23	0.0	4.2	0.0	-
24	0.0	4.4	0.0	-
25	0.0	0.2	0.0	-
26	7.8	0.0	0.0	-
27	0.0	0.0	21.0	-
28	0.2	0.0	0.0	-
29	1.4	5.0	0.8	-
30	0.0	11.0	0.4	-
31	1.0	-	0.0	-
TOTAL	59.8	101.6	109.2	22.4

Val D'Or Airport is located approximately 100 km east of Waite Amulet and is the synoptic station nearest in proximity to Waite Amulet. Val D'Or airport is not a stations from which an extended Waite Amulet record should be calibrated (Fig. 7.2) but the data was readily available, and the precipitation records from this station were used only as an index of daily snowfall and to summarize the regional monthly climate during 1990 (Table 7.3).

Table 7.3. Climatological Summary, Val D'Or Airport, 1990.

MONTH	AVERAGE DAILY TEMPERATURE (C) MEAN	AVERAGE DAILY TEMPERATURE (C) NORMAL	MAXIMUM DAILY TEMPERATURE (C) MEAN	MAXIMUM DAILY TEMPERATURE (C) NORMAL	MINIMUM DAILY TEMPERATURE (C) MEAN	MINIMUM DAILY TEMPERATURE (C) NORMAL	TOTAL PRECIPITATION (mm) TOTAL	TOTAL PRECIPITATION (mm) NORMAL	FRACTION AS SNOWFALL (%) MEAN	FRACTION AS SNOWFALL (%) NORMAL
January	-11.8	-16.8	-4.9	-10.9	-19.6	-22.7	64.4	60.1	83	94
February	-15.3	-14.9	-7.5	-8.6	-23.0	-21.2	59.8	50.7	96	96
March	-7.4	-8.3	-0.7	-1.9	-14.1	-14.6	45.0	59.0	40	75
April	2.1	0.9	8.0	6.6	-3.8	-4.9	60.4	50.9	72	43
May	8.5	8.8	15.3	15.4	1.7	2.2	51.8	63.8	7	6
June	14.8	14.6	20.8	21.2	8.9	8.0	124.6	93.9	-	-
July	17.2	17.1	23.3	23.3	11.1	10.8	123.6	101.5	-	-
August	16.3	15.5	22.7	21.4	9.8	9.6	86.6	101.1	-	-
September	9.1	10.4	14.3	15.8	4.0	5.1	153.0	107.4	4	1
October	3.5	4.6	8.0	9.0	-1.1	0.1	117.8	82.3	6	17
November	-2.9	-3.4	1.7	0.6	-7.5	-7.2	91.2	79.2	61	58
December	-11.8	-13.2	-5.2	-8.1	-18.4	-18.4	52.2	92.0	92	86
Annual	1.9	1.3	8.0	7.0	-4.3	-4.4	1030.4	941.9	28	31

Note: Normal 1951-1980

7.2 Air and Soil Temperature

Air temperature at Waite Amulet was measured at monitoring station WA15t in the aspen-birch grove, as per Section 6.4. The results of the hourly measurements encompass the period from September 13 through November 20 (Fig. 7.3). Hourly measurements of tailings temperature were conducted form October 7 through November 20 and were measured in the heat dissipation sensors at 15, 30, 45, 75, and 105 cm below the surface (see Section 6.1.1).

The temperature dynamics below the tailings surface are illustrated with the associated air temperature and precipitation. The temperature conditions below the tailings surface (WA15) is depicted with two vegetative covers: WA15g which is vegetated with a grass-legume cover (Fig. 7.4a), and at WA15t which is covered with an aspen-birch grove (Fig 7.4b). A similar figure depicts the temperature conditions below the surface of the tailings bench (WA30), vegetated with a grass-legume cover (Fig. 7.4c).

7.3 Soil-water Content

Soil-water content was measured several times during the study period by TDR method with soil transmission line lengths of 30, 60, 90, and 120 cm, as described in Section 6.2. At all three monitoring sites (WA15g, WA15g, and WA30) only transmission line lengths of 30 and 60 cm produced a TDR trace from which soil-moisture content was calculated (Table 7.4). The values for monitoring sites WA15g and WA30, the grass-legume sites, are depicted along with the climatic conditions (Fig. 7.5a,b). TDR soil-water content values for WA15t were fewer and are illustrated with all of the measured values (Fig. 7.6).

Table 7.4. Calculation of Soil-moisture Content by Time-domain Reflectometry Method.

SITE	DATE	TDR [a] DEPTH (cm)	TDR PROBE LENGTH (cm)	ONEWAY TRAVEL TIME (nsec)	DIELECTRIC [b] CONSTANT (K)	TDR [c] WATER CONTENT (θvb)
WA15g	23 Nov.	0-30	28.5	4.69	24.37	39.71
		0-60	60.5	11.73	33.83	47.96
		30-60	32.0	7.04	43.56	54.73
	07 Oct.	0-30	28.5	4.29	20.39	35.19
		0-60	60.5	10.72	28.26	43.45
		30-60	32.0	6.43	36.34	49.77
	06 Oct.	0-30	28.5	4.41	21.55	36.59
		0-60	60.5	10.87	29.05	44.15
		30-60	32.0	6.46	36.68	50.01
	04 Oct.	0-30	28.5	4.45	21.94	37.04
		0-60	60.5	10.95	29.48	44.51
		30-60	32.0	6.50	37.13	50.33
	03 Oct.	0-30	28.5	4.32	20.68	35.54
		0-60	60.5	10.65	27.89	43.12
		30-60	32.0	6.33	35.22	48.98
	14 Sept.	0-30	28.5	3.77	15.75	28.80
	12 Sept.	0-30	28.5	3.87	16.59	30.07
		0-60	60.5	9.03	20.05	34.76
		30-60	32.0	5.16	23.40	38.68
	07 Sept.	0-60	60.5	8.45	17.56	31.45
WA15t	23 Nov.	0-30	25.0	4.03	23.39	38.66
		0-60	61.0	10.49	26.62	41.94
		30-60	36.0	6.46	28.98	44.08
	07 Oct.	0-30	25.0	3.39	16.55	30.00
		0-60	61.0	9.20	20.47	35.29
		30-60	36.0	5.81	23.44	38.72
	06 Oct.	0-30	25.0	3.28	15.49	28.41
		0-60	61.0	9.22	20.56	35.40
		30-60	36.0	5.94	24.50	39.85
WA30	23 Nov.	0-30	28.5	4.52	22.64	37.84
		0-60	60.5	9.42	21.82	36.90
		30-60	32.0	4.90	21.10	36.06
	07 Oct.	0-30	28.5	4.39	21.35	36.36
		0-60	60.5	8.95	19.70	34.31
		30-60	32.0	4.56	18.28	32.44
	06 Oct.	0-30	28.5	4.28	20.30	35.07
		0-60	60.5	9.11	20.41	35.21
		30-60	32.0	4.83	20.50	35.33
	04 Oct.	0-30	28.5	4.38	21.26	36.24
		0-60	60.5	9.16	20.63	35.48
		30-60	32.0	4.78	20.08	34.80
	03 Oct.	0-30	28.5	4.30	20.49	35.31
		0-60	60.5	8.96	19.74	34.37
		30-60	32.0	4.66	19.09	33.52
	14 Sept.	0-30	28.5	3.49	13.50	25.20
		0-60	60.5	7.24	12.89	24.16
		30-60	32.0	3.75	12.36	23.24
	12 Sept.	0-30	28.5	3.35	12.43	23.37
		0-60	60.5	7.20	12.75	23.92
		30-60	32.0	3.85	13.03	24.40
	07 Sept.	0-30	28.5	2.94	9.58	18.02
		0-60	60.5	6.65	10.87	20.53
		30-60	32.0	3.71	12.10	22.77

a/ Two 3-rod TDR transmission lines, 30 and 60 cm long probes, were used and the depth segment from 30 to 60 cm was calculated with the difference in the two travel times.

b/ $K = (c * t[sec] / L[m])^2 = (30 * t[nsec] / L[cm])^2$
where, c = (0.3 E9) m/sec = 30 cm/nsec
L = length of transmission lines
t = signal one-way travel time.

c/ Soil-Water Content $(\theta_{vb}) = (4.3\ E\text{-}6) * K^3 - (5.5\ E\text{-}4) * K^2 + 0.0292 * K - 0.053$

Table 7.5. Depths of Tailings Oxidized/Unoxidized Interface.

Site	Bore Hole	Date (1990)	Depth (cm)
WA15g	Gravimetric water content	07 Oct.	35
WA15g	Gravimetric water content	16 Nov.	36
WA15g	Tensiometer, 75 cm.	17 Aug.	40
WA15g	Tensiometer, 105 cm.	17 Aug.	45
WA15g	Gypsum blocks, 75 & 105 cm.	17 Aug.	45
WA15t	Gravimetric water content	07 Oct.	49
WA15t	Gravimetric water content	16 Nov.	37
WA15t	Heat dissipation sensor, 75 cm.	11 Sept.	55
WA15t	Heat dissipation sensor, 105 cm.	11 Sept.	65
WA15t	Gypsum blocks, 75 & 105 cm.	11 Sept.	50
WA30	Gravimetric water content	07 Oct.	45
WA30	Gravimetric water content	16 Nov.	60
WA30	Heat dissipation sensor, 75 cm.	10 Sept.	45
WA30	Gypsum block, 105 cm.	10 Sept.	56

Measured from bore holes of gravimetric water content cores and instrument probe installation.

TDR measurements employing the longer transmission lines (90 and 120 cm) produced a signal trace on which the transmission-line end-point (T_2) was not discernible; the TDR signal attenuated in the soil prior to the transmission line end and no end reflection returned to the TDR instrument. TDR transmission lines of 20 cm (maximum 30 cm) seems appropriate in actively oxidizing tailings. Because the tailings oxidized-unoxidized zone contact is at approximately 50 cm depth (Table 7.5), soil-water content measurements by TDR are chiefly of the oxidized zone. Oxidized tailings apparently support longer transmission lines, suggesting a lower electrical conductivity above the actively oxidizing front.

Gravimetric measurements[1] of tailings-water content were conducted at close proximity to the TDR transmission line on October 7 and November 23. Table 7.6 shows these measurements with measurements of water content by TDR

[1]Gravimetric soil-water content (θ_{dw}) measures the mass of water present in a soil sample per unit mass of the sample after it has dried to a constant weight. TDR measures the volume of water present in a unit volume of soil sample (θ_{vb}). Soil bulk density (D_b) is the mass of the dry sample per unit volume of wet soil sample. The water density (D_w) is the mass of water per unit volume of water, which is typically taken as 1 g/cm^3.

$$\theta_{dw}\left(\frac{D_b}{D_w}\right) = \theta_{dw} D_b - \theta_{vb}$$

Table 7.6. Soil-moisture Content Measurements (θ) and Corresponding Measurements of Soil-moisture Potential (Ψ).

Site	Date (1990)	Time	Depth (cm)	TDR[a/] θ_{vb} (%)	Gravimetric θ_{vb} (%)	Probe Depth (cm)	Gypsum Block Output (Ω)	Gypsum Block Ψ[b/] (cm)	Aqwa-II Output (ΔT)	Aqwa-II Block Ψ[c/] (cm)
WA15g	07 Oct	1300	0-30	35.2	35.6	15	170	-320	3.25	-620
			0-60	43.4	40.0	30	150	-300	1.89	-540
			30-60	49.8	44.3	45	140	-290	3.36	-720
			60-90	d	43.2	75	1770	-1160	3.04	-950
			90-120	d	35.5	105	1070	-880	3.74	-1680
	23 Nov	1100	0-30	39.7	39.0	15	180	-330	2.91	-140
			0-60	48.0	47.4	30	170	-320	1.77	-80
			30-60	54.7	55.9	45	210	-360	3.01	-110
			60-90	d	45.4	75	1290	-980	2.80	-500
			90-120	d	36.8	105	680	-690	3.50	-1310
WA15t	07 Oct	1300	0-30	30.0	32.4	15	190	-340	3.01	-510
			0-60	35.3	34.9	30	250	-400	3.21	-940
			30-60	38.7	37.4	45	230	-380	3.34	-750
			60-90	d	35.9	75	310	-450	2.29	-910
			90-120	d	34.9	105	190	-340	4.00	-1800
	23 Nov	1100	0-30	38.7	36.2	15	290	-230	2.83	-30
			0-60	41.9	39.9	30	190	-340	1.85	-260
			30-60	44.1	43.5	45	180	-330	2.97	-40
			60-90	d	34.2	75	200	-350	2.62	-180
			90-120	d	39.5	105	190	-340	3.48	-1270
WA30	07 Oct	1300	0-30	36.4	35.7	15	210	-360	2.73	-270
			0-60	34.3	31.8	30	210	-360	4.47	-580
			30-60	32.4	27.8	45	200	-350	4.33	-1450
			60-90	d	13.0	75	580	-630	2.42	-450
			90-120	d	9.4	105	220	-370	3.52	e
	23 Nov	1100	0-30	37.8	35.3	15	200	-350	2.61	-100
			0-60	36.9	37.3	30	200	-350	4.47	-570
			30-60	36.1	39.4	45	250	-400	3.81	-690
			60-90	d	15.6	75	150	-300	2.25	-140
			90-120	d	19.2	105	110	-250	3.34	e

a/ The 30-60 depth value was calculated with the difference in ΔT values of the 0-30 and 0-60 TDR measurements.

b/ Gypsum block matric pressure head values were calculated from the sensor resistance and using a generalized correlation which is provided by the manufacture for agricultural purposes (Fig. 7.16d).

c/ Thermal conductivity sensor matric pressure head values were calculated from the temperature rise measurement (ΔT) with a correlation specific to each sensor (Appendix D2).

d/ The TDR energy was attenuated at tailings depth with the 0-90 and 0-120 transition probes, resulting in a trace with no indication of the probe end (i.e., T2).

e/ Thermal conductivity block calibration of ΔT to Ψ was inappropriate which resulted in a positive pressure head value.

method and Soil-moisture content by electrical resistivity and heat dissipation methods. Because gravimetric measurement units are per unit weight, tailings bulk density[1] values were also calculated from the gravimetric samples (Appendix C1). The bulk density values were used to calculate the gravimetric soil-water content values in volumetric units (Appendix C2), to facilitate comparison

[1]Bulk density (D_b) is defined as the ratio of the mass to the "bulk" or macroscopic volume of soil particles plus the space in a sample (Blake, 1986). Also called dry density, the mass is determined after drying to a constant weight at 105°C, and the volume is that of the sample as taken in the field.

with the TDR values. The bulk density depth profiles for the three monitoring sites are illustrated with the logged tailings bore-hole descriptions (Fig. 7.7a,b,c). The gravimetric tailings-water content depth profiles for the two sampling days at the three monitoring sites are illustrated with the corresponding TDR measurements (Fig. 7.8a..f).

The gravimetric tailings-water content at the specific TDR transmission line depth locations (i.e., 0-30 and 30-60 cm) were calculated (Appendix C3) to facilitate the comparison of the two methods (Table 7.6). The relation of gravimetric soil-water content to TDR soil-water content, delineated by probe depth (Fig. 7.9a) and by monitoring site (Fig. 7.9b), portrays a good fit. A statistical analysis of the data (Appendix C5) qualifies the soil-water content measurements by TDR method.

7.4 Soil-water Potential

Hourly soil-water matric potential measurements were conducted with heat-dissipation sensors at the three monitoring sites (WA15g, WA15t, and WA30) and at depths 15, 30, 45, 75, and 105 cm below the tailings surface, as described in Section 6.2. Measurements begin on October 7. The results are plotted with the air temperature and precipitation for the period October 7 through November 20 (Fig. 7.10a,b,c). Very few matric potential measurements were beyond the reported inflection at 1.75 bars.

All data is presented as pressure head and not as hydraulic head in order to illustrate the data with reference to tension free conditions (ψ_m=0) present at the water table. Units of hydraulic head were used to present the piezometric data, with zero elevation located at the base of the "V" of the weir at ST2. The presentation of the soil-water matric potential data in this format, however, complicated the temporal plot (providing a "busy"

illustration) which detracted from the intent of data analysis. The data is plotted as units of hydraulic head, however, are illustrated as depth profile plots (Fig. 7.11a..f) on the two days that gravimetric soil-water content measurements were conducted (Oct.7 and Nov.23), at the commencement and termination of the soil-water potential monitoring.

Table 7.7 shows the values of pressure, elevation, and hydraulic head at the 3 depth profiles on October 7 and November 23. The piezometric hydraulic head data is

Table 7.7. Groundwater Unsaturated Zone Head Values at Waite Amulet at the Time of Soil-moisture Content Measurements.

DATE (1990)	SITE	PROBE	HEAD[a/]	UNITS	GROUND SURFACE	15 cm DEPTH	30 cm DEPTH	45 cm DEPTH	75 cm DEPTH	105 cm DEPTH
07 OCT	WA15G	AGWA-II	ELEVATION	m	8.85	8.70	8.55	8.40	8.10	7.80
			PRESSURE	cm	-	-620	-540	-720	-950	-1680
			HYDRAULIC	m	-	2.50	3.15	1.20	-1.40	-9.00
		GYPSUM	ELEVATION	m	8.85	8.70	8.55	8.40	8.10	7.80
			PRESSURE	cm	-	-320	-300	-290	-1160	-880
			HYDRAULIC	m	-	5.50	5.55	5.50	-3.50	-1.00
	WA15T	AGWA-II	ELEVATION	m	9.00	8.85	8.70	8.55	8.25	7.95
			PRESSURE	cm	-	-510	-940	-750	-910	-1800
			HYDRAULIC	m	-	3.75	-0.70	1.05	-0.85	-10.05
		GYPSUM	ELEVATION	m	9.00	8.85	8.70	8.55	8.25	7.95
			PRESSURE	cm	-	-340	-400	-380	-450	-340
			HYDRAULIC	m	-	5.45	4.70	4.75	3.75	4.55
	WA30	AGWA-II	ELEVATION	m	5.90	5.75	5.60	5.45	5.15	4.85
			PRESSURE	cm	-	-270	-580	-1450	-450	b
			HYDRAULIC	m	-	3.05	-0.20	-9.05	0.65	b
		GYPSUM	ELEVATION	m	5.90	5.75	5.60	5.45	5.15	4.85
			PRESSURE	cm	-	-360	-360	-350	-630	-370
			HYDRAULIC	m	-	2.15	2.00	1.95	-1.15	1.15
23 NOV	WA15G	AGWA-II	ELEVATION	m	8.85	8.70	8.55	8.40	8.10	7.80
			PRESSURE	cm	-	-140	-80	-110	-500	-1310
			HYDRAULIC	m	-	7.30	7.75	7.30	3.10	-5.30
		GYPSUM	ELEVATION	m	8.85	8.70	8.55	8.40	8.10	7.80
			PRESSURE	cm	-	-330	-320	-360	-980	-690
			HYDRAULIC	m	-	5.40	5.35	4.80	-1.70	0.90
	WA15T	AGWA-II	ELEVATION	m	9.00	8.85	8.70	8.55	8.25	7.95
			PRESSURE	cm	-	-30	-260	-40	-180	-1270
			HYDRAULIC	m	-	8.55	6.10	8.15	6.45	-4.75
		GYPSUM	ELEVATION	m	9.00	8.85	8.70	8.55	8.25	7.95
			PRESSURE	cm	-	-320	-340	-330	-350	-340
			HYDRAULIC	m	-	5.65	5.30	5.25	4.75	4.55
	WA30	AGWA-II	ELEVATION	m	5.90	5.75	5.60	5.45	5.15	4.85
			PRESSURE	cm	-	-100	-570	-690	-140	b
			HYDRAULIC	m	-	4.75	-0.10	-1.45	3.75	b
		GYPSUM	ELEVATION	m	5.90	5.75	5.60	5.45	5.15	4.85
			PRESSURE	cm	-	-350	-350	-400	-300	-250
			HYDRAULIC	m	-	2.25	2.10	1.45	2.15	2.35

a/ The datum (z=0) is the base of "V" of the weir at surface water station #2 (elev.= 307.114 m).

b/ Thermal conductivity block calibration was in appropriate which resulted in a positive pressure head value.

presented in meters of water, and the matric pressure data is presented in cm of water (pF is also common).

7.5 Groundwater Hydraulic Head

There are several piezometers located along cross section A-A'. Their tip and top elevations, in addition to the elevations of the water levels which were measured during the study, are located in Appendix C6. Of these, only piezometer nests WA15 and WA30 were continuously monitored, as discussed in Section 6.3.

There are four piezometers located at WA15. During the period of study, September 13 through November 20, three of the four piezometers were monitored, the shallowest (WA15-2) being dry. The complete temporal record is plotted to illustrate both the hydraulic head and elevation head of the screened piezometric intervals at WA15 (Fig. 7.12a). A similar illustration for the piezometric data at WA30 are presented for the period October 7 through November 20 (Fig. 7.12b). Figures 7.13 and 7.14 detail the fluctuations of hydraulic head at WA15 by reducing the y-axis.

7.6 Gypsum Block Resistance

Hourly measurements of gypsum blocks were conducted at all three monitoring sites (WA15g, WA15t, and WA30) at depths 15, 30, 45, 75, and 105 cm below the tailing's surface, as described in Section 6.1.3. The gypsum block resistance during the monitoring period, September 13 through November 20, is illustrated with the air temperature and precipitation data (Fig. 7.15a,b,c).

Gypsum blocks measure the coupled influence of both the soil-water matric potential and the electrical conductance of the soil water. If electrical conductance remains constant, then matric potential can be estimated. In this case, a generalized calibration which relates soil suction to the resistance of the gypsum block (Fig. 7.16a) may be

utilized. The relation was developed for agricultural purposes where the wilting point is generally taken as 15 bars suction, and field capacity as ⅓ bar suction. During moist conditions, which prevail at Waite Amulet, the calibration can be represented by a power relation (Fig. 7.16b) which was developed from the manufacturer's calibration (Fig. 7.16a). This relation, however, looses credibility at soil-moisture states much above field capacity, as noted by the calculated suction of a saturated gypsum blocks[1].

In actively oxidizing tailings, the gypsum block electrical resistance is not independent of the soil-water electrical conductance (Table 7.8). The electrical conductance of saturated gypsum (of the gypsum block) is calculated at 3,850 µS/cm. Thus, the sensors may be used with the generalized relation to measure soil suction in soils with an electrical conductance approximately equal to, and less than, 4,000 µS/cm. At Waite Amulet, the calculated electrical conductance of the unsaturated unoxidized tailings pore water is 37,400 µS/cm, roughly an order of magnitude larger the electrical conductance of saturated gypsum. The soil,

Table 7.8. Comparison of Gypsum Block Resistance and the Electrical Conductance of Related Substances.

(1) Electrical Conductance of Distilled Water at Saturation with Gypsum (Appendix C8.1):	1200 µS/cm
(2) Electrical Conductance of Saturated Gypsum Used in Gypsum Blocks (Appendix C8.2):	3850 µS/cm
(3) Electrical Conductance of Unsaturated-Zone pore-waters of the Waite Amulet Unoxidized Tailings (Appendix C8.3):	37,400 µS/cm
(4) Electrical Resistance of Gypsum Blocks Saturated with De-ionized water (n=42, S=20.1 Ω):	82.6 Ω
(5) Electrical Resistance of Gypsum Blocks Saturated with a Solution Similar to that of the Unsaturated Zone Pore Waters of Waite Amulet Tailings (Appendix C8.4):	8.5 Ω

[1]Forty-two gypsum blocks were saturated with (soaked in) distilled water which was at saturation with gypsum. The mean of the measured resistance was 82.6 Ω with a standard deviation of 20.1 Ω. The calculated suction using the power relation (Fig. 7.16b) is 215 cm water (0.2 bars). The saturated resistances of the gypsum blocks installed at Waite Amulet appear in Appendix D3.4.

however, is unsaturated and will therefore exhibit a lower electrical conductance than that of a soil saturated with water at similar solute concentrations (i.e., pore-water conductivity), more similar to the electrical conductance reported at the water table, which varies widely up to 25,000 µS/cm. Nevertheless, in actively oxidizing tailings pore waters generally fluctuate in solute concentration and the generalized calibration curve will likely underestimate the soil suction. The calculations supporting these values are located in Appendix C8.

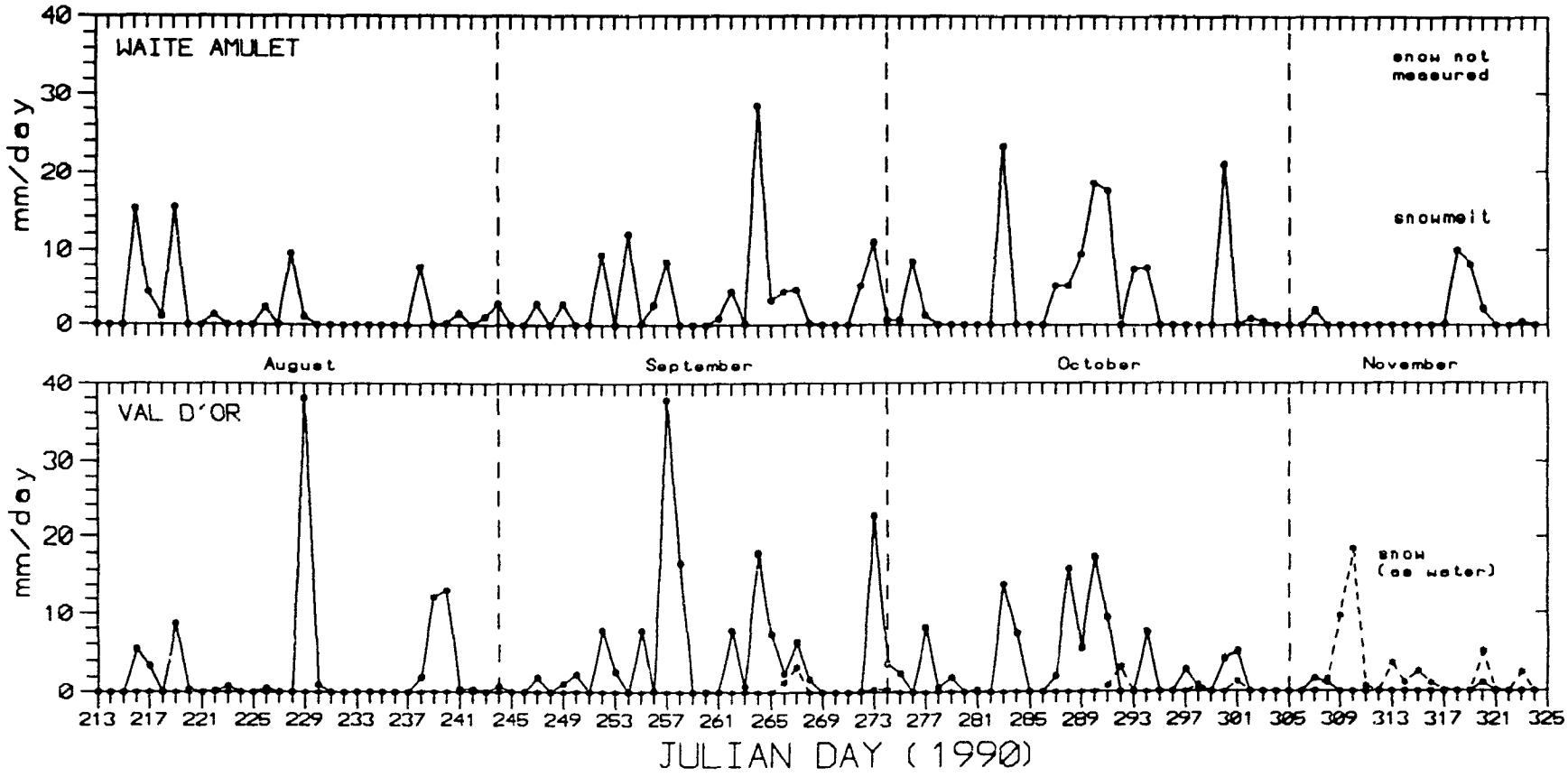

Figure 7.1. Precipitation at Val D'Or Airport and Waite Amulet During the Period of Study, Aug 1 – Nov 21, 1990.

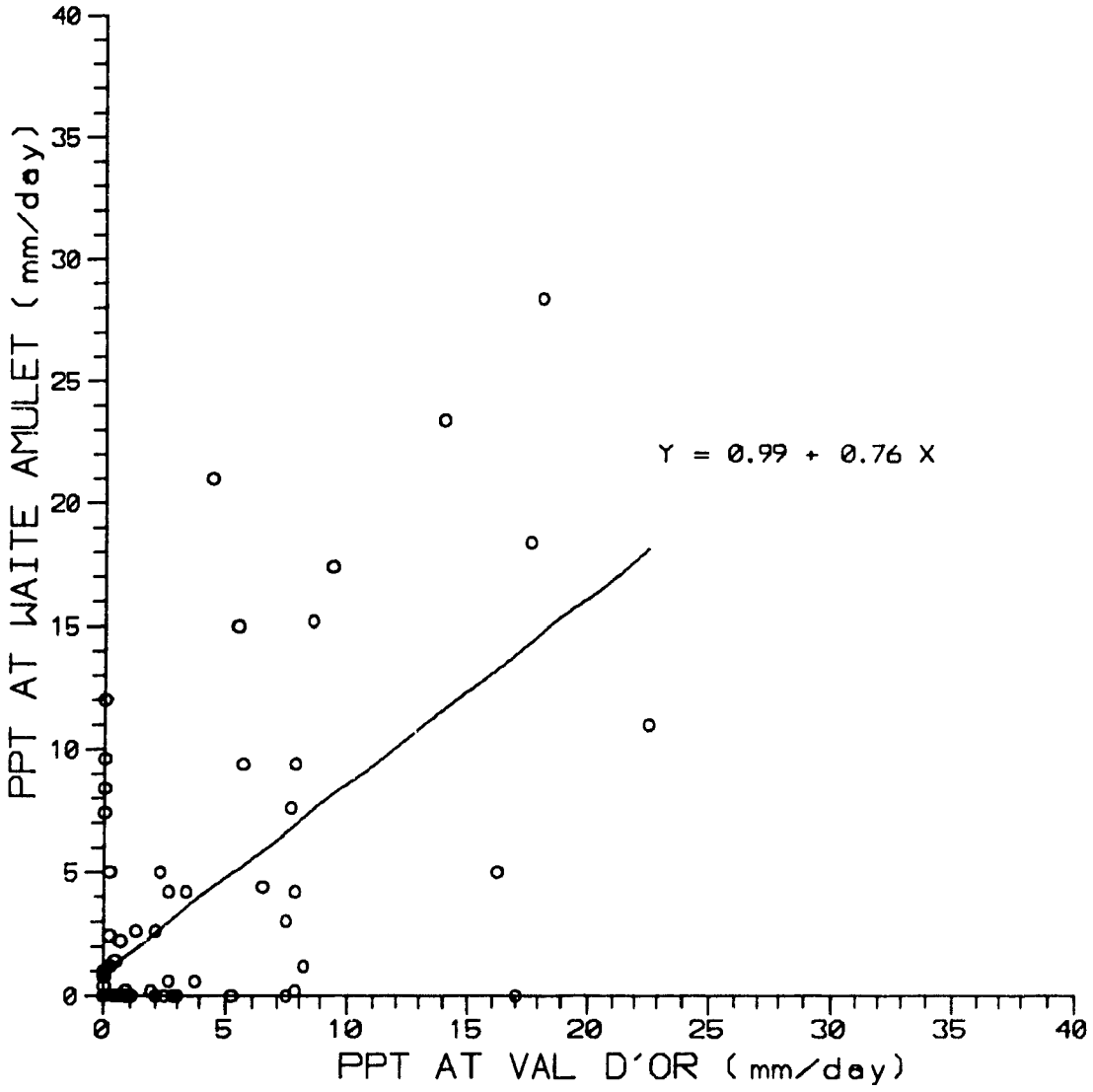

Figure 7.2. Daily Total Rainfall Relation, August, September, and October 1990, Excluding Thunderstorms.

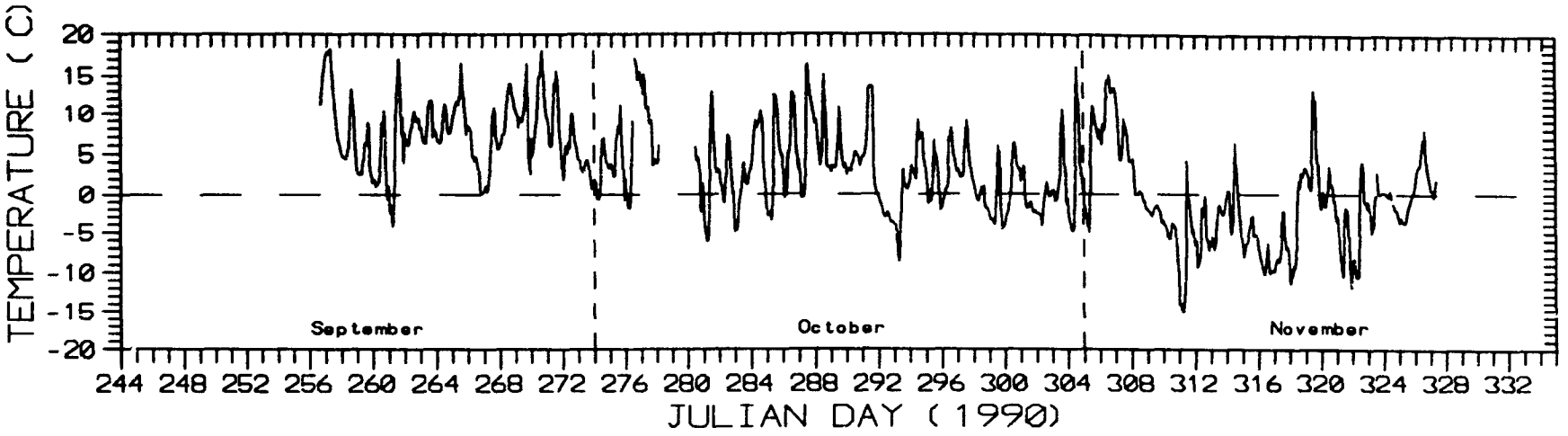

Figure 7.3. Air Temperatures in an Aspen/Birch Grove on Waite Amulet Tailings during the Period of Study.

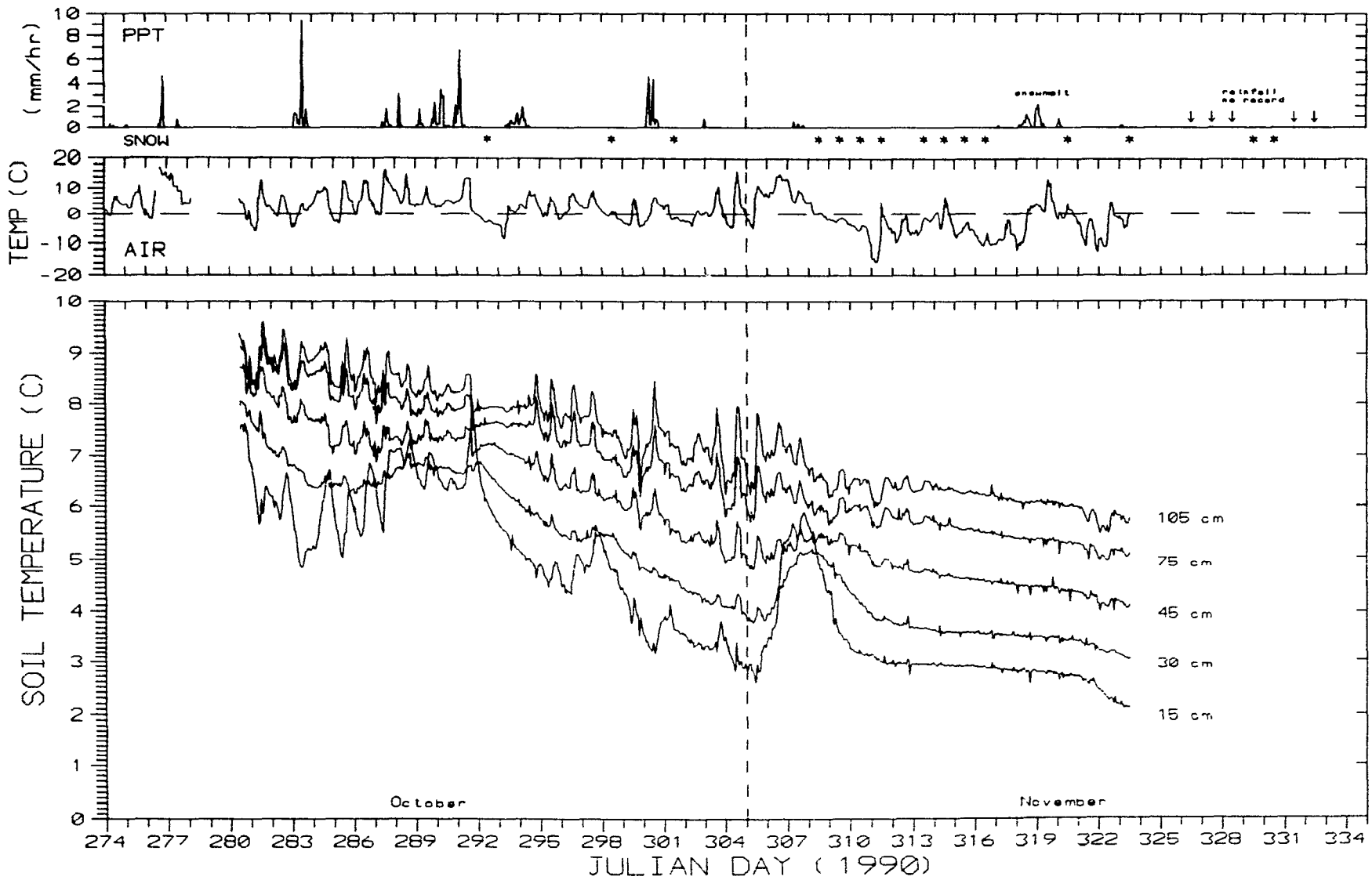

Figure 7.4a Soil Temperatures at Instrumentation Nest WA15g

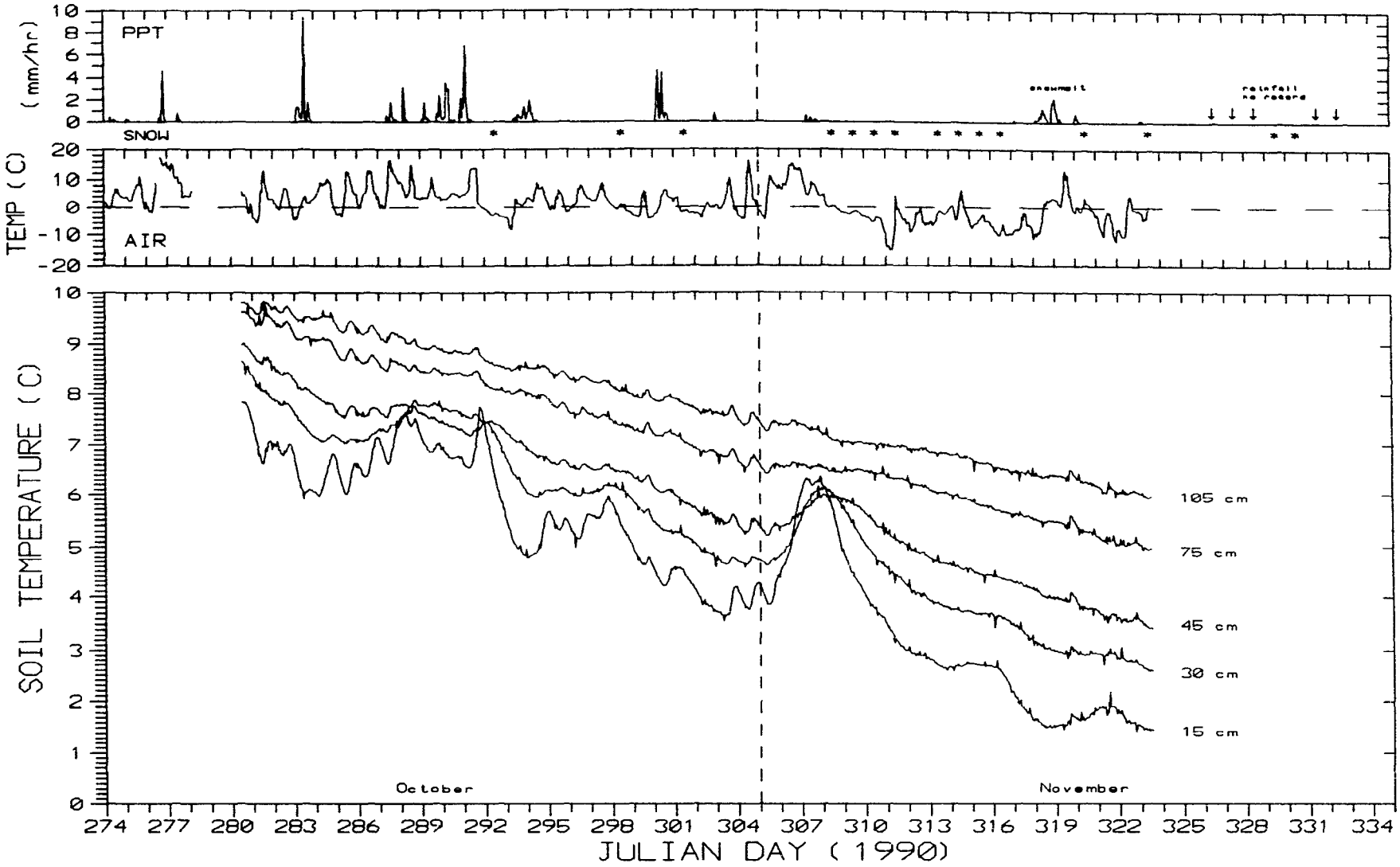

Figure 7.4b. Soil Temperatures at Instrumentation Nest WA15t.

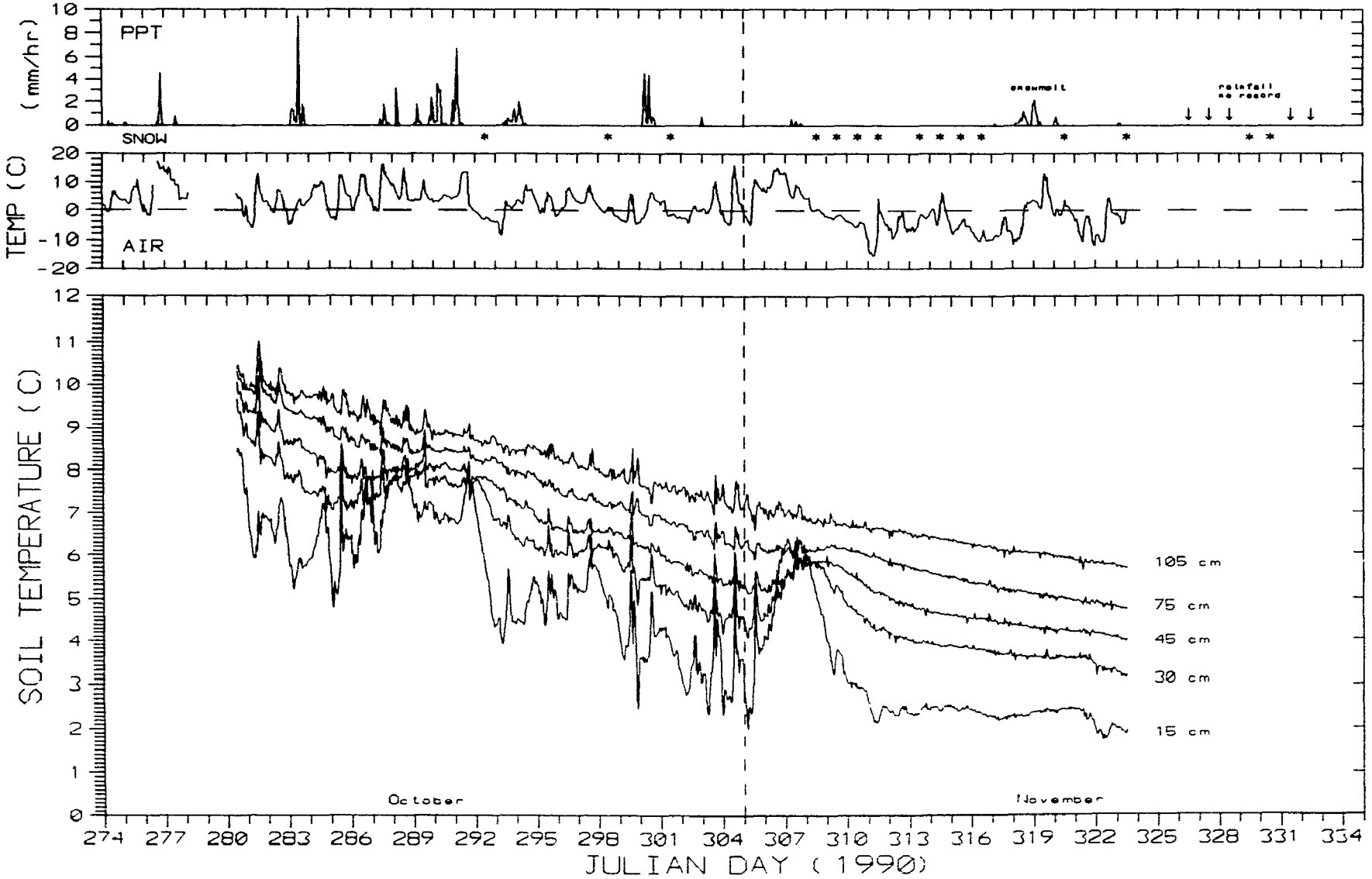

Figure 7.4c Soil Temperatures at Instrumentation Nest WA30.

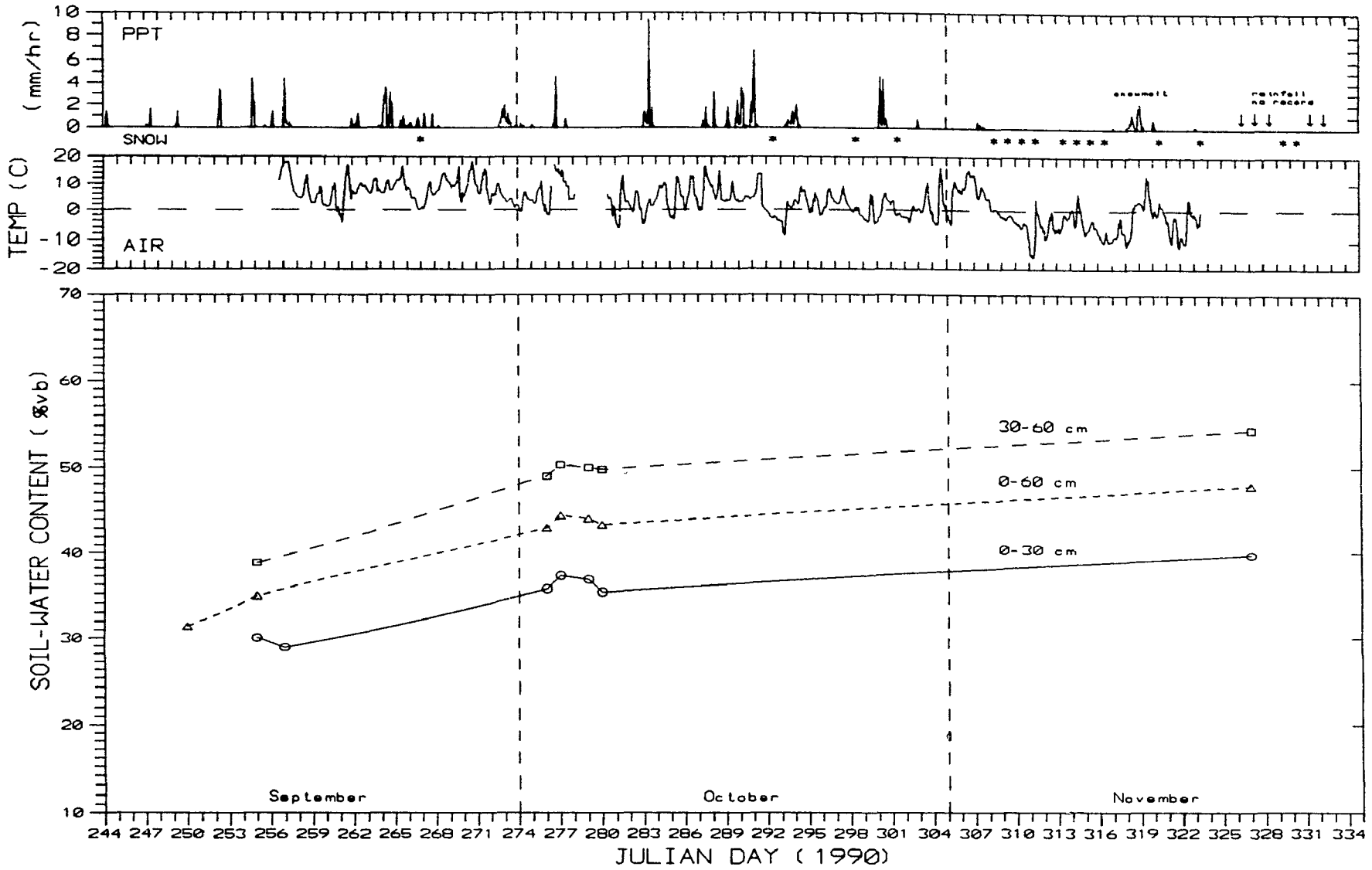

Figure 7.5a. Soil-moisture Content by TDR Method at WA15g.

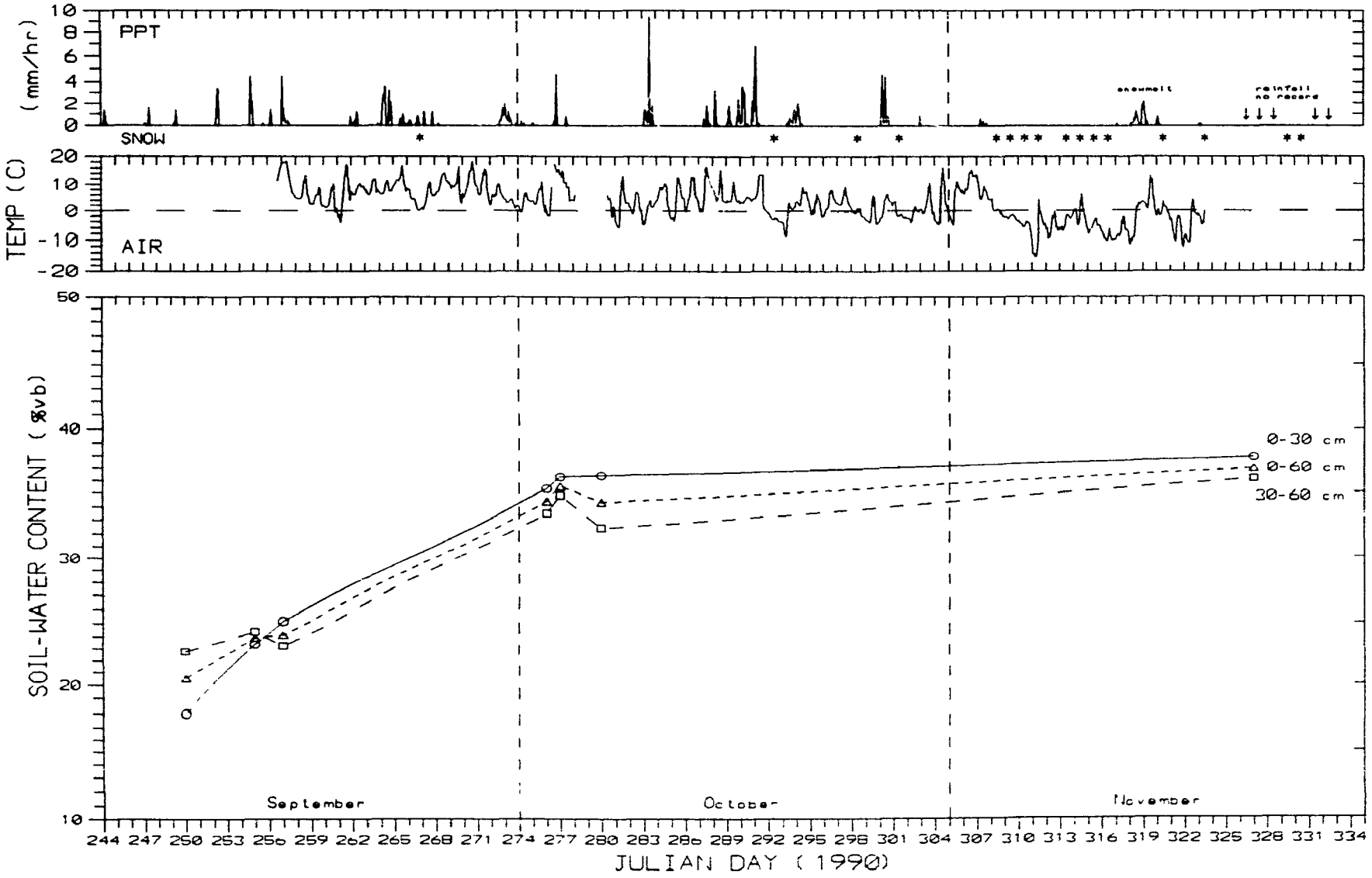

Figure 7 5b. Soil-moisture Content by TDR Method at WA30

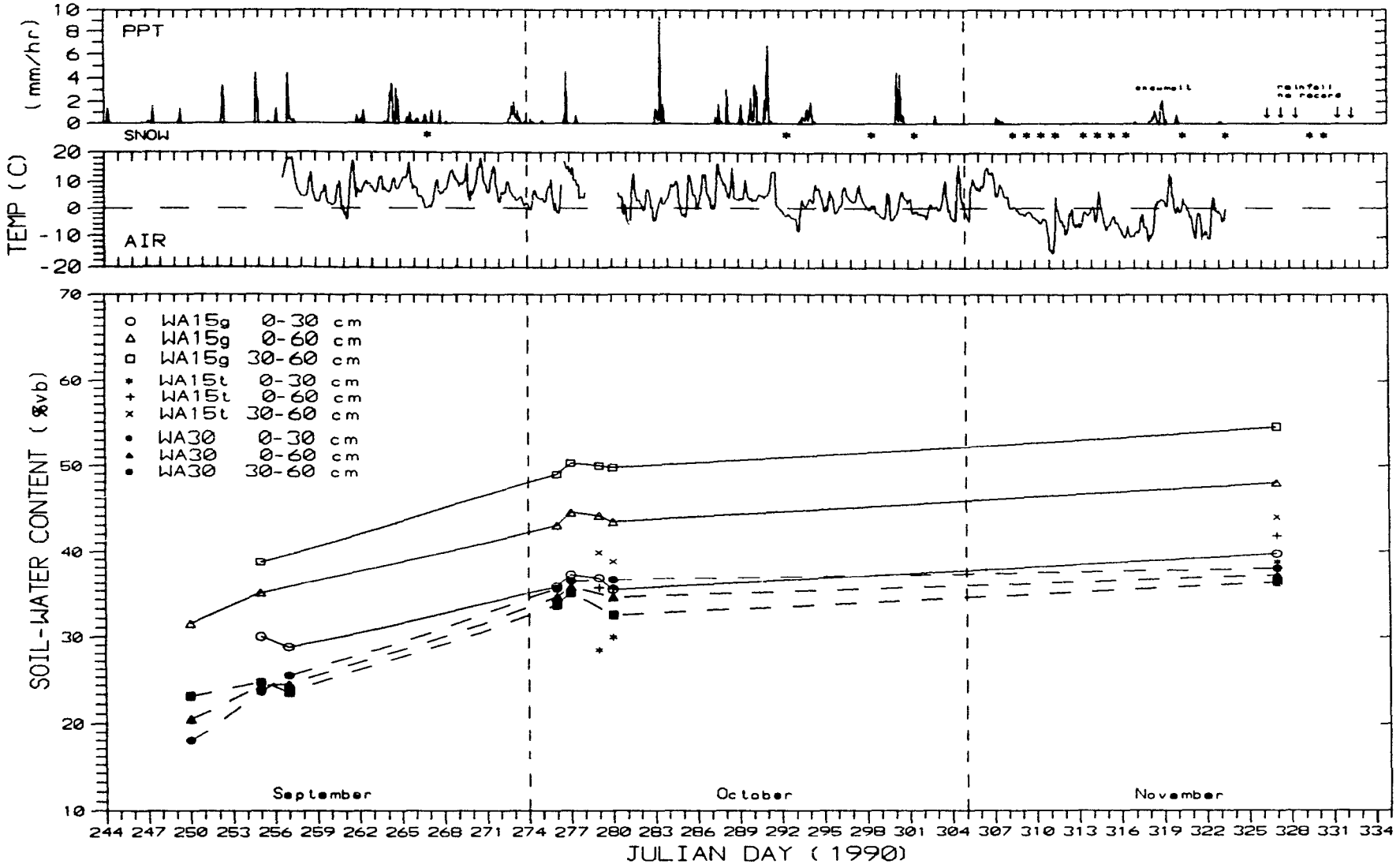

Figure 7.6. Soil-moisture Content by TDR Method at Waite Amulet.

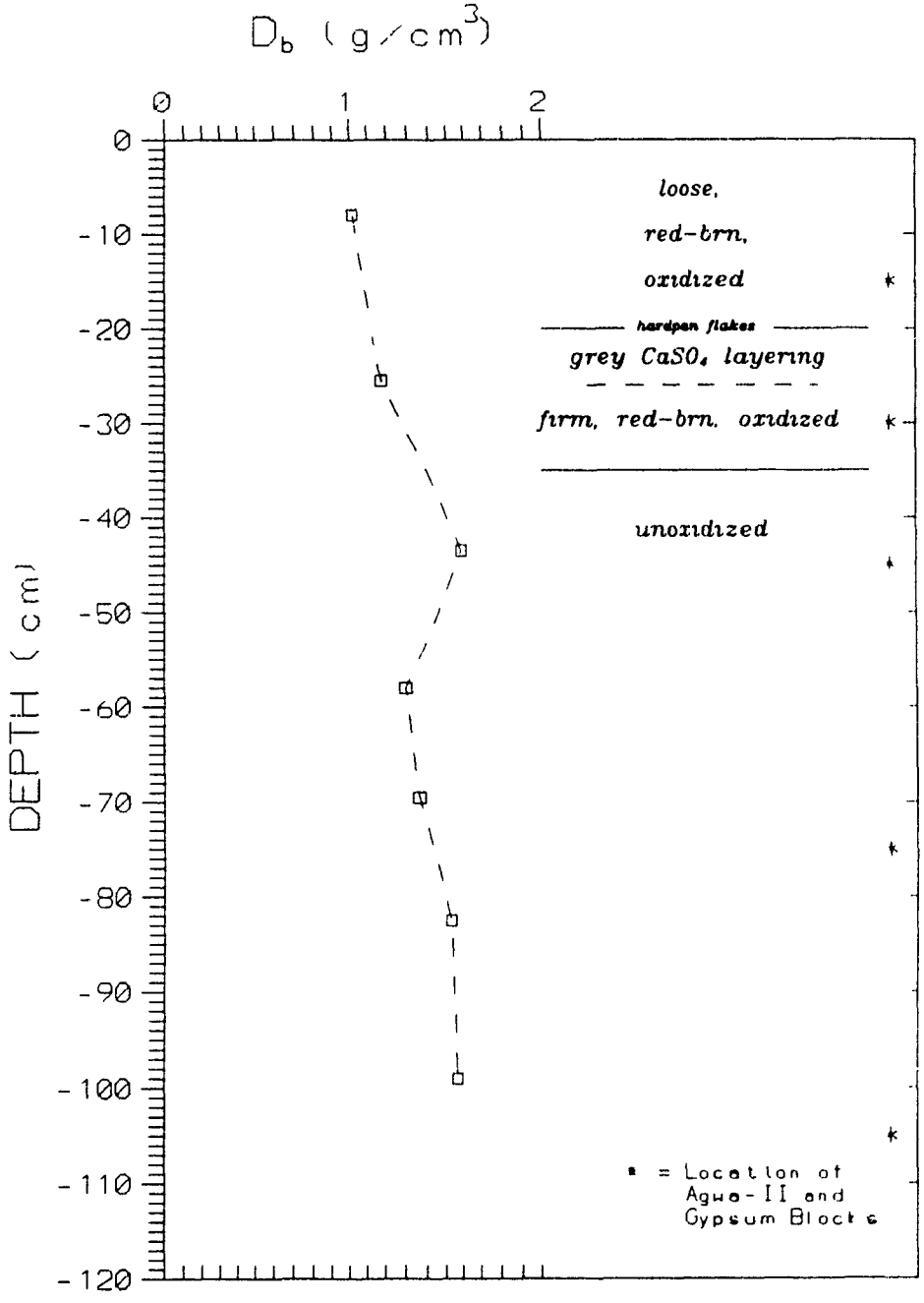

Figure 7.7a.
Bulk Density Measurements of Waite Amulet Tailings at WA15g taken on 7 October 1990.

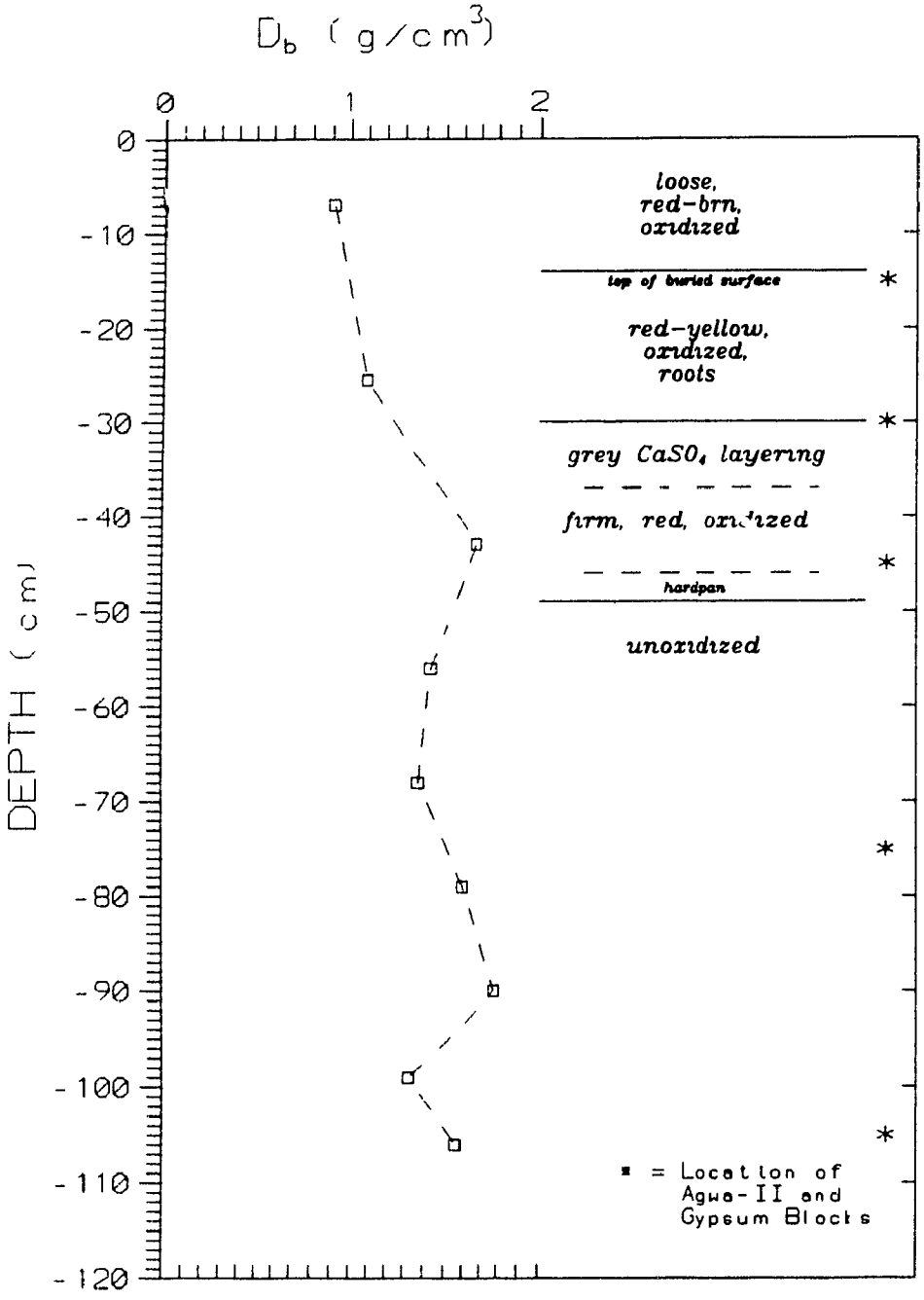

Figure 7.7b.
Bulk Density Measurements
of Waite Amulet Tailings at WA15t
taken on 7 October 1990.

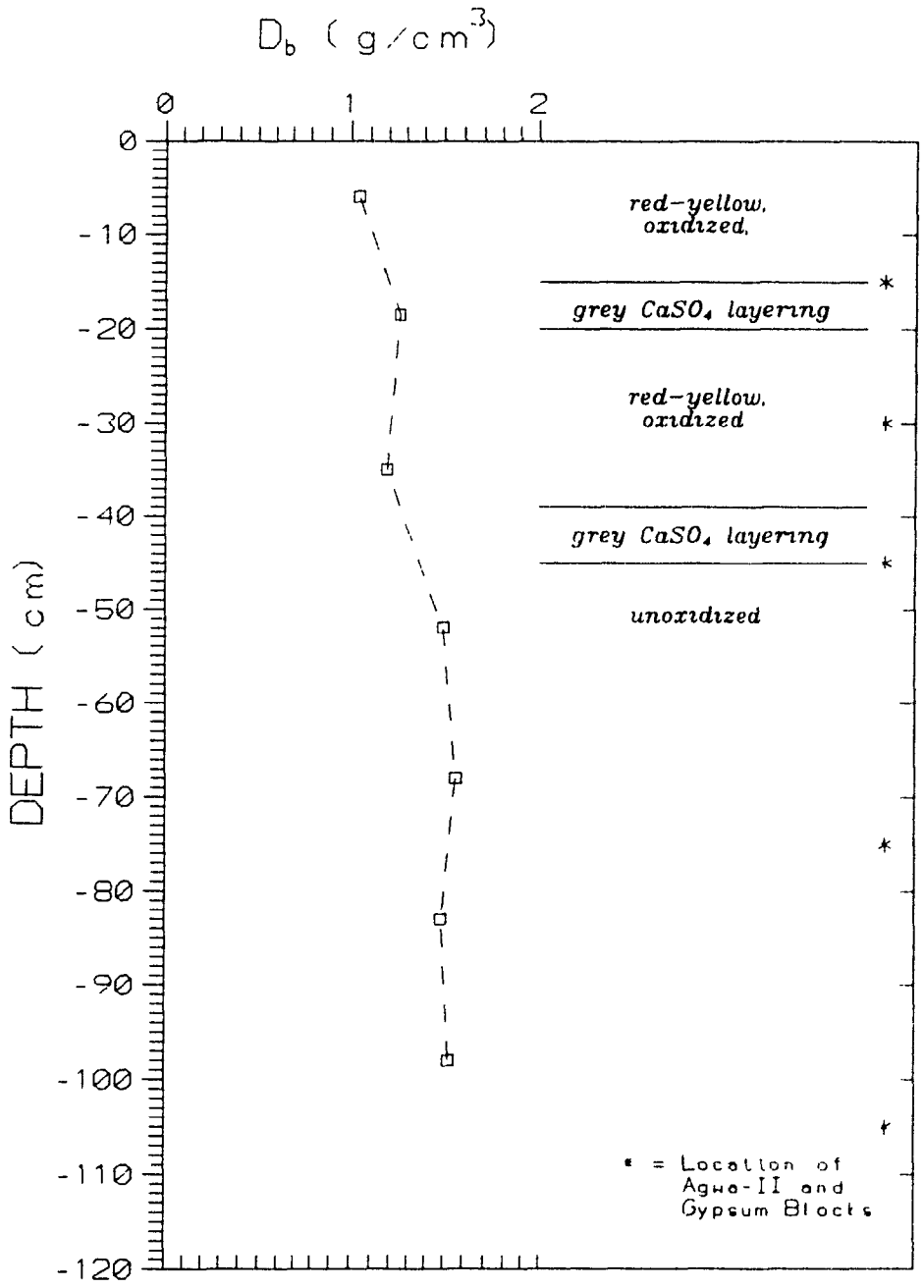

Figure 7.7c.
Bulk Density Measurements of Waite Amulet Tailings at WA30 taken on 7 October 1990.

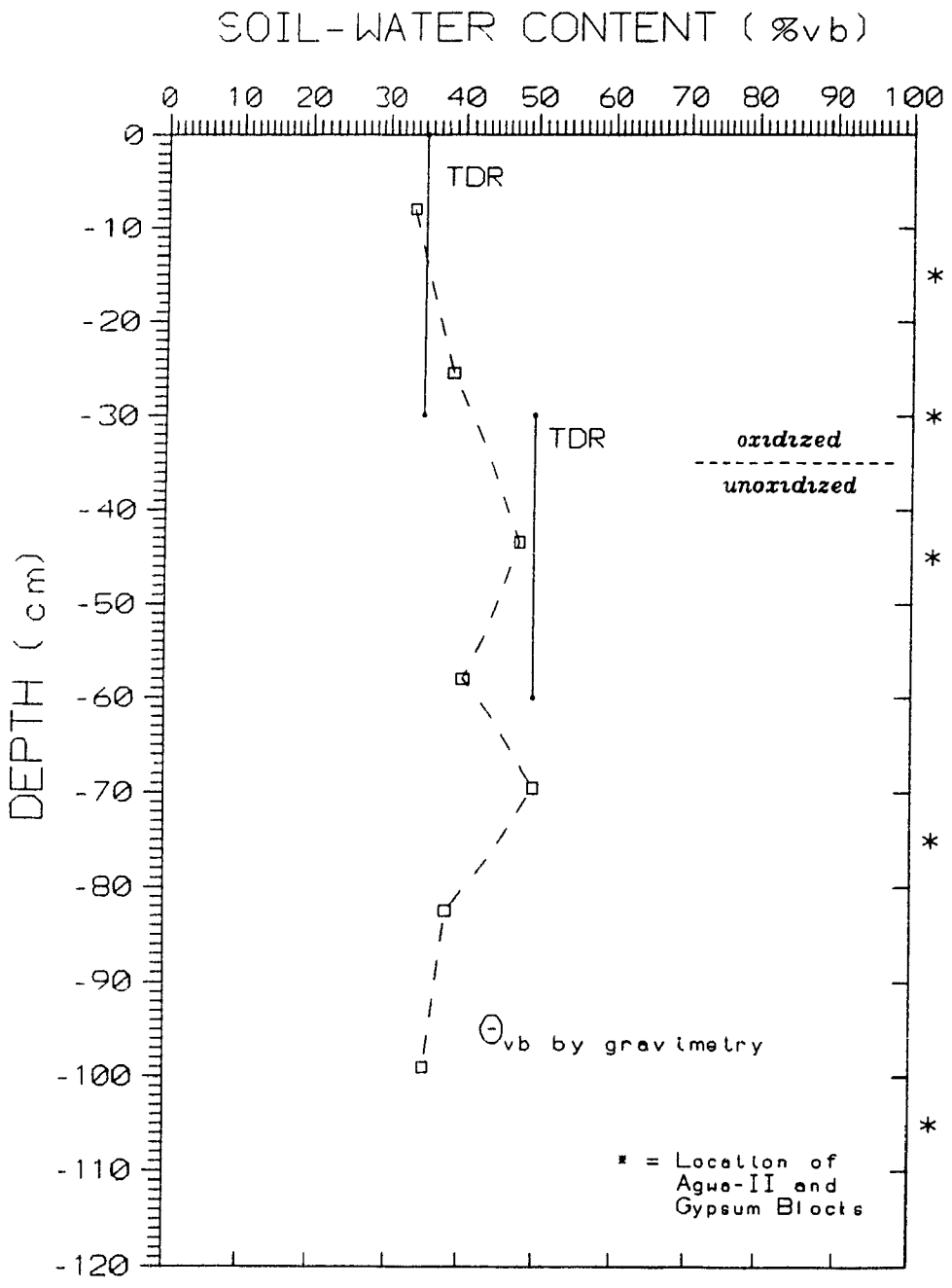

Figure 7.8a.
TDR and Gravimetric Soil-water Content Measurements of Waite Amulet Tailings at WA15g, taken on 7 October 1990.

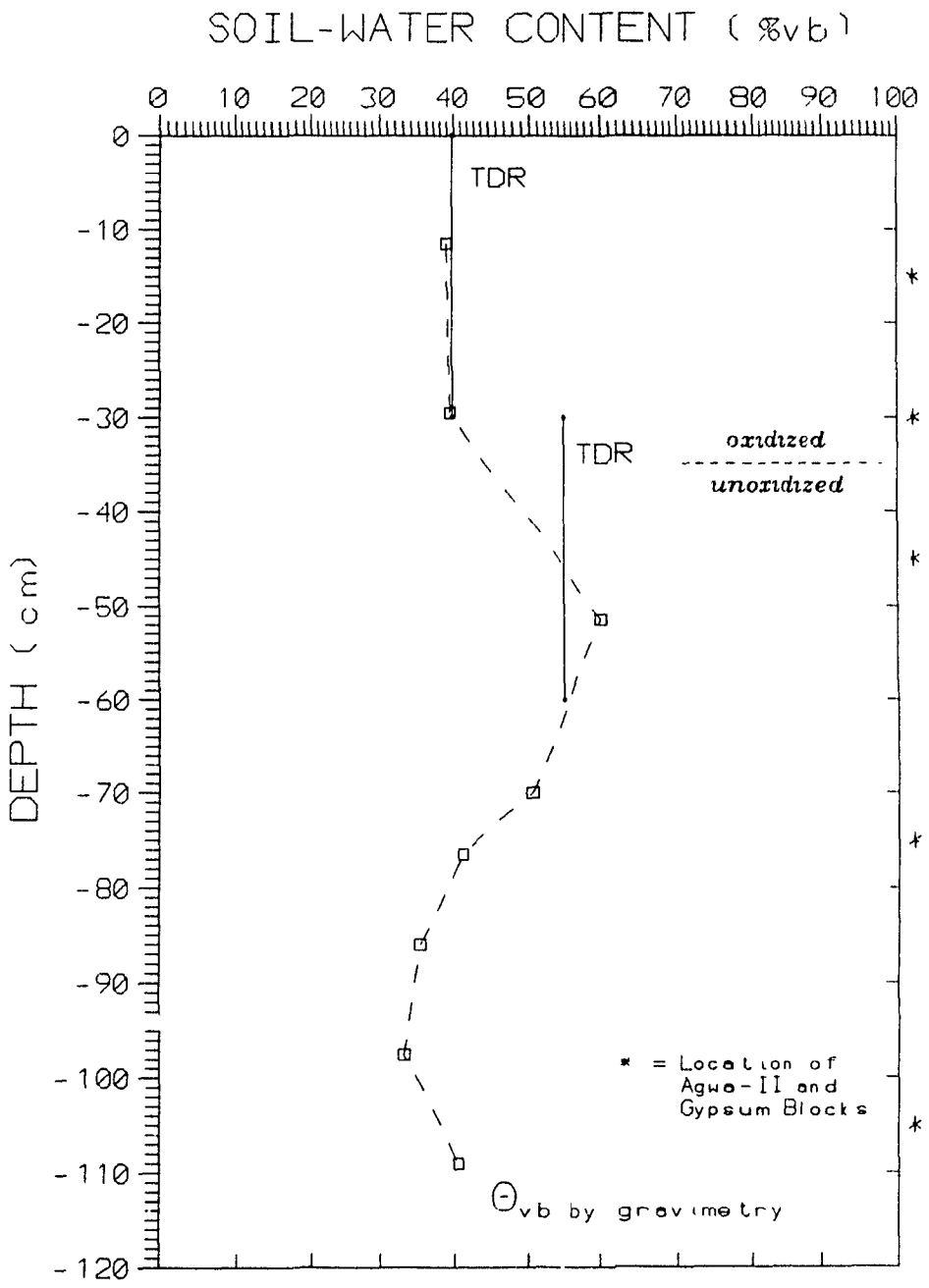

Figure 7.8b.
TDR and Gravimetric Soil-water Content Measurements of Waite Amulet Tailings at WA15g, taken on 23 November 1990.

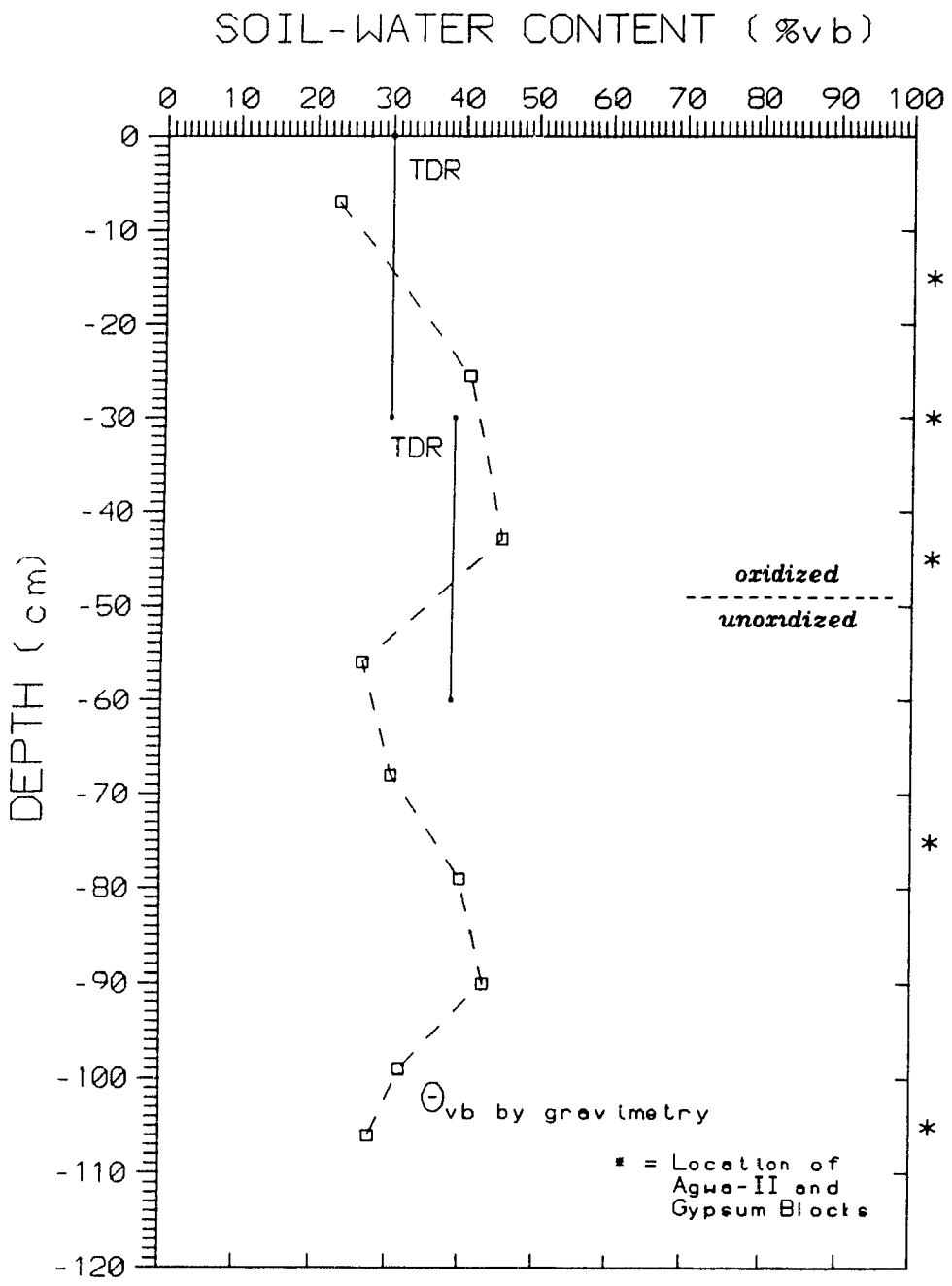

Figure 7.8c.
TDR and Gravimetric Soil-water Content Measurements of Waite Amulet Tailings at WA15t, taken on 7 October 1990.

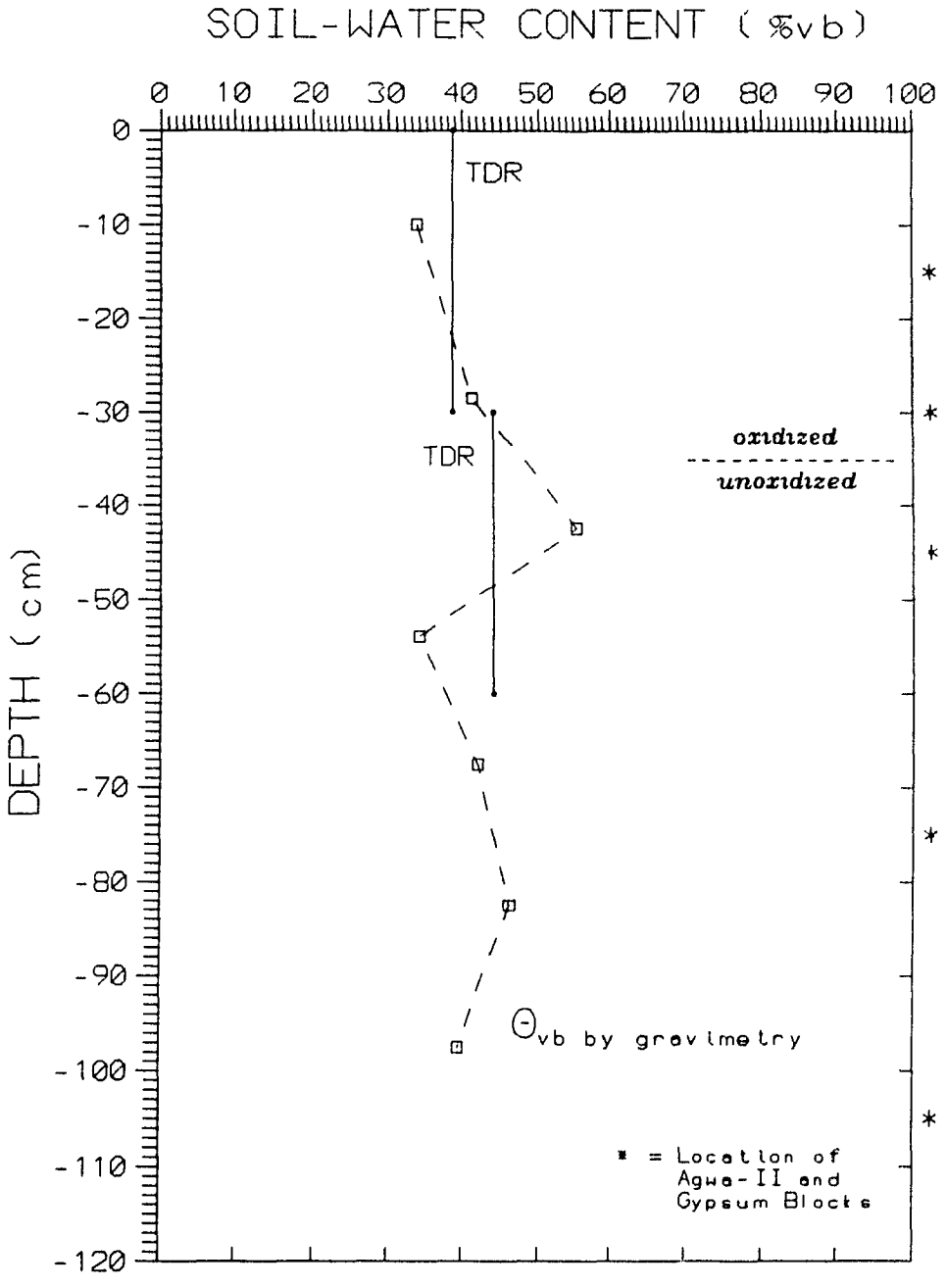

Figure 7.8d.
TDR and Gravimetric Soil-water Content Measurements of Waite Amulet Tailings at WA15t, taken on 23 November 1990.

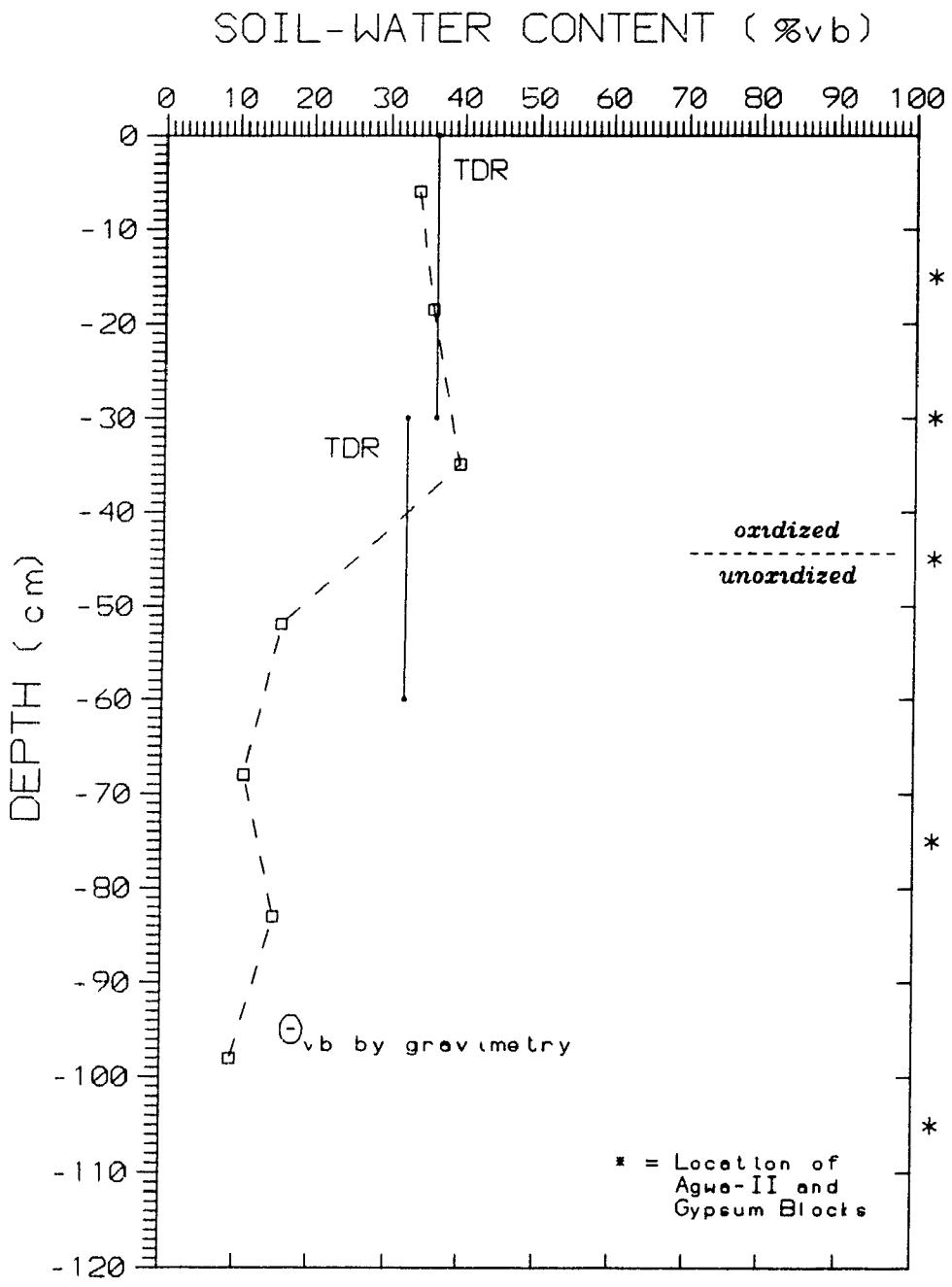

Figure 7.8e.
TDR and Gravimetric Soil-water Content Measurements of Waite Amulet Tailings at WA30, taken on 7 October 1990.

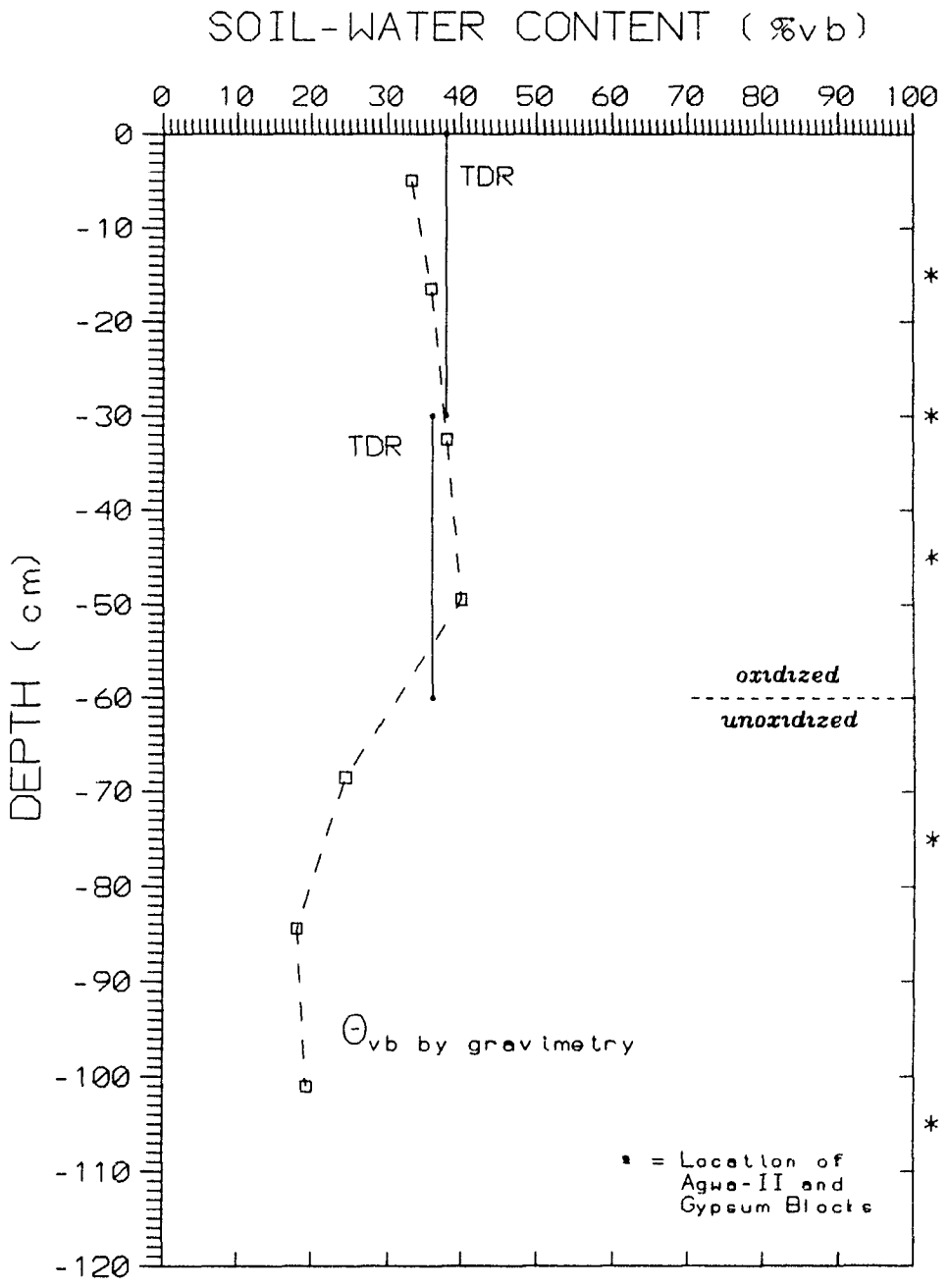

Figure 7.8f.
TDR and Gravimetric Soil-water Content Measurements of Waite Amulet Tailings at WA30, taken on 23 November 1990.

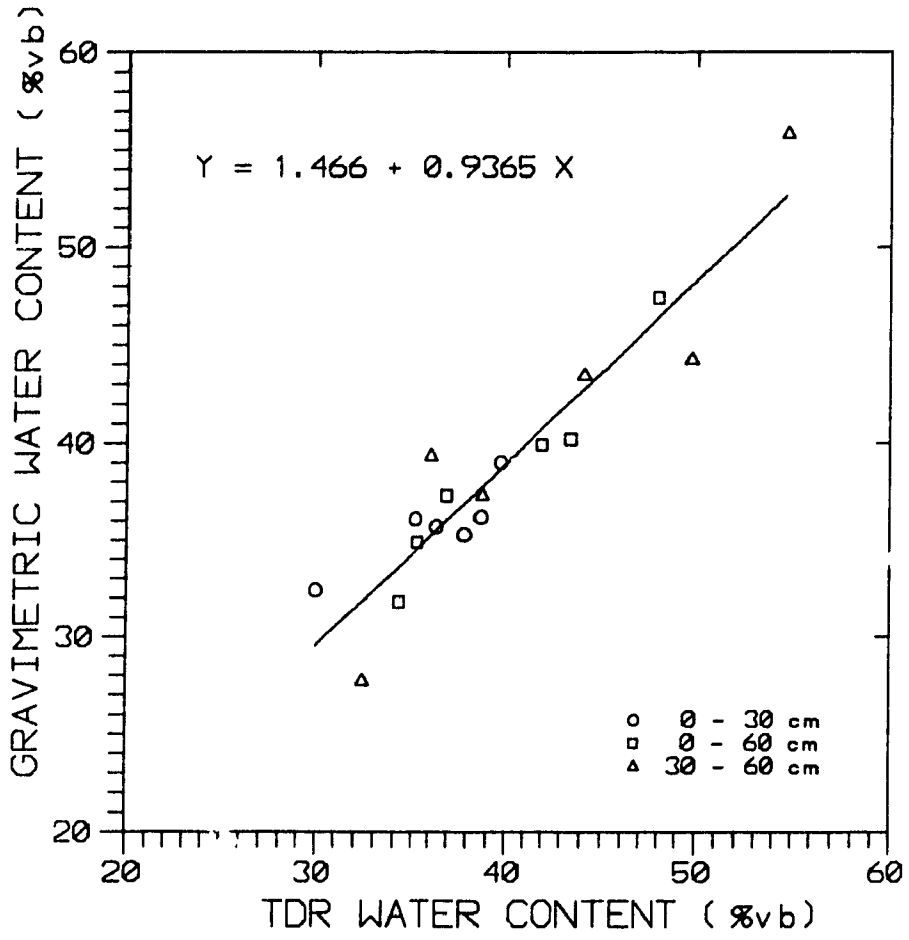

Figure 7.9a.
Correlation of Gravimetric Water Content to TDR Water Content, Delineated by Probe Depth.

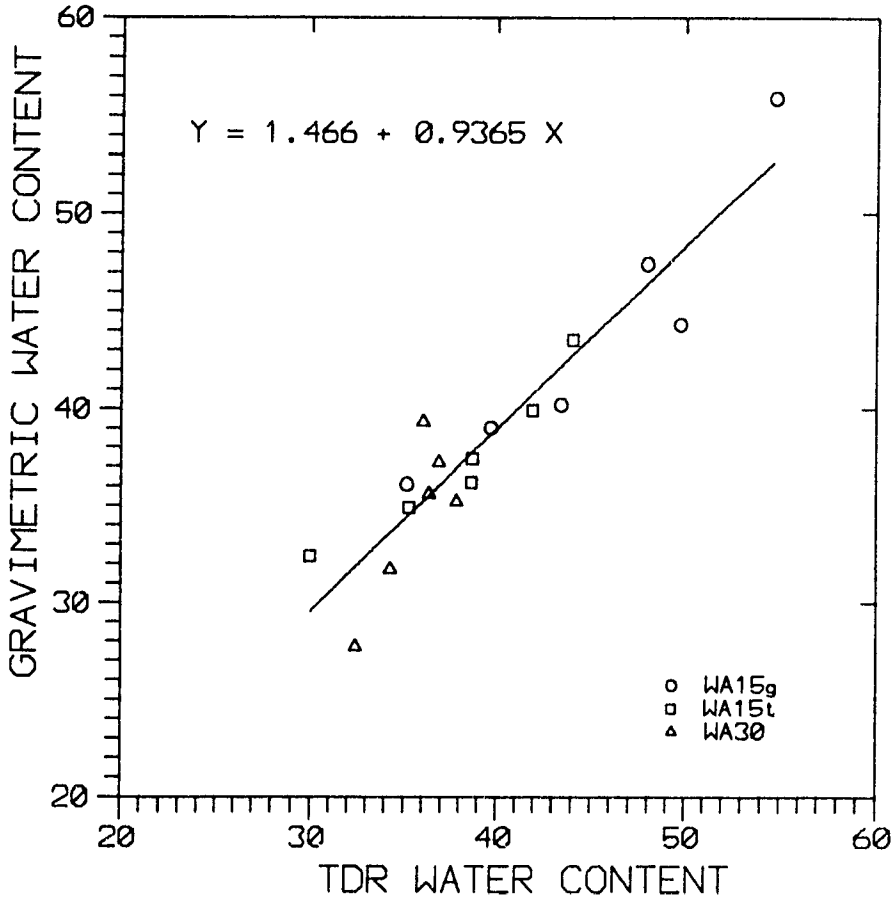

Figure 7.9b.
Correlation of Gravimetric Water Content to TDR Water Content, Delineated by Instrument Nest Site.

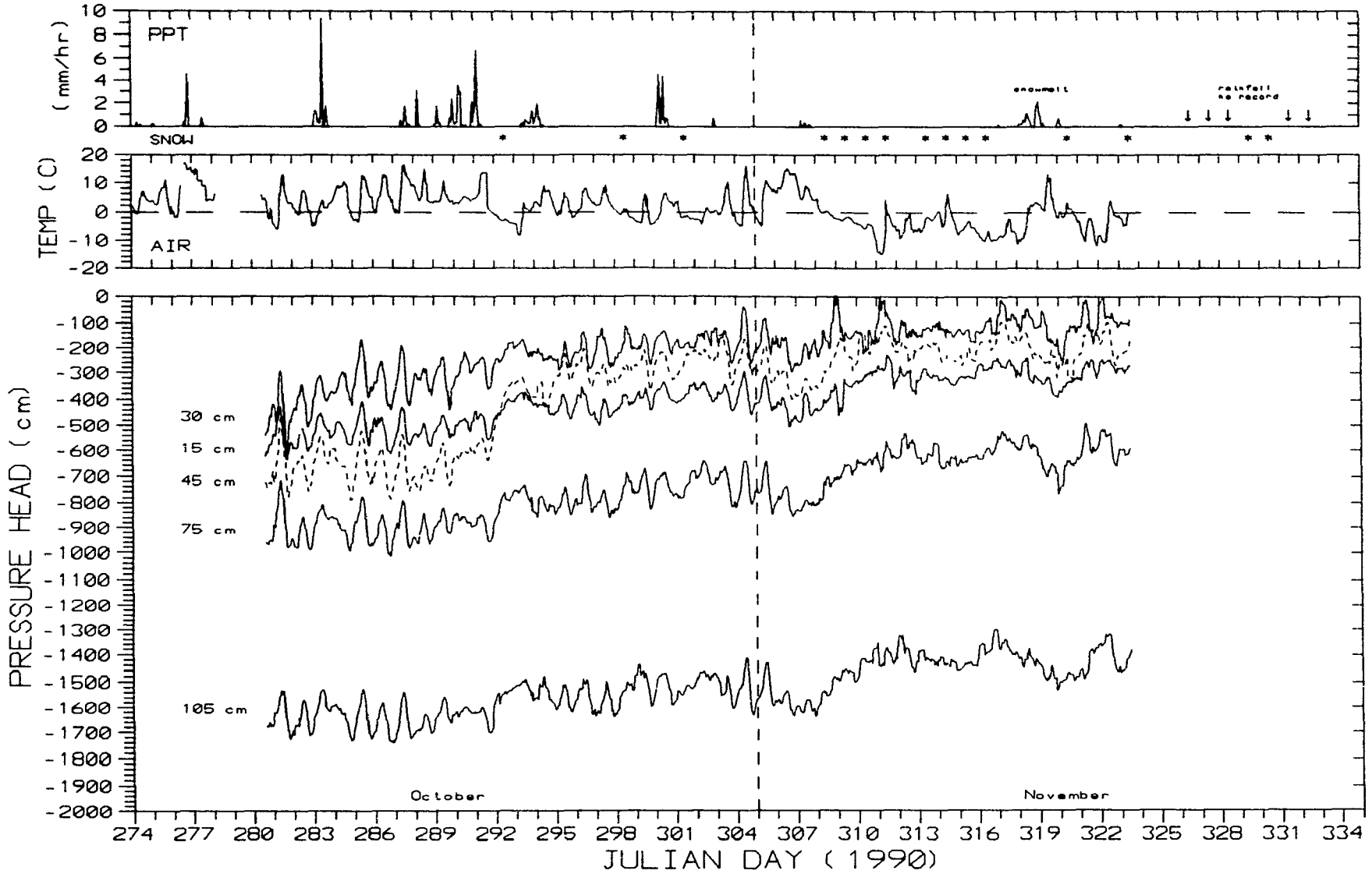

Figure 7.10a. Pressure Head from Agwa-II Blocks at WA15g.

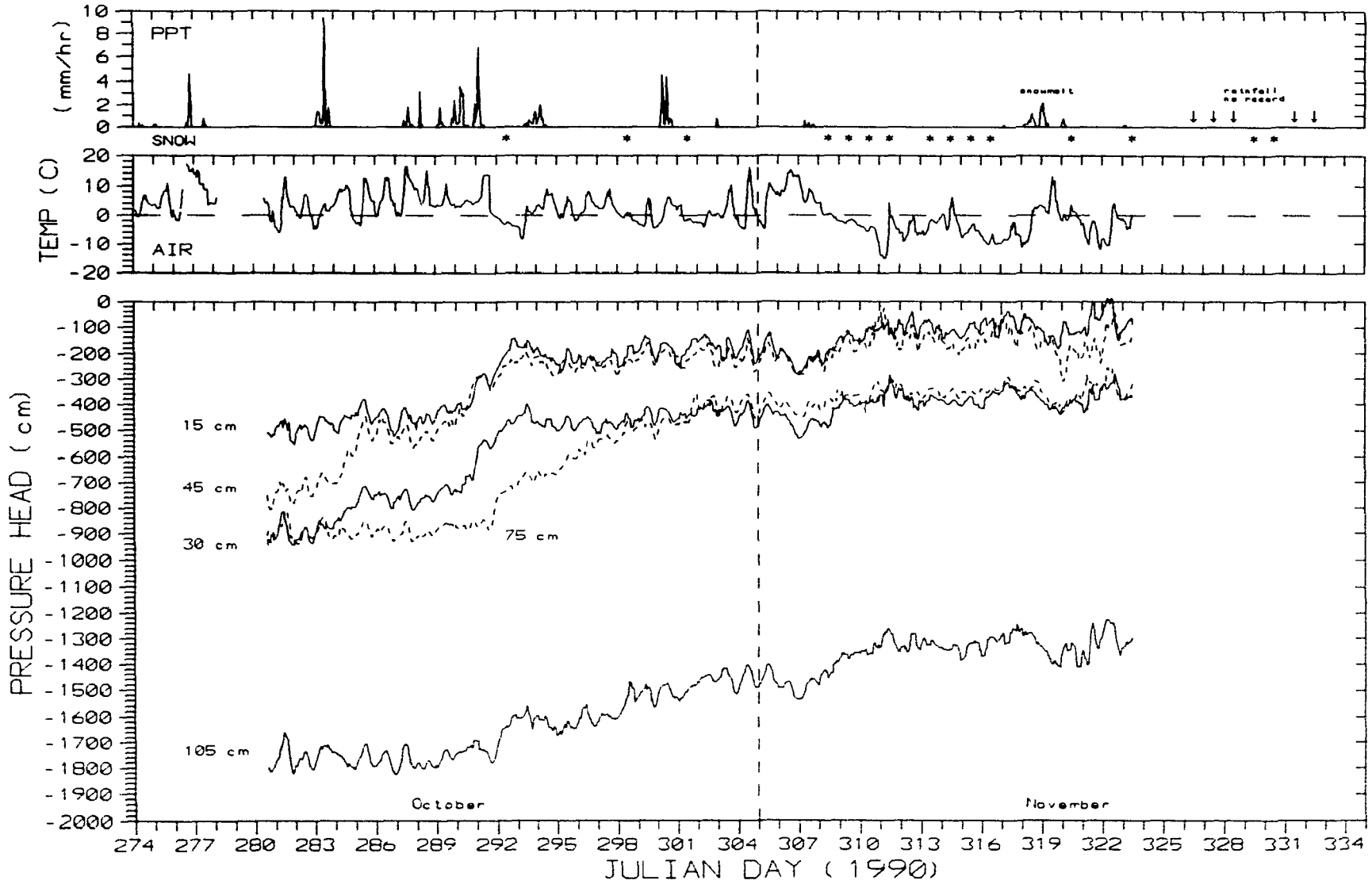

Figure 7.10b. Pressure Head from Agwa-II Blocks at WA15t

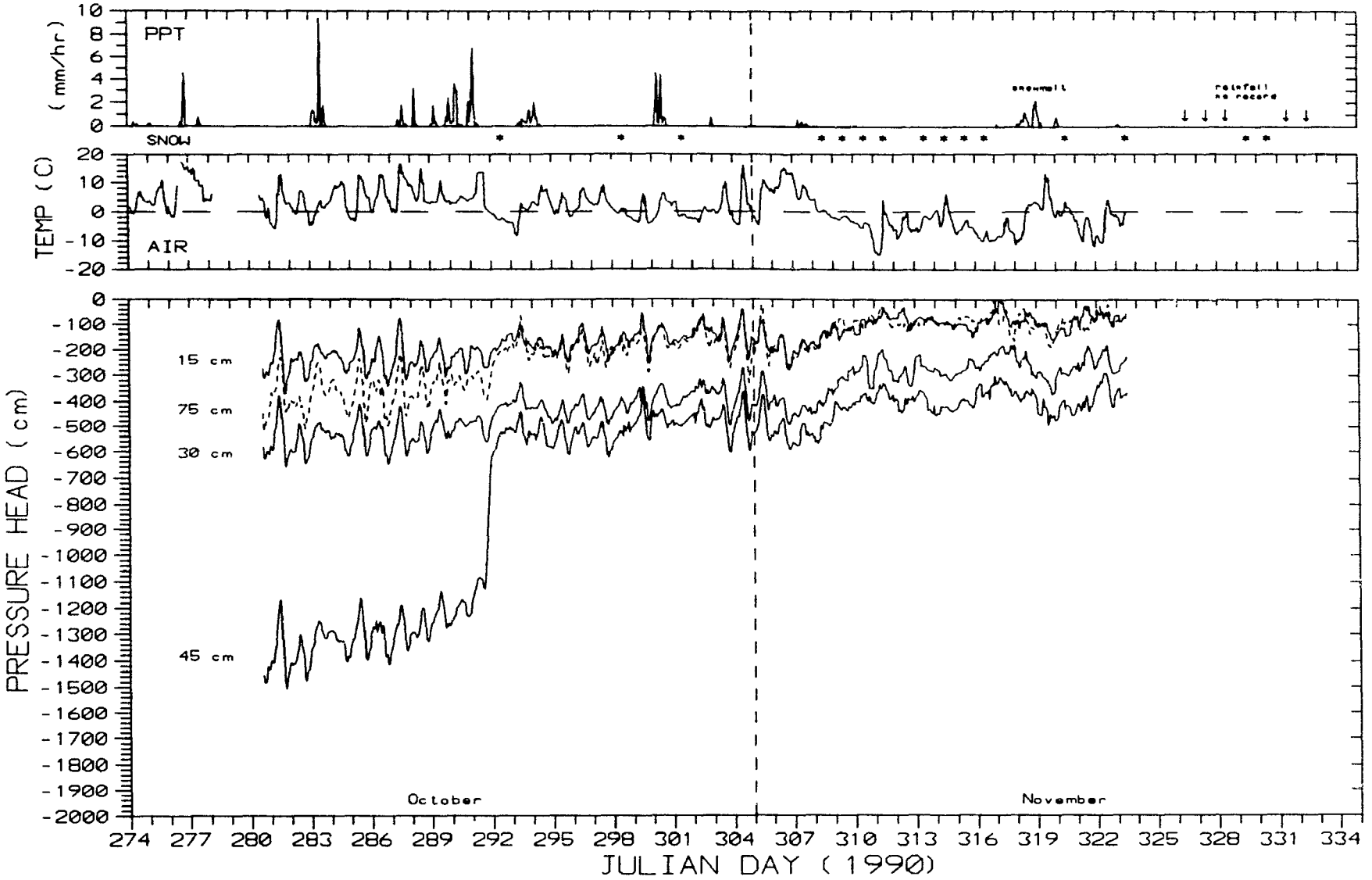

Figure 7.10c. Pressure Head from Agwa-II Blocks at WA30.

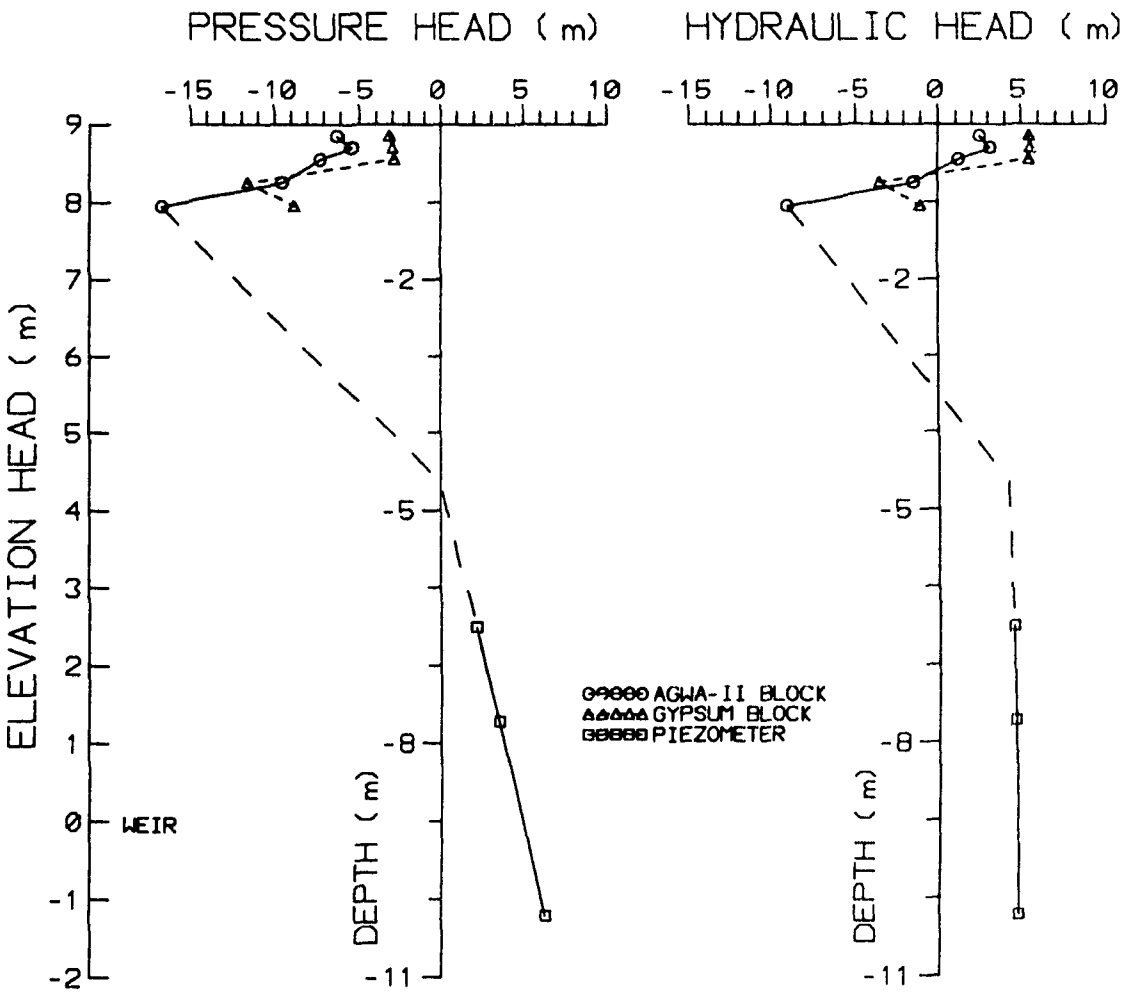

Figure 7.11a.
Groundwater Mechanical-energy Conditions near the Ground Surface at WA15g on 7 October 1990, Expressed as Energy per Unit Weight.

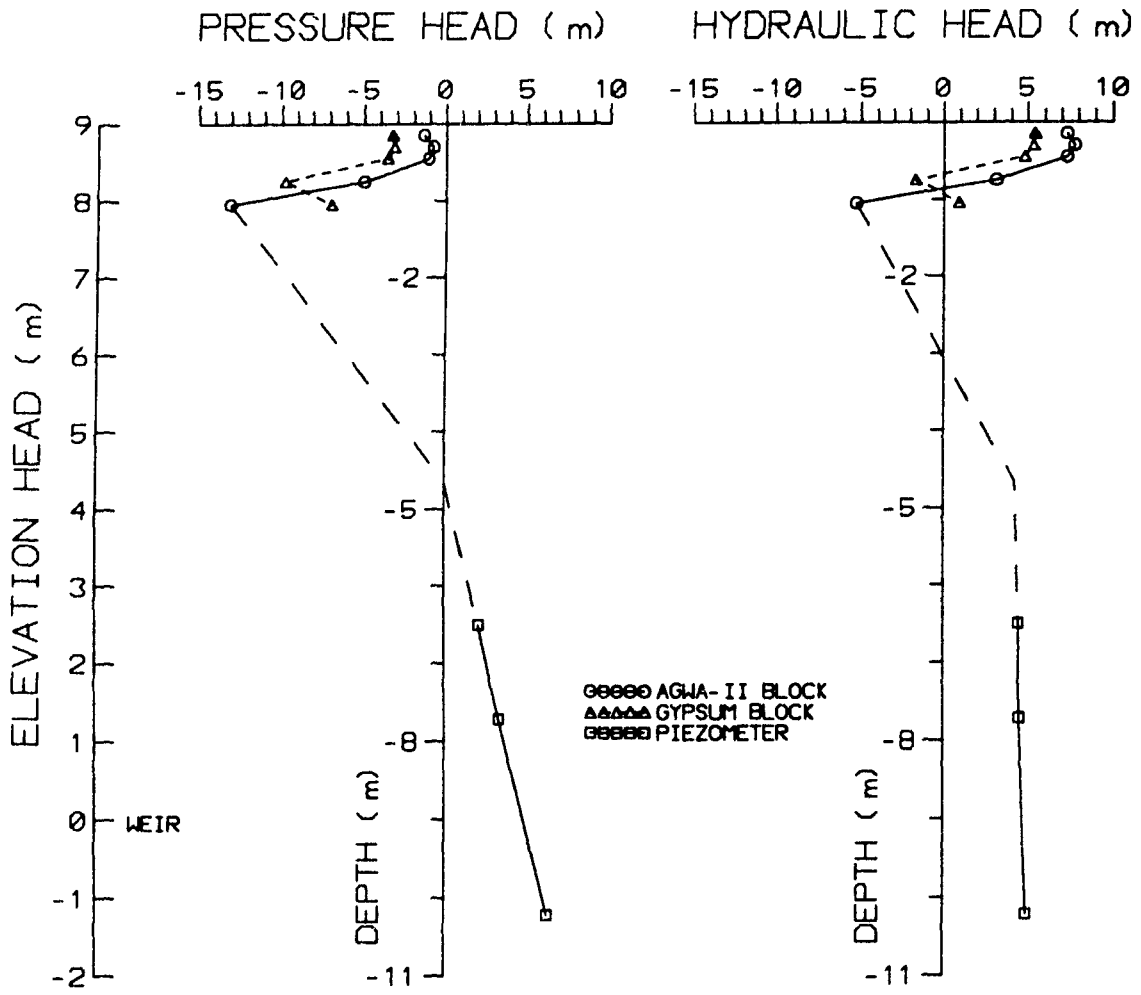

Figure 7.11b.
Groundwater Mechanical–energy Conditions near the Ground Surface at WA15g on 23 November 1990, Expressed as Energy per Unit Weight.

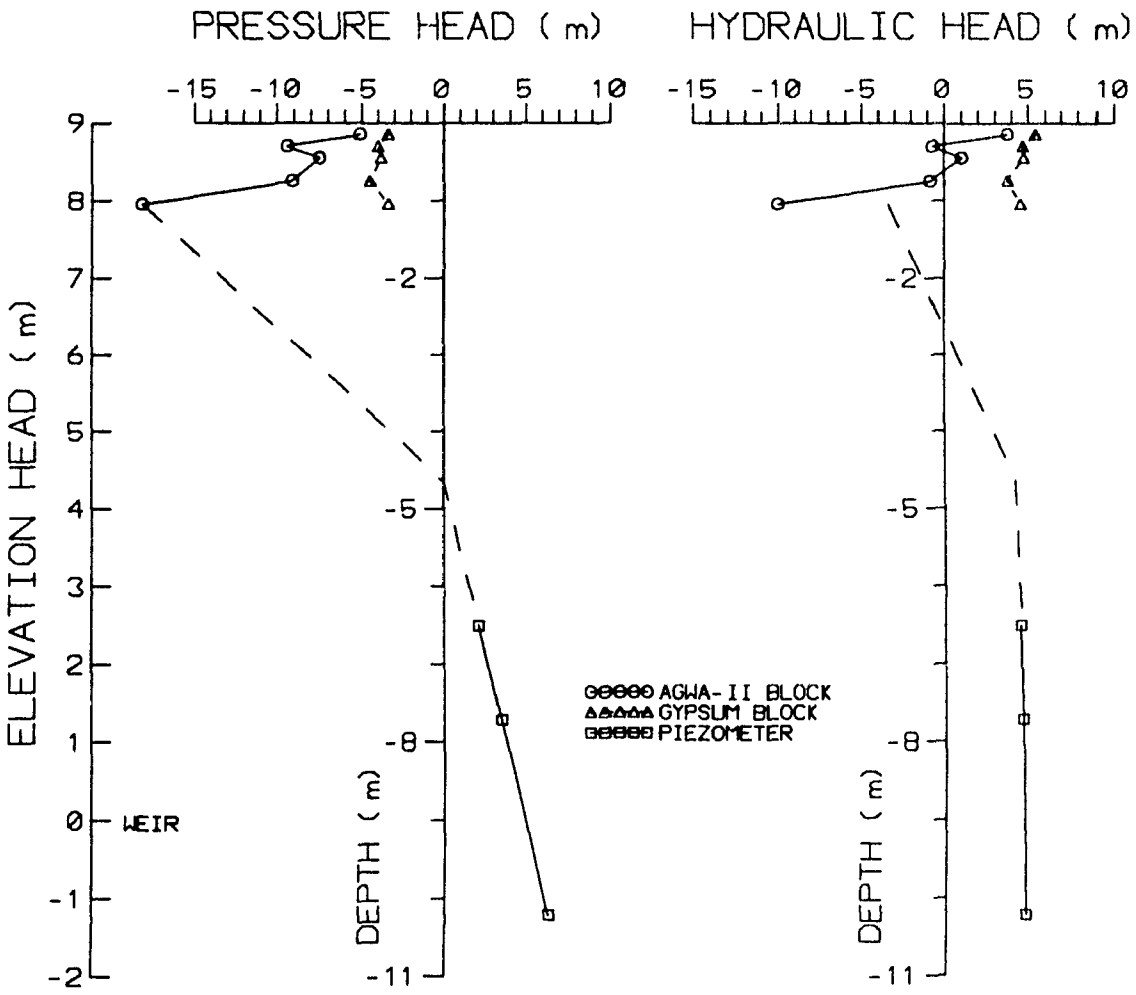

Figure 7.11c.
Groundwater Mechanical–energy Conditions near the Ground Surface at WA15t on 7 October 1990, Expressed as Energy per Unit Weight.

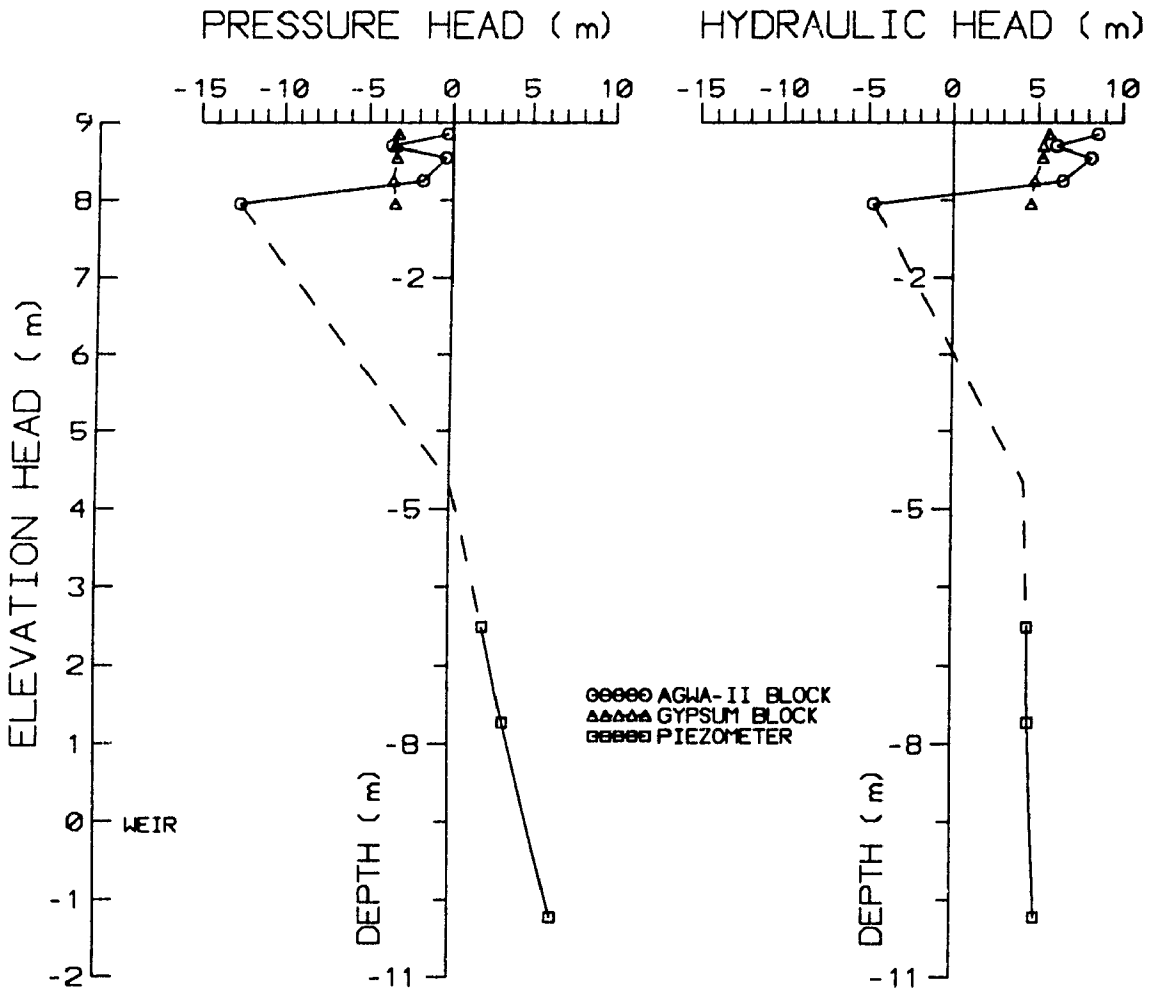

Figure 7.11d.
Groundwater Mechanical-energy Conditions near the Ground Surface at WA15t on 23 November 1990, Expressed as Energy per Unit Weight.

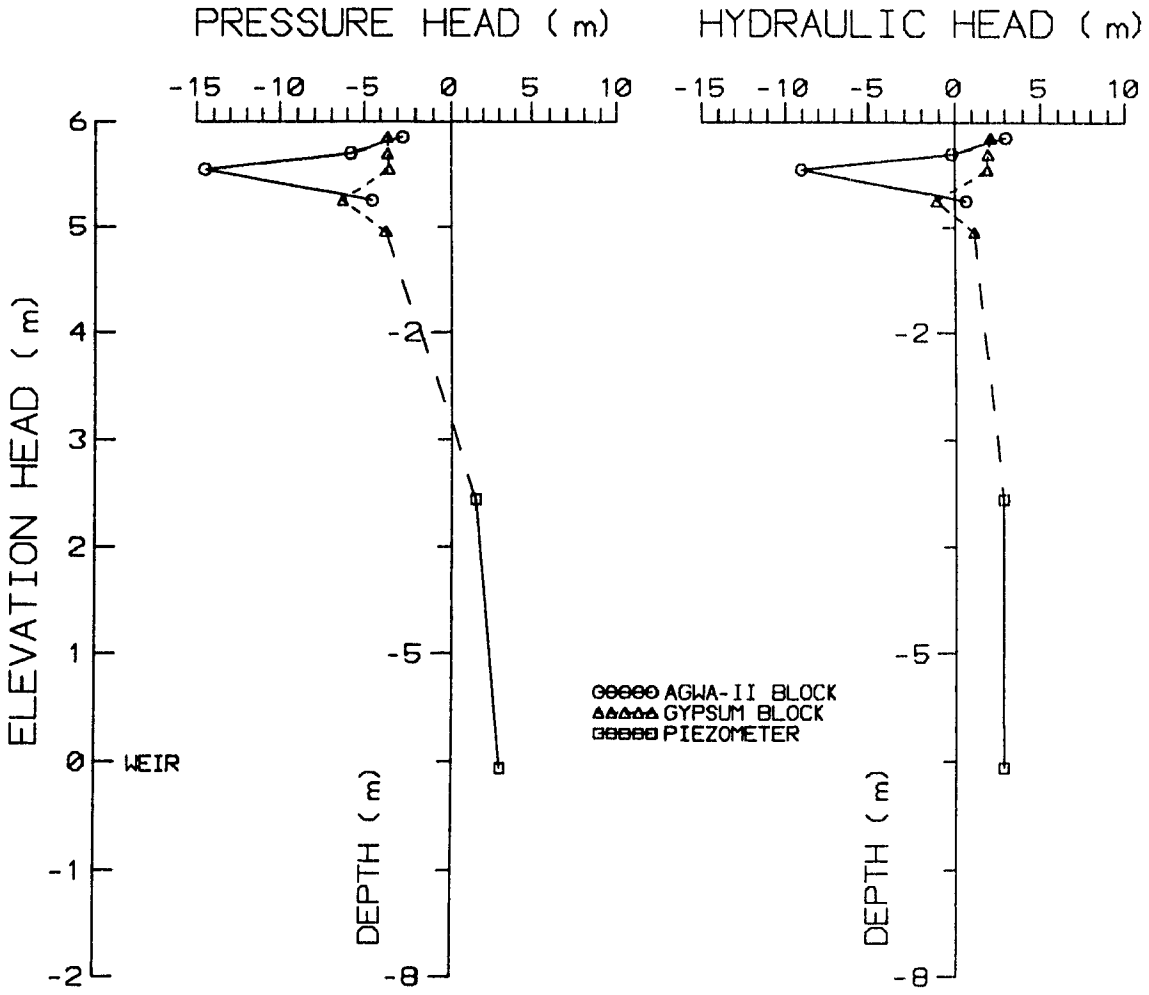

Figure 7.11e.
Groundwater Mechanical-energy Conditions near the Ground Surface at WA30 on 7 October 1990, Expressed as Energy per Unit Weight.

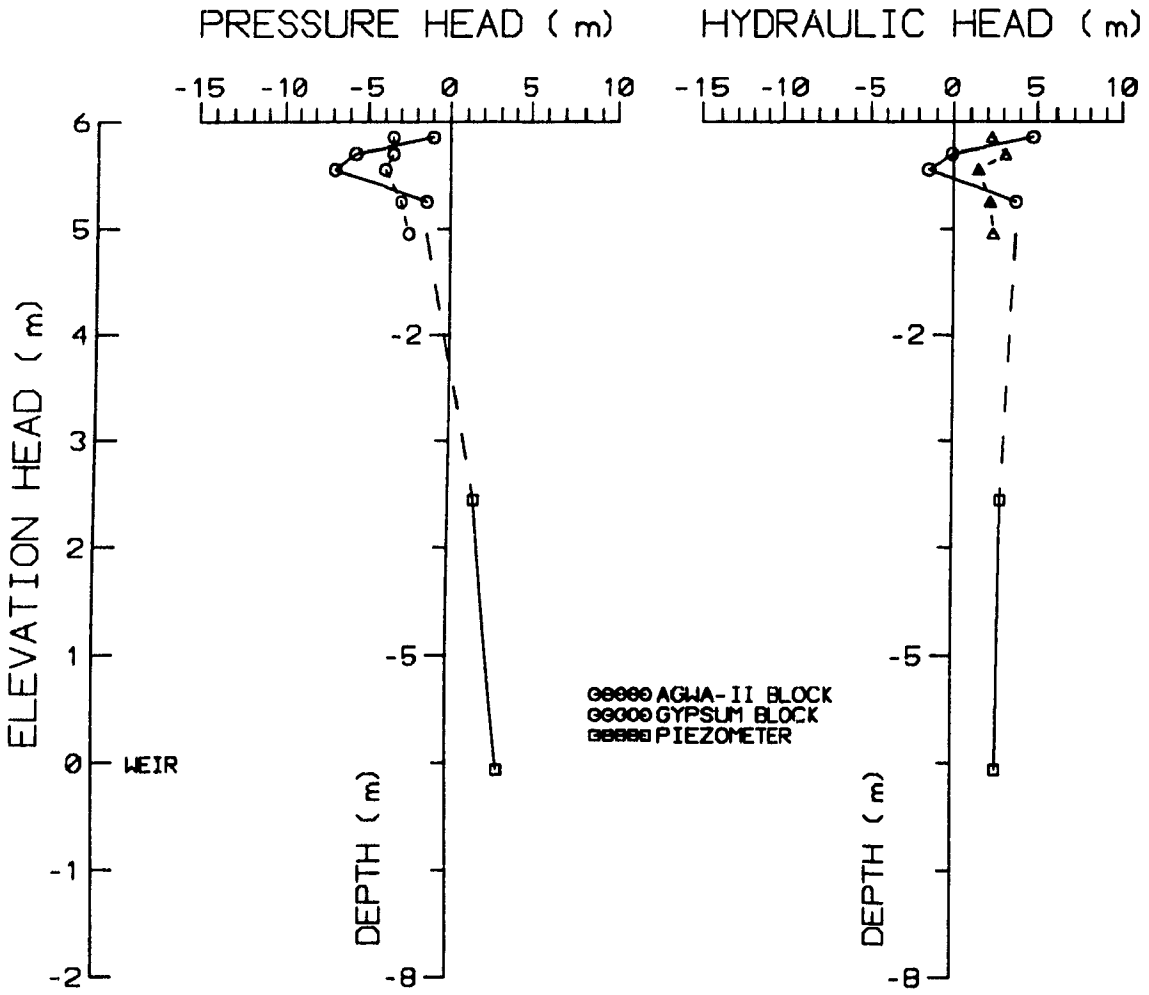

Figure 7.11f.
Groundwater Mechanical-energy Conditions near the Ground Surface at WA30 on 23 November 1990, Expressed as Energy per Unit Weight.

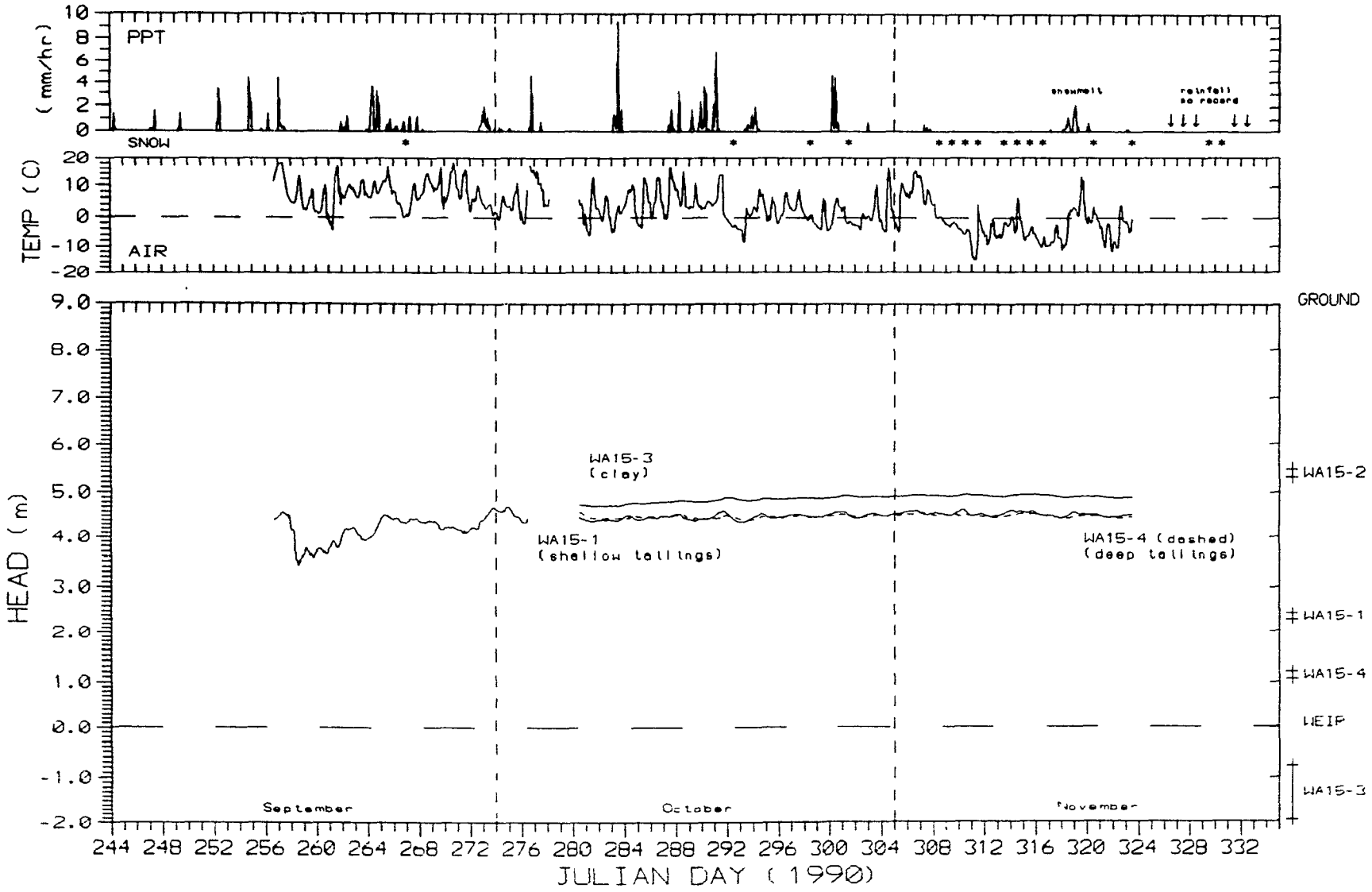

Figure 7 12a. Piezometric Hydraulic Head at WA15g

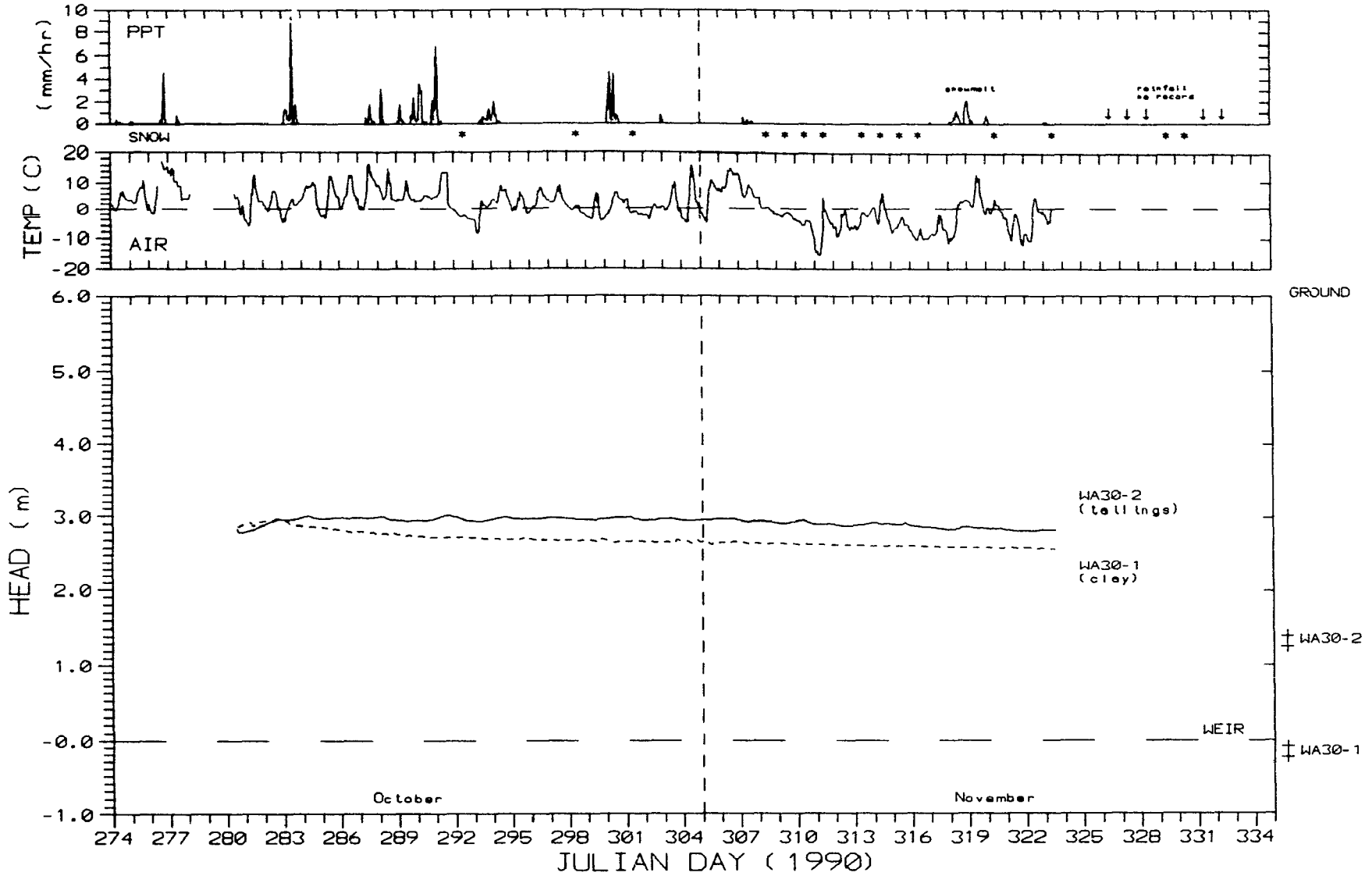

Figure 7.12b. Piezometric Hydraulic Head at WA30.

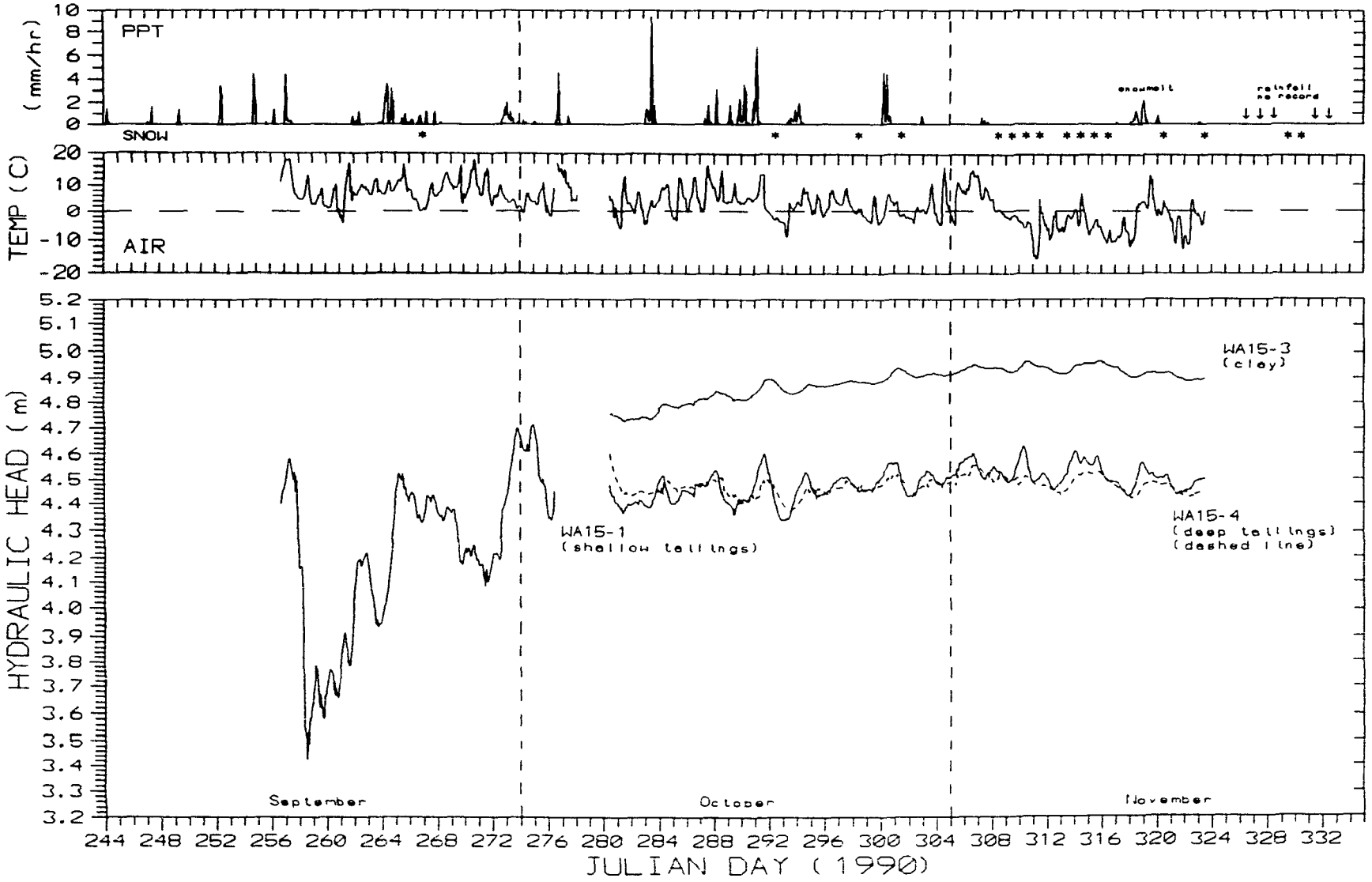

Figure 7.13. Piezometric Hydraulic Head at WA15g

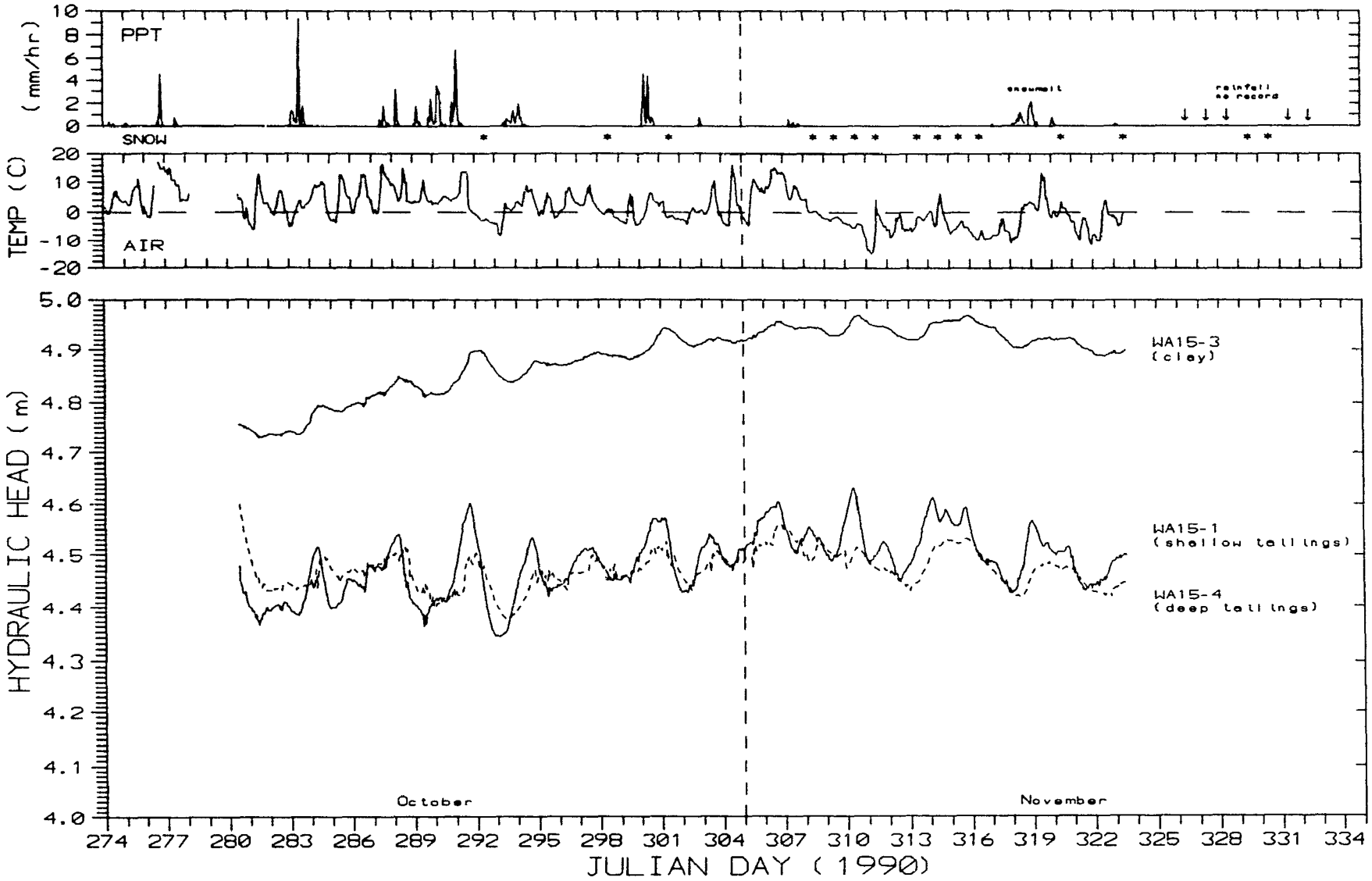

Figure 7.14. Piezometric Hydraulic Head at WA15g.

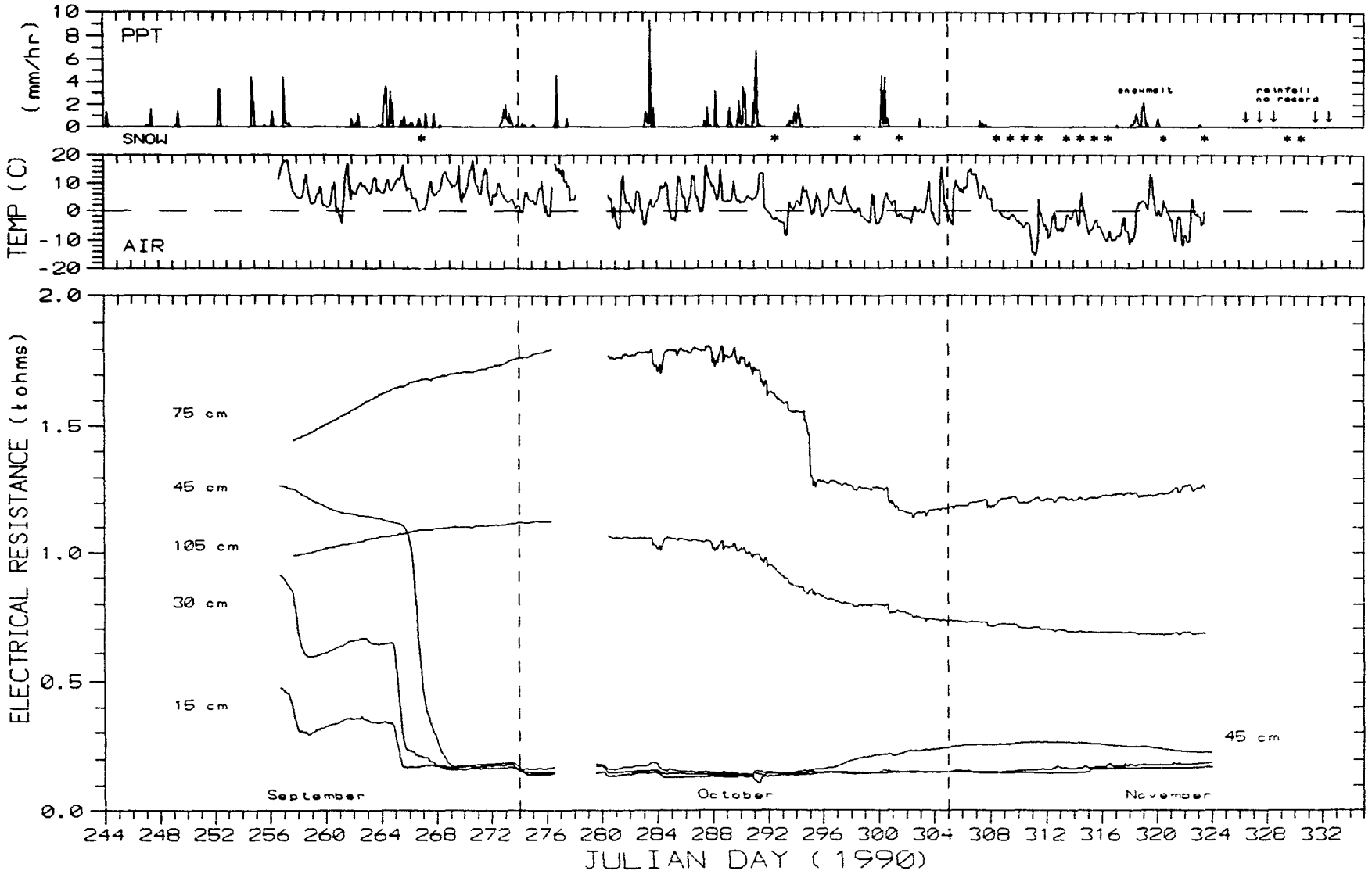

Figure 7.15a. Output from Gypsum Blocks at WA15g

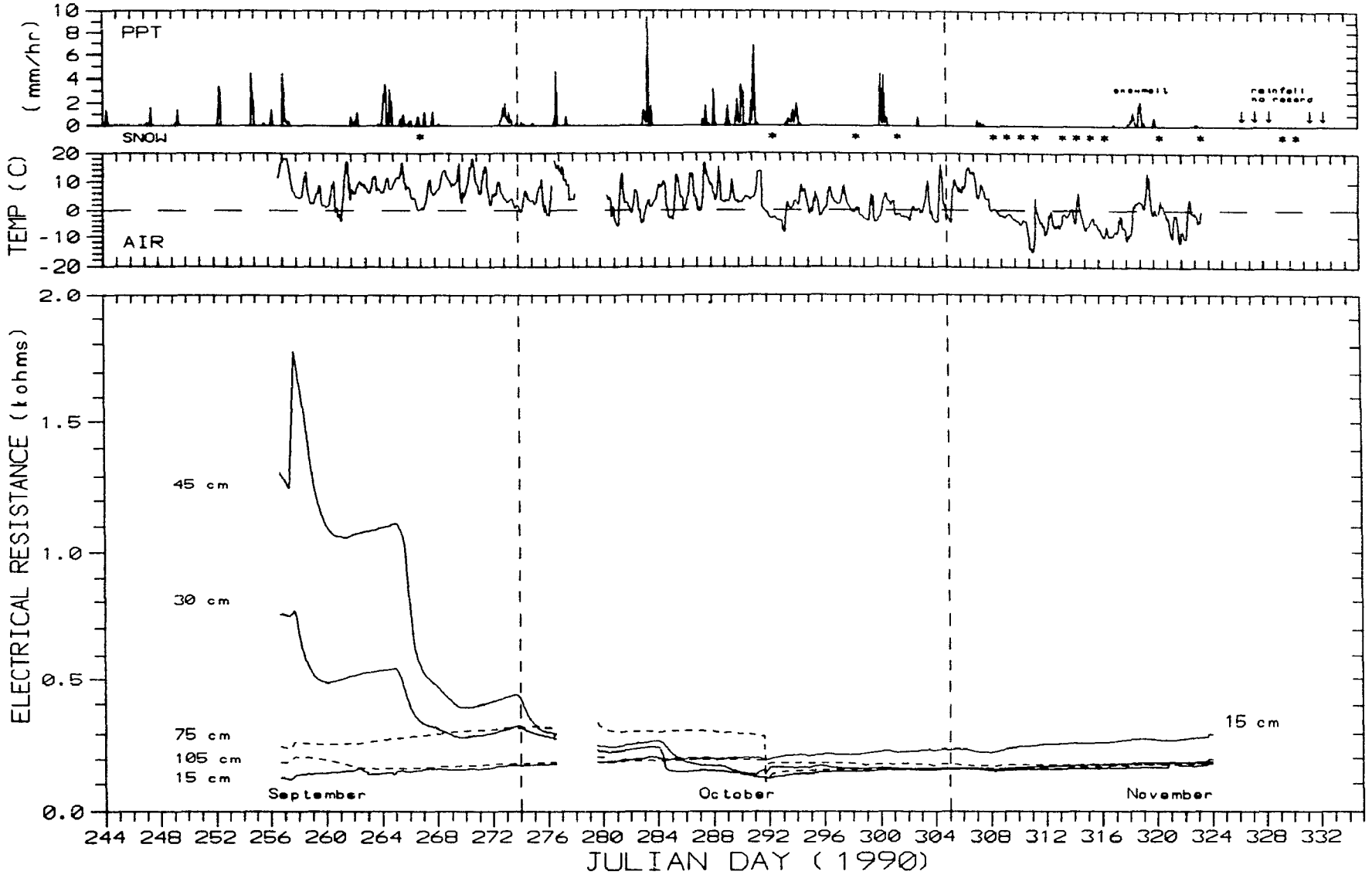

Figure 7.15b. Output from Gypsum Blocks at WA15t.

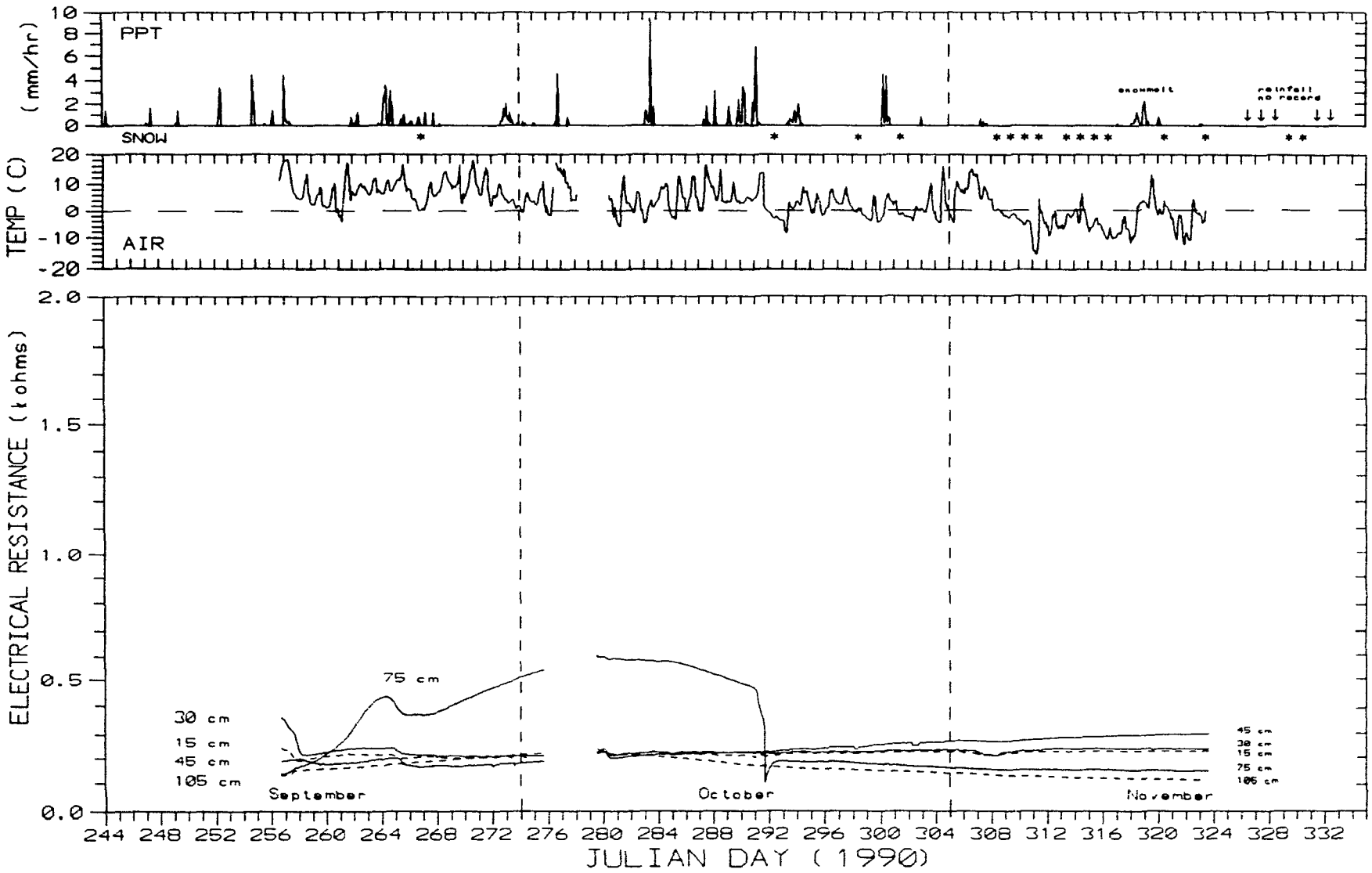

Figure 7.15c. Output from Gypsum Blocks at WA30.

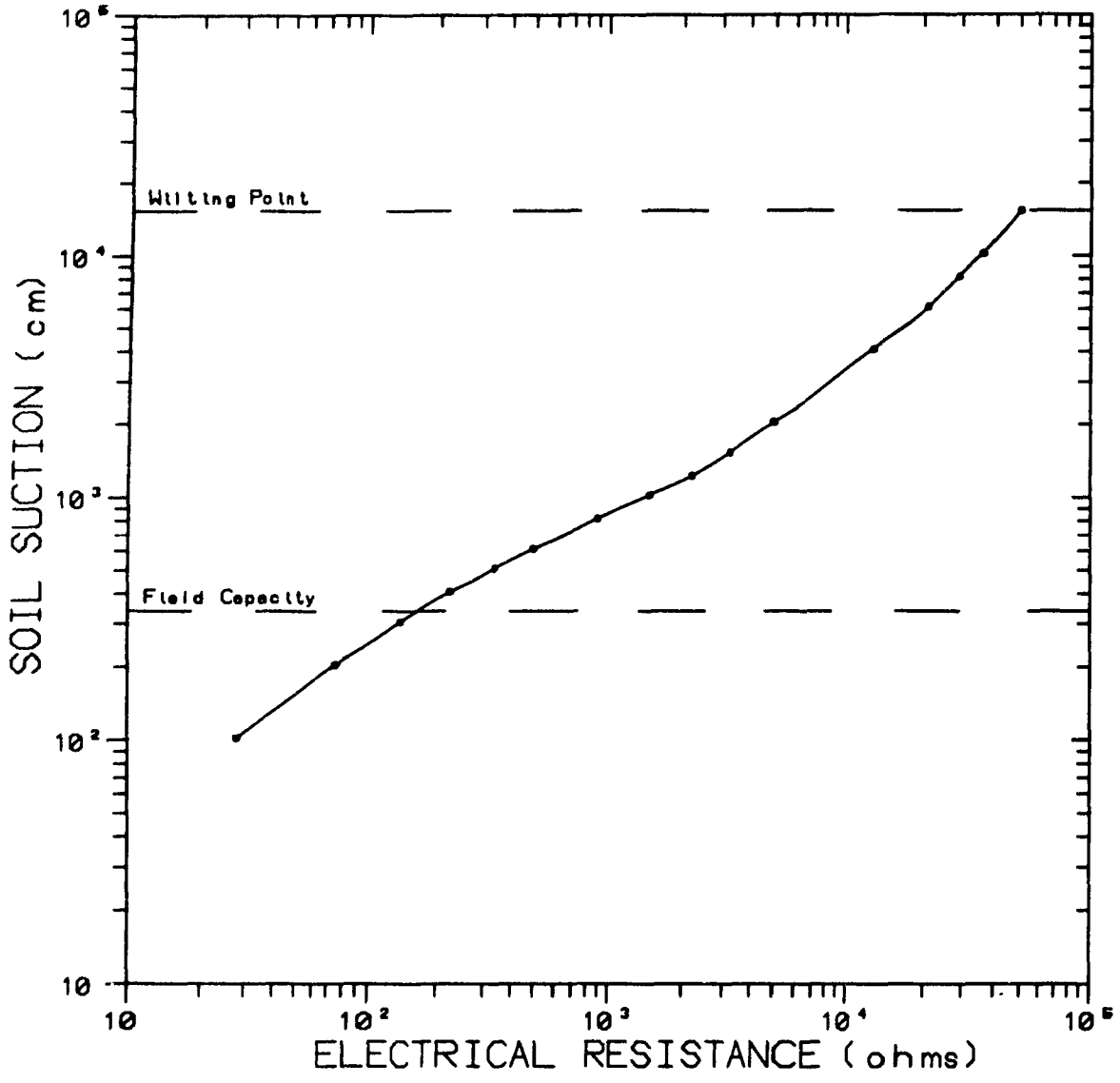

Figure 7.16a.
Generalized Gypsum Block Calibration which is Provided by the Manufacturer for Agricultural Purposes.

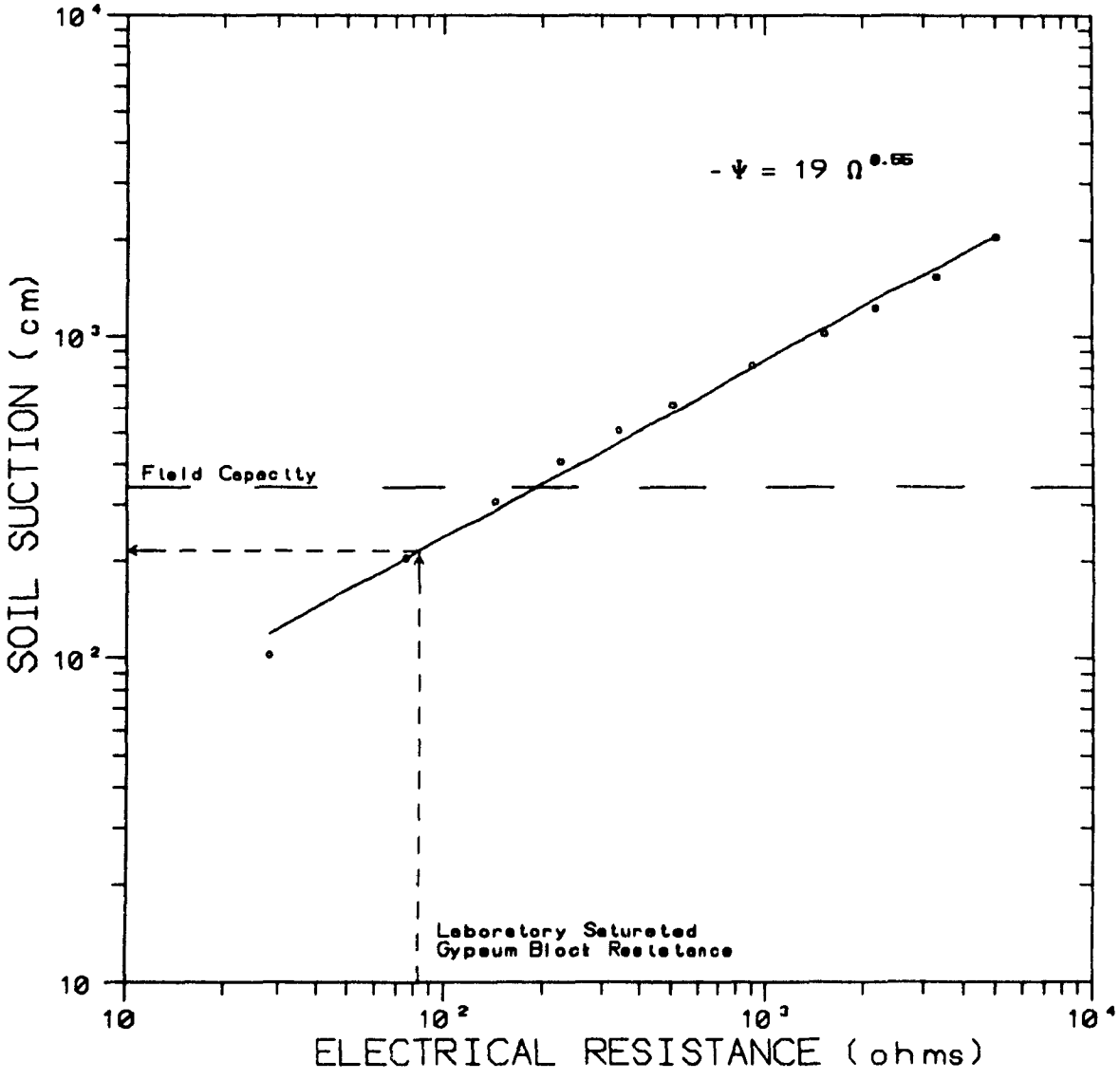

Figure 7.16b.
Generalized Gypsum Block Calibration Enveloping Moist Conditions (⟨ 2 bars suction).

8.0 Discussion of the Results

Three vadose zone monitoring sites were installed at Waite Amulet: two on the tailings surface (WA15g and WA15t) and one on the tailings bench (WA30). WA15g and WA30, were located under a grass-legume vegetation cover (the dominant vegetation of the tailings), and WA15g was located under an aspen-birch cover (occurring as isolated groves). A discussion of the results centers on the comparison of the three sites, thereby characterizing the subsurface hydrology during the autumn season of 1990. In addition, the performance of the vadose zone monitoring system is evaluated from the status of each measurement method.

8.1 Precipitation

Precipitation at Val D'Or Airport was 109% of normal for the calendar year 1990 (Table 7.3). January and February had above normal precipitation with at or below normal snowfall. Precipitation during March was below normal with an abnormal amount falling as rain (60%, as compared to a normal of 25%). April was snowy, 121% of normal precipitation with 72% as snow. Summer rainfall was above normal during June and July, and below normal during August. During the study period, September, October, and November, precipitation was 135% of normal.

During the study period, precipitation fell primarily as rain through October, with the exception of snow-flurries on September 23 and 24 and October 18, 19, 25, and 28. Precipitation during September was characterized by a contiguous series of small storms (< 10 mm/day) enveloping an isolated larger storm on September 21 (28.4 mm/day), which was the storm of highest intensity during the study period (Fig. 7.1). During October, storms were generally more defined in character, separated by several dry days. Nearly 50% of the monthly precipitation fell during an eight day wet period in the middle of the month (52.8 mm from

October 14 through 21). Two 1-day storm events (Oct. 10 and 27), similar to that which occurred on September 21, brought most of the remaining precipitation for October (41%). During early November snow accumulated (over 20 cm at Val D'Or), which later produced significant snowmelt on November 14 and 15. Unfortunately, during these periods of snowfall all of the precipitation were not recorded with the tipping bucket rain gauge in stalled at the site (ST1).

8.2 Bulk Density

Tailings bulk density was calculated on October 7 from the gravimetric soil-water content samples. The depth profiles (Fig 7.7a,b,c), illustrated with the logged tailings descriptions, depict increasing bulk density through the oxidized zone and a reasonably constant bulk density in the unoxidized zone; this trend reflects the higher specific gravity and packed structure of the unoxidized tailings. The bulk density data indicate greater homogeneity in the tailings bench (WA30) than on the tailings surface (WA15), displayed principally as bulk density variations in the unoxidized zone (Fig. 7.7a,b). In general, for the top 1 m of tailings, the oxidized tailings have a bulk density of 1.0 g/cm^3 and the unoxidized tailings have a bulk density of 1.6 g/cm^3. Assuming an tailings specific gravity of 4.8, the porosity[1] is 0.67 in the unoxidized zone, which intuitively seems high.

The variable depth of the contact between the unoxidized zone and the oxidized zone (Table 7.5) reflects the preferential transport channels of water and oxygen. In general, the contact is deeper on the tailings bench than that on the tailings surface, and deeper under tree cover.

---

[1]Porosity = 1 - (D_b/G), where D_b = Bulk Density and G = Specific Gravity; specific gravity (g/cm^3) of Pyrite = 5.0, Pyrrhotite = 4.6, Saphalerite = 3.9 to 4.1, and Chalcopyrite = 4.2.

8.3 Air and Soil Temperature

The earth's energy budget is an intercoupled system of energy transfer and transformation fluxes with the sun as the principal source (Oke, 1987). However at the scale of a particular site, the soil surface interacts within this global energy system. Three sources of energy may then be considered: the sun (i.e., short-wave radiation), the earth (i.e., heat conduction from the earth), and the atmospheric heat advection (i.e., heat conduction from advected air masses). Other sources, although significant, contribute more indirectly to transient dial cycles. For example, long-wave radiation and latent heat sources may be included as atmospheric heat advection in the form of cloud, and the net result of cloud is to damp the dial variation of the surface-radiation budget which serves to reduce the dial temperature range.

Temperature is the potential (force) of heat[1] (energy) flux, and in this sense, temperature is analogous to soil-water potential or hydraulic head. The transfer of heat to and from a soil surface through channels of radiation[2], advection-convection[3], or conduction[4], alters the soil

---

[1]Heat is defined generally as the aggregate internal energy of motion (by molecules, atoms, etc.) of a substance. It is the temperature (°K) of a body multiplied by its specific heat (W $°K^{-1}$ g^{-1}) and by its mass.

[2]Any object (not at a temperature of absolute zero) transmits energy to its surroundings by radiation in the form of electromagnetic waves traveling at the speed of light with no intervening medium. Radiation is characterized by its wave length which is inversely proportional to the temperature of the emitting body. When solar short-wave radiation is absorbed by soil, it becomes sensible heat (increasing the temperature) and latent heat of evaporation. Terrestrial long-wave radiation is subsequently emitted from the soil by sensible heat.

[3]Advection (*meteorology*) is the transfer of heat (or a property) by horizontal air (mass) movement. Convection is the transfer of heat (or a property) in a liquid by mass

temperature by sensible[1] heat and the state of soil-water by latent[2] heat (e.g., evaporation and condensation).

Tailings temperature was measured each hour at all three monitoring sites (WA15g, WA15t, and WA30) with the thermocouples of the heat dissipation sensors located at 15, 30, 45, 75, and 105 cm below the surface. The results (Fig. 7.4a,b,c) illustrate six phenomenon which are an outcome of the dominant heat transfer mechanism(s): (1) the net loss of heat from the soil by conduction (2) dial fluctuations in soil temperature by the absorption of solar radiation (and coupled soil conduction of the heat); (3) cooling by latent heat of evaporation, displayed as the increased amplitude of dial temperature fluctuation with soil depth; (4) warming by latent heat of condensation (and freezing), displayed at night and is similar to #3 in its evidence; (5) soil surface

---

movement of the liquid. In meteorology, convection often refers to vertical advection, particularly on the scale of an individual cloud (convective cell). Advection and convection is the dominant process in fluid systems (atmosphere and ocean).

[4]Conduction is the process of heat transfer through matter by molecular impact from regions of high temperature to low temperature without the transfer of matter. It is the process by which heat passes through solids but its effects in fluids (liquids and gases) are usually negligible in comparison to those of convection.

[1]Sensible heat is the same as enthalpy which represents the total heat or total energy content of a substance per unit mass and can be defined by $H = U + PV$ where U is internal energy, P is pressure, and V is volume. It is related to free energy (G) through entropy (S), $H = G + TS$ where T is temperature (°K). In the atmosphere, a change in sensible heat of a mass of gas is the heat gained or lost by the gas in an exchange at constant pressure.

[2]Latent heat is that part of thermal energy involved in the change of state (e.g., 2.4×10^6 J/kg of energy released when water vapor condenses to liquid). The evaporation of water stores solar energy in latent form until it can be released by a convective cell.

storage of heat by differential transfer rates, displayed as an earlier temperature crest (and trough) with soil depth; and, (6) warm period thermal fluxes by the transfer of advected atmospheric sensible heat, primarily by conduction. These mechanisms are elaborated in the succeeding text.

During the entire monitoring period temperature gradients indicate a net loss of heat from the upper 1 m of the tailings surface. Heat is clearly conducting to the soil surface and radiating to the atmosphere, resulting in the cooling of the tailings and a net decrease in temperature during autumn.

Each day the temperature of the tailings fluctuates in response to the transient flux in solar radiation. The fluctuations at depth, though, are compounded by the distribution of the heat and by the transfer of latent heat. Intuitively, one would expect the dial temperature fluctuations to be most pronounced at the shallow depth (15 cm sensor) and to diminish with depth (Oke, 1987, p. 47). Indeed, the fluctuations are most pronounced at 15 cm, but in some cases the results indicate the inverse at depth, which seems to suggests the coupling of more than one physical mechanism.

As the soil absorbs solar radiation the soil temperature increases and soil-water evaporates. Evaporation, in turn, cools the soil restricting the increase of soil temperature[1]. As the surface increases in temperature, heat is transfered to shallow depths by conduction (and to a minor extent by convection, temperature driven hydraulic flow). Evaporation is controlled by vapor

---

[1]In the absence of solar radiation, evaporation decreases the surface soil temperature which increases the soil temperature gradient, resulting in an increases the conduction of heat to the surface. In controlled laboratory experiments (Wilson, 1990), subsequent to the drop in soil temperature, surface temperature rises and equilibrium is obtained after soil-water evaporates (after 42 days).

pressure, and at soil depth, vapor pressure generally limits evaporation, being controlled by the flux of vapor to the soil surface (and atmosphere). Evaporation also lowers the soil-water potential which induces hydraulic flow, thereby distributing heat by convection. In the coupling of the dominant mechanisms of this heat system circulation an explanation exists for the inverted pattern of the dial-fluctuation amplitude with depth. The phenomenon is most

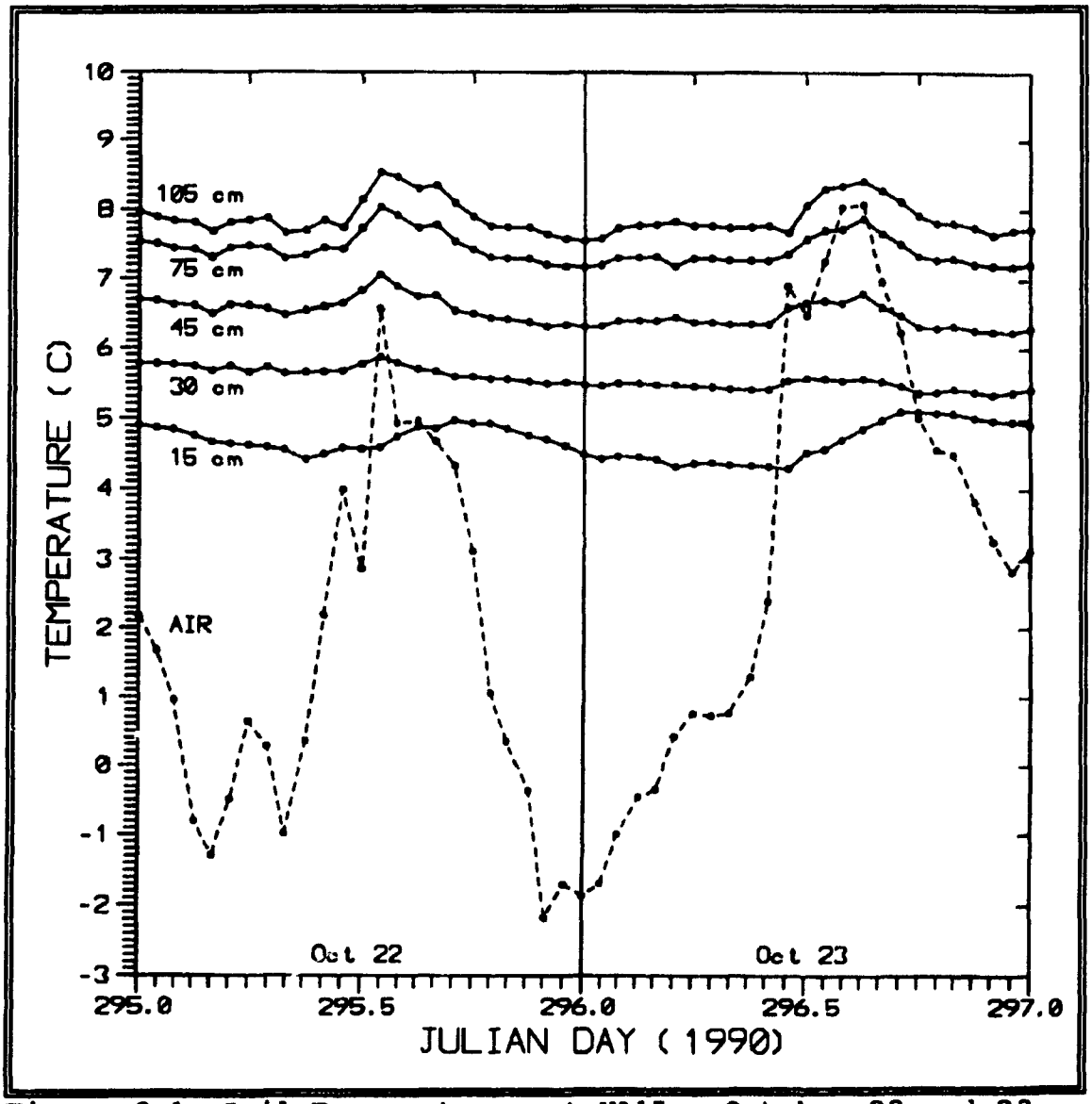

Figure 8.1. Soil Temperatures at WA15g, October 22 and 23.

pronounced at WA15g (Fig. 7.4a). Figure 8.1 illustrates October 21 and 22 (JD 294 and 295) of Figure 7.4a. At 30 cm depth, the rate of solar radiation influx generally equals the rate of latent heat transfer, resulting in minimal changes temperature. Below 30 cm, increasingly less energy is transferred as latent heat, and thus, dial temperature fluctuations increase with depth. Above 30 cm, the soil receives large amounts of solar radiation and evaporation simply limits the increase in soil temperature. When temperature decreases, the latent heat of condensation (and freezing) regulates the soil temperature in a similar fashion, particularly noted on the coldest days during the monitoring period (e.g., Nov. 7, JD 311, of Fig.7.4a).

Soil temperature generally increases throughout the morning and crests by afternoon. The crests, however, are generally earlier with increasing soil depth, reflecting the lag between solar radiation crest and air temperature crest. Above the soil surface the air temperature increases as the soil warms. Regarding heat transfer to the atmosphere, soil gas can be considered part of the atmosphere, or simply the interface between the atmosphere and the lithosphere. The air heated in the soil pores convects to the soil surface and rises with the heat at the soil surface, transferring heat through the atmosphere by convection, there by regulating the air temperature at the soil surface. After the peak in solar radiation, heat continues to transfer from the soil, thereby heating the air and producing a lag in the air temperature crest. Therefore, the loss of heat from the soil surface is controlled by the rate of heat transfer to the atmosphere, and the lag in the air temperature crest, produces a lag in the loss of heat from the soil, which produces the lag in soil temperature. Meanwhile, soil temperatures at depth (below the depth heat is conducted from the soil surface) vary chiefly by solar radiation

(short wave), and their crests are thereby coupled and precede the air temperature (and surface soil) crest.

At WA15t (Fig. 7.4b), the dial temperature fluctuation is less pronounced and exhibits less energy transfer as latent heat, representing the reduced solar radiation and soil evaporation under a forested cover (transpiration from the trees being nonexistent at this time). At WA30 (Fig. 7.4c), surface temperature dial fluctuation is similar to that at WA15g (Fig. 7.4a), both sites having a grass-legume cover, however, the transfer of energy as latent heat at WA30 occurs at greater depth, displayed by the smaller fluctuations at depth. The tailings bench, therefore, appears to have a higher vapor flux to the soil surface which allows for evaporation at greater depth. This explanation is in accord with the difference in tailings structure; the tailings bench (WA30) has a coarser texture and displays more homogeneity than the tailings surface (WA15).

Heat is also transferred to the soil from advected warm air masses that pass over the soil. Air masses which move through the region, typically from lower latitudes, bring with them sensible heat which is transferred to the soil and is manifested as thermal fluxes. The most pronounced warm-period thermal flux, which occurred in early November during a dry interlude, penetrated to the probe at 45 cm depth. Thermal flux rates calculated during this period are 0.6 cm/sec from the atmosphere to 15 cm depth and 1.64 cm/sec from 15 to 30 cm. Following this thermal flux, dial temperature fluctuations reduced due to the snow accumulation.

8.4 Soil-water Content

Soil-water content was measured principally by TDR method and validated by gravimetric measurements which were conducted on October 7 and November 23. The correlation

coefficient (R) of the relation (Fig. 7.9a,b) is 0.936 which indicated a good degree of linear association between the two methods of measurement. R^2 is 0.876 which is the percentage of variance TDR method predicts soil-water content by gravimetric method. In other words, TDR predicts the soil-water content of the tailings (chiefly oxidized tailings) with an 88% reliability. This accuracy also depicts the errors in the gravimetric measurement which is fundamentally in the calculation of bulk density. The two-tailed P-value is less than 0.0000 which indicates the relation is statistically significant. The statistical results appear in Appendix C5.

At all three monitoring sites during the study, the tailings soil-water content increased in magnitude (Fig. 7.6), which reflects the seasonal increase in precipitation and the wetter than normal precipitation during the study (September through November). Following a dryer than normal August, most of the increase in soil-moisture content occurred in September.

The tailings top 30 cm were generally similar in water content between the two grass-legume covered sites (WA15g and WA30) during October and November, but prior to this (in September), WA30 exhibited dryer surface conditions. In the aspen-birch grove (WA15t), however, the early October soil-water content measurements in the top 30 cm were lower than the grass-legume sites, which depicts the influence of interception by the woody vegetation. Following the larger storms of October, the surface measurements at all three sites, conducted on November 23, were similar in magnitude (approximately 39%). Since the measurements on November 23 were conducted several days following rain and snowmelt, 39% appears to be the oxidized tailings field capacity, although it may be slightly overestimated because measurements were conducted at a dry interlude during several days of light rainfall.

Although more soil-moisture replenishment occurred in September, the soil-water content depth profiles (Fig. 7.8a..f) all exhibit an advanced wetting front on November 23, as compared to October 7. On the tailing bench, at WA30 (Fig. 7.8e,f), the data depicts a profile which reflects the homogeneity of the tailings. In contrast, the layering of the tailings surface (WA15), which has different bulk densities and water holding capacities (e.g, at 40 cm depth), manifests as water content variations in the depth profile (Fig. 7.8a..d); because of differential layering, the soil-water content at WA15g and WA15t was greater at 30 to 60 cm than at 0 to 30 cm. Employing the depth profile data (Appendix C4), soil-water content increase from October 7 to November 23 was approximately 60% of the precipitation (Table 8.1): 53% at WA15g, 60% at WA15t, and 67% at WA30.

Table 8.1. Soil-water Content Increase from Oct 7 to Nov 23.

Description	WA15g	WA15t	WA30
Length of depth segment showing significant change in soil-water content (cm):	81	106	67
Average soil-water content (%) increase increase across depth segment:	8.17	7.08	12.65
Quantity of water within the depth segment (mm or L/m^2):	66.2	75.0	84.7
Percent of precipitation as soil-water (Total PPT = 126 mm):	53	60	67

Note: Calculations appear in Appendix C4.

8.5 Soil-water Potential

Soil-water matric potential was measured each hour at all three monitoring sites from October 7 through November 20 with heat dissipation sensors (Fig. 7.10a,b,c). Soil matric potential (negative pressure potential) is proportional to soil-water content; as water content increased, pressure potential increases. Three mechanisms influence the *in-situ* soil-water content and therefore the matric potential: (1) infiltration, (2) evaporation, and (3) groundwater recharge and discharge. The results from the

monitoring of soil-matric potential predominately illustrate the mechanisms of infiltration and evaporation.

Matric potential generally increased during the monitoring period due to infiltration, resembling the increasing trend noted in the soil-water content data. Most of the change transpired during the wet period, October 14 to 20 (JD 287 to 293). On October 18 (JD 291), a rapid change in matric potential is particularly evident at the 45 cm depth of WA30 (Fig. 7.10c), indicating the presence of a passing wetting front. Change in matric potential is also detected at the 45 cm depth of WA15g (Fig. 7.10a), although less in magnitude, which introduces more difficulty in its separation from the evaporative mechanism. At WA15t matric potential increased across 75 cm depth, demonstrating deeper wetting promoted by tree root pathways (Fig. 7.10b).

Interestingly, at WA15t all four sensors across 75 cm depth (15, 30, 45, and 75 cm depth) responded to precipitation during the 10 day stormy period, October 10 to 20 (JD 283-293) (Fig. 7.10b). At the grass-legume sites, however, response to infiltration occurred later on October 18 (JD 291) and only at the 45 cm depth. This illustrates two phenomena at WA15t: reduced moisture delivery due to interception, and delivery along root channels. Antecedent to soil-moisture monitoring, at the grass-legume sites, the tailings top 30 cm had been replenished by infiltration, indicated by little change in ψ at 15 and 30 cm depth (Fig. 7.10a,c), which corresponds to the water content data (Fig. 7.6), and by October 18 (JD 291), the wetting front reached 45 cm depth, noting a change in ψ. At WA15t, however, the tailings top 30 cm was not replenished, manifesting as ψ response to infiltration at 15 and 30 cm depth. This contrast depicts interception by the tree cover. In addition, infiltration that was delivered along root channels replenished reasonably equally to 45 cm depth and reaching 75 cm by the passing of the storms on October 19;

this root channel infiltration is also exhibited in the water content depth profiles (Fig. 7.8c,d) in their dissimilarity to a sharply-defined wetting front profile which is depicted at WA30 (Fig. 7.8e,f).

At WA30 (Fig. 7.10c), most of the change in matric potential occurred at the 45 cm depth, which reflects the depth of greatest change in soil-water content (Fig. 7.8e,f). Also in accordance with the trend in soil-water content data, matric potential decreases with depth, with the exception of the sensor at 75 cm. At this depth, the sensor is located in unoxidized tailings, which may have a different soil-water energy characteristic. This suggesting that, at a given water content, the unoxidized tailings exhibits less matric suction than oxidized tailings, which reflects the more open structure (larger voids) of oxidized tailings. In addition, at 75 cm depth, the tailings may be in a wetting trend (i.e., the dominant voids sizes unemptied), and at shallower depths, intermediate "scanning curve" states may reside (i.e., partially filled dominant void sizes), which results in an elevated suction for the shallower points at a given water content. Although less evident, a similar trend is interpreted at WA15g and WA15t (Fig. 7.10a,b).

At WA15g and WA15t (i.e., on the tailings surface) (Fig. 7.10a,b), the layering (particularly at the 45 cm depth) complicates analysis; each layer may have a different soil-water energy characteristic, inhibiting comparison with soil-water content measurements. However, excluding the data from the 45 cm depth (the layer with the higher bulk density and water content), the decreasing matric potential with depth resembles the trend observed in soil-water content profile.

While evapotranspiration is minimal during autumn (Table 5.1), dial fluctuations in matric potential are nevertheless evident. Transpiration generally ceases after

the first killing frost, thus, the dial fluctuation is principally due to evaporative demand during the monitoring period, although warm days may show a transpirative demand in October. Dial fluctuations additionally show a decrease in magnitude through the season which parallels the evaporative trend. The dial fluctuation of matric potential is generally inverse to the dial fluctuation in evaporation (and transpiration), which is evident in the comparison of matric potential with air temperature; as air temperature increases, so also does evaporation which decreases soil-water content and matric potential. The decreased matric potential induces hydraulic flow which lowers soil-water content and potential elsewhere.

Table 8.2. Average Lag in Matric Potential Response to ET as Indicated by Air Temperature in October, Grass-Legume Sites.

AIR TEMP. TIME[a/]	WA30-15 (hours)	WA30-30 (hours)	WA30-45 (hours)	WA30-75 (hours)	WA15g-15 (hours)	WA15g-30 (hours)	WA15g-45 (hours)	WA15g-75 (hours)	WA15g-105 (hours)
281.27	4.56	4.56	4.56	4.56	2.64	3.64	3.60	3.60	3.60
281.58	4.08	4.08	4.08	5.04	2.16	3.12	3.12	3.12	5.04
303.67	2.40	3.84	3.64	3.84	2.88	2.88	2.88	2.88	2.88
304.33	4.08	3.12	4.08	3.12	2.16	2.16	2.16	2.16	3.12
304.58	4.08	4.08	5.04	5.04	4.08	4.08	4.08	4.08	5.04
AVERAGE	3.84	3.94	4.32	4.32	2.78	3.18	3.17	3.17	3.94

a/ Julian time of air temperature peak or trough.

The peaks and troughs of the dial fluctuation in matric potential exhibit a lag in comparison to the temperature (and thus evaporation) fluctuations (Table 8.2). In addition, the lag increases with soil depth, demonstrating soil-moisture flow. Liquid and vapor fluxes are coupled in their relation to evaporation and, with regard to the presented data, the two mechanisms are difficult to

separate[1]; thus, they are grouped together as soil-moisture flow. The lag in the dial fluctuations of matric potential with soil depth represents the velocity of soil-moisture to the soil surface (Table 8.3), representing evapotranspiration. This flux may be related to pan evaporation through a proportionality constant, where pan evaporation (E_{pan}) equals the velocity (v) multiplied by a constant (C). Assuming 30 mm pan evaporation during October (Table 5.1):

$$C = \frac{E_{pan}}{v} = \frac{30\,mm}{(850\,mm/hr)(24\,hr/day)(31\,days)} = 4.7x10^{-5} \qquad (8.1)$$

The fact that C is small is explained by the fact that q is not an average daily rate, but more the peak rate for the day. In addition, *C* incorporates porosity and may be dependent on moisture content.

8.6 Groundwater Hydraulic Head

Piezometer water-level elevations located at nest sites WA15 and WA30 were measured with submersible pressure transducers every hour from October 7 through November 20. Additional monitoring data were also collected at WA15-1; hourly measurements began on September 15.

At WA15 (Fig. 7.12a), piezometer water level elevations gradually increased during the monitoring period, reflecting a rising watertable, caused by a larger recharge to the tailings ground water than that discharging. By November, recharge approximately equaled discharge, and at the end of the monitoring period (Nov. 20), the watertable showed a

---

[1]The soil temperature data illustrate increasingly less influence with soil depth by the transfer of latent heat, which suggests less loss of soil-water as vapor with depth. The matric potential data illustrates little consistent trend with depth, which suggests the coupling of vapor and fluid flow.

Table 8.3. Average Peak Velocity of Moisture to the Tailings Surface.

SITE	DEPTH TO (cm)	LAG[a/] (hr)	DEPTH FROM WHICH RATE IS MEASURED 15	30	45	75	AVERAGE (cm/hr)
WA15g	15	2.78	-				
	30	3.18	37.5	-			
	45	3.17	76.9	-	-		
	75	3.17	153.8	-	-	-	
	105	3.94	77.6	98.7	77.9	39.0	80.2
WA30	15	3.84	-				
	30	3.94	150.0	-			
	45	4.32	62.5	39.5	-		
	75	4.32	125.0	-	-	-	94.2
WA15G + WA30							85.3

Calculation: (depth from - depth to) / (lag at depth from - lag at depth to)

a/ Average lag in matric potential response to evaporation as indicated by air temperature in October, grass-legume sites.

slight decline, indicating less recharge. This trend, which was also observed at WA30 (Fig. 7.12b), generally corresponds to the increased (above normal) precipitation that succeeded a dryer than normal August. Depth to water measurement on August 15, however, indicate that the tailings watertable was higher than that observed at the onset of the piezometer monitoring period September 15 (Appendix C6), providing evidence of a declining watertable during the dry period of the latter part of August and early September.

Watertable fluctuations were greatest in September, despite storms of less magnitude than those of October (Fig. 7.13). The rapid rise of the watertable reflects the rapid conversion of tension-saturated soil-water of the capillary fringe to pressure-saturated ground-water. This conversion occurs by the percolation of a relatively small amount to water to the capillary fringe (much smaller than the specific yield). In addition, a declining watertable exhibits a larger capillary fringe than that of an advancing (rising) watertable. Therefore, following the watertable decline in late August, the September storms produced

greater rises in watertable than those of October, after the watertable elevation had advanced.

Similar to the rapid increase in watertable elevation with recharge of a small amount of water, thereby releasing tension saturated water, a rapid decline subsequently transpires by the passing vertical flow from the capillary fringe. In addition, lateral distribution (flow) of water in the capillary fringe may be encouraged if increased horizontal gradients develop; this flow is aided by the fact that the horizontal hydraulic conductivity of pyrite sediment is greater than the vertical hydraulic conductivity. Dependent on storm type, the watertable below a level surface may not rise as a level plane; precipitation is aerially and temporally transient resulting a similar recharge pattern, yet more pronounced due to soil heterogeneity. Thus, the fluctuating watertable may enhances the horizontal flow of capillary water. However, because water also flows vertically (following a potential gradient), the capillary water successively becomes ground water and follows a flow path of the saturated domain. Enhanced lateral flows at the watertable can flush the soils in proximity of a seepage face, which contributes to streamflow generation (Blowes and Gillham, 1988).

The rate at which the watertable rises and falls by the conversion of tension-saturated to pressure-saturated pore-water is presumably related to specific discharge. This soil water release mechanism can be therefore regarded as a multiplier in its relation to specific discharge. Studies of this mechanism may unfold a technique of calculating specific discharge (recharge) and hydraulic conductivity at the watertable. However less in magnitude, the capillary fringe fluctuation may also occur with a change in barometric pressure, which would produce a more level rise and fall of the watertable.

The fluctuations in water-table elevation caused by the conversion of tension-saturated to pressure-saturated pore-water exhibits a lag in the piezometric head across a vertical piezometer nest (Fig. 7.14). This lag, however, does not represent, the specific discharge (q), neither vertical nor horizontal. A fluctuation (i.e., the release and capture of tension saturated water) can be envisioned as a pore-water pressure pulse, and the vertical delivery through the medium exhibits a pore-water pressure velocity which is displayed as a lag in the piezometric data (Table 8.4). Clearly the velocity is much greater than expected; the specific discharge of a saturated silty soil with a hydraulic conductivity of 10^{-4} would require a hydraulic gradient of 83 ($\partial h/\partial z$) to produce such groundwater flow.

Table 8.4. Average Pore-water Pressure Wave Velocity Across Vertical Piezometer Nest WA15.

PIEZOMETER	ELEVATION (meter)	DEPTH (meter)	EVENT NUMBER	PEEK TIME (JD)	PRESSURE WA15-4 (cm/s)	VELOCITY TO WA15-3 (cm/s)
WA15-1	309.45	6.51	1	284.27	4.8E-03	-
			2	291.67	1.2E-02	1.0E-02
			3	293.04	3.1E-03	6.2E-03
WA15-4	308.25	7.71	1	284.56		-
			2	291.79		1.0E-02
			3	293.48		1.2E-02
WA15-3	305.74	10.22	1	-		
			2	292.08		
			3	293.73		
Average pressure velocity (n=7) = 8.28E-03 cm/sec						

Event #1 = piezometer crest following peek precipitation on Oct 10.
Event #2 = piezometer crest following precipitation on Oct 18.
Event #3 = piezometer trough following precipitation on Oct 18.

At WA15, hydraulic head gradients indicate a slight artesian pressure which describes groundwater flow from the clay to the tailings (Fig. 7.12a). In addition, other piezometer nests along cross section A-A′ also portray similar conditions (Table 8.5), which appear to be most pronounced below the tailings surface; artesian pressures

Table 8.5. Piezometric Hydraulic Head Values, Section A-A'.

PIEZOMETER	ELEVATION HEAD (m)	DEPTH (m)	HYDRAULIC HEAD (m) Aug 15	Oct 09	Nov 22
Ground	8.85	0.00	-	-	-
WA15-2	5.38	3.47	5.42	dry	dry
WA15-1	2.34	6.51	4.59	4.41	4.69
WA15-4	1.13	7.72	4.61	4.45	4.65
WA15-3	-1.37	10.22	4.79	4.74	4.93
Ground	9.09	0.00	-	-	-
WA28-3	6.09	3.00	dry	dry	dry
WA28-2	2.91	6.18	4.06	3.89	4.12
WA28-1	1.20	7.89	4.09	4.17	4.07
Ground	9.68	0.00	-	-	-
WA29-2	3.39	6.29	3.50	-	3.49
WA29-1	0.27	9.41	3.47	-	3.46
Ground	5.90	0.00	-	-	-
WA30-2	1.34	4.56	3.03	2.96	2.77
WA30-1	-0.16	6.06	2.96	2.96	2.58
Ground	2.47	0.00	-	-	-
WA31-3	1.89	0.58	2.40	-	2.50
WA31-2	-0.55	3.02	2.17	2.02	2.17
WA31-1	-2.05	4.52	2.27	2.15	2.27
Ground	1.02	0.00	-	-	-
WA32-3	-1.13	2.15	1.06	-	1.03
WA32-2	-1.98	3.00	0.96	-	0.94
WA32-1	-3.98	5.00	1.37	-	1.41
WEIR	0.00	-	-	-	-

appear successively deeper below the tailings benches. As the tailings watertable rose from recharge during the monitoring period, upward hydraulic gradients also increased from the clay (Fig. 7.12a), however, downward flow was also enhanced at the watertable (measured at piezometer nests WA15 and WA28 on November 22; Table 8.5). Because topographic relief does not appear to provide a regional pressure head, this phenomenon is presumably due to local groundwater flow patterns, possibly induced by the high watertable in the central tailings area (Fig. 5.3), west of the cross-section terminus. In addition, the flow pattern may be complicated by the heterogeneity of the clay (which previously supported forest and wetlands) and consolidation subsequent to burial.

8.7 Gypsum Block Resistance

Uncalibrated gypsum blocks were installed at WA15g on August 18, and at WA15t and WA30 on September 10, principally to indicate the trend in soil matric potential. They also, however, indicate large changes in soil electrical conductance. The results were in accord with other data (e.g., soil-water content and potential) in that the monitoring period from September 13 through November 20 is a period of soil wetting by infiltration (i.e., wetting front advancement). The results were particularly useful to indicate the state of wetting at a particular depth and the

relative change in soil-moisture content (i.e. wetting or drying). At times of rapid changes, the velocity of the wetting front can be measured, thereby characterizing the infiltration rate.

At WA15g (Fig. 7.15a), the advancing wetting front was displayed throughout the monitoring period: at 15 and 30 cm depth on September 14 (JD 257), to the 45 cm depth with the storms on September 21 (JD 264), and reaching 75 cm (and 105 cm minimally) by late October, following the storms that concluded on October 18 (JD 291). A similar trend was also depicted at WA15t (Fig. 7.15b) but with less wetting due to interception by the tree cover; wetting to the 45 cm depth did not reach that of WA15g (grass cover) until the storm of October 10 (JD 283), approximately 50 mm of precipitation succeeding the storms ending on September 25. This lag, however, may not be an accurate estimation of interception because infiltration advances further along root pathways which distributes the water at depth, resulting in a vertically exaggerated wetting front (less sharply defined). In other words, if the total quantity infiltrating is equal at both sites, a given depth exhibits different soil-water contents.

At WA15t, the gypsum blocks were installed dry (on August 18) which enhanced the detection of an advancing wetting front. At WA15g and WA30, however, the gypsum blocks were installed prior to the onset of monitoring (on September 10) in a moist state (with the exception of the 30 and 45 cm depth at WA15t). Thus, changes in resistance were less during infiltration; apparently, gypsum blocks equilibrate slowly in the soil environment (Fig. 7.15b,c). Although, when a gypsum block is at equilibrium with a soil, the soil and gypsum block will presumably change water contents at similar rates.

Gypsum-block measurements are less sensitive to changes in soil-water potential than measurements by heat-

dissipation sensors because the dial fluctuations in matric pressure were not detected. However, they may also equilibrate slower than the fluctuation frequency.

8.8 Energy State of Tailings Water *In Situ*

The pressure head, hydraulic head, and elevation head are illustrated collectively to describe the hydraulic-energy state (i.e., groundwater mechanical-energy state) near the ground surface of the tailings (Fig. 7.11a..f). The energy state is depicted for the commencement and conclusion of the principal monitoring period, October 7 and November 23. The results generally depict the wetting and storage of infiltrating water in the vadose zone, thereby rasing the energy state of the soil water.

The soil matric potential is plotted with both the heat-dissipation sensor data and gypsum block data. Because they are also dependent on the porewater chemistry, gypsum blocks are limited in their measurement of soil-suction. As a result, on October 7 measurements of gypsum-block resistance generally underestimate the soil suction, due to the high electrical conductance of the tailings pore waters. However, on November 23 this is not the case. In fact, the suction values (especially at 15, 30, and 45 cm depths) changed very little from the October measurement, when the heat-dissipation sensors indicated a decrease in suction. This can be explained by examination of gypsum block calibration curve (Fig. 7.16b). Apparently, the gypsum blocks are at their minimum suction value (i.e., the resistance of a saturated block). This value, approximately 300 cm water seems to be higher than that measured by gypsum blocks which were submerged in distilled water at saturation with gypsum (215 cm water).

These energy state figures are helpful to indicate the direction of flow, and with a hydraulic conductivity, specific discharge can be calculated. In general, there

appears to be a flow from both the tailings surface and the watertable toward the actively oxidizing region (50-100 cm depth), approximately to the base of wetting front. This seems to suggest exfiltration[1] and infiltration following a dry period. Interestingly, the profiles of November 23 are generally the same shape as that of October 7, but with a higher head overall; this indicates unchanged flow as soil-moisture is replenished. Although if soil moisture is replenished, the hydraulic conductivity will also increase, thus increasing the flow.

The hydraulic gradients are quite large -- from the surface, i = 12/1, and from the watertable, i = 3/1. To provide a perspective on these values an estimate is developed to quantify the flow at WA15g, where the observed flow condition appears most pronounced. Given the quantity of water that infiltrated and replenished soil-moisture during this 47 day period (approximately 66 mm, Table 8.1), an estimate of hydraulic conductivity would be 10^{-6} cm/s, which is reasonable (Section 5). However, given these conditions, infiltrating water would not reach the watertable without flowing solely through a secondary porosity (e.g., root channels or fractures), which seems unlikely. On the other hand, the suggestion of a calibration error is lessened due tho the fact the situation repeats at all the stations. Therefore, it is difficult to state confidence in this data without further study. One can state, though, that a phenomenon exists, whether it is an artifact of the measurement technique is unknown.

---

[1]*Exfiltration* is defined as the removal of water from the surface across the ground surface, together with the associated flow towards the ground surface within the unsaturated zone. The process is often referred to as evaporation, but this leads to confusion to whether the meteorological processes in the atmosphere are included. See Freeze and Cherry (1979), p. 211.

9.0 Hydrologic Analysis of the Results

The results of subsurface hydrologic monitoring at the cross section A-A' (i.e. at WA15g, WA15t, and WA30) provided appropriate findings for which a hydrologic analysis is justified. Estimates of infiltration, soil-moisture storage, groundwater recharge, and evapotranspiration are balanced against the measurement of precipitation to generate a hydrologic budget of the vadose zone during the monitoring period, October 7 through November 23. This water balance quantifies the subsurface hydrology of Waite Amulet tailings during a wet autumn.

9.1 Infiltration

When isolated storms produce a detected advancement of a wetting front, the infiltration rate and average hydraulic conductivity of the unsaturated zone can be calculated with the matric-potential monitoring data. The wet period of October 14 to 20 provided ideal conditions at the 45 cm depth of monitoring site WA30 (Fig. 7.10c). Precipitation during this period was generally light with a defined peak on October 18 (JD 291). Following the increased precipitation intensity, infiltrating water produced a defined decrease in matric potential. The difference in time between the two peaks represents the maximum velocity (v) of the wetting front:

$$v = \left(\frac{45cm}{12hr}\right) = 3.75\frac{cm}{hr} \qquad (9.1)$$

given n = 0.6, the infiltration rate (q) is 2.25, and by applying Darcy,s law of fluid flow,

$$v = \frac{K(\psi)\, i}{n} \qquad (9.2)$$

$K(\psi)$ can be calculated with antecedent matric-pressure head at the depth of interest:

$$K(\psi) = q\frac{\partial x}{\partial h} = (2.25\frac{cm}{hr})(\frac{1hr}{3600s})(\frac{45cm}{1100cm}) = 2.6x10^{-5}\frac{cm}{sec} \qquad (9.3)$$

This calculation of $K(\psi)$, that of a passing wetting front is similar to saturated hydraulic conductivity (Section 5).

The gypsum block data provided more opportunities for which to measure the velocity of a wetting front (Table 9.1). Unfortunately, all but one event occurred in September, prior to the onset of monitoring the soil-matric potential with heat-dissipation sensors. Thus, without the potential gradients, estimates of hydraulic conductivity are not possible. Nevertheless, the velocity of the wetting front on October 10 (JD 283) was calculated at the 75 cm depth of monitoring site WA15t and utilizing the potential gradients from the heat dissipation sensors, the hydraulic conductivity is calculated:

$$K(\psi) = nv\frac{\partial x}{\partial h} = (0.6)(3.7x10^{-4}\frac{cm}{sec})(\frac{75cm}{800cm}) = 2.1x10^{-5}\frac{cm}{sec} \qquad (9.4)$$

Average wetting-front velocities are characterized by depth interval in Table 9.2. In general, the velocity and thus the infiltration rate is an order of magnitude higher on the tailings bench (WA30) than on the tailings surface (WA15g), with a tree cover increasing the infiltration by a factor of three (WA15t), exemplified by the segment 30 to 45 cm:

Site	Velocity		Velocity	x	Porosity		Infiltration
WA15g	= 0.000128	cm/s	= 0.46 cm/h	x	0.6	=	0.28 cm/h
WA15t	= 0.000409	cm/s	= 1.47 cm/h	x	0.6	=	0.88 cm/h
WA30	= 0.00121	cm/s	= 4.36 cm/h	x	0.6	=	2.61 cm/h

The interception by vegetation, however, alters these proportions and the variance with storm type and antecedent moisture conditions.

TABLE 9.1. Measured Wetting-Front Velocities at Waite Amulet Tailings, 1990.

MONITORING SITE	TIME OF RAIN PEAK (JD)	PRECIPITATION PEAK INTENSITY (mm/hr)	SENSOR DEPTH (cm)	TIME OF MAXIMUM CHANGE IN RESISTANCE (JD)	VELOCITY (cm/s) TO SENSOR DEPTH 15 cm	30 cm	45 cm
WA15g	257.104	4.4	Ground	-	3.07E-04	4.92E-04	
			15	257.67		1.24E-03	
			30	257.81			
	264.438	3.6	Ground	-	2.88E-04	5.21E-04	2.58E-04
			15	265.04		2.67E-03	2.45E-04
			30	265.11			1.28E-04
			45	266.46			
	264.771	3.2	Ground	-	3.11E-04	5.04E-04	
			15	265.33		1.34E-03	
			30	265.46			
WA15t	257.104	4.4	Ground	-		3.75E-04	3.84E-04
			15	-			
			30	258.03			4.04E-04
			45	258.46			
	264.438	3.6	Ground	-		3.33E-04	3.56E-04
			15	-			
			30	265.48			4.13E-04
			45	265.90			
	283.521	9.4	Ground	-		3.70E-04	
			15	-			
			30	284.46			
WA30	264.438	3.6	Ground	-	3.33E-04	5.77E-04	6.75E-04
			15	264.96		2.17E-03	1.39E-03
			30	265.04			1.02E-03
			45	265.21			
	264.771	3.2	Ground	-	3.35E-04	6.16E-04	7.56E-04
			15	265.29		3.86E-03	2.04E-03
			30	265.33			1.39E-03
			45	265.46			

Note: Infiltration rate was calculated by the response of a gypsum block nest following a significant precipitation event.

Note: Ground refers to measurements at a rain gauge, which refers to the vegetation surface.

Table 9.2. Average Wetting-Front Velocities at Waite Amulet.

MONITORING SITE	DEPTH INTERVAL	AVERAGE[a/] VELOCITY (cm/s)	SAMPLE SIZE (n)
WA15g	Ground to 15 cm depth	3.02E-04	3
	Ground to 30 cm depth	7.45E-04	3
	Ground to 45 cm depth	2.58E-04	1
	15 to 30 cm depth	1.75E-03	3
	15 to 45 cm depth	2.45E-04	1
	30 to 45 cm depth	1.28E-04	1
WA15t	Ground to 15 cm depth	-	0
	Ground to 30 cm depth	3.59E-04	3
	Ground to 45 cm depth	3.70E-04	2
	15 to 30 cm depth	-	0
	15 to 45 cm depth	-	0
	30 to 45 cm depth	4.09E-04	2
WA30	Ground to 15 cm depth	3.34E-04	2
	Ground to 30 cm depth	5.96E-04	2
	Ground to 45 cm depth	7.15E-04	2
	15 to 30 cm depth	3.01E-03	2
	15 to 45 cm depth	1.72E-03	2
	30 to 45 cm depth	1.21E-03	2

a/ Average of several events, each calculated from the response of a gypsum block nest to a significant precipitation event.

Note: Ground refers to measurements at a rain gauge, which actually refers to the vegetation surface.

9.2 Soil-moisture Storage

Soil-moisture can be calculated by the difference in water content succeeding an infiltration event. The specific soil-moisture storage, $C(\psi)$, can be calculated by the reciprocal of soil moisture storage with the difference in matric potential.

$$C(\psi) = \frac{\partial\theta}{\partial\psi} \qquad (9.5)$$

During the study, however, soil-water content was periodically measured, with no regard to infiltration; measured at the convenience of site visits. Therefore, data describing the soil-moisture storage related to infiltration events was not collected. However, the total storage during the monitoring period, October 7 through November 23 (as described in Section 8.4), was approximately 60% of the precipitation (Table 8.1): 53% at WA15g, 60% at WA15t, and 67% at WA30.

9.3 Groundwater Recharge

During the monitoring period October 7 through November 23, the tailings water table exhibited little net change, which is illustrated in the piezometer hydraulic head temporal plots (Fig. 7.12a,b). A maximum net increase during October is estimated at 10 cm with nearly an equal decline in November. This increase, however does not reflect the total recharge to the tailings water table, it simply represents the net change from the total recharge less the discharge. In absence of discharge data, the sum of the recharge events displayed as capillary fringe fluctuations (described in Section 8.6) best represents the total recharge. Both approaches include specific yield, although an increase in the capillary fringe (i.e., the release of tension saturated water) entails a greatly reduced

"effective" specific yield (approximated at an order of magnitude).

At Waite Amulet, specific yield has not been estimated. However, assuming a porosity of 0.60 (Section 8.2) and a field capacity of 0.35 (Section 8.4), an approximated specific yield would be 0.25. A sum of the water table increases in the capillary fringe approximates the total recharge to the tailings water table during the 47 days as 40 mm (1.3 m multiplied by 0.03 "effective" specific yield), which is a factor of 1.3 greater than that calculated by a net rise in water table during the monitoring period (1 m multiplied by 0.3). Therefore discharge would roughly be 10 mm. If half of the tailings drained to surface water station #2 then 10 mm would equal approximately 2,000 m^3 or an average flow for the 47 days of 0.5 L/s (8 gpm).

9.4 Evapotranspiration

The dial fluctuation of soil-water content portrays the flux of water affected by the demand for evapotranspiration. As a result of the depletion of soil moisture, evapotranspirative gradients are established towards the soil surface and water moves upward to supply the deficiency. During the day, the movement of water is more rapid as the evapotranspirative demand is greatest, resulting in a loss of soil water and a decline in soil-water potential. During the night, transpiration and evaporation losses are small, the soil-water content and potential increases.

The dial fluctuation in response to evapotranspiration was initially observed at the water table by plants reaching the capillary fringe. A study by White (1932) documented fluctuations in water table under various vegetation types in Escalante valley, Utah. Observations concluded that in the evening and morning from about 6 to 10, the recharge approximately balances discharge, and the water table is

still. The state of equilibrium would be reached earlier if it were not for the replenishment of water to plants in the evening, following the decline in transpiration; a similar lag occurs during the morning, as plants begin to discharge water to the atmosphere. By approximately midnight, the demand for water by plants has discontinued and capillary equilibrium has been established in the capillary fringe. Between midnight and 4 a.m. the water table is approximately at a mean elevation for the 24 hour period (disregarding the net gain or loss). Therefore, neglecting the very slight evapotranspirative losses during midnight and 4 a.m., in addition to the net loss or gain, the hourly rate of discharge during this period may be given as the average rate for the 24 hour period. The total discharge for the day thus includes the rate of discharge and net loss or gain in water table elevation (i.e., the net loss or gain in water content).

From a hydrologic budget perspective, a change in the water table elevation for the day (i.e., the amount of water lost or gained during 24 hours) is equal to the mean hourly rate of groundwater discharge or recharge (r) multiplied by 24 hours less the evapotranspirative losses for the day (E_t).

$$\Delta z = 24r - E_t \qquad (9.6)$$

where, $\Delta z = z_2 - z_1$ is negative when water is lost and positive when water is gained; r is the hourly rate during midnight and 4 a.m., and is positive during discharging groundwater conditions and negative during recharging groundwater conditions; and E_t is a positive number. If $\Delta z = 0$, then $E_t = 24r$. If $E_t = 0$ then $\Delta z = 24r$.

The White method of calculating evapotranspiration is most applicable when recharge and discharge rates are reasonably steady and minimal (i.e., Δz primarily due to E_t); large losses and gains by groundwater recharge and

discharge tend to eclipse the effect of E_t. At Waite Amulet, for example, the effect of E_t on the tailings water table elevation seems to be minimal in comparison to the dynamics of tailings groundwater recharge. For this reason, the White method of calculating E_t does not apply well to the piezometer data collected at the monitoring sites.

A similar line of reasoning can be applied to unsaturated soils, above the water table:

$$\Delta\theta = 24r - E_t \qquad (9.7)$$

where, $\Delta\theta$ is the amount of soil-water content lost or gained during 24 hours ($\theta_2 - \theta_1$) and is negative if soil water is lost and positive if soil water is gained; r is the daily mean rate of discharge taken between midnight and 4 a.m.; and E_t is the amount of water lost by evapotranspiration. If soil-water content is measured each hour (by TDR), then r can be calculated, and thus, E_t can be estimated with an adapted White method. With the data collected during this thesis investigation (i.e., periodic soil-water content measurements and hourly measurements of matric potential) estimates are futile because *r* could only be calculated with the slope of the matric potential data (between 12 and 4 a.m.) which is dependent on the specific soil-moisture capacity, $C(\psi)$, a unknown value.

$$r = \frac{\partial\theta}{\partial t} = \frac{\partial\theta}{\partial\psi}\frac{\partial\psi}{\partial t} = C(\psi)\frac{\partial\psi}{\partial t} \qquad (9.8)$$

An estimation of specific soil-moisture capacity can be attempted by continuity of mass and momentum, where for one-dimensional, transient, unsaturated flow:

$$\frac{\partial}{\partial z}(K(\psi)\frac{\partial h}{\partial z}) - C(\psi)\frac{\partial \psi}{\partial t} \qquad (9.9)$$

substituting $h=\psi+z$

$$\frac{\partial}{\partial z}(K(\psi)(\frac{\partial \psi}{\partial z}+1)) - C(\psi)\frac{\partial \psi}{\partial t} \qquad (9.10)$$

and isolating $C(\psi)$

$$C(\psi) - \frac{\partial t}{\partial \psi}\frac{\partial}{\partial z}(K(\psi)(\frac{\partial \psi}{\partial z}+1)) \qquad (9.11)$$

For homogeneous soil and water-content:

$$C(\psi) - \frac{\partial t}{\partial \psi}\frac{\partial}{\partial z}(\frac{\partial \psi}{\partial z}+1) - \frac{\partial t}{\partial \psi}\frac{\partial^2 \psi}{\partial z^2} \qquad (9.12)$$

It is noted that $C(\psi)$ is always positive, therefore, during wetting conditions $\partial t/\partial \psi$ is negative and $\partial^2\psi/\partial z^2$ is negative, and during drying conditions $\partial t/\partial \psi$ is positive and $\partial^2\psi/\partial z^2$ is positive. This method of calculating $C(\psi)$, however, has limited practical application and when coupled with Equation 9.7 with which to estimate evapotranspiration, the accuracy of the estimate is greatly reduced. Revising equation 9.8,

$$r - \frac{\partial \theta}{\partial t} - \frac{\partial \psi}{\partial t}C(\psi) - \frac{\partial \psi}{\partial t}(\frac{\partial t}{\partial \psi}\frac{\partial^2 \psi}{\partial z^2}) - \frac{\partial^2 \psi}{\partial z^2} \qquad (9.13)$$

therefore equation 9.7 is:

$$\Delta\theta - 24\frac{\Delta^2 \psi}{\Delta z^2} - E_t \qquad (9.14)$$

9.5 Water Balance

A water budget of the inflows and outflows at the soil surface includes the balance of precipitation (P) with runoff (RO), infiltration (I), and Evapotranspiration (ET).

$$P = RO + I + ET \tag{9.15}$$

Similarly, a water budget below the soil surface would include balance of infiltration (I) with soil moisture storage (C) and recharge to groundwater (R).

$$I = C + R \tag{9.16}$$

Thus, a water balance of the soil column (vadose zone) consists of:

$$P = RO + ET + C + R \tag{9.17}$$

Regarding a water balance of the tailings, the period from October 7 through November 23 envelopes the monitoring period appropriate for analysis. During the 47 days, 126 mm of precipitation fell primarily as rain, but also as snow that subsequently melted. A major portion of the precipitation was stored as soil-moisture (Section 8.4). An estimate of soil-moisture storage for the tailings surface is 67 mm (WA15g of Table 8.1). The balance of these two components estimates a total of 59 mm for the combined recharge, evapotranspiration, and runoff.

Evapotranspiration during the monitoring period is minimal, approximately 15 to 20 mm by extrapolation of the regional climatic records (Table 5.1), and the remaining 39 to 44 mm approximates groundwater recharge, which is similar to the estimate using water table monitoring data (Section 9.3). Of the amount that recharged, a rough estimate of discharge is 10 mm (Section 9.3). Runoff, as Hortonian overland flow, is therefore minimal, a maximum of 5 mm (4% of precipitation), which seems reasonable for light

precipitation on a level, primarily grass-legume covered, silty soil, although, the runoff-infiltration ratio is 1/20, a low value. If pan evaporation data and streamflow (at ST2) data were collected the records could validate these approximations of runoff, evapotranspiration, and groundwater recharge. Of the percent of precipitation (100%), water balance estimates are:

- Soil-moisture storage at 53%,
- Evapotranspiration at 12%,
- Tailings groundwater recharge at 31%, and
- Runoff at 4%.

10.0 Summary and Conclusions

Acid discharge from mine and mill tailings sites constitute an important environmental problem. At such sites, investigations are generally hydrogeochemical, hydrogeological, or geotechnical in nature, interpreting the geochemical evolution of the porewater and evaluating the saturated flow. In response, a soil-water (i.e., geohydrologic; sub-surface hydrologic) approach was undertaken in this thesis to shed light on the hydrology of the unsaturated zone, the region of sulfide mineral oxidation.

A review of the physics of soil water concentrated on the theories of soil-water energy -- soil structure, water-retention mechanisms, analytical approaches, and soil-water energy characterization. The *in-situ* techniques of soil-moisture measurement were thoroughly reviewed regarding soil-moisture potential and soil-moisture content. In particular, a rigorous account of the principles of time-domain reflectometry (TDR), including a comprehensive literature review, evaluated this method of soil-moisture content determination.

In-situ vadose-zone monitoring was conducted at 3 vertical profiles along a cross-section of the Waite Amulet Tailings near Rouyn-Noranda, Quebec. Two profiles were located on the top surface, one under a grass-legume cover, the dominant vegetation type of the tailings, and the other in an young aspen-birch grove. The third profile was located in a bench lower in elevation and towards the edge of the tailings. At this profile the material was coarser and more homogenous than that of the two sites on the tailings top surface, and had a grass legume cover. The study characterized the fall of 1990, September 13 to November 23 (71 days).

The continuous monitoring data that were successfully collected included that from gypsum blocks, heat dissipation

sensors, and pressure-transducer piezometers, in addition to rainfall and air and soil temperatures. Soil-moisture content was periodically measured by time-domain reflectometry and gravimetric methods.

The TDR measurements, conducted with vertical soil-transmission lines, were successful to a depth of 60 cm; beyond this, the wave attenuated in unoxidized tailings. The relation of soil-moisture content by TDR method to that by gravimetric method indicated a good degree of linear association ($r=0.936$) that was statistically significant ($p<0.0000$). Therefore, TDR predicted the soil-water content of oxidized tailings with an 88% reliability. This level of accuracy, however, required careful interpretation of the TDR trace.

During the study period an increase in tailings-water content was measured. This increase was estimated at 53% of the precipitation. The TDR data detected advancing wetting fronts and interception by woody vegetation. Following a significant infiltration event, the field capacity of the oxidized tailings was measured at 0.39.

Measured with heat dissipation sensors, the tailings matric potential data evidenced infiltration and evaporation. The velocity of the wetting front was determined at 3.75 cm/h, the infiltration rate at 2.25 cm/h, and the hydraulic conductivity, $K(\Psi)$, at 2.5×10^{-5} cm/s. Not surprisingly, infiltration at the aspen-birch site demonstrated interception by the woody vegetation and deeper wetting promoted by tree-root pathways. Evapotranspiration caused dial fluctuations in matric potential, which exhibited an increasing lag with depth. Employing this data, the average peak velocity of the soil-moisture flow towards the surface was calculated at 85 cm/h (0.24 mm/s).

The gypsum blocks were most useful to indicate the state of wetting at a particular depth, relative changes in moisture content, and the velocity of a wetting front (i.e.,

infiltration rate). The infiltration rate was highest on the tailings bench (2.16 cm/hr), which was about an order of magnitude higher than the tailings top surface (0.28 cm/h) and 3 times that of the tailings surface with tree cover (0.88 cm/h). Apparently during the fall, a tree cover increases infiltration into tailings by a factor of three. Gypsum blocks are more sensitive to changes in matric potential than heat dissipation sensors, however are slower to equilibrate, and thus do not detect dial fluctuations caused by evapotranspiration.

The watertable showed a net rise during the study period, indicating recharge conditions. Hydraulic gradients indicated a slight artesian pressure from the underlying clay to the tailings.

Watertable fluctuations were largest early in the study period, subsequent to a decline in the water table (i.e., a discharge period); coupled with an extended capillary fringe, the rapid rise (and fall) of the watertable (a recharge peak) reflected the conversion of tension-saturated to pressure-saturated pore-waters by the percolation of a relatively small amount of water. This phenomenon may result in elevated flushing of the tailings porewaters, particularly those of the tailings bench. At distance from the seepage face, porewaters may distribute more laterally. This phenomenon also produced a porewater pressure pulse which was detected as a lag in the peak with depth.

Recharge to the watertable was approximated by the sum of the recharge peaks multiplied by an "effective" specific yield, resulting in 31% of precipitation. Three-quarters of this was detected as a net change in waterlevel, and one quarter was estimated to discharge as seepage, which presumably produced an average baseflow of 0.5 L/s (8 gpm) at surface water station #2.

A water budget was developed for the study period, the fall of 1990. The budget characterized a wetter than normal

fall antecedent to a dryer than normal August. The budget, therefore, characterized recharge conditions. Of the percent of precipitation (100%), water balance estimates are:

- Soil-moisture storage at 53%,
- Evapotranspiration at 12%,
- Tailings groundwater recharge at 31%, and
- Runoff at 4%.

10.1 Review of Sensor Effectiveness

Time-domain reflectometry (TDR) measurements proved valuable when conducting a water balance. Periodic measurements along a vertical profile yields changes in soil-moisture storage, which is integral to infiltration. TDR, however, is has a maximum resolution in sandy soils with a low solute content. As the electrical nature of the soil increases, the resolution decreases. In this study no useable measurements were obtained in unoxidized tailings, where the E_c is elevated; the wave soon attenuated after passing though approximately 0.5 m of oxidized tailings. Under these circumstances, horizontal installation of shorter soil-transmission lines are recommended along a vertical profile. The reliability of the measurements in oxidized tailings was 88%, but not without careful methodology.

TDR was also useful to determine the field capacity following a significant infiltration event. The wetting front and interception by woody vegetation were also detected. These and other applications would be greatly enhanced by more frequent measurements (i.e., automated measurements). For example, application of the White method (1932) of determining evapotranspiration could be adapted to changes in soil-water content. Infiltration rate could also be measured if a vertical profile were multiplexed.

Heat dissipation sensors respond readily to changes in matric potential, detecting small dial fluctuations in response to evapotranspiration. In addition, they provide a measurement of temperature. They suffer, however, by needing a precise calibration, which is difficult and time consuming. Doubt was cast on some data collected in this study as to the precision of the calibration provided by the manufacturer. The calibration may be checked *in situ* with a tensiometer but this is not always applicable, as it was not in this study. With a weak calibration, though, heat dissipation sensors are useful in detecting wetting fronts and calculating infiltration rates and hydraulic conductivities, as they were in this study.

Gypsum blocks, though dependent on porewater chemistry, are useful to indicate the state of wetting (i.e., dry or wet) and large changes in water content. They proved valuable in detecting wetting fronts and calculating infiltration rates, and simply as a confirmation to events detected by other instrumentation. Gypsum blocks are not sensitive to the dial fluctuations driven by evapotranspiration.

Tensiometers were not effective in this study due to the freezing temperatures that were encountered. Prior to fieldwork, attempts to equip the tensiometers with pressure transducers in addition to a dial gage proved arduous; the fittings inclined to leak. Tensiometers generally require weekly maintenance.

The continuous record of watertable elevation collected from Pressure-transducer piezometers proved invaluable to detect the rapid changes in piezometric head resulting in the conversion from tension-saturated to pressure-saturated pore-water. With this data, an estimate of recharge was feasible, and with the net change in waterlevel, an estimate of discharge was also feasible. These estimates were useful in the water balance.

10.2 Thesis Critique and Recommendations

This thesis study provides a sound foundation for soil-water, geohydrologic, and sub-surface hydrologic investigations, particularly those *in situ*. Two overall objectives were proposed in Chapter 2: (1) develop a soil-water monitoring system suitable for study in the corrosive environment of sulfide tailings; and, utilizing this methodology (2) evaluate the hydrologic controls in the vadose zone of the Waite Amulet tailings site. This thesis was successful in fulfilling both of these objectives.

With regard to the questions posed in Chapter 1, all of them were addressed except for the first two questions.

Question (a), "What is the infiltration capacity of the tailings surface, and what storm events exceed the infiltration capacity, resulting in Hortonian overland flow?" was not addressed because the usable data that were collected did not facilitate appropriate analysis. Data permitted the calculation of infiltration for the entire study period, which was not sensitive to infiltration events. If soil-moisture content were measured regarding these events an appropriate analysis would be possible. Automating TDR would facilitate such an analysis.

Question (b), "Are there partial-area or variable-source-area contributions to overland flow and how does the watertable fluctuation contribute to these areas?" was indirectly answered but not strictly addressed. Overland flow was minimal and partial-area and variable-source-area contributions were not observed.

Question (c), "Are there significant increases in the hydraulic gradient of the saturated zone due to the conversion of tension-saturated water of the capillary fringe to pressure-saturated porewaters?" was addressed in Section 8.6.

Question (d) "What are the typical exfiltration hydraulic gradients and evapotranspiration estimates?" was touched on in Section 8.8. In short, exfiltration gradients may exist in the unsaturated zone but data reliability is uncertain.

Question (e) "What is the soil-moisture storage of the tailings? How does infiltration contribute to soil-moisture storage and recharge to the tailings saturated zone, and what storm events contribute to recharge?" was addressed in Section 8.4 and in the water balance. Although, particular storm events were not addressed due to available data.

Question (f) "What are the hydrogeologic properties with regard to Darcian flow?" was addressed in Section 9.1.

Question (g) "What are the dynamics of the tailings hydrologic system?" was generally addressed throughout the entire thesis, however Section 8.5, 8.7, 8.9, and 9.1 addressed unsaturated flow.

Question (h) "What are the quantitative changes of the hydrologic system (i.e., water balance) during the monitoring period" was addressed in many parts of the thesis and summarized in Section 9.5.

In addition to fulfilling the proposed objectives, several problems were confronted and partially resolved.

(1) As an artifact of the measurement of soil suction with the heat dissipation sensor, soil temperature is also measured. Although not directly used in this hydrologic study, the data was discussed in Section 8.3. In the process, several hypotheses were developed on which further study is recommended.

(2) Evapotranspiration was estimated in this thesis with pan evaporation records. However, two theories were developed which may yield good estimates of evapotranspiration if further studied. The most promising is the application of the White method of evapotranspiration measurement to the unsaturated zone (Section 9.4). Less interesting, a proportionality constant was developed utilizing an observed lag in dial fluctuations of matric potential, measured with heat dissipation sensors (Section 8.5).

(3) In the analysis involving the conversion of tension-saturated to pressure-saturated pore-water (Section 8.6), a pressure wave was observed in the piezometric head data. This may have geophysical applications if further studied.

The results of this thesis were strictly physical in nature with no attempt of incorporating geochemical studies. It is recommended that the hydrologic controls be coupled with geochemical reaction rates or morphology to access the hydrologic impact on tailings oxidation. In addition, this approach would be generously compounded with a complete year of monitoring data. Several years of data would be ideal.

11.0 References Cited

Annan, A.P. (1977). Time-domain reflectometry - air gap problem for parallel-wire transmission line. Report of activities, part B. *Geol. Surv. Can.*, Paper 77-1B:59-62.

Baker, J.M., and R.R. Allmaras (1990). System for automating and multiplexing soil moisture measurement by time-domain reflectometry. *Soil Sci. Soc. Am. J.* 54(1):1-6.

Baker, J.M., and R.J. Lascano (1989). The Spatial sensitivity of time-domain reflectometry. *Soil Sci.* 147:378-384.

Blackport, R. (1986). A preliminary hydrogeological investigation of the Waite Amulet tailings - 1985 field season. A report prepared for Centre de technologie Noranda. Terraqua Investigations LTD., Waterloo, ON, N2L 1L5.

Blackport, R. (1987). Hydrogeological sampling and instrumentation of the Waite Amulet tailings - 1986 field season. A report prepared for Centre de technologie Noranda. Terraqua Investigations LTD., Waterloo, ON, N2J 1N8.

Blake, G.R. (1986). Bulk density. *In* Methods of soil analysis, Part 1, Physical and Mineralogical Methods, 2nd ed., A.L. Page (ed), Agronomy Series Monograph No. 9, Soil Sci. Soc. Am., Madison, Wis., p. 374.

Bloodworth, M.E., and J.B. Page (1957). Use of thermistors for the measurement of soil moisture and temperature. *Soil Sci. Soc. Am. Proc.* 21:11-15.

Blowes, D.W. and J.A. Cherry (1987). Hydrogeochemical investigations of the unsaturated zone of the Waite Amulet tailings site, WRI Award No. 1142401. A final report prepared of the Centre de technologie Noranda.

Blowes, D.W., and R.W. Gillham (1988). The generation and quality of streamflow on inactive uranium tailings near Elliot Lake, ON. *J. Hydro.* 97:1-22.

Blowes, D.W., and J.L. Jambor (1988). The pore-water geochemistry and the mineralogy of the vadose zone of sulphide tailings, Waite Amulet, PQ. Report to CANMET, DSS Contr. No. 23440-7-9161/01-SQ.

Bouyoucous, G.J., and A.H. Mick (1940). An electrical resistance method for the continuous measurement of soil moisture under field conditions. *Michigan Agric. Exp. Sta. Tech. Bull.* 172.

Bouyoucous, G.J. (1949). Nylon electrical resistance unit for continuous measurement of soil moisture in the field. *Soil Sci.* 67:319-330.

Bouyoucous, G.J. (1953). More durable plaster of paris moisture blocks. *Soil Sci.* 76:447-451.

Brown, R.W., and D.L. Bartos (1982). A calibration model for screen-caged Peltier thermocouple psychrometers. U.S. For. Serv. Res. Paper INT-293, Ogden, UT, 84401, 155 p.

Campbell, J.E. (1990). Dielectric properties and influence of conductivity in soils at one to fifty megahertz. *Soil Sci. Soc. Am. J.* 54(2):332-341.

Campbell Scientific, Inc. (1991). TDR soil-moisture measurement system manual., P.O. Box 551, Logan, UT, 84321, USA.

Chudobiak, W.J., B.A. Syrett, and H.M. Hafez (1979). Recent advances in broad-band VHF and UHF transmission line methods for moisture content and dielectric constant measurement. *IEEE Transactions on Instrumentation and Measurement*, IM-28(4):284-289.

Colman, E.A., and T.M. Hendrix (1949). Fiberglass electrical soil-moisture instrument. *Soil Sci.* 67:425-438.

Dalton, F.N., and S.L. Rawlins (1968). Design criteria for Peltier-effect thermocouple psychrometers. *Soil Sci.* 105:12-17.

Dalton, F.N., W.N. Herkelrath, D.S. Rawlins, and J.D. Rhoades (1984). Time domain reflectometry: Simultaneous measurement of soil water content and electrical conductivity with a single probe. *Science* 224:989-990.

Dalton, F.N., and M.Th. van Genuchten (1986). The time-domain reflectometry method for measuring soil water content and salinity. *Geoderma* 38:237-250

Dasberg, S., and F.N. Dalton (1985). Time-domain reflectometry field measurements of soil water content and electrical conductivity. *Soil Sci. Soc. Am J.* 49:293-297

Davis, J.L. (1975). Relative permittivity measurements of a sand and clay soil *in situ*. *Geol. Surv. Can.*, paper 75-1C:361-365.

Davis, J.L., and A.P. Annan (1977). Electromagnetic detection of soil moisture: Progress report I. *Can. J. Remote Sensing* 3(1):76-86.

Davis, J.L., and Chudobiak, W.J. (1975). *In-situ* meter for measuring relative permittivity of soils. *Geol. Surv. Can.*, paper 75-1, part A, pp.75-79.

Davis, J.L., R. Singh, M.J., Waller, and P. Gower (1983). Time-domain reflectometry and acoustic-emission monitoring techniques for locating linear failures. *U.S. Environmental Protection Agency*, Office of Research and Development, Cincinnati, Ohio, 45268. Contr. #68-03-3030.

Dejager, J.M., and J. Charles-Edwards (1969). Thermal conductivity probe for soil moisture determinations. *J. Ex. Bot.* 20:46-51.

Denbigh, K.G. (1981). The principles of chemical equilibrium, 4th ed., Cambridge University Press, New York.

Drungil, C.E.G., K. Abt, and T.J. Gish (1989). Soil moisture determination in gravelly soils with time-domain reflectometry. *Trans. ASAE* 32(1):177-180.

Fellner-Feldegg, H (1969). The measurement of dielectrics in the time-domain. *J. Phys. Chem.* 73(3):616-623.

Ferroni, G.D., and L.G. Leduc (1985). Quantification of *Thiobacillus ferrooxidans* and sulfate-reducing bacteria in core samples from the Waite Amulet tailings. A report prepared for Centre de technology Noranda. Laurentian U., Sudbury, ON, P3E 2C6.

Fredlund, D.G., and D.K.H. Wong (1989). Calibration of thermal conductivity sensors for measuring soil suction. *Geotech. Test. J.* 12(3):188-194.

Freeze, R.A., and J.A. Cherry (1979). Groundwater. Prentice-Hall, Inc., New Jersey, 604 p.

Gardner, W.O., W. Israelsen, N.E. Edlefsen, and H. Conrad (1922). The capillary potential function and its relation to irrigation practice. *Phys. Rev.* Ser. 2, 20, 196.

Gardner, W.H. (1986). Water Content. *In* Methods of soil analysis, Part 1, Physical and Mineralogical Methods, 2nd ed., A.L. Page (ed), Agronomy Series Monograph No. 9, Soil Sci. Soc. Am., Madison, Wis., pp. 82-127.

Geotechnical Research Centre (1990). Geotechnical properties of selected samples from the Waite Amulet tailings, Noranda, Quebec. Report to Centre de technologie Noranda. McGill U., Montreal, PQ.

Hall, A.D., and R.E. Fagen (1956).Definition of system. General systems yearbook I, pp. 18-28.

Hallikainen, M.T., F.T. Ulaby, M.C. Dobson, M.A. El-Rayes, and L.K. Wu (1985). Microwave dielectric behaviour of wet soil, I. Empirical models and experimental observations. *IEEE Trans. Geosci. Remote Sens,* GE-23(1):25-34.

Handbook of Chemistry and Physics (1977). 57th ed., CRC press, Cleveland, Ohio.

Hasted, J.B. (1973). Aqueous Dielectrics. J. Wiley and Sons, New York, 302 p.

Hayhoe, H.N., G.C. Topp, and W.G. Bailey (1983). Measurements of soil-water contents and frozen water depths during a thaw using time-domain reflectometry. *Atmos-Ocean* 21:299-311.

Heimovaara, T.J., and W. Bouten (1990). A computer-controlled 36-channel time-domain reflectometry system for monitoring soil-water contents. *Water Resour. Res.* 26:2311-2316.

Herkelrath, W.N., S.P. Hamburg, and F. Murphy (1991). Automatic, real-time monitoring of soil moisture in a remote field area with time-domain reflectometry. *Water Resour. Res.* 27(5):857-864.

Hillel, D. (1972). Soil and water, physical principles and processes. Academic Press, Inc., New York, 288 p.

Hoekstra, P, and A. Delaney (1974). Dielectric properties of soil at UHF microwave frequencies. *J. Geophys. Res.* 79:1969-1706.

Intergovernmental Working Group on the Mineral Industry (IGWGMI) (1988). Report on the economic and policy aspects of acid discharge. Canadian agency report by the federal-provincial-industrial sub-committee on mine waste.

Iwata S., and T. Tabuchi (1988). Soil-water interactions, mechanisms and application. Marcel Dekker, Inc., New York. 380p.

Jambor, J.L. (1986). Detailed mineralogical examination of alteration products in core WA20 from Waite Amulet tailings. Report prepared for Centre de technology Noranda. CANMET Mineral Sci. Lab., project 30.86.02, report 86-45 (IR).

Jambor, J.L. (1987a). Mineralogical and chemical investigation of cores from Waite Amulet tailings, Noranda, Quebec. Report prepared for Centre de technology Noranda. CANMET Mineral Sci. Lab., project 30.86.02, report 87-32 (IR).

Jambor, J.L. (1987b). Character and depth of oxidation of the reactive acid tailings at the Waite Amulet mine site, Noranda, Quebec. Report prepared for Centre de technology Noranda. CANMET Mineral Sci. Lab., project 30.86.02, report 87-97 (IR).

Jenny, H. (1961). Derivation of state factor equations of soil ecosystems. *Soil Sci. Soc. Am. Proc.* 25:385-388.

Johnson, L.N. (1942). Water permeable jacketed thermal radiators as indicators of field capacity and permanent wilting percentage in soils. *Soil Sci.* 54:123-126.

Keng, J.C.W., and G.C. Topp (1983). Measuring water content of soil columns in the laboratory: a comparison of gamma ray attenuation and TDR techniques. *Can. J. Soil Sci.* 63:37-43.

Knight,J.H. (1991). The sensitivity of time-domain reflectometry measurements to lateral variations in soil moisture content. *Water Resour. Res.* (submitted).

Lambe, T.W., and R.V. Whittman (1969). Soil Mechanics. J. Wiley and Sons, New York, 553 p.

Ledieu, J.,P. DeRidder, P. DeClerck, and S. Dautrebande (1986). A method of measuring soil moisture by time-domain reflectometry. *J. Hydro.* 88:319-328.

Litynski, J.K. (1983). The numerical classification of the world climates. World Meteoro. Org., Geneva, 46 p.

Litynski, J.K. (1987). Analysis des climats du Québec Méridional, section IV. *In* Climatologie du Québec Méridional, H. Proulx *et al.*, Ministére de L'Environnement de Québec direction de la Météorolgie, pp. 85-94.

Lowery, B., B.C. Datiri, and B.J. Andraski (1986). An electrical readout system for tensiometers. *Soil Sci. Soc. Am. J.* 50:494-496.

Mangold, D.C., and C.-F.Tsang (1991). A summary of subsurface hydrological and hydrochemical models. *Rev. of Geophys.* 29(1):51-79.

Markus, J. (1966). Electronics and Nucleotonics Dictionary, 3rd ed., McGraw-Hill, New York.

Marthaler, H.P., W. Vogelsanger, F. Richard, and P.J. Wierenga (1983). A pressure transducer for field tensiometer. *Soil Sci. Soc. J.* 47:624-627.

Mitchell, J.K. (1976). Fundamentals of soil behavior. J. Wiley and Sons, New York. 422 p.

Nikodem, H.J. (1966). Effects of soil layering on the use of VHF radio waves for remote terrain analysis. *Proceedings of the 4th Symposium on Remote Sensing of Environment*, Univ. Mich., Ann Atbor, pp. 691-703.

Oke, T.R. (1987). Boundary Layer Climates, 2nd ed. Routledge, New York. 435 p.

Patterson, D.E., and M.W. Smith (1981). The measurement of unfrozen water content by time domain-reflectometry: Results from laboratory tests. *Can. Geotech. J.* 18:131-144.

Patterson, D.E., and M.W. Smith (1984). Unfrozen water content in saline soils: results using time-domain reflectometry. *Can. Geotech. J.* 22:95-101.

Patterson, D.E., and M.W. Smith (1985). Comment on " Monitoring the unfrozen water content of soil and water using time-domain reflectometry" by J. Stein and D.L. Kane. *Water Resour. Res.* 21:1055-1056.

Peck, A.J. (1968). Theory of Spanner psychrometer 1. The thermocouple. *Agric. Meteorol.* 5:433-447.

Peck, A.J. (1969). Theory of Spanner psychrometer 2. Sample effects and equilibration. *Agric. Meteorol.* 6:111-124.

Petruk, W., and R. Pinard (1986). Mineralogical and image analysis study of samples from core WA20 of the Waite Amulet tailings. Report prepared for Centre de technologie Noranda. CANMET Mineral Proc. Lab., project 30.86.02, report 86-87 (IR).

Phene, C.J., G.J. Hoffman, and S.L. Rawlins (1971a). Measuring soil matric potential *in situ* by sensing heat dissipation within a porous body: I. Theory and sensor construction. *Soil Sci. Soc. Am. Proc.* 35:27-33.

Phene, C.J., G.J. Hoffman, and S.L. Rawlins (1971b). Measuring soil matric potential *in situ* by sensing heat dissipation within a porous body: II. Experimental results. *Soil Sci. Soc. Am. Proc.* 35:225-229.

Phene, C.J. (1986). Operational principles, chapter 3.3, Automation. *In* Trickle Irrigation for Crop Production. F.S. Nakayama and D.A. Bucks (eds). Elsevier Publication, pp. 188-215.

Phene, C.J., C.P Allee, and J. Pierro (1987). Measurement of soil matric potential and real-time irrigation scheduling. *In* Proceedings of the international conference on measurement of soil and plant water status, Utah State U., vol. 2, pp 258-265.

Ramo, S., J.R. Whinnery, T. Van Duzer (1984). Fields and Waves in Communication Electronics. John Wiley and Sons, Inc., New York.

Rawlins, S.L. (1966). Theory for thermocouple psychrometers used to measure water potential in soil and plant samples. *Agr. Meteorol.* 3:293-310.

Rawlins, S.L, and F.N. Dalton (1967). Psychrometer measurement of soil-water potential without precise temperature control. *Soil Sci. Soc. Am. Proc.* 31:297-301.

Rawlins, S.L. (1971). Some new methods for measuring the components of water. *Soil Sci.* ??:8-16.

Reynolds, T.D., R.B. Shepard, J.W. Laundré, and C.L. Winter (1987). Calibrating resistance-type soil-moisture units in a high clay-content soil. *Soil Sci.* 144(4):237-241.

Richards, L.A., and W. Gardner (1936). Tensiometers for measuring the capillary tension of soil water. *J. Am. Soc. Agron.* 28:352-358.

Richards, L.A. (1949). Methods of measuring soil moisture tension. *Soil Sci.* 68:95-112.

Richards, S.J. (1986). Soil suction measurements with tensiometers. *In* Methods of soil analysis, Part 1, Physical and Mineralogical Methods, 2nd ed., A.L. Page (ed), Agronomy Series Monograph No. 9, Soil Sci. Soc. Am., Madison, Wis., pp. 153-163.

Richter, J. (1987). The soil as a reactor, modelling processes in the soil. *Catena paperback* Catena Verlag, W. Germany.

Ripley, E.A., R.E. Redmann, and J. Maxwell (1978). Environmental Impact of Mining in Canada. Centre for Resource Studies, Queen's University, Kingston, ON, 274 p.

Roth, K., R. Schulin, H. Fluhler, and W. Attinger (1990). Calibration of time-domain reflectometry for water content measurement using a composite dielectric approach. *Water Resour. Res.* 26:2267-2273.

Runge, E.C.A. (1973). Soil development sequences and energy models. *Soil Sci.* 115(3):183-193.

Sattler, P., and D.G. Fredlund (1989). Use of thermal conductivity sensors t measure matric suction in the laboratory. *Can. Geotech. J.* 26:491-491.

Schmugge, T.J., T.J. Jackson, and H.L. McKim (1980). Survey methods for soil-moisture determination. *Water Resour. Res.* 16:961-978.

Scotter, D.R. (1972). The theoretical and experimental behaviour of the spanner psychrometer. *Agric. Meteorol.* 10:125-136.

Shaw, B., and L.D. Bauer (1939a). Heat conductivity as an index of soil moisture. *J. Am. Soc. Agron.* 31:886-891.

Shaw, B and L.D. Bauer (1939b). An electrothermal method for following moisture changes of the soil *in situ*. *Soil Sci. Soc. Am. Proc.* 4:78-83.

Siwik, R. (1986). Hydrogeochemical investigation of reactive tailings at Waite Amulet tailings site, Noranda, Quebec, phase 1, 1985 program. Report to CANMET, DDS contr. no. 23SQ.23440-5-9120.

Siwik, R.S., R. Prairie, and S. Payant (1987). Hydrogeochemical investigation of reactive tailings at Waite Amulet tailings site, Noranda, Quebec, phase 2, 1986 program. Report to CANMET, DDS contr. no. 01SQ.23440-6-9099.

Siwik. R.S., L. St-Arnaud, R.Prairie, and L. Labrosse (1988). Hydrogeochemical investigation of reactive tailings at Waite Amulet tailings site, Noranda, Quebec, phase 3, 1987 program. Report to CANMET, DDS contr. no. 03SQ.23440-7-0161

Smith-Rose, R.L. (1933). The electric properties of soil for alternating currents at radio frequencies. *Proc. R. Soc. London* 140:359-377.

Soilmoisture Equipment, Inc. (1987). Porous ceramics by soilmoisture., 600 series, P.O. Box 30025, Santa Barbara, CA, 93105, USA, 20 p.

Soilmoisture Equipment, Corp. (1990). Trace system I. operating instructions., P.O. Box 30025, Santa Barbara, CA, 93105, USA.

Spanner, D.C. (1951). The peltier effect and its use in the measurement of suction pressure, *J. Exptl. Bot.* 2:145-168.

Sposito, G. (1981). The thermodynamics of soil solutions. Oxford Clarendon Press, New York. 223 p.

Stannard, D.I. (1990). Tensiometers - theory, construction, and use. *In* Ground water and vadose zone monitoring, ASTM STP 1053, D.M. Nielsen and A.I. Johnson (eds), Am. Soc. Test. Mat., Phil., pp. 34-51.

Stein, J., and D.L. Kane (1983). Monitoring the unfrozen water content of soil and snow using time-domain reflectometry. *Water Resour. Res.* 19(6):1573-1584.

Strangeways, I.C. (1983). Interfacing soil-moisture gypsum blocks with a modern data-logging system using a simple, low-cost, DC method. *Soil Sci.* 136(5):322-324.

Stumm E., and J.J. Morgan (1981). Aquatic chemistry, an introduction emphasizing chemical equilibria in natural waters. J. Wiley and Sons, New York, 780 p.

Topp, G.G., J.L. Davis, A.P. Annan (1980). Electromagnetic determination of soil water content using TDR: Measurements in coaxial transmission lines. *Soil Sci. Soc. Am. J.* 46:672-678.

Topp, G.C., and J.L. Davis (1981). Detecting infiltration of water through soil cracks by time-domain reflectometry. *Geoderma* 26:13-23.

Topp, G.G., J.L. Davis, A.P. Annan (1982a). Electromagnetic determination of soil water content using TDR: I. Applications to wetting fronts and steep gradients. *Soil Sci. Soc. Am. J.* 46:672-678.

Topp, G.G., J.L. Davis, A.P. Annan (1982b). Electromagnetic determination of soil water content using TDR: II. Evaluation of installation and configuration of parallel transmission lines. *Soil Sci. Soc. Am. J.* 46:678-684.

Topp, G.C., J.L. Davis, and J.H. Chinnick (1983). Using TDR water content measurements for infiltration studies. *In* Advances in Infiltration. ASAE Publication 11-83:231-239.

Topp, G.G., J.L. Davis, W.G. Bailey, and W.D. Zebchuk (1984). The measurement of soil water content using a portable TDR hand probe. *Can. J. Soil Sci.* 64:313-321.

Topp, G.C., and J.L. Davis (1985). Time-domain reflectometry (TDR) and its application to irrigation scheduling. *In* Advances in Irrigation, Volume 3. Academic Press, Inc.

Topp, G.C., and J.L. Davis (1985). Measurement of soil water content using time-domain reflectometry (TDR): A field evaluation. *Soil Sci. Soc. Am. J.* 49:19-24.

Topp, G.C., and J.L. Davis (1985). Comment on "Monitoring the unfrozen water content of soil and water using time-domain reflectometry" by J. Stein and D.L. Kane. *Water Resour. Res.* 21:1059-1060.

Topp, G.C., M. Yanuka, W.D. Zebchuk, and S. Zegelin (1988). Determination of electrical conductivity using time-domain reflectometry: Soil water experiments in coaxial lines. *Water Resour. Res.* 24:945-952.

Ulrich, B. (1987). Stability, elasticity, and resilience of terrestrial ecosystems with respect to matter balance. *In* Potentials and limitations of ecosystem analysis. E.D. Schulze and H. Zwolfer (eds). Springer-Verlag, 435 p.

Villa Nova, N.A., K. Reichardt, P.L. Libardi, and S.O. Moraes (1989). Direct reading "air-pocket" tensiometer. *Soil Tech.* 2:403-407.

Wang, B.W. (1986). Compositional effects on soil suction. M.Eng. thesis, McGill U., Montreal, Quebec, Canada.

Wilson, W. (1990). Soil evaporative fluxes for geotechnical engineering problems. Ph.D. Thesis, Dept. of Eng., U. Saskatchewan, Saskatoon, 464 p.

White, W.N. (1932). A method of estimating ground-water supplies based on discharge by plants and evaporation from soil. U.S. Geo. Surv. Water Supply Paper 659A, 105 p.

Yanuka, M., G.C. Topp, S. Zegelin, and W. D. Zebchuk (1988). Multiple reflection and attenuation of time-domain reflectometry pulses: Theoretical considerations for applications to soil and water. *Water Resour. Res.* 24:939-944.

Yanful, E.K., L. St-Arnaud, and R. Pairie (1989). Generation and evolution of acid pore waters at the waite amulet tailings, final report. Centre de Technology Noranda. N-8523G:RR89-1.

Yong, R.Y. (1980). Some aspects of soil suction, shear strength and soil stability. *Geotech. Eng.* 11:55-76.

Yong, R.Y., T.H. Govert, L.S. Madan, Z.-C. Moh, and Y.C. Chiang (1982). Composition effect on suction of a residual soil. *ASCE Conf. Proc. on* Engineering and construction in tropical and residual soils, Honolulu, HA, Jan. 11-15, 1982. pp. 296-313.

Yong, R.N., and E.J. Hoppe (1989). Application of electric polarization to contaminant detection in soils. *Can. Geotech. J.* 26(4):536-550.

Yong, R.N., and B.P. Warkentin (1975). Soil properties and behaviour. Elsevier Scientific Publishing Co., New York, 449 p.

Zegelin, S.J., and I. White (1989) Improved field probes for soil water content and electrical conductivity measurement using time-domain reflectometry. *Water Resour. Res.* 25(11):2367-2376.

Zegelin, S.J., I. White, and G.F. Russell (1992). A critique of the time-domain reflectometry technique for determining field soil-water content. *Soil Sci. Soc. Am. J.* (submitted).

12 APPENDICES

A1 SURFACE TENSION (after Kohnke, 1968)

Fluid surfaces exhibit certain features resembling the properties of a stretched elastic membrane; hence the name "surface tension". When dissimilar substances make contact at an interface, the inequalities of molecular attraction (cohesion) tend to change the shape of the interface until, in accordance with the "least energy principal," the potential energy of the whole molecular system attains a minimum value.

Surface tension is a force pulling inward at (normal to) the surface of a liquid, tending to make the surface a small as possible. It is due to the unbalancing of the forces of attraction between the molecules, the surface molecules having only the relatively distant gas molecules to pull them outward.

To make it easier to visualize and calculate the nature and dimensions of surface tension, consider the force that holds a soap bubble together. At an imagined central plane of a soap bubble the upper half is held to the lower half by surface tension. Surface tension acts all along the length of the circle that forms the contact between the upper half and the lower half. As there is a surface on the outside as well as on the inside of the bubble, the length over which surface tension acts is twice as long as the circumference of the bubble:

$$2(2\pi r)\gamma \qquad \text{(A1.1)}$$

where γ = surface tension of the water-air interface. The dimensions of surface tension are energy per area (ergs/cm^2) or force per distance (dyne/cm). The pressure on the inside of the bubble (P_B) is greater than the atmospheric pressure (P_A) on the outside of the bubble. Consequently, the difference on the pressures ($P_B - P_A$) acting over the entire area of the cross section of the bubble (πr^2) is the force counteracting the inward pull of the surface tension.

$$4\pi r\gamma = (P_B - P_A)\pi r^2 \qquad \text{(A1.2)}$$

This becomes

$$4\gamma = (P_B - P_A) r \qquad \text{(A1.3)}$$

or

$$P_B - P_A = \frac{4\gamma}{r} \qquad \text{(A1.4)}$$

This shows that the pressure difference is directly proportional to the surface tension and inversely proportional to the radius of the bubble; thus, the bigger radius of the bubble, the smaller the difference in pressure, or in other words, the smaller the inside pressure because the atmospheric pressure can be taken as a constant. This can also be stated: the greater the curvature of the bubble, the greater is the inside pressure.

If a spherical bubble of gas is blown into a liquid, there is only one liquid-gas interface and the length over which surface tension acts is now solely the circumference of the bubble.

$$\Delta P = \frac{2\gamma}{r} \qquad \text{(A1.5)}$$

If the bubble is not spherical,

$$\Delta P = \gamma\left(\frac{1}{r_1} + \frac{1}{r_2}\right) \qquad \text{(A1.6)}$$

where, r_1 and r_2 are the principal radii of curvature for a given point on the interface.

The surface tension of water does not change greatly with temperature, within the temperature limits normally occurring in soil. If the solute concentration is increased, the cohesive forces of the water will increase, and thereby increasing the surface tension of the water.

A2 CONTACT ANGLE (after Hillel, 1972)

If we place a drop of liquid upon a dry solid surface, the liquid will usually displace the gas which covered the surface of the solid and spread over that surface to a certain extent. Where this spreading will cease and the edge of the drop will come to rest, the interface with the gas will form a typical "contact angle" (Fig A2.1).

We can perhaps simplify the matter by stating that, if the adhesive forces between the solid and the liquid are greater than the cohesive forces inside the liquid, and greater than the forces of attraction between the gas and the solid, then the solid-liquid contact angle will tend to be acute and the liquid will wet the solid. A contact angle of zero would mean the complete flattening of the drop and perfect wetting of the solid surface by the liquid. A contact angle of 180° (if it were possible) would mean a complete non-wetting or rejection of the liquid by the gas-covered solid (i.e., the drop would retain its spherical shape without spreading over the surface (assuming no gravity effect).

In order for a drop resting on a solid surface to be in equilibrium with that surface and with the gas phase, the vector sum of the three forces arising from the three types of surface tension present must be zero. In Figure A3.1, the sum of the forces pulling leftward at the edge of the drop must equal the sum of the forces pulling to the right:

$$\gamma_{gs} = \gamma_{sl} + \gamma_{lg}\cos\alpha \qquad \text{(A2.1)}$$

and therefore,

$$\cos\alpha = \frac{\gamma_{gs} - \gamma_{sl}}{\gamma_{lg}} \qquad \text{(A2.2)}$$

where, γ_{sl} is the surface tension between sold and the liquid, γ_{gs} is the surface tension between the gas and the solid, and γ_{lg} is the surface tension between the liquid and the gas. Each of these surface tensions ten to decrease its own interface. Reducing the interfacial tensions γ_{lg} and γ_{sl} (as with the aid of a detergent) can increase cos α and decrease the contact angle α, thus promoting the wetting of the solid surface by the liquid.

The contact angle of a liquid on a solid is generally constant under stable physical conditions. This angle, however, can be different in the case of a liquid advancing upon the solids ("wetting angle" or "advancing angle") than for a liquid that is receding upon the solid surface ("retreating" or "receding" angle). The wetting of pure water upon clean smooth surfaces is generally zero, but where the surface is rough or coated with adsorbed surfactants of a hydrophobic nature, the contact angle, and especially the wetting angle, can be considerably greater than zero.

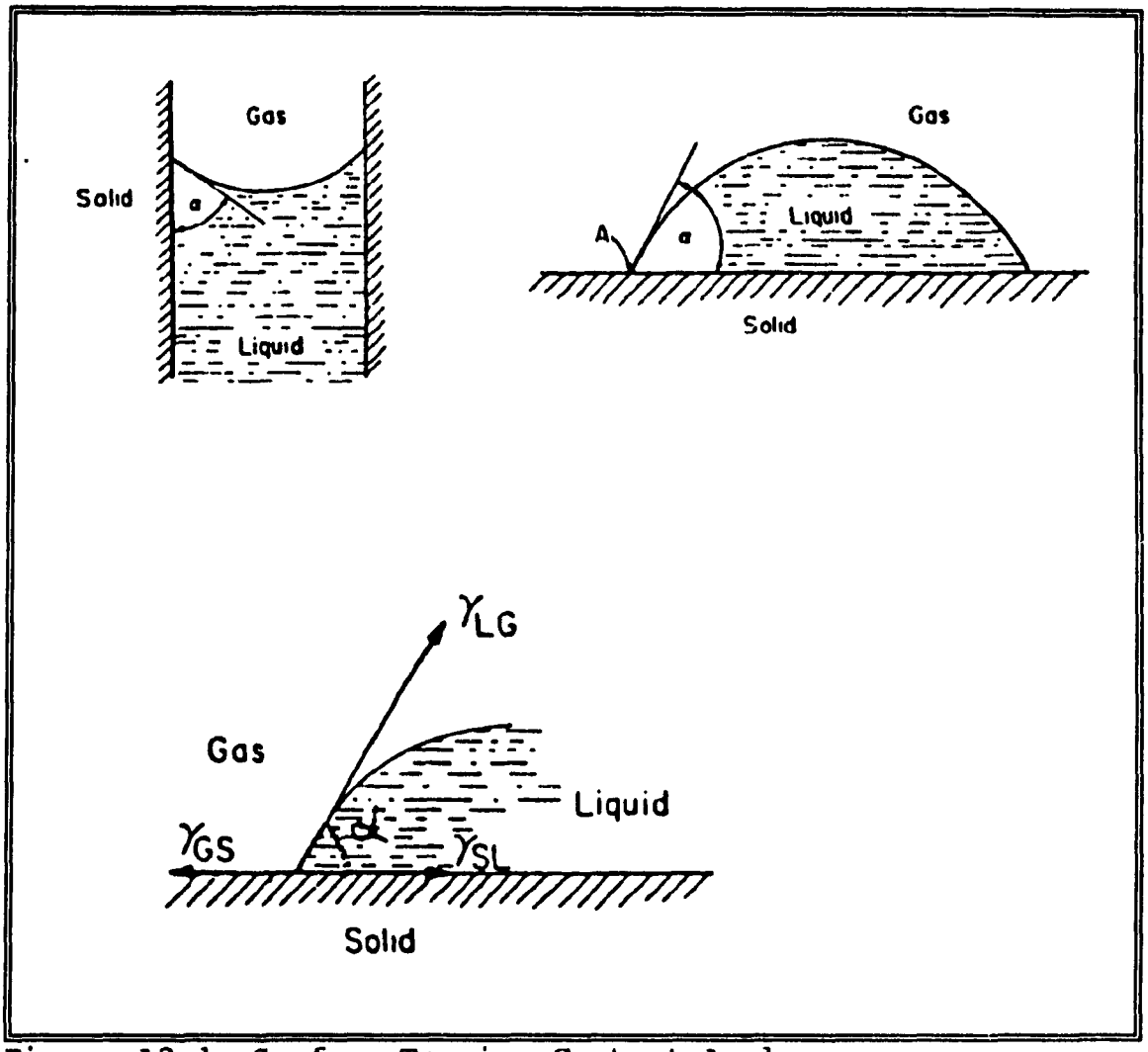

Figure A2.1. Surface-Tension Contact Angle (after Hillel, 1972).

A3 CAPILLARITY (after Hillel, 1972; and Kohnke, 1968)

An important phenomena of surface tension in soil is capillarity (latin *capilla* = hair), the attraction of water into openings of the approximate diameter of a hair. A capillary tube dipped in a body of water will form a meniscus as the result of the contact angle of water with the walls of the tube. The curvature of this meniscus will be greater (i.e. the radius of curvature smaller) with a narrower tube. The occurrence of curvature causes a pressure difference to develop across the liquid-gas interface. A liquid with an acute contact angle (e.g., water on glass) will form a meniscus concave towards the air, and therefore the liquid pressure under the meniscus (P_1) will be smaller than the atmospheric pressure (P_o) (Fig. A3.1). For this reason, the water inside the tube, and the meniscus, will be driven up the tube by a pressure greater than that of free water (i.e., water at atmospheric pressure, under a horizontal air-water interface).

Water is not pulled up by capillarity, it is pushed up by a pressure difference. The height to which the liquid rises is determined by the surface tension and the weight of the liquid column. The water will be driven up the tube until the pressure difference between the water inside the tube (P_1) and the water under the flat surface outside the tube (P_o) is in equilibrium with the hydrostatic pressure of the water column in the capillary tube.

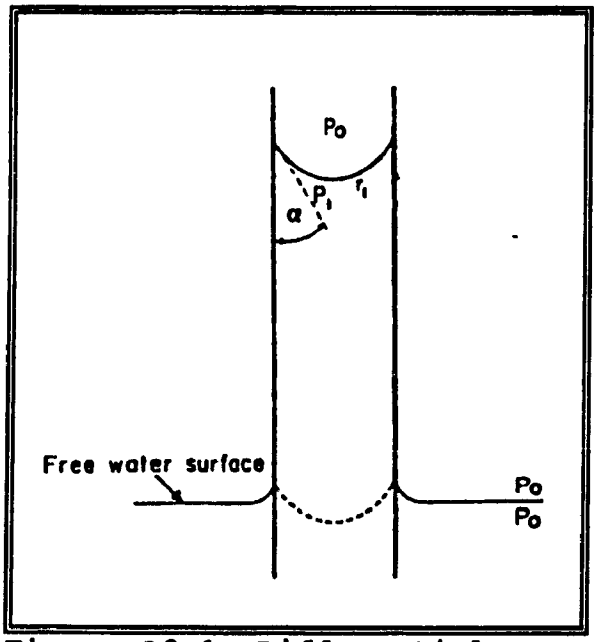

Figure A3.1. Differential Pressure Causing Capillary Rise (after Hillel, 1972).

An equation that permits the calculation of the height of rise of a liquid in a cylindrical capillary tube can be derived in the following manner. At equilibrium the force tending to move the liquid downward must equal the force tending to move the liquid upward.

The downward force is the product of:

h, height of the liquid above its free surface (L);
ρ, density of the liquid (ML^{-3});
g, acceleration due to gravity (LT^{-2}); and,
πr^2, cylindrical capillary cross-sectional area (L^2).

The upward force is the product of:

γ, surface tension of the liquid (ML^{-2});
$2\pi r$, line of contact between the liquid and tube (L);
$\cos \alpha$, cosine of the contact angle (dimensionless).

Equilibrating the two forces,

$$h\rho g(\pi r^2) = \gamma(2\pi r)\cos\alpha \qquad \text{(A3.1)}$$

and solving for h:

$$h = \frac{2\gamma\cos\alpha}{\rho g r} \qquad \text{(A3.2)}$$

For water, the contact angle small and cos α is very close to 1; therefore,

$$h = \frac{2\gamma}{\rho g r} = \frac{4\gamma}{\rho g d} \qquad \text{(A3.3)}$$

where d is the diameter of the capillary.
Assuming water at 20°C, γ = 72.75 dyne/cm, ρ = 0.998 g/cm^3, and g = 981 ergs/g-cm:

$$h = \frac{0.297}{d} \approx \frac{0.3}{d} \qquad \text{(A3.4)}$$

This serves to calculate the height of water rise in a capillary tube. This equation, although, overestimates the height of the capillary fringe above the water table; soil voids are not bundles of capillary tubes, they are variously sized pores interconnected through openings of various sizes ("breathing" channels).

In a cylindrical capillary tube, the meniscus assumes a spherical shape. When the contact angle of the liquid on the walls of the tube is zero, the meniscus is a hemisphere (a 2-D section is represented as a semicircle) with the radius of curvature equal to the radius of the capillary tube. If, on the other hand, the liquid contacts the tube at an angle greater than zero (but smaller than 90°), then the diameter of the tube (2r) is length of the chord cutting a section of a circle with an angle of $\pi-2\alpha$ (Fig. A3.2).

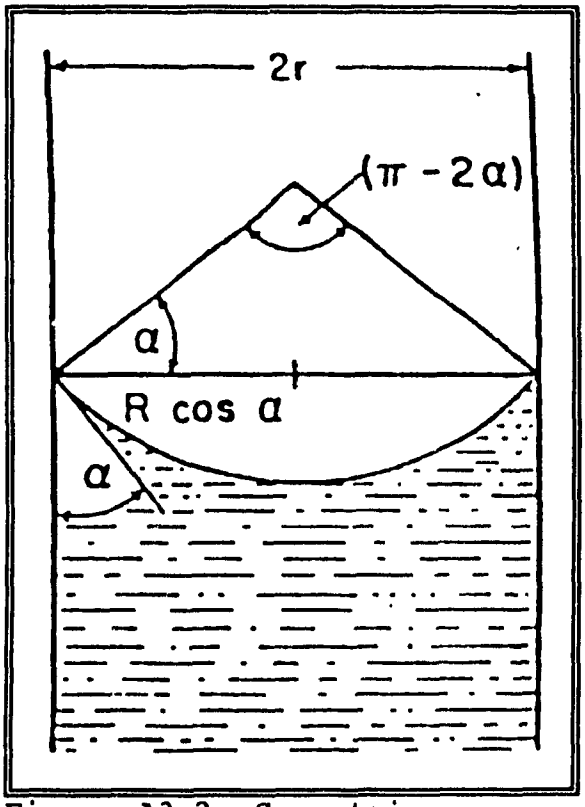

Figure A3-2. Geometric Relationship between the Radius of Curvature (R), the Radius of the Capillary (r), and the Contact Angle (α) (after Hillel, 1972).

Thus,

$$R = \frac{r}{\cos\alpha} \qquad \text{(A3.5)}$$

where R is the radius of curvature of the meniscus;
r is the radius of the capillary tube; and,
α is the contact angle.

The pressure difference across a spherically curved liquid-gas surface is, therefore, given by the equation:

$$\Delta P = \frac{2\gamma}{R} = \frac{2\gamma\cos\alpha}{r} \qquad \text{(A3.6)}$$

Assuming the shape of soil pores resembles close packed spheres, this equation serves to calculate the pressure which must be applied to remove water from a soil sample, and hence it is the soil-water potential.

When the liquid surface is concave, the center of curvature lies outside the liquid and the curvature, by convention, is regarded as negative. Thus, for a concave meniscus such as that of water in a clean glass capillary, ΔP is negative with reference to the atmosphere, indicating a capillary pressure deficit (or sub-pressure). With regard to the atmosphere, ΔP is simply P when atmosphere is assumed to be zero (i.e., gauge pressure). For a convex meniscus, such as mercury in a glass tube or water in an oily (or hydrophobic) tube, ΔP is positive and a capillary depression, rather than a capillary rise, will result.

Values of pressure (i.e., soil-water matric potential) are equivalent to the height of a capillary rise and, therefore, values of pressure can be converted to the pore radius which would be emptied at that pressure. From the desorption portion of the soil-water energy characteristic curve, the amount of water held between two values of pressure and, therefore, the amount of pore space between

two sizes can be calculated, and hence, the pore-size distribution of the soil can be calculated. An example is presented from Yong and Warkentin (1975).

Given: 100 g of soil with a bulk density of 1.2 g/cm^3; a pressure increase from 60 to 100 cm water head, and 6 cm^3 of water drain out of the soil. The soil temperature is 20°C, therefore, γ is 72.75 dyne/cm, and ρ_w is 0.99823 g/cm^3. g is 981 ergs/g-cm [erg = dyne-cm = g-cm^2/s^2] and 1.0 cm H_2O is 980 dyne/cm^2. Assume the soil voids have equivalent radii between r_1 and r_2, and cos α = 1. Thus, the calculations with Equation A3.6:

$$r_1 = \frac{2\gamma\cos\alpha}{P} = \frac{2(72.75\,dynes\,cm^{-1})\,1}{(60\,cm_{H_2O})\,(980)} = 0.0025\,cm \qquad \textbf{(A3.7)}$$

$$r_2 = \frac{2\gamma\cos\alpha}{P} = \frac{2(72.75\,dynes\,cm^{-1})\,1}{(100\,cm_{H_2O})\,(980)} = 0.0015\,cm \qquad \textbf{(A3.8)}$$

or with equation A3.2:

$$r_1 = \frac{2\gamma\cos\alpha}{\rho g h} = \frac{2(72.75\,dynes\,cm^{-1})\,1}{(0.998\,g\,cm^{-3})\,(981\,dyne\,cm\,g^{-1}\,cm^{-1})\,(60\,cm)} = 0.0025\,cm \qquad \textbf{(A3.9)}$$

$$r_2 = \frac{2\gamma\cos\alpha}{\rho g h} = \frac{2(72.75\,dynes\,cm^{-1})\,1}{(0.998\,g\,cm^{-3})\,(981\,dyne\,cm\,g^{-1}\,cm^{-1})\,(100\,cm)} = 0.0015\,cm \qquad \textbf{(A3.10)}$$

The 6 cm^3 of voids is:

$$\frac{6\,cm^3}{(100\,g)\,(1.2\,g\,cm^{-3})}\,100 = 5\%\ of\ the\ total\ soil\ volume. \qquad \textbf{(A3.11)}$$

A4 SOIL-MOISTURE POTENTIAL AND SOIL SUCTION

Basic research associated with soil-water was initiated by soil physicists and agronomists during the late 1800's. Buckingham (1907) introduced the concept that the flow of water in soils result from a difference in "capillary potential" between two points in the soil, and the soil exerts an attraction sufficient to hold water against gravitational force; the concept, which was latter known as soil-moisture suction or tension, was further developed to include the effects of solutes and other forces (for a historical review, refer to Iwata and Tabuchi, 1988).

A soil physics terminology committee of the International Soil Science Society (Aslyng et al., 1963) developed definitions of the total potential of soil water (ψ) and its components. Following this, a review panel for the soil mechanics symposium (Aitchison, 1965) adopted the subdivision of soil suction and the definitions quoted by the International Society of Soil Science. In 1976, the second Terminology Committee of Commission I of the International Society of Soil Science adopted the total potential as an energy concept to express the state of water in soils. The total soil-water potential was defined as follows:

> *"The total potential, ψ_t, of the constituent water in soil at temperature T_0, is the amount of useful work per unit mass of pure water that must be done by the means of externally applied forces to transfer reversibly and isothermally an infinitesimal amount of water from the state S_0 to the soil liquid phase at the point under consideration. It is convenient to divide the transfer process referred to above into several steps, by introducing substandards. S_1: a pool of pure water, free water as in S_0, but situated at the same height as the soil liquid phase under consideration, h_x (i.e., S_1 is at T_0, h_x, and P_0). S_2: a pool of free solution (identical in composition with the liquid phase at the point under consideration), thus having an osmotic pressure, π, but otherwise identical with S_1 (i.e., S_2 is at T_0, h_x, and P_0."*

The total potential, therefore, is composed of three potentials which are all defined by the concept of useful work in the same manner as the total potential: gravitational potential (ψ_g), the osmotic potential (ψ_o), and the pressure potential (ψ_p). The pressure potential is negative as soil-water (termed matric pressure in non-swelling soils) and positive as ground water[1]. At water table (free water; tension free) the pressure potential is zero. The relation between the total potential and the three components is :

$$\psi_t = \psi_g + \psi_\pi + \psi_p = g\Delta h - \int_0^\pi \overline{V_w}\,\partial P + \int_0^P \overline{V_w}\,\partial P \qquad \text{(A4.1)}$$

where, Δh is the difference in height between S_0 and S_1; π is the value of the experimentally accessible osmotic pressure of the soil solution; P is the value of the experimentally accessible tensiometric pressure (or piezometric pressure for a saturated soil) of the soil liquid phase in situ, and V_w is the partial specific volume of the constituent water in the soil solution. Osmotic and matric potentials, separately and in combination, are illustrated in Figure A4.1.

---

[1]In groundwater hydrology ψ refers to the pressure head (h_p), energy per unit weight, and ϕ refers to fluid potential, energy per unit mass, where $\gamma=gh$. Total head (h_T) is the sum of the elevation head (h_z or z), the pressure head (h_p or ψ), and the velocity head (h_v or $v^2/2g$), and for the special case where $h_v=0$, the total head is equal to the hydraulic head (h), and $h=z+\psi$.

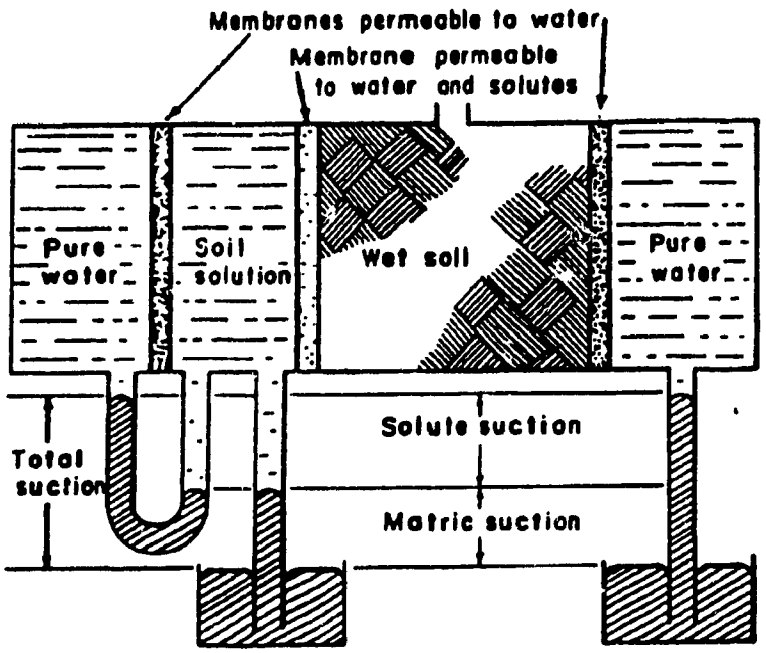

Fig. 3.3. In an isothermal equilibrium system, matric suction is the pressure difference across a membrane separating soil solution *in situ* from the same solution in bulk, the membrane being permeable to solution but not to solid particles or air; osmotic suction is the pressure difference across a semipermeable membrane separating bulk phases of free water and the soil solution; and total suction is the sum of the matric and osmotic suction values, and is thus the pressure difference across a semipermeable membrane separating pure water from a soil that contains solution. An ideal semipermeable membrane is permeable to water only. (After L. A. Richards, 1965).

Figure A4.1. Total Suction, Matric Suction, and Osmotic (solute) Suction (after Hillel, 1972).

The total soil-water potential, with regard to the chemical potential of pure liquid, is equivalent to the chemical potential of the soil water at a given temperature and pressure (Taylor and Ashcroft, 1972; Sposito, 1981). The osmotic potential of soil-water is equal to one component of the chemical potential related to solutes existing in the water and the pressure potential of soil-water (the matric potential) is equal to another component of chemical potential related to surface tension and/or adsorption (electric and van der Waals forces). The pressure potential of ground water is equal to the piezometric pressure.

The matric potential and osmotic potential together determine the vapor pressure or relative humidity in the soil as given by:

$$\psi_m + \psi_\pi = \frac{RT}{V_m} \ln(RH) \qquad \text{(A4.2)}$$

where, R = universal gas constant = 8.324 J/°K-mol, 1.987 cal/°K-mol, or 0.082057 L atm/°K-mol, T = absolute temperature (°K), and, V_m = molecular volume of liquid water.

Soil-water potential for non-swelling soils can be further described by six components, adapted from Yong and Warkentin (1972). For swelling soils, see ~~Appendix A6~~.

(1) ψ, the total potential, is the work required to transfer a unit quantity of water from a reference pool to a point in the soil. It is a negative number.

(2) ψ_g, the gravitational potential, is the work required to transfer water from a reference elevation to a soil elevation.

$$\psi_g = \rho_w g z \qquad \text{(A4.3)}$$

where, ρ_w = density of water, g = acceleration due to gravity, and, z = height above the free water level.

(3) ψ_o, the osmotic potential, is the work required to transfer water from a reference pool of pore water to a pool of soil solution at the same elevation, temperature, and pressure. The osmotic pressure is the pressure which must be applied to a solution to prevent the diffusive flow of the solvent. The osmotic pressure can be expressed by Van't Hoff equation:

$$P_o = nRT(c_1 - c_2) \qquad \text{(A4.4)}$$

where, P_o = osmotic pressure, n = number of molecules per mole of salt (i.e., ionic species), R = universal gas constant, T = absolute temperature (°K), c_1 = concentration of solute in solution, and, c_2 = concentration of solute in external solution. c_2 is zero for pure water and the work defined is to move pure water to a solution, therefore:

$$\psi_o = nRT(c_2 - c_1) = -nRTc \qquad \text{(A4.5)}$$

(4) ψ_m, the matric potential, is a soil matrix property. This is analogous to Buckingham's capillary potential. It is the work required to transfer a unit quantity of soil solution from a reference pool at the same elevation and temperature as the soil, to a point in the soil. The matric potential cannot be calculated except for uniform spheres where it is related to the curvature of the air-water interfaces,

$$\psi_m = -\gamma\left(\frac{1}{r_1} + \frac{1}{r_2}\right) \qquad \text{(A4.6)}$$

or in free swelling clay plates,

$$\psi_m = -RT\cosh(y_c - 1) \qquad \text{(A4.7)}$$

where, γ is the surface tension of the air-water interface, r_1 & r_2 = air-water interface radii of the curvature, R = universal gas constant, T = absolute temperature (°K), and, y_c = electrical potential between two clay plates. Matric potential can be subdivided into a component related to swelling forces in clays, but these components cannot be separated experimentally. In the water content range where the air-water interfaces may be observed, the matric potential can be generalized as a function of the radius of the air-water interface:

$$\psi_m = -\rho g z = \frac{-2\gamma}{r} \qquad \text{(A4.8)}$$

where, ρ = density of the water, γ = surface tension of the water-air interface, and, z = height of water column in equilibrium with soil.

(5) ψ_p, the piezometric potential, is the work required to transfer water to a point below the water table.

$$\psi_p = \gamma_w g d \qquad \text{(A4.9)}$$

where, γ_w = density of water, g = acceleration due to gravity, and, d = depth below free water level.

(6) ψ_a, the pneumatic of a pressure potential, refers to the transfer of water from atmospheric pressure to the air pressure, P, on the soil.

$$\psi_a = P \qquad \text{(A4.10)}$$

The matric, piezometric, and pneumatic potentials are typically taken together as the pressure, ψ_p.

$$\psi_p = \psi_m + \psi_p + \psi_a \qquad \text{(A4.11)}$$

The definition of total potential is more commonly applied with mechanical terminology, than with thermodynamic terminology, because mechanical concepts are more suitable for studies on water movement in soil. This poses a theoretical problem (Iwata and Tabuchi, 1988), whether or not the amount of useful work in the definition is dissipated to increase the potential energy or the free energy of the transferred water. If the work was done reversibly on the transferred water, the amount of work must be equal to the increase in the potential energy of water. However, the amount of useful work does not satisfy this condition except for the gravitational potential; entropy is produced.

Soil-water potential measurements are generally used to describe the energy status of water with soil; relating the soil-water content to the soil-water potential. The relation of hydraulic conductivity to soil-water potential is also commonly applied in flow in the unsaturated zone. In addition, soil-water potential measurements can be useful in

defining the integrity ar stability of the soil system. Incorporation of the soil-water potential term into an effective stress equation can also be used to describe the volume change and shear strength behavior.

Soil-water potential is given in terms of the water phase and, therefore, the values (of soil-water free energy) decrease as water content decreases, which indicates that water is held more strongly by dry soil than by wet soil. If the potential were defined in terms of the soil phase, as did Buckingham, the algebraic sign would be positive and the potential would decrease as water content increases. This definition of soil-water is referred to as soil suction (or tension). It is only semantics to avoid the use of the negative sign which generally characterizes the pressure of soil water, and allows one to speak of the osmotic and matric potentials in positive terms.

A5 Quantitative Expression of Soil-Water Potential

The soil-water potential is typically expressed in three ways (after Hillel, 1972):

(1) Energy per unit mass: This is often taken to be the fundamental expression of potential, using units of ergs per gram or joules per kilogram. The dimensions of energy per unit mass are L^2T^{-2}.

(2) Energy per unit volume: Since water is practically an incompressible liquid, its density is almost independent of potential. Hence, there is a direct proportion between the expression of the potential as energy per unit mass and its expression as energy per unit volume. The latter expression yields the dimensions of pressure (for, just as energy can be expressed as the product of pressure by volume, so the ratio of energy to volume gives pressure). This equivalent pressure can be measured in terms of dyne per square centimeter, bars, or atmospheres. The basic dimensions are those of force per unit area: $ML^{-1}T^{-2}$. This method of expression is convenient for the osmotic and pressure potentials, but is seldom used for the gravitational potential.

(3) Energy per unit weight (hydraulic head): Whatever can be expressed in units of hydrostatic pressure can also be expressed in terms of an equivalent hydraulic head, which is the height of a liquid column corresponding the given pressure. For example, a pressure of 1 atm is equivalent to a vertical water column (or hydraulic head) of 1033 cm, and to a mercury head of 76 cm. This method of expression is certainly simpler, and often more convenient, than the previous methods. Hence, it is common to characterize the state of soil water in terms of terms of total head (h_T) which is the sum of the elevation head (h_z or z), the pressure head (h_p or ψ), and the velocity head (h_v or $v^2/2g$), and for the special case where $h_v=0$, the total head is equal to the hydraulic head (h), and $h=z+\psi$.

In attempt to express the negative pressure potential of soil water in equivalent hydraulic head, we must content with the face that this head may be as much as -10,000 or -100,000 cm of water. To avoid the use of large numbers, Schofield (1935) suggested the use of *pF* (by analogy to the pH scale) which he defined as the logarithm of the negative pressure (tension or suction) head in centimeters of water.

It ϕ is the potential in terms of energy per unit mass, P is the potentials in terms of pressure, and h is the potential in terms of head, then

$$\phi = \frac{P}{\rho_w} \qquad \text{(A5.1)}$$

and,

$$h = \frac{P}{\rho_w g} = \frac{\phi}{g} \qquad \text{(A5.2)}$$

where, ρ_w is the density of liquid water, and,
g is the acceleration due to gravity.

Appendix B: Notes on Electrical Charge and Dielectrics

The question "what is a charge?" cannot be answered directly. All that can be said is that "charge" is the name given to a certain concept that accounts for the physical behavior of electrostatic systems. The same difficulty is encountered with "gravity" which is the name of the concept used to account for the fact that all objects fall to the ground (Sharpe, 1988).

The unit quantity of charge is given as that of an electron, and this charge is equal to 1 electrostatic unit (esu). A practical unit of quantity (volume) of electricity is defined as the amount of electricity passing in a circuit when 1 ampere (i.e., voltage per resistance) flows for 1 second; this quantity, being 1 coulomb, is 6×10^{18} esu. Electricity implies a current, or flow of electrons (or charge) in a electodynamic system. The practical unit of electrostatic capacitance, 1 farad (F), is defined as that capacitance which, when charged to a potential of one volt, carries a charge of one coulomb (i.e., 1 coulomb per volt); 1 farad is equal to 9×10^{11} esu.

The direction of the force from an electric field at a charged surface is perpendicular to the object's surface, along a flux line. The flux (θ), that effect of a charged surface is equal to the object's charge (q) in coulombs. This restates that the term "charge" is given to a phenomenon, that of electrostatic systems.

For two parallel plates separated by a dielectric, the electrostatic flux density (D) (i.e, the specific flux or electric displacement) is equal to the charge (q) divided by the plate surface area (A), in coulombs/m^2.

$$D = \frac{q}{A} = \frac{\theta}{A} \qquad \text{(B1)}$$

Similar to Darcy's law, the flux density is equal to a potential gradient multiplied by a proportionality constant.

$$D = \varepsilon E = \varepsilon \nabla V = \varepsilon \frac{V}{L} \qquad \text{(B2)}$$

where, D = flux density, E = electric field strength, V = voltage potential across the two plates, L = distance between the two plates (m), ε = proportionality constant. In other words, the potential gradient is the electric field strength.

$$E = \frac{D}{\varepsilon} = \frac{V}{L} = \nabla V \qquad \text{(B3)}$$

The proportionality constant (ε) is known as the permittivity which is a measure of the capacity of the surrounding medium to support an electrical stress.

$$\varepsilon = \varepsilon_o \varepsilon_r \qquad \text{(B4)}$$

where, ε_o = permittivity of free space (vacuum), 1 coul^2/dyne-cm^2 (CGS system), $10^{-9}/36\pi$ F/m or coul^2/N-m^2 (MKS system), and, ε_r = relative permittivity or dielectric constant.

A summary of a rigorous discussion of dielectric properties (von Hillel, 1958) is presented here, which was adapted from Ledieu et al. (1986). An additional explanation of the theory as they apply to the electrical properties of soils is found in Davis and Annan (1977).

Given the charge density,

$$D = \varepsilon E \qquad \text{(B5)}$$

then,

$$\frac{\textit{the charge density}}{\textit{electric field strength}} = \frac{D}{E} = \varepsilon = \varepsilon_o \varepsilon_r \qquad \text{(B6)}$$

therefore, the complex dielectric constant

$$\varepsilon_r = \varepsilon_o \frac{D}{E} \qquad \text{(B7)}$$

The dielectric constant (ε_r) is a capacity ratio and has a real and imaginary part that are frequency dependent.

$$\varepsilon_r = K^* = K' + j\left(\frac{\sigma_{dc}}{\omega \varepsilon_o} + K''\right) \qquad \text{(B8)}$$

where, K^* = complex dielectric constant, K' = real dielectric constant, K'' = dielectric loss, ε_o = permittivity of free space, σ_{dc} = zero frequency DC conductivity (Siemens/m), ω = angular frequency ($2\pi f$ radian/sec), and $j = (-1)^{1/2}$, the imaginary number.

The permittivity expresses the polarization of the material submitted to an electric field (D) and the polarization tends to reduce the field strength (E).

$$E = \frac{D}{\varepsilon} = \frac{q}{\varepsilon A} \qquad \text{(B9)}$$

Similarly, in geohydrology the term hydraulic conductivity (K) expresses the ability of water to flow in a porous media submitted to a discharge (q), and the conductivity tends to reduce the hydraulic head (h).

Two main classes of phenomena cause the polarization induced by an electric field:

(1) an electronic, atomic and molecular distortion of nonpolar molecules, causing an indirect dipolar moment in the direction of the field; and

(2) a rotation of dipolar elements, tending to align then with the field.

In the imaginary part of K*, the term K" represents the dielectric losses due to the vibration or rotation of the molecules and the term $\sigma_{dc}/\omega\varepsilon_o$, which is the characteristic of materials containing free charge, represents the losses due to conductivity (ohmic). The imaginary part of K* results in a phase shift between the applied electric field (D) and the resulting polarization.

At low frequencies (e.g., direct current) the ions can move to the limits of the conducting microdomains of soils to create an extra polarization, which can be greater than the original dielectric permittivity of the soil. At high frequencies the term $\sigma_{dc}/\omega\varepsilon_o$ becomes negligible. For water at high frequencies, K' is no longer strongly dependent on frequency and also K"<< K' (Davis and Annan, 1977). In this case, K* is nearly real and constant, therefore, it can be represented as K, an apparent dielectric constant. For water (and therefore soil) the assumption is valid between 10 MHz and 1 GHz.

Given the electrostatic flux density

$$D = \frac{Q}{A} = \varepsilon\frac{V}{L} = \varepsilon\left(\frac{1}{L}\right)V \qquad \text{(B10)}$$

1/L is useful in the field of surface chemistry. It is generally taken to be the extent of the double-diffuse layer of a charged surface. Rearranging this to express the charge of a parallel plate capacitor,

$$q = \left(\frac{\varepsilon A}{L}\right)V = CV \qquad \text{(B11)}$$

where, C = capacity of a parallel plate capacitor (farad). An analogy to Darcy's law, thus, would include the product of the hydraulic conductivity and the area per depth ratio.

$$Q = -\left(K\frac{A}{\partial z}\right)\partial h \qquad \text{(B12)}$$

Capacitance is useful to understand the principles of TDR, although, with one important note. The capacitance of a capacitor, or the capacity of two plates (conductors) to hold an electric charge, depends on the geometry of the capacitor and on the insulating material (dielectric) between the plates.

$$C = \frac{\varepsilon A}{L} \qquad \text{(B13)}$$

Furthermore, the capacitance of a coaxial cable is given by:

$$C = \frac{2\pi\varepsilon d}{\ln(a/b)} \qquad \text{(B14)}$$

where, d = length of the cable (m), b = inside radius of shield (outer conductor) (m), a = radius of the inner conductor (m). However, in the TDR technique the effect of changes in the dielectric constant are measured by determining signal propagation velocity in a transmission line which is independent of both the line geometry and the capacitance.

$$K = \left(\frac{ct}{2L}\right)^2 \qquad \text{(B15)}$$

where, K_a = apparent dielectric constant, c = velocity of electromagnetic wave in a vacuum (30 cm/ns), t = signal 2-way travel time (ns), L = length of transition line (cm). This is the major advantage of the TDR technique compared to other high-frequency electrical techniques (Topp and Davis, 1985).

Table B1. Approximate Dielectric Constants at 20°C and 1 atm.

Material	ε_r	Material	ε_r
Acetone	21.3	Mineral oil	2.24
Air	1.00059	Mylar	2.8–3.5
Alcohol	16–31	Olive oil	3.11
Amber	2.9	Paper	2.0–2.6
Asbestos paper	2.7	Paper (kraft)	3.5
Asphalt	2.7	Paraffin	1.9–2.5
Bakelite	3.5–10	Polyethylene	2.25
Benzene	2.284	Polystyrene	2.6
Carbon dioxide	1.001	Porcelain	5.7–6.8
Carbon tetrachloride	2.238	Quartz	5
		Rock	≈ 5
Castor oil	4.7	Rubber	2.3–5.0
Diamond	16.5	Shellac	2.7–3.7
Glass	5–10	Silicon oil	2.2–2.7
Glycerine	56.2	Slate	6.6–7.4
Hydrogen	1.003	Sulfur	3.6–4.2
Lucite	3.4	Teflon	2.0–2.2
Marble	8.3	Vacuum	1.000
Methanol	22	Water	80.37
Mica	2.5–8	Wood	2.5–7.7

Appendix C1. Calculation of Bulk Density of Waite Amulet Tailings, Samples Collected on October 7, 1990, 1300-1500 Hours.

SITE	SAMPLE DEPTH (cm)	VOLUME (cc)	DISH WEIGHT (g)	WET WEIGHT SAMPLE + DISH (g)	WET WEIGHT SAMPLE WEIGHT (g)	DRY WEIGHT SAMPLE + DISH (g)	DRY WEIGHT SAMPLE WEIGHT (g)	BULK DENSITY (g/cc)	REMARKS
WA15g	0-16	50.27	15.83	84.27	68.44	67.35	51.52	1.02	oxidized
	16-35	59.69	15.89	109.36	93.47	86.50	70.61	1.18	oxidized
	35-52	53.41	15.76	64.38	48.62	54.14	38.38	1.59	unoxidized
	"	"	16.01	76.40	60.39	62.73	46.72	---	unoxidized
	52-64	37.70	16.01	79.37	63.36	65.20	49.19	1.30	unoxidized
	64-76	37.70	15.84	85.38	69.54	67.12	51.28	1.36	unoxidized
	76-90	43.98	15.95	100.55	84.60	83.32	67.37	1.53	unoxidized
	90-108	56.55	16.06	126.19	110.13	105.11	89.05	1.57	unoxidized
WA15t	organic	15.71	16.04	18.67	2.63	17.21	1.17	0.07	organic
	0-15	47.12	15.76	66.75	50.99	55.87	40.11	0.85	oxidized
	15-37	69.12	15.96	65.61	49.65	51.30	35.34	1.16	oxidized
	"	"	15.79	76.02	60.23	60.68	44.89	---	oxidized
	37-49	37.70	15.79	95.97	80.18	79.14	63.35	1.68	oxidized
	49-63	43.98	15.87	91.55	75.68	79.41	63.54	1.44	unoxidized
	63-73	31.42	15.87	68.78	52.91	59.29	43.42	1.38	unoxidized
	73-85	37.70	16.21	92.63	76.42	76.54	60.33	1.60	unoxidized
	85-95	31.42	16.04	88.18	72.14	72.12	56.08	1.78	unoxidized
	95-103	25.13	16.00	56.60	40.60	49.51	33.51	1.33	unoxidized
	103-109	18.85	16.18	50.94	34.76	45.51	29.33	1.56	unoxidized
WA30	organic	6.28	15.98	19.26	3.28	17.56	1.58	0.25	organic
	0-12	37.70	19.07	71.11	52.04	58.41	39.34	1.04	oxidized
	12-25	40.84	15.98	82.24	66.26	67.48	51.50	1.26	oxidized
	25-45	62.83	16.09	76.64	60.55	61.85	45.76	1.19	oxidized
	"	"	16.03	54.14	38.11	45.21	29.18	---	oxidized
	45-60	47.12	15.66	93.82	78.16	86.25	70.59	1.50	unoxidized
	60-76	50.27	16.33	100.47	84.14	94.62	78.29	1.56	unoxidized
	76-90	43.98	15.87	88.24	72.37	81.60	65.73	1.49	unoxidized
	90-106	50.27	16.41	98.06	81.65	93.22	76.81	1.53	unoxidized

Appendix C2.1. Calculation of Soil-moisture Content by Gravimetric Method, Waite Amulet Tailings Samples Collected on October 7, 1990, 1500-1700 hours.

SITE	SAMPLE DEPTH (cm)	DISH WEIGHT (g)	WET WEIGHT SAMPLE + DISH (g)	WET WEIGHT SAMPLE WEIGHT (g)	DRY WEIGHT SAMPLE + DISH (g)	DRY WEIGHT SAMPLE WEIGHT (g)	BULK a/ DENSITY (g/cc)	WATER Mass (g)	WATER CONTENT (%dw)	WATER CONTENT (%vb)	REMARKS
WA15g	0-16	15.83	84.27	68.44	67.35	51.52	1.00	16.92	32.84	32.84	oxidized
	16-35	15.89	109.36	93.47	86.50	70.61	1.10	22.86	32.38	35.61	oxidized
	35-52	15.76	64.38	48.62	54.14	38.38	1.70	23.91	28.10	47.76	unoxidized
	"	16.01	76.40	60.39	62.73	46.72	---	---	---	---	unoxidized
	52-64	16.01	79.37	63.36	65.20	49.19	1.40	14.17	28.81	40.33	unoxidized
	64-76	15.84	85.38	69.54	67.12	51.28	1.40	18.26	35.61	49.85	unoxidized
	76-90	15.95	100.55	84.60	83.32	67.37	1.50	17.23	25.58	38.36	unoxidized
	90-108	16.06	126.19	110.13	105.11	89.05	1.50	21.08	23.67	35.51	unoxidized
WA15t	organic	16.04	18.67	2.63	17.21	1.17	0.07	1.46	124.79	8.74	organic
	0-15	15.76	66.75	50.99	55.87	40.11	0.85	10.88	27.13	23.06	oxidized
	15-37	15.96	65.61	49.65	51.30	35.34	1.10	29.65	36.96	40.65	oxidized
	"	15.79	76.02	60.23	60.68	44.89	---	---	---	---	oxidized
	37-49	15.79	95.97	80.18	79.14	63.35	1.70	16.83	26.57	45.16	oxidized
	49-63	15.87	91.55	75.68	79.41	63.54	1.40	12.14	19.11	26.75	unoxidized
	63-73	15.87	68.78	52.91	59.29	43.42	1.40	9.49	21.86	30.60	unoxidized
	73-85	16.21	92.63	76.42	76.54	60.33	1.50	16.09	26.67	40.00	unoxidized
	85-95	16.04	88.18	72.14	72.12	56.08	1.50	16.06	28.64	42.96	unoxidized
	95-103	16.00	56.60	40.60	49.51	33.51	1.50	7.09	21.16	31.74	unoxidized
	103-109	16.18	50.94	34.76	45.51	29.33	1.50	5.43	18.51	27.77	unoxidized
WA30	organic	15.98	19.26	3.28	17.56	1.58	0.25	1.70	107.59	26.90	organic
	0-12	19.07	71.11	52.04	58.41	39.34	1.05	12.70	32.28	33.90	oxidized
	12-25	15.98	82.24	66.26	67.48	51.50	1.25	14.76	28.66	35.83	oxidized
	25-45	16.09	76.64	60.55	61.85	45.76	1.25	23.72	31.65	39.56	oxidized
	"	16.03	54.14	38.11	45.21	29.18	---	---	---	---	oxidized
	45-60	15.66	93.82	78.16	86.25	70.59	1.50	7.57	10.72	16.09	unoxidized
	60-76	16.33	100.47	84.14	94.62	78.29	1.50	5.85	7.47	11.21	unoxidized
	76-90	15.87	88.24	72.37	81.60	65.73	1.50	6.64	10.10	15.15	unoxidized
	90-106	16.41	98.06	81.65	93.22	76.81	1.50	4.84	6.30	9.45	unoxidized

a/ Bulk density values were based on measurements made on Oct. 7 and Nov. 23.

Appendix C2.2. Calculation of Soil-moisture Content by Gravimetric Method, Waite Amulet Tailings Samples Collected on November 23, 1990, 1300-1500 hours.

SITE	SAMPLE DEPTH (cm)	DISH WEIGHT (g)	WET WEIGHT SAMPLE + DISH (g)	WET WEIGHT SAMPLE WEIGHT (g)	DRY WEIGHT SAMPLE + DISH (g)	DRY WEIGHT SAMPLE WEIGHT (g)	BULK a/ DENSITY (g/cc)	WATER MASS (g)	WATER CONTENT (%dw)	WATER CONTENT (%vb)	FIELD REMARKS
WA15g	0-23	15.97	96.37	80.40	74.65	58.68	1.05	21.72	37.01	38.87	oxidized
	23-36	15.88	82.74	66.86	66.22	50.34	1.20	16.52	32.82	39.38	oxidized
	36-67	15.91	108.65	92.74	86.48	70.57	1.50	48.37	39.99	59.98	unoxidized
	"	16.00	92.60	76.60	66.40	50.40	---	---	---	---	---
	67-73	16.26	81.84	65.58	64.51	48.25	1.40	17.33	35.92	50.28	unoxidized
	73-80	16.13	62.50	46.37	52.52	36.39	1.50	9.98	27.43	41.14	unox., wet
	80-92	15.94	78.97	63.03	66.99	51.05	1.50	11.98	23.47	35.20	unox., dryer
	92-103	16.18	77.08	60.90	66.06	49.88	1.50	11.02	22.09	33.14	unoxidized
	103-115	15.67	83.90	68.23	69.40	53.73	1.50	14.50	26.99	40.48	unoxidized
WA15t	organic	15.76	27.67	11.91	24.12	8.36	0.10	3.55	42.46	4.25	organic
	0-20	15.82	86.21	70.39	66.24	50.42	0.85	19.97	39.61	33.67	oxidized
	20-37	15.80	85.79	69.99	66.69	50.89	1.10	19.10	37.53	41.29	oxidized
	37-48	15.87	81.46	65.59	65.36	49.49	1.70	16.10	32.53	55.30	unoxidized
	48-60	16.06	95.69	79.63	81.00	64.94	1.50	14.69	22.62	33.93	unoxidized
	60-75	16.03	95.81	79.78	78.33	62.30	1.50	17.48	28.06	42.09	unoxidized
	75-90	16.09	116.04	99.95	92.49	76.40	1.50	23.55	30.82	46.24	unox., wet
	90-105	15.83	121.67	105.84	99.62	83.79	1.50	22.05	26.32	39.47	unox., wet
WA30	0-10	16.14	57.43	41.29	47.50	31.36	1.05	9.93	31.66	33.25	oxidized
	10-26	16.40	92.06	75.66	75.20	58.80	1.25	16.86	28.67	35.84	oxidized
	26-39	16.45	78.48	62.03	64.02	47.57	1.25	14.46	30.40	38.00	oxidized
	39-60	16.26	114.08	97.82	93.50	77.24	1.50	20.58	26.64	39.97	oxidized
	60-77	16.05	121.39	105.34	106.67	90.62	1.50	14.72	16.24	24.37	unox., dry
	77-92	15.90	98.18	82.28	89.35	73.45	1.50	8.83	12.02	18.03	unox., dry
	92-110	15.94	122.84	106.90	110.61	94.67	1.50	12.23	12.92	19.38	unox., dry

a/ Bulk density values were based on measurements made on Oct. 7 and Nov. 23.

Appendix C3.1. Calculation of Gravimetric Soil-moisture Content at TDR Probe Locations

SITE	DATE	TDR PROBE LOCATION (cm)	GRAVIMETRIC WATER CONTENT (%vb)	LENGTH OF GRAVIMETRIC WATER CONTENT COLUMN (cm)	% COLUMN LENGTH IS OF TOTAL TDR PROBE LENGTH	PARTIAL WATER CONTENT OF TDR PROBE LENGTH AT COLUMN LOCATION (%vb)	TOTAL WATER CONTENT AT TDR PROBE LOCATION (%vb)
WA15g	07 Oct.	0-30	32.84	16.00	0.53	17.51	
			38.85	14.00	0.47	18.13	35.64
		0-60	32.84	16.00	0.27	8.76	
			38.85	19.00	0.32	12.30	
			47.74	17.00	0.28	13.53	
			40.33	8.00	0.13	5.38	39.96
		30-60	38.85	5.00	0.17	6.47	
			47.74	17.00	0.57	27.05	
			40.33	8.00	0.27	10.75	44.28
		60-90	40.33	4.00	0.13	5.38	
			49.85	12.00	0.40	19.94	
			38.36	14.00	0.47	17.90	43.22
		90-108	35.51	18.00	1.00	35.51	35.51
	23 Nov.	0-30	38.87	23.00	0.77	29.80	
			39.38	7.00	0.23	9.19	38.99
		0-60	38.87	23.00	0.38	14.90	
			39.38	13.00	0.22	8.53	
			59.98	24.00	0.40	23.99	47.42
		30-60	39.38	6.00	0.20	7.88	
			59.98	24.00	0.80	47.98	55.86
		60-90	59.98	7.00	0.23	14.00	
			50.28	6.00	0.20	10.06	
			41.14	7.00	0.23	9.60	
			35.20	10.00	0.33	11.73	45.38
		90-115	35.20	2.00	0.08	2.82	
			33.14	11.00	0.44	14.58	
			40.48	12.00	0.48	19.43	36.83

Appendix C3.2. Calculation of Gravimetric Soil-moisture Content at TDR Probe Locations

SITE	DATE	TDR PROBE LOCATION (cm)	GRAVIMETRIC WATER CONTENT (%vb)	LENGTH OF GRAVIMETRIC WATER CONTENT COLUMN (cm)	% COLUMN LENGTH IS OF TOTAL TDR PROBE LENGTH	PARTIAL WATER CONTENT OF TDR PROBE LENGTH AT COLUMN LOCATION (%vb)	TOTAL WATER CONTENT AT TDR PROBE LOCATION (%vb)
WA15t	07 Oct.	0-30	23.06	14.00	0.47	10.76	
			40.65	16.00	0.53	21.68	32.44
		0-60	23.06	14.00	0.23	5.38	
			40.65	23.00	0.38	15.58	
			45.16	12.00	0.20	9.03	
			26.75	11.00	0.18	4.90	34.90
		30-60	40.65	7.00	0.23	9.48	
			45.16	12.00	0.40	18.06	
			26.75	11.00	0.37	9.81	37.36
		60-90	25.75	3.00	0.10	2.58	
			30.60	10.00	0.33	10.20	
			40.00	12.00	0.40	16.00	
			42.96	5.00	0.17	7.16	35.94
		90-109	42.96	5.00	0.26	11.31	
			31.74	8.00	0.42	13.36	
			27.77	7.00	0.37	10.23	34.90
	23 Nov.	0-30	33.67	20.00	0.67	22.45	
			41.29	10.00	0.33	13.76	36.21
		0-60	33.67	20.00	0.33	11.22	
			41.29	17.00	0.28	11.70	
			55.30	11.00	0.18	10.14	
			33.93	12.00	0.20	6.79	39.85
		30-60	41.29	7.00	0.23	9.63	
			55.30	11.00	0.37	20.28	
			33.93	12.00	0.40	13.57	43.48
		60-90	42.09	15.00	0.50	21.05	
			26.24	15.00	0.50	13.12	34.16
		90-105	39.47	15.00	1.00	39.47	39.47

Appenxix C3.3. Calculation of Gravimetric Soil-moisture Content at TDR Probe Locations

SITE	DATE	TDR PROBE LOCATION (cm)	GRAVIMETRIC WATER CONTENT (%vb)	LENGTH OF GRAVIMETRIC WATER CONTENT COLUMN (cm)	% COLUMN LENGTH IS OF TOTAL TDR PROBE LENGTH	PARTIAL WATER CONTENT OF TDR PROBE LENGTH AT COLUMN LOCATION (%vb)	TOTAL WATER CONTENT AT TDR PROBE LOCATION (%vb)
WA30	07 Oct.	0-30	33.90	12.00	0.40	13.56	
			35.83	13.00	0.43	15.53	
			39.56	5.00	0.17	6.59	35.68
		0-60	33.90	12.00	0.20	6.78	
			35.83	13.00	0.22	7.76	
			39.56	20.00	0.33	13.19	
			16.09	15.00	0.25	4.02	31.75
		30-60	39.56	15.00	0.50	19.78	
			16.09	15.00	0.50	8.04	27.83
		60-90	11.21	16.00	0.53	5.98	
			15.15	14.00	0.47	7.07	13.05
		90-106	9.45	16.00	1.00	9.45	9.45
	23 Nov.	0-30	33.25	10.00	0.33	11.08	
			35.84	16.00	0.53	19.11	
			38.00	4.00	0.13	5.07	35.26
		0-60	33.25	10.00	0.17	5.54	
			35.84	16.00	0.27	9.56	
			38.00	13.00	0.22	8.23	
			39.97	21.00	0.35	13.99	37.32
		30-60	38.00	9.00	0.30	11.40	
			39.97	21.00	0.70	27.98	39.38
		60-90	24.37	17.00	0.57	13.81	
			18.03	3.00	0.10	1.80	15.61
		90-110	18.03	2.00	0.10	1.80	
			19.38	18.00	0.90	17.44	19.25

Appencix C4. Calculation of Soil-Water Content Accumulation from October 7 to November 23, 1990.

DEPTH	WA15g OCT 7	WA25g NOV 23	WA15g WETTING ACCUMULATION	WA15t OCT 7	WA25t NOV 23	WA15t WETTING ACCUMULATION	WA30 OCT 7	WA30 NOV 23	WA30 WETTING ACCUMULATION
0	32.84	38.87	6.03	23.06	33.67	10.61	33.90	33.25	-
1	32.84	38.87	6.03	23.06	33.67	10.61	33.90	33.25	-
2	32.84	38.87	6.03	23.06	33.67	10.61	33.90	33.25	-
3	32.84	38.87	6.03	23.06	33.67	10.61	33.90	33.25	-
4	32.84	38.87	6.03	23.06	33.67	10.61	33.90	33.25	-
5	32.84	38.87	6.03	23.06	33.67	10.61	33.90	33.25	-
6	32.84	38.87	6.03	23.06	33.67	10.61	33.90	33.25	-
7	32.84	38.87	6.03	23.06	33.67	10.61	33.90	33.25	-
8	32.84	38.87	6.03	23.06	33.67	10.61	33.90	33.25	-
9	32.84	38.87	6.03	23.06	33.67	10.61	33.90	33.25	-
10	32.84	38.87	6.03	23.06	33.67	10.61	33.90	33.25	-
11	32.84	38.87	6.03	23.06	33.67	10.61	33.90	35.84	-
12	32.84	38.87	6.03	23.06	33.67	10.61	33.90	35.84	-
13	32.84	38.87	6.03	23.06	33.67	10.61	35.83	35.84	-
14	32.84	38.87	6.03	23.06	33.67	10.61	35.83	35.84	-
15	32.84	38.87	6.03	23.06	33.67	10.61	35.83	35.84	-
16	32.84	38.87	6.03	23.06	33.67	10.61	35.83	35.84	-
17	35.61	38.87	3.26	23.06	33.67	10.61	35.83	35.84	-
18	35.61	38.87	3.26	40.65	41.29	0.64	35.83	35.84	-
19	35.61	38.87	3.26	40.65	41.29	0.64	35.83	35.84	-
20	35.61	38.87	3.26	40.65	41.29	0.64	35.83	35.84	-
21	35.61	38.87	3.26	40.65	41.29	0.64	35.83	35.84	-
22	35.61	38.87	3.26	40.65	41.29	0.64	35.83	35.84	-
23	35.61	38.87	3.26	40.65	41.29	0.64	35.83	35.84	-
24	35.61	39.38	3.77	40.65	41.29	0.64	35.83	35.84	-
25	35.61	39.38	3.77	40.65	41.29	0.64	35.83	35.84	-
26	35.61	39.38	3.77	40.65	41.29	0.64	39.56	35.84	-
27	35.61	39.38	3.77	40.65	41.29	0.64	39.56	38.00	-
28	35.61	39.38	3.77	40.65	41.29	0.64	39.56	38.00	-
29	35.61	39.38	3.77	40.65	41.29	0.64	39.56	38.00	-
30	35.61	39.38	3.77	40.65	41.29	0.64	39.56	38.00	-
31	35.61	39.38	3.77	40.65	41.29	0.64	39.56	38.00	-
32	35.61	39.38	3.77	40.65	41.29	0.64	39.56	38.00	-
33	35.61	39.38	3.77	40.65	41.29	0.64	39.56	38.00	-
34	35.61	39.38	3.77	40.65	41.29	0.64	39.56	38.00	-
35	35.61	39.38	3.77	40.65	41.29	0.64	39.56	39.97	0.41
36	47.76	59.98	12.22	40.65	41.29	0.64	39.5	39.97	0.41
37	47.76	59.98	12.22	40.65	41.29	0.64	39.5	39.97	0.41
38	47.76	59.98	12.22	45.16	55.30	10.14	39.5	39.97	0.41
39	47.76	59.98	12.22	45.16	55.30	10.14	39.5	39.97	0.41
40	47.76	59.98	12.22	45.16	55.30	10.14	39.5	39.97	0.41
41	47.76	59.98	12.22	45.16	55.30	10.14	16.0	39.97	23.88
42	47.76	59.98	12.22	45.16	55.30	10.14	16.0	39.97	23.88
43	47.76	59.98	12.22	45 16	55.30	10.14	16.0	39.97	23.88
44	47.76	59.98	12.22	45.16	55.30	10.14	16.0	39.97	23.88
45	47.76	59.98	12.22	45.16	55.30	10.14	16.0	39.97	23.88
46	47.76	59.98	12.22	45.16	55.30	10.14	16.0	39.97	23.88
47	47.76	59.98	12.22	45.16	55.30	10.14	16.0	39.97	23.88
48	47.76	59.98	12.22	45.16	55.30	10.14	16.0	39.97	23.88
49	47.76	59.98	12.22	45.16	55.30	10.14	16.0	39.97	23.88
50	47.76	59.98	12.22	26.75	33.93	7.18	16.0	39.97	23.88
51	47.76	59.98	12.22	26.75	33.93	7.18	16.0	39.97	23.88
52	47.76	59.98	12.22	26.75	33.93	7.18	16.0	39.97	23.88
53	40.33	59.98	19.65	26.75	33.93	7.18	16.0	39.97	23.88
54	40.33	59.98	19.65	26.75	33.93	7.18	16.0	39.97	23.88
55	40.33	59.98	19.65	26.75	33.93	7.18	16.0	39.97	23.88
56	40.33	59.98	19.65	26.75	33.93	7.18	16.0	39.97	23.88
57	40.33	59.98	19.65	26.75	33.93	7.18	16.0	39.97	23.88
58	40.33	59.98	19.65	26.75	33.93	7.18	16.0	39.97	23.88
59	40.33	59.98	19.65	26.75	33.93	7.18	16.0	39.97	23.88
60	40.33	59.98	19.65	26.75	33.93	7.18	16.0	39.97	23.88
61	40.33	59.98	19.65	26.75	42.09	15.34	11.2	24.37	13.16
62	40.33	59.98	19.65	26.75	42.09	15.34	11.2	24.37	13.16
63	40.33	59.98	19.65	26.75	42.09	15.34	11.2	24.37	13.16
64	40.33	59.98	19.65	30.60	42.09	11.49	11.2	24.37	13.16
65	49.85	59.98	10.13	30.60	42.09	11.49	11.2	24.37	13.16
66	49.85	59.98	10.13	30.60	42.09	11.49	11.2	24.37	13.16
67	49.85	59.98	10.13	30.60	42.09	11.49	11.2	24.37	13.16
68	49.85	50.28	0.43	30.60	42.09	11.49	11.2	24.37	13.16
69	49.85	50.28	0.43	30.60	42.09	11.49	11.2	24.37	13.16
70	49.85	50.28	0.43	30.60	42.09	11.49	11.2	24.37	13.16

Appendix C4. (continued)

DEPTH	WA15g OCT 7	WA25g NOV 23	WA15g WETTING ACCUMULATION	WA15t OCT 7	WA25t NOV 23	WA15t WETTING ACCUMULATION	WA30 OCT 7	WA30 NOV 23	WA30 WETTING ACCUMULATION
71	49.85	50.28	0.43	30.60	42.09	11.49	11.2	24.37	13.16
72	49.85	50.28	0.43	30.60	42.09	11.49	11.2	24.37	13.16
73	49.85	50.28	0.43	30.60	42.09	11.49	11.2	18.03	6.82
74	49.85	50.28	0.43	40.00	42.09	2.09	11.2	18.03	6.82
75	49.85	50.28	0.43	40.00	42.09	2.09	11.2	18.03	6.82
76	38.36	41.14	2.78	40.00	46.24	6.24	11.2	18.03	6.82
77	38.36	41.14	2.78	40.00	46.24	6.24	15.1	18.03	2.88
78	38.36	41.14	2.78	40.00	46.24	6.24	15.1	18.03	2.88
79	38.36	41.14	2.78	40.00	46.24	6.24	15.1	18.03	2.88
80	38.36	41.14	2.78	40.00	46.24	6.24	15.1	18.03	2.88
81	38.36	35.20	-	40.00	46.24	6.24	15.1	18.03	2.88
82	38.36	35.20	-	40.00	46.24	6.24	15.1	18.03	2.88
83	38.36	35.20	-	40.00	46.24	6.24	15.1	18.03	2.88
84	38.36	35.20	-	40.00	46.24	6.24	15.1	18.03	2.88
85	38.36	35.20	-	40.00	46.24	6.24	15.1	18.03	2.88
86	38.36	35.20	-	42.96	46.24	3.28	9.4	18.03	8.58
87	38.36	35.20	-	42.96	46.24	3.28	9.4	18.03	8.58
88	38.36	35.20	-	42.96	46.24	3.28	9.4	19.38	9.93
89	38.36	35.20	-	42.96	46.24	3.28	9.4	19.38	9.93
90	38.36	35.20	-	42.96	46.24	3.28	9.4	19.38	9.93
91	35.51	35.20	-	42.96	46.24	3.28	9.4	19.38	9.93
92	35.51	35.20	-	42.96	46.24	3.28	9.4	19.38	9.93
93	35.51	33.14	-	42.96	46.24	3.28	9.4	19.38	9.93
94	35.51	33.14	-	42.96	46.24	3.28	9.4	19.38	9.93
95	35.51	33.14	-	42.96	46.24	3.28	9.4	19.38	9.93
96	35.51	33.14	-	31.74	39.47	7.73	9.4	19.38	9.93
97	35.51	33.14	-	31.74	39.47	7.73	9.4	19.38	9.93
98	35.51	33.14	-	31.74	39.47	7.73	9.4	19.38	9.93
99	35.51	33.14	-	31.74	39.47	7.73	9.4	19.38	9.93
100	35.51	33.14	-	31.74	39.47	7.73	9.4	19.38	9.93
101	35.51	33.14	-	31.74	39.47	7.73	9.4	19.38	9.93
102	35.51	33.14	-	31.74	39.47	7.73	-	19.38	-
103	35.51	33.14	-	31.74	39.47	7.73	-	19.38	-
104	35.51	40.48	-	27.77	39.47	11.70	-	19.38	-
105	35.51	40.48	-	27.77	39.47	11.70	-	19.38	-
106	35.51	40.48	-	27.77	-	-			
107	35.51	40.48	-	27.77	-	-			
108	35.51	40.48	-	27.77	-	-			
L	81	81	81	106	106	106	67	67	67
A (%)	40.38	48.55	8.17	34.62	41.69	7.08	15.31	27.96	12.65
TOTAL	327.09	393.27	66.18	366.96	441.95	75.00	102.61	187.34	84.74

Note: Change in soil-water content was calculated only for the profile segment which exhibited a significant increase.
Data Source: Gravimetric soil-water content measurements, Appendix C2.
L = Segment Length = cm
A = Average
TOTAL = (%θ/100)(segment length)(10 mm/cm) = mm or L/m^2.

Appendix C5. Statistical Results of TDR Water content verses Gravimetric Water Content.

Scatterplot File: tdr Date: 12-10-1990

FILTER: None

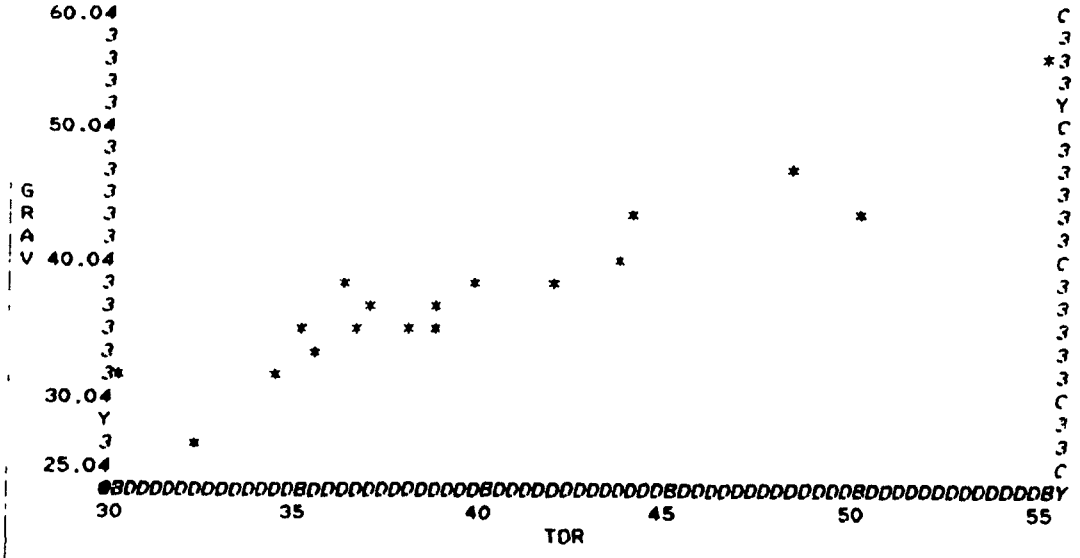

X Variable: TDR
Y Variable: GRAV

	GRAV	TDR
Mean:	38.583	39.634
Standard deviation:	6.360	6.358
Minimum:	27.800	30.000
Maximum:	55.900	54.730
N:	18	
N Missing:	0	

Std dev of Y given X: 2.306

Correlation and two-tailed P-value: 0.9361 (P(0.0000)

Regression line for predicting GRAV from TDR:	GRAV =	INTERCEPT 1.46577 +	SLOPE 0.93651 * TDR
Std Errors:		3.52916	0.08798

Appendix C6. Piezometer and Water Level Information at Section A-A', Waite Amulet Tailings, Expressed in Meters.

DATE	TIME	NOTES	WA15-2 *	WA15-1 *	WA15-4 *	WA15-3 *	WA28-3	WA28-2	WA28-1	WA28b	WA29-2	WA29-1	WA30-2 *	WA30-1 *	WA31-3	WA31-2	WA31-1	WA32-3	WA32-2	WA32-1
		PIEZOMETER INFORMATION:																		
22 Nov	PM	TOP	317.14	317.16	316.85	316.77	316.94	316.67	317.22	317.64	317.66	317.47	313.87	313.78	310.57	310.49	310.39	309.09	309.00	309.24
22 Nov	PM	TPTG	1.15	1.22	0.85	0.75	0.75	0.50	1.02	1.12	0.90	0.90	0.88	0.78	0.89	1.00	0.76	0.61	0.61	0.87
		Elev	315.99	315.94	316.00	316.02	316.19	316.17	316.20	316.52	316.76	316.57	312.99	313.00	309.68	309.49	309.63	308.48	308.39	308.37
22 Nov	PM	GSE	315.96	315.96	315.96	315.96	316.21	316.21	316.21	316.56	316.80	316.80	313.01	313.01	309.58	309.58	309.58	308.14	308.14	308.14
			4.62	7.68	8.57	11.52	3.70	6.62	8.88	8.17	7.13	10.06	5.24	6.65	1.39	3.75	5.15	2.93	3.69	5.93
			4.73	7.79	8.68	11.63	3.81	6.73	8.99	8.28	7.24	10.17	5.35	6.76	1.50	3.86	5.26	3.04	3.80	6.04
	1500	DTBP	4.73	7.79	8.68	11.63	3.81	6.73	8.99	8.28	7.24	10.17	5.50	6.91	1.65	4.01	5.41	3.19	3.95	6.19
		Elev	312.42	309.37	308.17	305.14	313.13	309.94	308.23	309.36	310.42	307.30	308.38	306.87	308.93	306.48	304.98	305.90	305.05	303.06
		PTE	312.50	309.45	308.25	305.74	313.21	310.02	308.31	309.44	310.50	307.38	308.45	306.95	309.01	306.56	305.06	305.98	305.13	303.14
		WATER LEVEL INFORMATION:																		
15 Aug	1500	DTW	4.61	5.46	5.12	4.86	dry	5.50	6.02	6.83	7.04	6.89	3.73	3.70	1.06	1.21	1.00	0.91	0.92	0.76
		Elev	312.53	311.70	311.73	311.91	-	311.17	311.20	310.81	310.62	310.58	310.14	310.08	309.51	309.28	309.39	308.18	308.08	308.48
		Head	5.42	4.59	4.61	4.79	-	4.06	4.09	3.70	3.50	3.47	3.03	2.96	2.40	2.17	2.27	1.06	0.96	1.37
01 Oct	1200	DTW	dry	5.60	5.33	4.96							3.97	3.78	1.03	1.18	0.97			
		Elev	-	311.56	311.52	311.81							309.90	310.00	309.54	309.31	309.41			
06 Oct	1200	DTW					dry	5.63	6.17											
		Elev					-	311.04	311.05											
06 Oct	1830	DTW	dry	5.64	5.28	4.91	dry	5.67	5.94				3.80	3.70	-	1.36	1.12			
		Elev	-	311.52	311.57	311.86	-	311.00	311.28				310.07	310.08	-	309.13	309.27			
07 Oct	1100	DTW	dry	5.57	5.13	-														
		Elev	-	311.59	311.72	-														
07 Oct	1220	DTW					dry	5.81	6.39				3.92	3.80						
		Elev					-	310.86	310.83				309.95	309.98						
19 Nov	1300	DTW	dry	5.55	5.28	4.75	dry	5.67	6.47	6.81	7.07	6.91	3.92	4.07	0.99	1.14	1.01			
		Elev	-	311.61	311.57	312.02	-	311.00	310.75	310.83	310.59	310.56	309.95	309.71	309.58	309.35	309.38			
22 Nov	PM	DTW	dry	5.36	5.08	4.72	dry	5.44	6.04	7.01	7.06	6.90	3.99	4.08	0.96	1.21	1.00	0.94	0.94	0.72
		Elev	-	311.80	311.77	312.05	-	311.23	311.18	310.63	310.60	310.57	309.88	309.70	309.61	309.28	309.39	308.15	308.06	308.52

TOP: Elevation of top of uncapped piezometer, by level survey.
TPTG: Distance from top of piezometer (uncapped) to ground surface, measured with tape.
GSE: Ground Surface Elevation, by level survey.
BTBP: Depth to bottom of piezometer from top of uncapped piezometer.
PTE: Piezometer tip elevation (average of porous segment), calculated from top of uncapped piezometer.
DTW: Depth to water level from top of piezometer (uncapped).
Elev: Elevation calculated from top of uncapped piezometer.

Appendix C7. THERMAL CONDUCTIVITY (Agwa-II Block) AND ELECTRICAL RESISTIVITY (Gypsum Block) INFORMATION.

INSTRUMENTATION NEST	DEPTH (cm)	ELEVATION (m)	ELEVATION HEAD (m)	AGWA-II BLOCK SERIAL NUMBER	AGWA-II BLOCK CALIBRATION a/ SLOPE (b)	AGWA-II BLOCK CALIBRATION a/ OFFSET (a)	AGWA-II BLK INSTALLATION DATE	SATURATED GYPSUM BLK RESISTANCE (ohms)	GYPSUM BLK INSTALLATION DATE
Ground Surface	0	315.933	8.82	-	-	-	-	-	-
WA15g-15	15	315.783	8.67	2397	-1.375	3.868	23 Aug	80	18 Aug
WA15g-30	30	315.633	8.52	2391	-2.087	3.607	23 Aug	126	18 Aug
WA15g-45	45	315.483	8.37	2364	-1.743	5.143	23 Aug	77	18 Aug
WA15g-75	75	315.183	8.07	2370	-1.800	4.546	23 Aug	125	18 Aug
WA15g-105	105	314.883	7.77	2383	-1.507	3.996	23 Aug	54	18 Aug
Ground Surface	0	316.110	9.00	-	-	-	-	-	-
WA15t-15	15	315.960	8.85	2361	-1.488	3.983	11 Sept	85	10 Sept
WA15t-30	30	315.810	8.70	2362	-1.225	3.007	11 Sept	78	10 Sept
WA15t-45	45	315.660	8.55	2388	-1.673	3.183	11 Sept	67	10 Sept
WA15t-75	75	315.360	8.25	2394	-1.312	2.113	11 Sept	77	10 Sept
WA15t-105	105	315.060	7.95	2404	-1.329	3.546	11 Sept	74	10 Sept
Ground Surface	0	312.804	5.69	-	-	-	-	-	-
WA30-15	15	312.654	5.54	2363	-1.396	3.546	10 Sept	62	10 Sept
WA30-30	30	312.504	5.39	2365	-1.235	4.957	10 Sept	62	10 Sept
WA30-45	45	312.354	5.24	2380	-1.444	4.826	10 Sept	61	10 Sept
WA30-75	75	312.054	4.94	2382	-1.776	3.862	10 Sept	63	10 Sept
WA30-105	105	311.754	4.64	2390	-1.160	4.379	10 Sept	62	10 Sept
Weir "V"	-	307.114	0.00	-	-	-	-	-	-

a/ Linear calibration (y=a+bx), where the independent variable is DELTA TEMPERATURE (C) the dependent variable is the PRESSURE HEAD (bars).

Appendix C8.1. Calculation of the Specific Electrical Conductance of Distilled Water at Saturation with Gypsum.

Given:

$$CaSO_{4\,(s)} \rightleftharpoons Ca^{2+} + SO_4^{2-}$$

$$K_{sp} = 2.5 \times 10^{-5}$$

Concentrations of each ion:

$$K_{sp} = [Ca^{2+}]\,[SO_4^{2-}]$$

$$2.5 \times 10^{-5} = M^2$$

$$M = 0.005 \text{ mole/L}$$

$$\text{mg } Ca^{2+}/L = (0.005 \text{ mole/L})(40.08 \text{ g/mole})(1000 \text{ mg/L}) = 200 \text{ mg/L}$$

$$\text{mg } SO_4^{2-}/L = (0.005 \text{ mole/L})(96.06 \text{ g/mole})(1000 \text{ mg/L}) = 480 \text{ mg/L}$$

Ionic Strength (I):

$$I = 1/2 \sum c_i z_i$$

where, c_i = concentration of ith species (moles/L)

z_i = oxidation number of the ith species.

$$I = \tfrac{1}{2}[(.005)(2)^2 + (0.005)(2)^2] = 0.020$$

Specific Conductivity (after Kemp, 1971):

$$I = (2.5 \times 10^{-5})(EC)(g)$$

where, EC = electrical conductance at 20°C (μmho cm^{-1}) otherwise, specific conductivity

g = proportionality factor, 0.55 to 0.70 (typ. 0.67)

$$EC = (40{,}000)(I)/g$$
$$= (40{,}000)(0.02)/(2/3)$$
$$= 1200 \text{ } \mu\text{mho cm}^{-1}$$

Appendix C8.2. Calculation of Specific Electrical Conductance of Saturated Gypsum Used in Gypsum Block Probes.

Construction of Gypsum Blocks:

Dimensions of the cylindrical gypsum blocks (manufactured by Soil Moisture Corp.) are 1¼ inch length by ⅞ inch diameter. The electrode system imbedded in the gypsum consists of a cylindrical stainless steel screen (½ inch ID) surrounding a smaller cylindrical stainless steel screen (¼ inch OD).

Specific Electrical Conductance:

Measured resistance of 42 gypsum blocks which were saturated with de-ionized water has a mean of 82.6 Ω with a standard deviation of 20.9 Ω.

The 82.6 Ω is across a ⅛ inch radial distance. Therefore, the average resistance of the saturated gypsum is 260 Ω/cm.

Since conductivity is the reciprocal of resistance, EC = $10^6/260$ = 3850 µmhos/cm.

Appendix C8.3. Calculation of Maximum Specific Electrical Conductance of Unsaturated-Zone Pore-Waters of Waite Amulet Unoxidized Tailings.

Ion	Atomic Weight (g/mol)	Concentration[a/] (mg/L)	(mol/L)
Fe^{2+}	55.85	10,000	0.179
SO_4^{2-}	96.06	10,000	0.104
Na^+	22.99	20	0.001
K^+	39.10	60	0.002
Ca^{2+}	32.06	600	0.019
Mg^{2+}	24.31	850	0.035
H^+	1.00	3	0.003

Ionic Strength = 0.623

Specific Electrical Conductance[b/] = 37,366 µS/cm

a/ Source: Blowes and Jambor (1988).

b/ Specific Electrical Conductance = (40,000)(I)/g
where, I = Ionic Strength,
g = proportionality factor,
0.55 to 0.70 (typ. 0.67)
after, E.C. Kemp (1971).

Appendix C8.4. Calculation of the Resistance of Gypsum Blocks Saturated with a Solution Similar to that of the Unsaturated-Zone Pore-Waters of Waite Amulet Unoxidized Tailings.

Construction of Gypsum Blocks:

Dimensions of the cylindrical gypsum blocks (manufactured by Soil Moisture Corp.) are 1¼ inch length by ⅞ inch diameter. The electrode system imbedded in the gypsum consists of a cylindrical stainless steel screen (½ inch ID) surrounding a smaller cylindrical stainless steel screen (¼ inch OD).

Assumptions:

The electrical conductance of the gypsum that is saturated with unsaturated zone porewaters is equal to the electrical conductance of the porewaters, i.e., 37400 µmhos/cm.

Gypsum Block Resistance:

Since resistance is the reciprocal of conductivity, the resistance of gypsum (in Ω/cm) = 10^6/EC

= (10^6)/(37400 µmhos/cm)

= 26.7 Ω/cm

The resistance of the gypsum block is across a ⅛ inch radial distance of gypsum. Therefore, the resistance of the gypsum block

= (26.7 Ω/cm)(2.54 cm/inch)(⅛ inch)

= 8.5 Ω

As the resistance of gypsum blocks, saturated with de-ionized water, is 82.6 Ω with a standard deviation of 20.9, the resistance measurement as a result of the increased conductivity by tailings unsaturated zone porewaters is an order of magnitude less than that by de-ionized water, 3.5 standard deviations outside of the mean. The difference is 82.6 - 8.5 = 74.1 Ω.

Appendix C9. Julian Day Calendar Year.

DAY	JAN	FEB	MAR	APR	MAY	JUN	JUL	AUG	SEP	OCT	NOV	DEC
1	1	32	60	91	121	152	182	213	244	274	303	335
2	2	33	61	92	122	153	183	214	245	275	304	336
3	3	34	62	93	123	154	184	215	246	276	305	337
4	4	35	63	94	124	155	185	216	247	277	306	338
5	5	36	64	95	125	156	186	217	248	278	307	339
6	6	37	65	96	126	157	187	218	249	279	308	340
7	7	38	66	97	127	158	188	219	250	280	309	341
8	8	39	67	98	128	159	189	220	251	281	310	342
9	9	40	68	99	129	160	190	221	252	282	311	343
10	10	41	69	100	130	161	191	222	253	283	312	344
11	11	42	70	101	131	162	192	223	254	284	313	345
12	12	43	71	102	132	163	193	224	255	285	314	346
13	13	44	72	103	133	164	194	225	256	286	315	347
14	14	45	73	104	134	165	195	226	257	287	316	348
15	15	46	74	105	135	166	196	227	258	288	317	349
16	16	47	75	106	136	167	197	228	259	289	318	350
17	17	48	76	107	137	168	198	229	260	290	319	351
18	18	49	77	108	138	169	199	230	261	291	320	352
19	19	50	78	109	139	170	200	231	262	292	321	353
20	20	51	79	110	140	171	201	232	263	293	322	354
21	21	52	80	111	141	172	202	233	264	294	323	355
22	22	53	81	112	142	173	203	234	265	295	324	356
23	23	54	82	113	143	174	204	235	266	296	325	357
24	24	55	83	114	144	175	205	236	267	297	326	358
25	25	56	84	115	145	176	206	237	268	298	327	359
26	26	57	85	116	146	177	207	238	269	299	328	360
27	27	58	86	117	147	178	208	239	270	300	329	361
28	28	59	87	118	148	179	209	240	271	301	330	362
29	29	60	88	119	149	180	210	241	272	302	331	363
30	30	-	89	120	150	181	211	242	273	303	332	364
31	31	-	90	-	151	-	212	243	-	304	-	365

Note: Add 1 to values after 29 Feb during leap years.

Appendix D. References of the Appendices

Aitchison, G.D. (1965). Moisture equilibria and moisture changes in soils beneath covered areas. Butterworths, Sydney, 278 p.

Aslyng *et al.* (1963). Soil Physics terminology. Inter. Soc. of Soil Sci. Bull. 23, p.7

Davis, J.L., and A.P. Annan (1977). Electromagnetic detection of soil moisture: Progress report I. *Can. J. Remote Sensing* 3(1):76-86.

Blowes, D.W., and J.L. Jambor (1988). The pore-water geochemistry and the mineralogy of the vadose zone of sulphide tailings, Waite Amulet, PQ. Report to CANMET, DSS Contr. No. 23440-7-9161/01-SQ.

Hillel, D. (1972). Soil and water, physical principles and processes. Academic Press, Inc., New York, 288 p.

Iwata S., and T. Tabuchi (1988). Soil-water interactions, mechanisms and application. Marcel Dekker, Inc., New York. 380p.

Kemp, P.H. (1971). Chemistry of natural waters - I. *Water Research*, 5, p. 297.

Kohnke, H. (1968). Soil Physics. McGraw-Hill Book Co., New York, 224 p.

Ledieu, J.,P. DeRidder, P. DeClerck, and S. Dautrebande (1986). A method of measuring soil moisture by time-domain reflectometry. *J. Hydro.* 88:319-328.

Schofield, R.K. (1935). The pF of water in soil. Trans. Int. Congr. Soil Sci., 3d, II:37-48.

Sharpe, C. (ed) (1988). Kempes' Engineers Year-Book. 93rd ed., vol. 1., p. A7/6.

Sposito, G. (1981). The thermodynamics of soil solutions. Oxford Clarendon Press, New York. 223 p.

Taylor, S.A., and G.L. Ashcroft (1972). Physical Edaphology, W.H. Freeman, San Francisco.

Terminology Committee, Commission I, ISSS, Terminology in soil physics, *ISSS Bull.* 49:26-36.

Topp, G.C., and J.L. Davis (1985). Comment on "Monitoring the unfrozen water content of soil and water using time-domain reflectometry" by J. Stein and D.L. Kane. *Water Resour. Res.* 21:1059-1060.

von Hillel, A.R. (1958). Dielectrics. *In* Handbook of Physics. E.V. Condon and H. Odishaw (eds), McGraw-Hill, New York, N.Y.

Yong, R.N., and B.P. Warkentin (1975). Soil properties and behaviour. Elsevier Scientific Publishing Co., New York, 449 p.